Functional characterization and plasticity of extraocular motor responses in *Xenopus laevis*

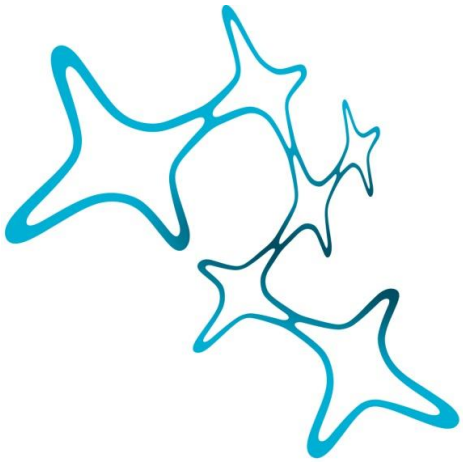

Graduate School of
Systemic Neurosciences
LMU Munich

Dissertation der Graduate School of Systemic Neurosciences der
Ludwig-Maximilians-Universität München

Haike Dietrich

August 2016

Supervisor:	**Prof. Dr. Hans Straka**
Second reviewer:	**Prof. Dr. Stefan Glasauer**
Date of defense:	**9.3.2017**

Acknowledgements

Only some time after becoming a doctoral student – apparently all of a sudden – I now look back at these exciting and challenging years, wondering how they could have possibly passed so quickly. Out of the numerous interesting people that came and went during this time, I am especially happy about the many who have supported me in one way or another.

Most of all I want to thank my supervisor Hans Straka for offering me to conduct my thesis in his laboratory and for the continuous support, interesting projects and inspiring discussions that helped me at any time. Thank you for an "open door" whenever I needed it!

I would also like to thank my colleagues for the good time in and outside of the laboratory! Thank you, Kathi, for always lending an ear to me and for cheering me up if needed. Thanks, Francisco, for always knowing an answer and the instant setup-help whenever necessary. Thank you, Boris, for being honest, even when the truth was not too comfortable. Thank you Johanna, Michi, Céline, Sara, Elisabeth, Carlana and all of you for the many laughs, chats and lovely cake and coffee breaks!

Thanks, Sara and Hans, for the thorough proof-reading of this manuscript!

I also want to thank my thesis advisory committee (Hans Straka, Lars Kunz and Stefan Glasauer) for their useful input during our regular meetings. Stefan, thank you also for all the work during our long and successful collaboration!

Furthermore, I would like to thank the Graduate School of Systemic Neurosciences for providing an international and interdisciplinary framework for this thesis and offering such helpful events and courses as part of the PhD program.

For their financial support I thank the IFB, the graduate program RTG[1373] and the GSN.

Last but not least I want to thank my family and friends for always standing by my side. Thank you for sharing these past years with me and for all the great memories that will remain!

Index

Summary ... **1**

Introduction ... **3**

I Why animals move their eyes – principles of gaze stabilization ... 3

I.1 Acquisition of visual information requires a stable visual environment ... 3

I.2 Gaze stabilization in *Xenopus laevis*: an ideal model organism ... 5

I.3 Mechanisms underlying the vestibulo-ocular reflex (VOR) ... 7

I.3.a The angular VOR (aVOR) ... 8

I.3.b The linear VOR (lVOR) ... 10

II Different cellular subtypes shape responses at all stages of the VOR circuitry ... 11

II.1 Sensory Periphery: Hair cells and afferents ... 12

II.2 Vestibular nuclei ... 16

II.3 Extraocular motoneurons and muscle fibers ... 19

II.4 Neurotransmitter systems of the basic VOR network ... 21

III Plasticity ... 22

III.1 The VOR is plastic ... 22

III.1.a Demands for motor system plasticity ... 22

III.1.b Mechanisms underlying VOR plasticity ... 23

III.2 Homeostatic plasticity ... 26

IV Aim of this thesis ... 27

Results Part I ... **29**

Results Part II ... **75**

Results Part III ... **87**

Discussion ... **103**

I The developing *Xenopus laevis*: an ideal model organism for studying the VOR ... 103

II Electrophysiological properties of abducens motoneurons ... 104

II.1 Abducens motoneurons: both continuum and distinct groups ... 105

II.1.a The origin of two different subgroups ... 106

II.1.b Functional relevance of the two different subgroups for VOR eye motion ... 107

II.2 Different subgroups of abducens motoneurons: evidence for parallel channels?. 109

III Calcium imaging and morphological correlates to physiology ... 110

IV Pharmacology of the VOR ... 114

IV.1 Excitatory neurotransmitter systems ... 115

IV.2 Inhibitory neurotransmitter systems 116
V Plasticity of the VOR 118
VI Summary and Outlook 120
VI.1 Classification of abducens motoneurons 120
VI.2 Homeostatic plasticity of the VOR 122
References/Bibliography 125
Appendix 139
I Abbreviations 139
II List of publications 139
III Declaration of author contributions 140
IV Copyrights 145
V Affidavit (Eidesstattliche Erklärung) 147

Summary

Vestibulo-ocular reflexes (VOR) provide an essential contribution to gaze stabilization in vertebrates that is required to maintain visual acuity during movements of the head or body. Eye movements that counteract head motion in the horizontal plane are mediated by a pair of antagonistic horizontal eye muscles that cause an adduction (medial rectus muscle) or abduction (lateral rectus muscle) of each eye. Each muscle is controlled by a separate set of extraocular motoneurons located in the oculomotor and abducens nucleus respectively. Abducens motoneurons receive bilateral vestibular signals about ongoing head motion and integrate them into temporally precise motor commands. The major part of this thesis aimed at investigating the mechanistic basis of this neuronal integration by deciphering the morpho-physiological and pharmacological properties of abducens motoneurons. Experiments were performed in semi-intact preparations of *Xenopus laevis* tadpoles that allowed *in vitro* studies of the fully intact vestibulo-ocular reflex network from the vestibular endorgans to the oculomotor plant. A morphological approach revealed that abducens motoneurons display a variety of somal sizes and shapes, likely related to the observed continuum of recruitment thresholds and resting firing rates. Investigation of the discharge during sinusoidal head rotation suggested that abducens motoneurons subdivide into at least two functional subgroups with respect to generated motor commands during sinusoidal head rotation: one group responds with changing discharge peak amplitude and phase to different frequencies of head rotation, whereas a second group only responds to differences in stimulus velocity, insensitive to changes in the frequency of head motion. This physiological segregation into two motoneuronal subgroups also correlates with differences in the excitatory neurotransmitter profile: inputs to group I motoneurons are mediated by a relatively higher NMDA than AMPA receptor contribution, whereas in group II motoneurons, the opposite relation was observed. Inhibitory vestibular inputs to all abducens motoneurons were found to be glycinergic in nature and supplemented by a tonic GABAergic inhibition of extra-vestibular origin. A computational approach suggested that group II motoneurons are relatively more important for the generation of compensatory eye movements than group I motoneurons. The second part of this thesis revealed that homeostatic plasticity shapes the output of the VOR in the absence of visual feedback. Prolonged sinusoidal head rotation induces an attenuation or facilitation of VOR responses depending on the magnitude of the motion stimulus. This type of plasticity is plane-specific, reversible and critically depends on the integrity of the vestibulo-cerebellar side-loop. Given the evolutionarily conserved organization of the VOR, this thesis thus contributes to the general understanding of how gaze stabilizing eye movements in vertebrates are controlled at the motoneuronal level.

Introduction

I Why animals move their eyes – principles of gaze stabilization

I.1 Acquisition of visual information requires a stable visual environment

Around half a billion years ago, vertebrates started colonizing the planet (Shu et al., 1999). In an environment full of competitors, through evolution numerous strategies emerged that improved the species' individual chances of survival. Critical to this was the development of sensory systems, out of which the visual system again played a crucial role. The ability to "see" soon became an important aspect for life, whether being a predator searching for food or prey that needs to escape, fight or hide. Furthermore, the evolution of a large spectrum of eye movement dynamics not only allowed animals to scan the surroundings (saccades) or, for example, follow moving objects (smooth pursuit; in foveate mammals) while resting in a fixed position, but also to counteract any changes in head position that otherwise would have caused a shift of the visual scene during the large spectrum of passive or self-generated movements of the head and body (see Land, 1999).

First of all, keeping a stable, focused image on the retina is especially important considering the fact that visual processing is relatively slow compared to other sensory organs. Perception of an image requires it to be still for around 300 ms (for review see Land, 1999) – without gaze-stabilizing mechanisms, the visual world would continuously be blurred during head motion. Thus, scanning of the environment, even if it might appear smooth, actually comprises a sequence of fast, small movements (saccades) where the eyes "jump" from one stable image to another. Secondly, even though gaze stabilization appears to be mainly important for foveate animals, also species with less accurate vision require counteracting eye movements, in particular to distinguish self-motion from movements within the environment and thus discriminate between inanimate objects and other animals (Walls, 1962). In order to distinguish whether objects move in space or remain stationary, the animal's eyes must be stable relative to that object. For example, if we actively follow a person running from left to right with our eyes, we can tell that the runner is moving although he stays at a similar position on our retina, since our brain knows that our eyes are moving at the same time. However, if our eyes were passively moved during head displacements, the resulting movement of the visual environment would be misinterpreted as objects moving around us even though they are stable, and such delusion is prevented by gaze-stabilizing reflexes. Thirdly, a stable gaze enables some animals to retrieve appropriate information about optic flow speed during translational self-motion such as flying, in order to determine whether objects are near (faster visual flow) or distant (slow visual flow) (see Land, 1999).

All of these advantages have promoted the evolution of image stabilizing mechanisms not only in vertebrates but also for instance in arthropods such as crustaceans (rock crabs, Paul et al., 1990) and insects. Although e.g. blowflies cannot move their eyes, they move their head relative to the neck to stabilize the eyes against body movements (Land, 1973). On the other hand, such a "head stabilization mechanism" is also found in vertebrates: for example, most birds, although they can move their eyes, mainly use head movements to counteract image slip during body motion in space (e.g. Pratt, 1982). It can thus be concluded that, even though the general strategies and underlying neurobiological mechanisms for gaze stabilizing eye movements may differ widely among species, their importance persists throughout the long history of evolution.

Generally in vertebrates, an essential part of gaze stabilization is mediated by the evolutionarily well conserved vestibulo-ocular reflex (VOR) that transforms vestibular signals during head motion into extraocular motor commands for counteractive eye movements (see below). However, depending on the species, the VOR alone would be insufficient to achieve the accuracy of image stabilization required e.g. by foveate animals over the entire range of naturally experienced head motion frequencies (see e.g. Walls, 1962); hence other inputs, such as from the visual system, are necessary to fine-tune compensatory eye movements. Concerning visuo-ocular motor transformations, a substantial component is mediated by the optokinetic reflex (OKR) that enables tracking of a large-field moving visual scene and thus acts as an online feed-back control of the VOR output (Batini et al., 1979; Cochran et al., 1984; see Ito, 1982; Barnes, 1993). OKR performance becomes especially apparent in the absence of vestibular and/or proprioceptive stimuli. Imagine for example a person looking out of the window in a train moving at a slow, constant speed, such that no acceleration activates the vestibular system. Stable images are produced by the OKR when the eyes follow the moving environment for a while, jump back (resetting fast phase) when the most eccentric eye position is reached, and then continue following the scene.

On the other hand, gaze stabilization is assisted by proprioceptive feedback, activating the cervico-ocular reflex, which collects information about head position from the neck musculature to produce compensatory eye movements. In many species, such as humans, this reflex plays a minor role, but gains importance in replacing the VOR in patients with vestibular deficits (Bronstein and Hood, 1986; Kelders et al., 2003; Sadeghi et al., 2011; Yakushin et al., 2011). Furthermore, it appears likely that at least some vertebrates are capable of anticipating image slip caused by their own active body and head movements during walking, running, swimming or flying (Chagnaud et al., 2012). During many of these locomotor strategies, central pattern generators (CPG) in the spinal cord generate motor commands for the necessary rhythmic trunk muscle contractions (for review, e.g. see Marder and Bucher, 2001; Hultborn and Nielsen, 2007). In fact, the spinal CPG in *Xenopus laevis*

sends an efference copy of its motor commands to central VOR brain regions to supplement or even replace vestibular sensory inputs with the expected head movement signal during the upcoming locomotion (Combes et al., 2008; Lambert et al., 2012; von Uckermann et al., 2013). In a complementary fashion, the discharge of one class of neurons in the vestibular nuclei ("vestibular-only neurons") in primates is actively suppressed during active head motion by an efference copy of the voluntary motor command (see e.g. Cullen et al., 2011).

In conclusion, various mechanisms that are adapted to the species' individual requirements act in concert to mediate gaze stabilization in vertebrates. During my thesis, I focused on the vestibulo-ocular reflex, using *Xenopus laevis* tadpoles as a model organism that shall now be described in more detail.

I.2 Gaze stabilization in *Xenopus laevis*: an ideal model organism

In choosing an appropriate model organism for a certain field of study, various aspects from the ease of maintenance and accessibility of the species to their applicability for the specific area of investigation must be considered. For example, model systems for clinical research are mainly chosen according to their similarity with humans, whereas the understanding of fundamental biological mechanisms that persist across evolution is so far often facilitated by studies in animals that have less complex neural circuitries and additionally allow employing a variety of experimental techniques. Next to "classical" model organisms like mice, zebrafish, *Drosophila* and monkeys, amphibian species such as the African clawed frog (*Xenopus laevis*) have so far played a minor role in basic neurobiological research. However, in many aspects frogs were proven to be highly advantageous (see Straka and Simmers, 2012; Straka et al., 2016). First of all, keeping these animals is relatively simple, and growth occurs rapidly such that after hatching tadpoles usually take no longer than 3 months to reach metamorphosis. Developmental stages, that consider e.g. the size and shape of fore- and hindlimbs and other morphologically characteristic features, are well described and allow the classification of larval maturation independent of individual growth rates and body dimensions (example pictures of developmental stages are depicted in figure 1A, modified from "The normal table of *Xenopus laevis*", Nieuwkoop and Faber, 1994). This in turn facilitates studies investigating the formation of neural circuitries in a developmental and behavioral context, such as the remodeling of locomotor networks during metamorphosis where animals rapidly change from undulatory swimming to limb-kick propulsion (Combes et al., 2004). In addition, trans- or implantation studies of certain organs such as the eyes (Blackiston and Levin, 2013) or ears (Elliott and Fritzsch, 2010; Elliott et al., 2015a,b) significantly contributed to the understanding of how neuronal connections are established during critical periods of development. With respect to gaze stabilization, investigating the

normal development of visual (for review, see Udin, 2007) and vestibular circuitries (Lambert et al., 2008; Branoner and Straka, 2015) in *Xenopus* made significant contributions to understanding functional principles of the directly involved sensory systems. Furthermore, the recently sequenced full genome of *Xenopus tropicalis* (Hellsten et al., 2010) now enables the potential use of genetic tools in these animals.

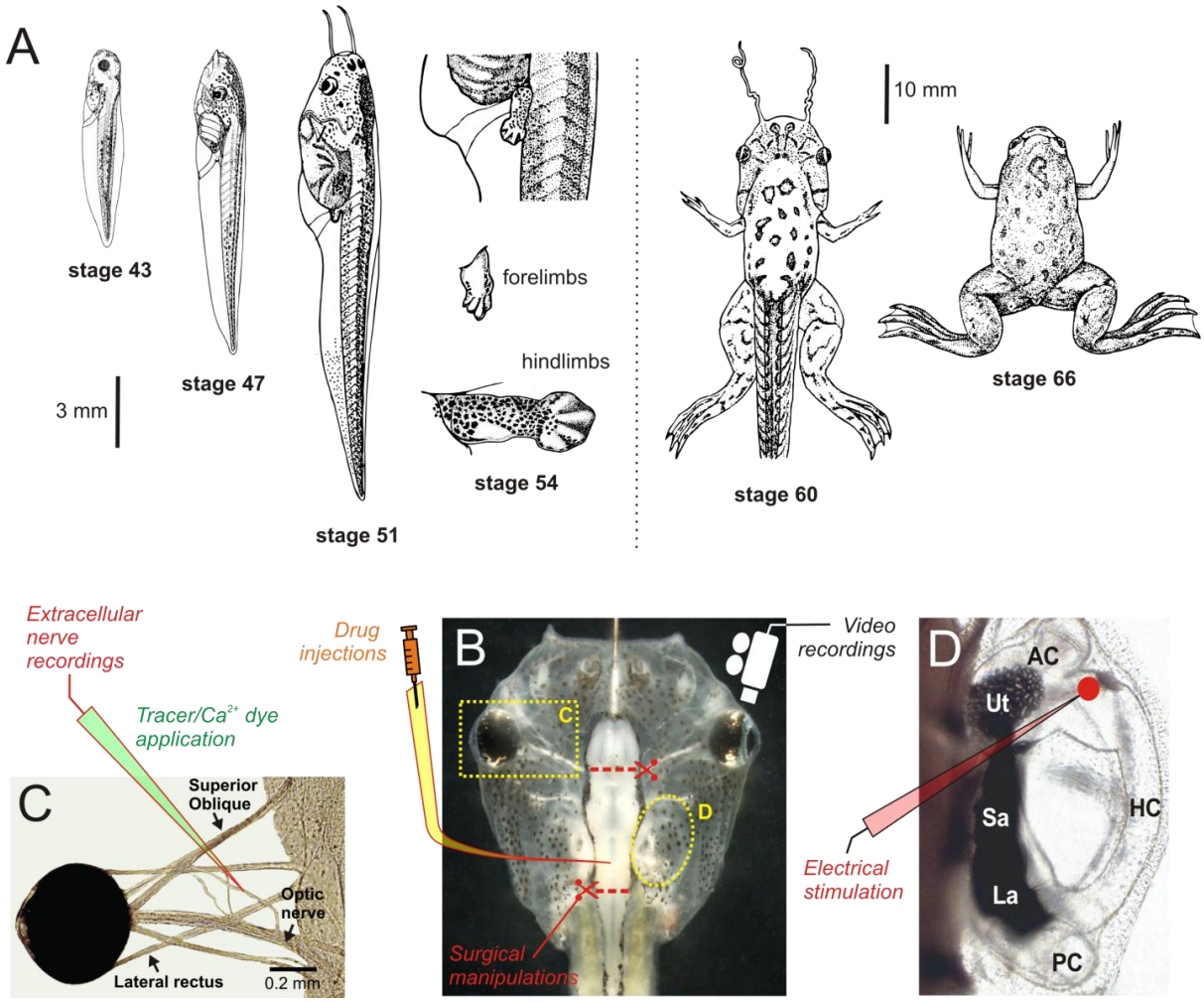

Figure 1: *Xenopus laevis* as a model organism. *A,* Drawings depicting different stages during the development of *Xenopus laevis*; note the development of fore- and hindlimbs in growing larvae (left side) and loss of the tail and tentacles during metamorphic climax (right). Scale bars apply to all drawings on the respective side. Modified from Niewkoop and Faber, 1994. Permission granted by Garland Pub. ***B-D,*** Overview of methods applied to semi-intact *in vitro* preparations of larval *Xenopus* (***B***), eye muscles with innervating nerve branches (***C***) and vestibular endorgans (***D***). ***B*** and ***C*** were modified from Dietrich and Straka, 2016; ***D*** was adapted from Gensberger et al., 2016. AC/HC/PC, anterior/horizontal/ posterior semicircular canals; La, lagena; Sa, saccule; Ut, utricle.

Another tremendous advantage of using *Xenopus* as a model organism is the ability to employ amphibian semi-intact *in vitro* preparations (Luksch et al., 1996; Straka and Simmers, 2012) that have long been used in neurobiological research ever since the isolated frog whole brain was described by Hackett (1972). *Xenopus* tadpole preparations (Fig. 1B) allow retaining fully functional networks within and outside the central nervous system, such as all components required for gaze stabilizing reflexes. For example the entire circuitry of the vestibulo-ocular reflex, including vestibular endorgans (Fig. 1D) and the oculomotor plant (Fig. 1C), remain intact which allows a "natural" activation of the VOR with motion stimuli and the recording of functional eye movements as a direct behavioral readout. Hence, an *in vivo* like investigation of the VOR can be achieved while at the same time being able to use *in vitro* anatomical, electrophysiological and imaging techniques as well as pharmacological and surgical manipulations (Fig. 1B-D). Furthermore, these preparations survive for several days in oxygenated Ringer's solution (Straka and Dieringer, 1993), thus allowing prolonged experimentation required e.g. for over-night retrograde labeling of neurons for anatomical tracing or subsequent Ca^{2+} -imaging studies.

During my thesis, I aimed to isolate extraocular motor commands as readout of the VOR and exclude interferences by the optokinetic reflex and spinal efference copy. Taking advantage of the *Xenopus in vitro* preparation, this was achieved by dissecting both optic nerves as well as the rostral spinal cord (lower red dashed line in Fig. 1B). Predominantly, *Xenopus* tadpoles at developmental stage 54 were used for experimentation, since their semicircular canals have reached a size where angular accelerations are already detectable and VOR responses are robust (Lambert et al., 2008).

I.3 Mechanisms underlying the vestibulo-ocular reflex (VOR)

The vestibulo-ocular reflex in vertebrates has its origin early in evolution, and its principle mechanism – simple as it is – has not changed ever since (Straka et al., 2014). As the name suggests, the "vestibulo"-"ocular" reflex relays inputs from the vestibular to the oculomotor system, and in its simplest form, this transfer is almost direct. The basic VOR network consists of a three-neuronal reflex arc (first described by Lorente de Nó, 1933) that transmits information about angular or linear head movements from the different vestibular endorgans via afferents of the VIIIth cranial nerve to central vestibular neurons in the brainstem that in turn directly project to extraocular motoneurons. The beauty of this reflex lies in this simplicity: the very few processing stages allow an extremely fast transformation of sensory- into motor commands and thus the generation of temporally precise eye movements that counteract head motion of up to at least 25 Hz on-line and almost instantly (Huterer and Cullen, 2001). In primates, for example, the onset of the VOR response has a latency of only

5-6 ms (Huterer and Cullen, 2001). The VOR contains both linear and angular components that are mediated by functionally different vestibular endorgans. The networks underlying these individual components shall be considered below.

I.3.a The angular VOR (aVOR)

Angular accelerations generated by rotational movements of the head are sensed by the three semicircular canals in each inner ear that are filled with a fluid – the so called endolymph – that is maximally forced in one or the other direction when the head turns in the orientation of the respective canal. This fluid motion then forces cilia of the hair cells, located in the canal cupulae, in one or the other direction, causing excitation or inhibition of the hair cell respectively, that in turn induces an increase or decrease in the firing rate of the postsynaptic afferent fiber (see below; Guth et al., 1998).

Spatial specificity of the angular VOR is facilitated by the approximate geometric alignment of the six extraocular muscles with the orientation and activation planes of the six semicircular canals (Fig. 2A), that allows a direct transformation of vestibular signals into extraocular motor commands both in frontal- and lateral-eyed species (Simpson and Graf, 1981). Probably most intuitive is the relation between the horizontal canals and lateral and medial rectus eye muscles that move the eye in the horizontal plane. Connections between these approximately aligned systems are called principal connections, whereas supplemental information is retrieved from additional, "auxiliary" connections that bring together vestibular signals from other semicircular canals and combine the different three-dimensional activation vectors for a final, precise motor output (for review, see Straka and Dieringer, 2004). These connections thus compensate for the remaining portion of species-dependent eye muscle – semicircular canal misalignments (Simpson and Graf, 1981; Pantle and Dieringer, 1998; Cox and Jeffery, 2008). Angular head movements are detected by hair cells of the semicircular canals that pass the information on to second order vestibular neurons (2°VN) in the brainstem via vestibular afferents of the VIIIth cranial nerve. Vestibular

---

Figure 2: Principles of the angular VOR. ***A,*** Schematic showing the alignment of the pulling directions of extraocular muscles with the orientation of the semicircular canals. Modified with courtesy from Dr. Francisco Branoner, 2016. ***B,C,*** Schematics of the *semi-intact* larval *Xenopus* preparation depicting the pathways underlying the horizontal aVOR (***B***) and the optimal orientation on the turntable for activation of the vertical aVOR innervating the left superior oblique eye muscle (***C***). ***D,*** Multiple-unit abducens nerve recording of the modulated aVOR activity during sinusoidal head rotation. ***E,F,*** Schematics depicting neuronal circuitries of the horizontal (***E***) and vertical (***F***) aVOR. 1/2°VN, first/second order vestibular neurons; AC/HC/PC, anterior/ horizontal/posterior semicircular canals; int, abducens internuclear neurons; IR, inferior rectus; LR, lateral rectus; MN, motoneurons MR, medial rectus; SO, superior oblique.

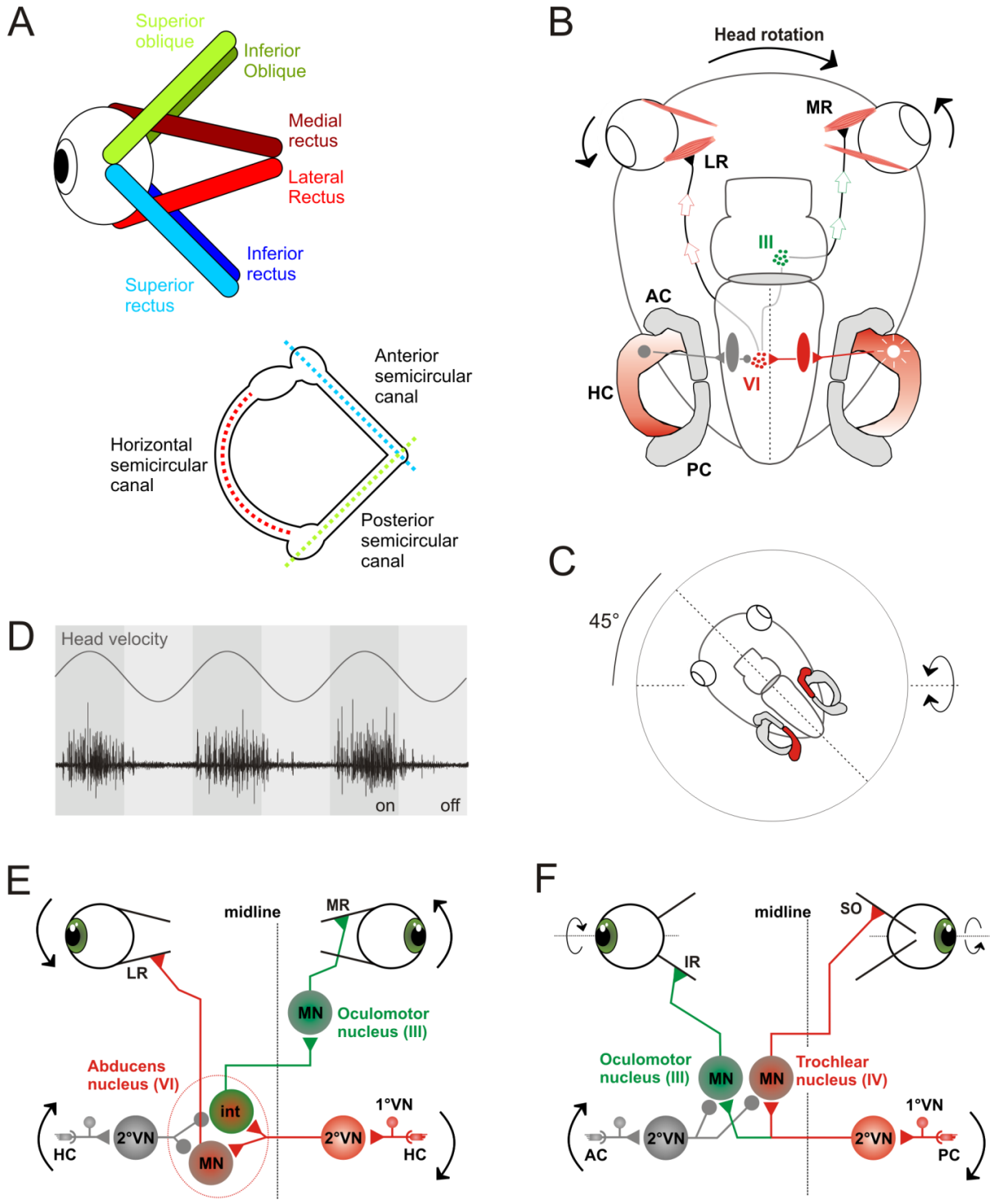

neurons then project to the three cranial motor nuclei – oculomotor (III), trochlear (IV) and abducens (VI) – that innervate the extraocular musculature.

Via principal connections of the horizontal aVOR, abducens motoneurons receive excitatory inputs from contralateral 2°VNs that in turn are contacted by vestibular afferents from the contralateral horizontal canal (red in Fig. 2B,E) (Baker et al., 1969). Hence, maximal

excitation results from a head movement in the direction that maximally activates the contralateral horizontal canal (on-direction of the movement). In addition, inhibitory connections from the ipsilateral vestibular nucleus reach abducens motoneurons that are weakest during this contraversive motion (gray in Fig. 2B,E) and maximally activated during head motion in the opposite direction (Baker et al., 1969). Furthermore, in order to synchronize the motion of both eyes, abducens internuclear neurons receive similar vestibular inputs and relay them to medial rectus innervating motoneurons of the contralateral oculomotor nucleus (green in Fig. 2B,E) (Baker and Highstein, 1975; Highstein and Baker, 1978). Hence, whenever the head rotates e.g. clockwise, both eyes jointly move counter-clockwise to counteract motion-induced image slip (Fig. 2B). During vertical head rotation, for example, principal aVOR connections supplying the superior oblique muscle can be investigated. This muscle receives innervation from trochlear (IV) motoneurons that are maximally activated during rotation in the plane of the ipsilateral posterior (PC) and contralateral anterior (AC) vertical semicircular canals, approximately when the animal is rotated vertically at a 45° horizontal position angle (Fig. 2C). Maximal contraction of the ipsilateral superior oblique and contralateral inferior rectus muscles occurs during head motion that optimally activates the ipsilateral PC and inactivates the contralateral AC via midline-crossing projections (Fig. 2F; Graf et al., 1997).

In general, when the head remains stable, extraocular motoneurons display a resting rate – probably due to the resting discharge of vestibular afferents (e.g. Blanks and Precht, 1976) that is relayed via 2°VNs – for the tonic activation of muscle fibers that stabilizes the eye in its resting position. During sinusoidal head rotation the resting discharge of motoneurons is cyclically modulated depending on the direction of the head motion (Fig. 2D).

I.3.b The linear VOR (lVOR)

Unlike angular head acceleration which is sensed by the semicircular canals, linear accelerations, comprising translational movements or head position within the gravitational field, are detected by the otolith organs of the inner ear in all vertebrates. In most species, hair cell sensory epithelia of these organs are covered by a gelatinous matrix coated with small calcium carbonate crystals, called otoconia (“ear stones”), that give the gelatinous layer a mass to be moved by linear acceleration. Hair cell cilia embedded in this layer are deflected by the resulting shearing motion, and due to their arrangement in 360°, the direction-specific degree of activation or inhibition of each hair cell afferent firing rate allows the precise calculation (vector summation) of the direction of translational motion or, in the vertical plane, position of the head relative to gravity. Compared to the semicircular canals, these organs are more heterogeneous with respect to function and occurrence within vertebrate

species. Common to all mammals are two otolith organs: the utricle, detecting horizontal linear motion, and the saccule that senses vertical acceleration and head position changes relative to gravity. In non-mammalian species, such as frogs, the utricle also perceives horizontal linear acceleration (Rohregger and Dieringer, 2002), and utricular afferents often converge on the level of 2°VNs with inputs from the horizontal semicircular canals (Straka et al., 2002). However, the saccule in these animals is considered to predominantly act as an auditory organ and substrate vibration sensor (Lewis et al., 1982). All non-mammalian species and also some mammals (monotremes) thus possess a third organ – the lagena – that mainly functions as a vestibular organ (see Khorevin, 2008) and detects vertical linear movements (e.g. in frogs: Caston et al., 1977), converging with posterior and anterior vertical canal inputs on the level of 2°VNs (Straka et al., 2002). In conclusion, not the saccule, but lagena and utricle in non-mammalian species sense vertical and horizontal linear motion respectively (e.g. in frogs: Straka et al., 2002).

With respect to gaze stabilization, the lVOR in frogs mainly comprises utriculo-ocular pathways (Hess and Precht, 1984), mediating compensatory eye movements during horizontal linear motion, whereas purely vertical linear acceleration causes negligible responses in extraocular motoneurons of all – horizontal, vertical and oblique – eye movement planes (Rohregger and Dieringer, 2002). Furthermore, compared to the continuously conjugate eye motion that counteracts horizontal angular acceleration, horizontal lVOR responses can be more diverse, depending on the direction of linear acceleration. In fact, left- and rightward linear head motion elicits counteracting conjugate right- and leftward eye movements, whereas forward-/backward motion causes con- and divergence of the eyes respectively, to account for the changes in object distance when the head moves towards or away from a visual target (see Straka and Dieringer, 2004).

II Different cellular subtypes shape responses at all stages of the VOR circuitry

During natural behavior, the VOR must cover a large spectrum of widely differing head motion dynamics. Since rapid, high frequency head turns must be equally well counteracted as slow, low frequency displacements, the underlying neural and/or network integrations must display an equally large dynamic range. Indeed, a variety of neuronal subtypes with different intrinsic and synaptic properties is present at each level of the VOR circuitry, ranging from hair cells in the sensory periphery to muscle fibers of the extraocular motor plant (see below). In turn, to facilitate network computations, one can imagine that cells of a particular subtype (e.g. afferent fibers) relay information to cells with similar characteristics

at the next processing stage (2°VNs), creating parallel, "frequency-tuned" channels for the sensory-motor transformation, each with different dynamic properties (see Straka et al., 2009). Differential rabies-virus retrograde labeling (Ugolini, 2010) of pathways terminating in different sectors of extraocular muscles revealed such separate processing streams in primates. In fact, distal lateral rectus muscle injections labeling "slow" muscle fibers, stain "slow" abducens motoneurons that are located in different parts of the nucleus and receive inputs from different presynaptic regions compared to "fast" motoneurons that are labeled by central muscle injections in the monkey (Ugolini et al., 2006). Although separate pathways were only confirmed between 2°VNs and muscle fibers, it appears likely that the parallel channels extend throughout the entire VOR circuitry. Although convergence of inputs originating from spatially related otolith and semicircular canal endorgans (see above) or, to a smaller extent, from more than one semicircular canal (Beraneck et al., 2007) were demonstrated at the level of the vestibular nucleus, distinct dynamic properties of 2°VNs probably remain independent from their input origin(s) (Beraneck et al., 2007).

To date, numerous studies identified different cellular subtypes of vestibular hair cells, afferent fibers, 2°VNs, extraocular motoneurons and muscle fibers. In the following chapters I will give a brief overview of hitherto characterized subtypes at all levels of the VOR network to provide a framework that will facilitate the discussion of present findings with respect to the parallel channel hypothesis.

II.1 Sensory Periphery: Hair cells and afferents

All vestibular endorgans use mechanoreceptive hair cells to detect head motion. On top of these cells is a bundle of cilia, named stereocilia, that is forced in one or the other direction by endolymph or otolith motion in the semicircular canals and otolith organs respectively (see Guth et al., 1998). These stereocilia contain mechanically gated ion channels that open or close depending on the direction of motion. When the head is in a resting position (white in Fig. 3A), a small fraction of these non-specific cation channels are open, continuously depolarizing the membrane such that a certain amount of excitatory neurotransmitter (glutamate) is tonically released from the hair cell synapse (see Guth et al., 1998). This generates the individual resting rate of vestibular afferent fibers that, depending on the species, can range from less than 1 Hz in amphibians (Gensberger et al., 2015) to around 100 Hz in primates (see Goldberg, 2000). It should be noted that afferent fibers deprived of their synaptic inputs do not fire spontaneously (see Eatock and Songer, 2011). Hair bundle bending towards the longest cilium (kinocilium) and the concurrent shearing forces pull further ion channels open which in turn allows more positive ions to flow into the hair cell, causing a depolarization of its membrane (receptor potential, red in Fig. 3A), an increase in

neurotransmitter release and thus increased firing rate of vestibular afferent fibers (Fig. 3A). Notably, this ion channel opening is gradual, and the resulting magnitude of depolarization encodes the angle of deflection in a nonlinear manner (see e.g. Guth et al., 1998). On the other hand, movement in the direction away from the kinocilium causes channels to close and the hair cell membrane to hyperpolarize (gray in Fig. 3A) which decreases neurotransmitter release and afferent discharge (Fig. 3A).

With respect to their morphology, different subtypes of vestibular hair cells have been demonstrated in all vertebrates. In amniotes, two types of hair cells are classically described that differ mostly with respect to their afferent synaptic endings: type I hair cells are bottle-shaped and comprise a large, calyx-like synapse whereas type II hair cells are rather cylindrically shaped with bouton-like afferent terminations (Fig. 3B, from Chen and Eatock, 2000; see Guth et al., 1998). In chinchillas, calyx afferents contact only 1 – 3 type I hair cells in the center of the sensory epithelium, whereas bouton afferents terminate on 15 – 100 type II hair cells in the peripheral zones (Fernández et al., 1988). However, most vestibular afferents display a mixture of type I and II terminations (Fig. 3B; Fernández et al., 1988).

Anamniotes (fish and amphibians) in general possess only type II hair cells (see e.g. Goldberg and Brichta, 1998) although also in these species, a large spectrum of receptor and afferent morphologies can be found: in frogs, for example, three hair cell body shapes were described – club-, cigar-, and pear-shaped (Fig. 3C; Guth et al., 1994) – as well as a large variety of otolith organ cilial bundle types (types “a” – “f”) (Fig. 3D; Lewis and Li, 1975). Furthermore, also in frogs, claw-like synapses, reminiscent of the type I calyx shape, were observed (Honrubia et al., 1989). In general, a large spectrum of afferent diameters was demonstrated both in anamniotes (frogs: Honrubia et al., 1989; toadfish: Boyle et al., 1991) and amniotes (squirrel monkeys: Goldberg, 2000) and in all cases larger afferents terminated predominantly in the central region, smaller in the peripheral regions of the vestibular sensory epithelia.

It is widely accepted that afferent diameters correlate with discharge regularity and sensitivity to motion stimuli such that thicker axons have higher conduction velocities, lower thresholds to electrical (galvanic) stimulation and are more irregular and sensitive compared to thin, regular afferent fibers (Goldberg and Fernández, 1977; Honrubia et al., 1989; see also Goldberg, 2000; Eatock and Songer, 2011). Furthermore, irregular fibers in mammals in general represent the afferent population that mostly innervates type I hair cells in the central zone of semicircular canal sensory epithelia and displays phasic, rapidly adapting responses to vestibular stimulation. Regularly firing afferents in turn predominantly receive peripheral type II hair cell input and respond with slowly adapting, tonic and low-gain responses during head motion (see Goldberg, 2000; Eatock and Songer, 2011), although, a substantial fraction

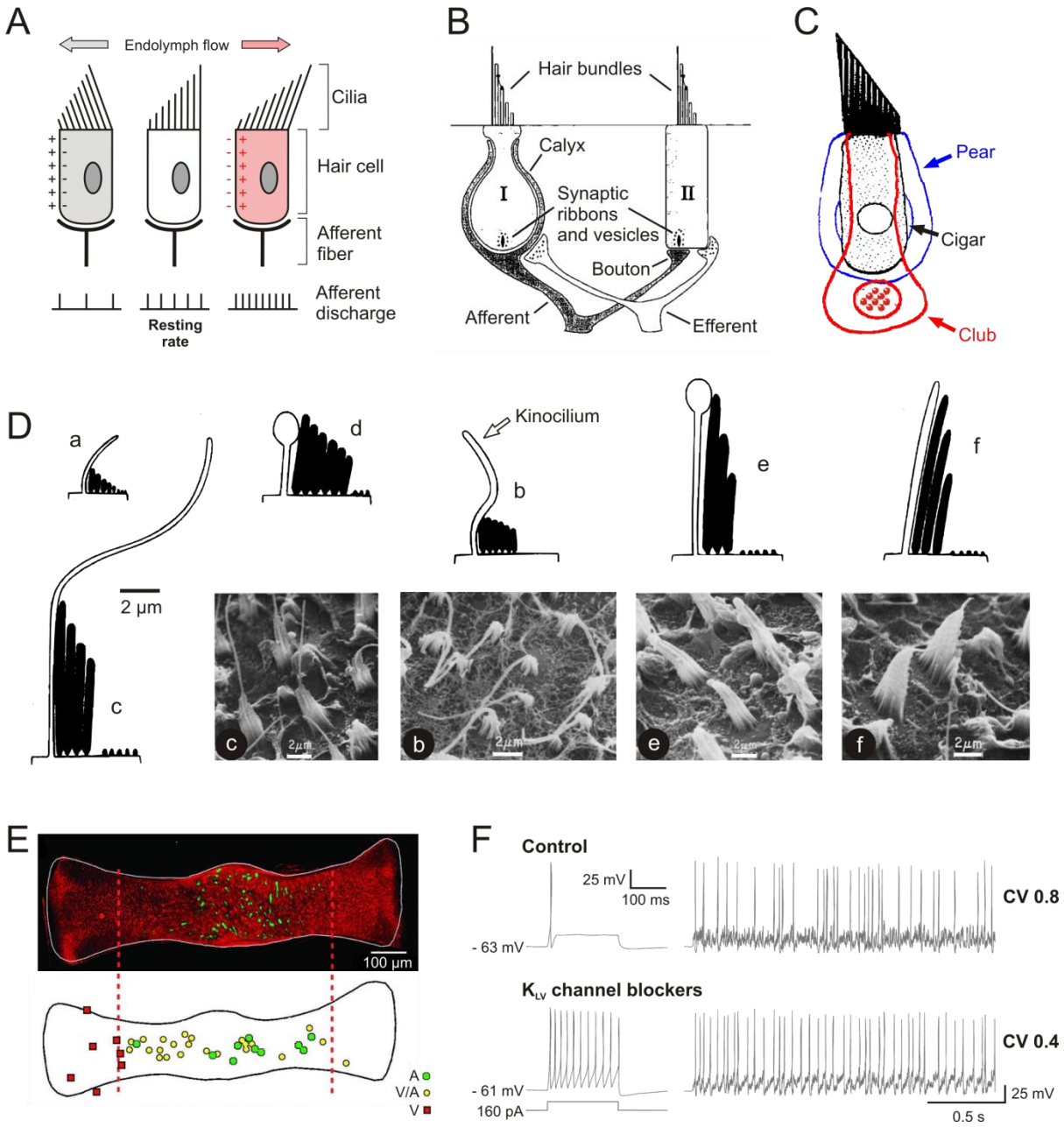

Figure 3: Vestibular hair cells and afferent fibers. ***A,*** Schematic depicting polarization changes of vestibular hair cells and corresponding changes in afferent firing rates upon bending of the hair cell cilia. ***B,*** Drawing showing the different synaptic terminations on type I and II hair cells. From Chen and Eatock, 2000 (permission not required). ***C,*** Three types of hair cell morphologies in the frog. From Guth et al., 1994, with permission from ELSEVIER. ***D,*** Schematics and pictures depicting differences in kinocilium length and shape in an otolith organ of the frog. From Lewis and Li, 1975, with permission from ELSEVIER. ***E,*** Immunohistochemical staining of GABAergic hair cells in the central zone in toadfish. From Holstein et al., 2004b, with permission from PNAS. ***F,*** Effects of blocking K_{LV} channels on regularity (right) and phasic-tonic discharge characteristics (left) of mammalian vestibular afferent fibers. From Kalluri et al., 2010 (permission not required).

of afferents innervates both type I and II hair cells (Fernández et al., 1988). A wide ranging continuum of afferent discharge regularities (coefficient of variation; CV) was demonstrated in several amniote and anamniote vertebrate species, e.g. toadfish (Boyle and Highstein, 1990), frogs (Honrubia et al., 1989) and chinchillas (Kim et al., 2011), assuming that this represents a general principle of information processing in the vertebrate vestibular afferent system. In fact, experimental and theoretical approaches suggest that these differences in regularity might reflect different coding strategies of regular (spike time code) *vs* irregular (rate code) fibers (Sadeghi et al., 2007). However, it is not commonly assumed that differences in discharge regularity are the direct cause of other response characteristics of afferent fibers (see Highstein et al., 2005).

As briefly mentioned in context with discharge regularity, afferent fibers also distinguish into different subtypes with respect to other response characteristics such as gain and timing. In toadfish, Boyle and Highstein (1990) described a continuum between low-gain velocity- and high-gain acceleration sensitive afferent fibers. These differences cannot be explained by varying hair cell responses alone: although different morphologies (see above) and membrane properties of hair cells and cilia contribute to differences in sensitivity and gain (Baird and Lewis, 1986; Baird, 1992; Peterson et al., 1996; see Straka and Dieringer, 2004; Eatock and Songer, 2011), with respect to response timing, their receptor potentials rather faithfully follow the dynamics of the vestibular stimulation (Highstein et al., 1996). This suggests that – at least in some cases – a major integration of hair cell responses has to occur at the hair cell-afferent synapse or within the afferent fibers themselves. Evidence for synaptic integration mechanisms arises from studies demonstrating GABA co-release from a specific subset of otherwise glutamatergic hair cells (toadfish: Holstein et al., 2004a; chicken: Usami et al., 1989) that is believed to shunt afferent responses via $GABA_B$ receptors and thus create a phase advance of the response that is more aligned with the acceleration component of the head movement (Holstein et al., 2004b). This fits well with the fact that GABAergic hair cells are found predominantly in central regions of the sensory epithelia where larger, irregular acceleration-sensitive afferent fibers (and, in mammals, type I hair cell terminations) are located (Fig. 3E, from Holstein et al., 2004b). Moreover, the intrinsic properties of afferent fibers play a major role in determining their respective response characteristics. For example, low-voltage activated K^+ (K_{LV}) channels create phasic response patterns to current steps of irregular vestibular afferent fibers that become more regular and tonically active during current steps in the presence of the particular K^+ channel blockers (Fig. 3F, from Kalluri et al., 2010).

In conclusion, various anatomical, pharmacological and physiological studies have revealed different subtypes of vestibular hair cells and afferent fibers that act in concert to encode different dynamic aspects of head movements. Although a certain level of convergence

between thick and thin afferent fibers on 2°VNs has been suggested (Straka and Dieringer, 2000), it appears plausible that – at least in part – parallel channels of irregular and phasic *vs* regular and tonic afferents exist between the sensory periphery and 2°VNs (Straka et al., 2004; see Straka et al., 2009). This is supported by anatomical studies that demonstrate at least partial segregation of regular and irregular fiber terminations within the vestibular nuclei (Sato and Sasaki, 1993).

II.2 Vestibular nuclei

Vestibular afferents terminate with both electrical and chemical synapses on neurons of the ipsilateral vestibular nuclei as the first stage of signal processing of the vestibulo-ocular reflex (Fig. 4A). Electrical coupling via gap junctions (purple in Fig. 4A) occurs predominantly between thick afferents and 2°VNs with large somal diameters, as shown both anatomically and physiologically in several species such as frogs, toadfish, chicken and most mammals (for review, see Straka and Dieringer, 2004). On the other hand, chemical transmission (red in Fig. 4A) is mainly glutamatergic (Cochran et al., 1987). In frogs and rats, all vestibular afferents are immunopositive for glutamate; however, a subgroup of 10 – 20% of afferents in addition is stained for glycine (Reichenberger and Dieringer, 1994). This subpopulation comprises larger afferent cell bodies and thicker axons (see Straka and Dieringer, 2004), consistent with results from glutamate and glycine uptake experiments in frogs (Straka et al., 1996a). As a cotransmitter, glycine is believed to mainly regulate glutamate responses as a co-agonist of NMDA receptors, in accordance with a study in frogs suggesting that NMDA receptors predominantly mediate inputs originating from thick vestibular afferents that also possess glycine (Straka et al., 1996a,b; see Straka and Dieringer, 2004). In addition to the monosynaptic afferent input, excitatory and inhibitory (GABA- and glycinergic) side loops were demonstrated in frogs that potentially serve as a feed-forward regulator of 2°VN responses (Fig. 4A; Straka and Dieringer, 1996; 2000). Furthermore, vestibular neurons receive inputs from the visual and proprioceptive systems (Fig. 4A; see Straka et al., 2005), which allows them to combine different sensory modalities for a precise calculation of head position or motion in space.

Although a continuum of different vestibular neurons is often suggested (e.g. in chicken, du Lac and Lisberger, 1995), generally two main types of 2°VNs can be distinguished in all vertebrates examined so far (for review, see Straka et al., 2005). In mammals, typically type A and B neurons are described *in vitro* with respect to action potential shape and discharge properties during current injection (Serafin et al., 1991, Johnston et al., 1994). Spikes of type A 2°VNs are broad with a monophasic afterhyperpolarization whereas action potentials of

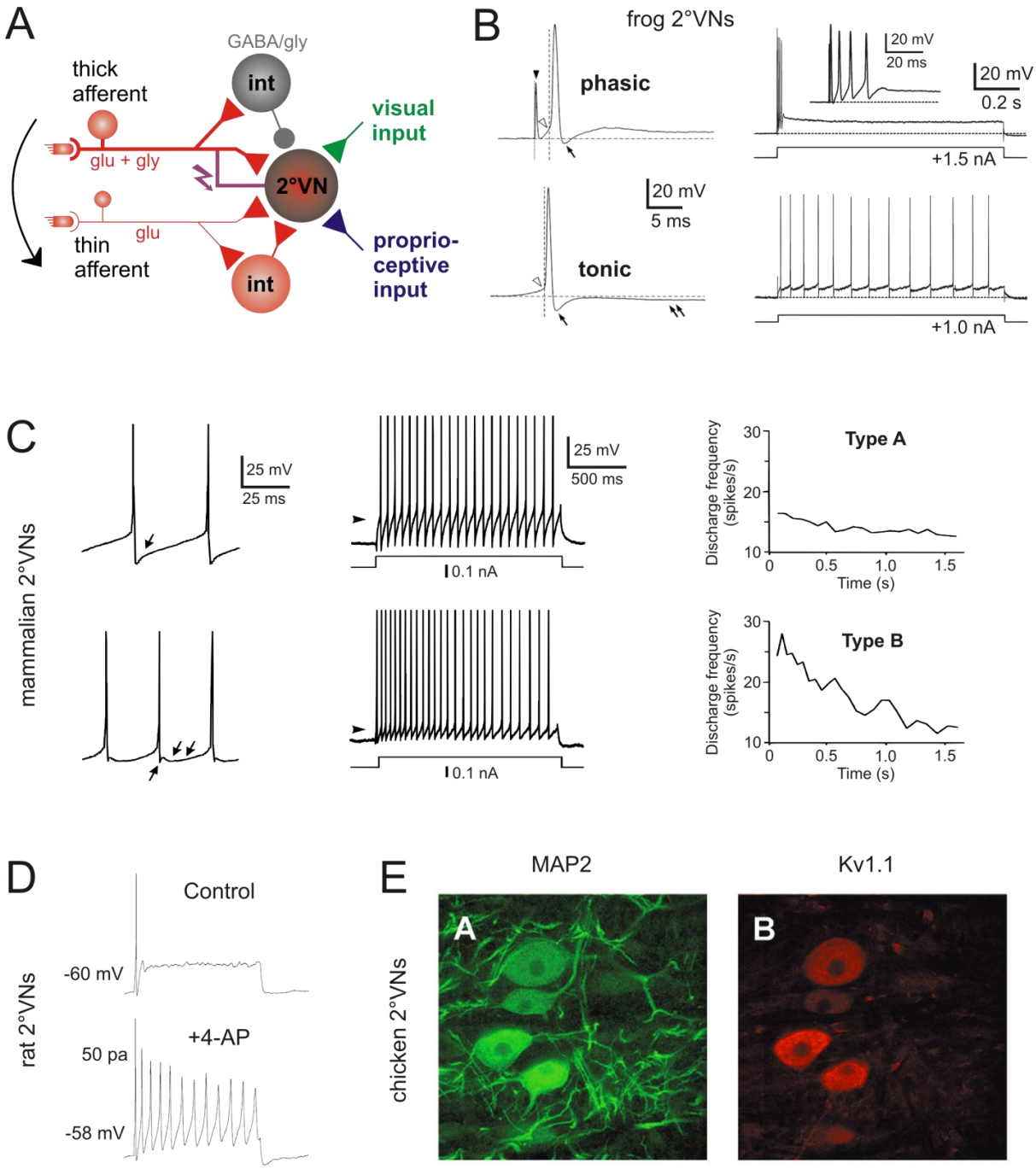

Figure 4: Characteristics of second order vestibular neurons (2°VNs). ***A,*** Schematic depicting the convergence of vestibular, visual and proprioceptive information in the vestibular nucleus. ***B,*** Action potential shapes (left) and firing behavior during current step injection (right) of phasic (above) and tonic (below) frog 2°VNs respectively. From Straka et al., 2004 (permission not required). ***C,*** Action potential shapes (left) and firing behavior (middle) with the respective discharge frequency (right) during current step injection of mammalian (guinea pig) type A (above) and type B (below) 2°VNs. From Straka et al., 2005, with permission from ELSEVIER. ***D,*** Dependency of phasic characteristics of rat 2°VNs on low-voltage activated K^+ channels, blocked in the presence of 4-Aminopyridine (4-AP). From Iwasaki et al., 2008 (permission not required). ***E,*** Immunohistochemical staining confirming the presence of a type of low-voltage activated K^+ channels (Kv1.1 channels) (right) on vestibular neurons in chicken; microtubule-associated protein 2 (MAP2) counterstain was used as a neuronal marker (left). From Shao et al., 2009, with permission from IOS press.

type B neurons are thinner and display biphasic afterhyperpolarizations (arrows in left plots of Fig. 4C). Moreover, type A neurons display a more regular resting rate than type B and resemble tonic, non-adaptive discharge patterns during current injections, whereas type B neurons fire more rapidly at the beginning of depolarizing steps in a phasic-tonic manner (Serafin et al., 1991; see Straka et al., 2005; middle and right plots in Fig. 4C). In most species investigated to date, type B 2°VNs are more prevalent than type A neurons, similar to the large population of phasic compared to tonic 2°VNs in frogs (see Straka et al., 2005). One can argue that type A and B neurons in mammals more or less resemble tonic and phasic 2°VNs in amphibians (Fig. 4B, from Straka et al., 2004) both with respect to action potential shape and responses to current injections, however, purely phasic cells like those observed in frogs appear to be unique for anamniotes, where they predominantly mediate high frequency vestibular inputs (Beraneck et al., 2007).

Several distinct membrane ion channel compositions – most importantly K^+ and Ca^{2+} channels – contribute to the physiological characteristics of different subtypes of 2°VNs (see Straka et al., 2005). Crucial in this context are low-voltage activated K^+ channels (K_{LV}), such as Kv1.1 channels, that, similarly as described above for vestibular afferent fibers, play a crucial rule in generating phasic responses in 2°VNs in rats (Johnston et al., 1994, Iwasaki et al., 2008) and frogs (Beraneck et al., 2007). In both species, pharmacological blockade of these K^+ channels with 4-Aminopyridine (4-AP) causes phasic neurons to become more tonic (Fig. 4D (rats); Johnston et al., 1994; Beraneck et al., 2007; Iwasaki et al., 2008), confirming their large impact on the dynamics of 2°VNs. Furthermore, a link to morphology was demonstrated in frogs, where phasic neurons that are immunopositive for K_{LV} channels (Beraneck et al., 2007) also display larger cell diameters and correspondingly lower input resistances (Straka et al., 2004; Beraneck et al., 2007; see discussion), similarly to vestibular afferent fibers (see above). The importance of Kv1.1 channels in vestibular neurons has been demonstrated electrophysiologically and pharmacologically in several other vertebrate species (see Straka et al., 2005), and was confirmed immunocytochemically in e.g. chicken (Fig. 4E, Shao et al., 2009), suggesting a common functional relevance of these channels throughout vertebrates. Another striking difference related to pharmacological properties was described by Takazawa et al. (2004) who investigated the neurotransmitter profile of the two subtypes of vestibular neurons in rats: type A 2°VNs are mainly GABAergic, whereas type B neurons can be either glutamatergic or GABAergic.

In conclusion, distinct subtypes with respect to morphological, electrophysiological and pharmacological features can also be observed in 2°VNs that serve as the first central processing stage of the VOR circuitry. Due to a certain level of afferent fiber convergence (in cats: Zakir et al., 2000; in frogs: Straka et al., 2002; in primates: Dickman and Angelaki, 2002; in pigeons: McArthur et al., 2011) and, for example, convergence with commissural (in

frogs: Malinvaud et al., 2010) or cerebellar inputs (in frogs: Magherini et al., 1975), information can be integrated at the level of the vestibular nucleus. The final output of 2°VNs is then distributed to various brain regions (see Straka et al., 2005) such as the contralateral vestibular nuclei (commissural connections, Malinvaud et al., 2010), cerebellum (see chapter on VOR plasticity below), hippocampus and thalamus (spatial cognition and orientation), the spinal cord (vestibulospinal reflexes, posture control) and extraocular motoneurons as a final stage of VOR processing.

II.3 Extraocular motoneurons and muscle fibers

Compared to vestibular hair cells, afferents and 2°VNs, fewer studies have so far investigated the different physiological subtypes of extraocular motoneurons with respect to VOR processing. Experiments on these motoneurons are facilitated with respect to spatial specificity by the fact that three separate cranial motor nuclei innervate the extraocular musculature (see above): abducens (N.VI, innervating the lateral rectus), trochlear (N.IV, innervating the superior oblique) and oculomotor (N.III, innervating the medial, superior, inferior recti and inferior oblique). Notably, although similar functional properties of all extraocular motoneurons are likely, findings related to a single nucleus might not be sufficient for generalization.

To date, numerous studies have investigated the morphology of extraocular motoneurons in several vertebrate species. A continuum of somal sizes exists in e.g. the abducens nucleus of fish (Sterling, 1977), frogs (Dieringer and Precht, 1986) and cats (Grantyn et al., 1977), the trochlear nucleus of turtles (Jones and Ariel, 2008), and all extraocular motor nuclei in monkeys (Büttner-Ennever et al., 2001), assuming this to be a general principle of morphological organization of extraocular motoneurons across vertebrate species. Cell size seems to play a functional role both with respect to the inverse relation between cell diameter and input resistance (see discussion) as well as in determining the type of targeted muscle fibers. In frogs, Dieringer and Precht (1986) demonstrated a bimodal distribution of abducens nerve fiber diameters: one peak of smaller axons around 3 µm, and a second larger population of axons with diameters around 8 µm. This in turn appears to correlate with findings in monkeys, where a dual pathway of extraocular muscle innervation has been suggested (Büttner-Ennever et al., 2001; Büttner-Ennever and Horn, 2002a,b; Ugolini et al., 2006): Small motoneurons with thin axons project to slow, tonic, non-twitch, multiply-innervated muscle fibers (MIF), whereas larger motoneurons with thicker axons innervate fast, twitch, singly-innervated fibers (SIF) that are spatially restricted to the central region of extraocular muscles. Furthermore, smaller motoneurons innervating MIFs are localized in the periphery of the respective motor nucleus unlike larger, SIF innervating motoneurons that are

spread out through the entire center of extraocular motor nuclei (Büttner-Ennever et al., 2001; see Büttner-Ennever and Horn, 2002a,b). Slow, MIF and fast, SIF innervating motoneurons also differ in several immunohistochemical properties such as the presence of perineuronal nets that is restricted to the population of SIF motoneurons (Eberhorn et al., 2005). In addition, slow and fast abducens motoneurons can be distinguished according to differences in premotor innervation. In monkeys, the two subtypes at least partially receive inputs from functionally distinct brain regions respectively (Ugolini et al., 2006).

In general, vertebrate extraocular muscles are somewhat compartmentalized and in most species consist of an inner global layer with larger SIF muscle fibers, surrounded by an outer orbital layer comprising smaller diameter MIF fibers (Stirn Kranjc et al., 2009; see Büttner-Ennever, 2007). As their names suggest, multiply innervated fibers receive motor commands via numerous “en-grappe” (grape-like) clusters of synapses. They display slower contraction times than SIFs and can retain the contractile force for long periods of time (see Büttner-Ennever, 2007). On the other hand, singly innervated fibers undergo “all-or-nothing” twitch responses upon innervation via a central “en-plaque” endplate. This suggests a task sharing of MIFs for gaze holding and eye stabilization and SIFs for fast VOR-driven eye movements or saccades respectively (Büttner-Ennever and Horn, 2002a).

As observed for 2°VNs (see above), two classes of extraocular motoneurons can be distinguished according to their action potential shapes and discharge during current injection. In rat oculomotor (Nieto-Gonzalez et al., 2007) and abducens (Russier et al., 2003) motoneurons, spikes display mono- and biphasic afterhyperpolarizations, similar to those observed in mammalian type A and type B 2°VNs. Mono- and biphasic action potentials were also demonstrated in other species such as in turtle trochlear motoneurons (Jones and Ariel, 2008). Furthermore, in rats, the two spike shapes coincide with tonic and phasic-tonic characteristics respectively (Nieto-Gonzalez et al., 2007), again similar to what was shown for 2°VNs, and tonic and phasic abducens motoneurons can be observed in goldfish (Gestrin and Sterling, 1977).

Extracellular nerve recordings in frogs (Dieringer and Precht, 1986) demonstrated three types of abducens motoneuronal responses to natural optokinetic stimulation that differ in their relative spike amplitudes: the first subtype with largest spikes encodes eye velocity; another with smallest spikes mediates eye position signals, and the third subtype displays responses in between the two extremes. Although this is a first indication for the function and potential task-sharing of different motoneuronal subtypes, a complete picture combining morphological, physiological and pharmacological properties of extraocular motoneurons with their implications for VOR processing still remains to be drawn.

II.4 Neurotransmitter systems of the basic VOR network

The differential use of excitatory and inhibitory neurotransmitters at different stages of the VOR as well as the distribution and expression levels of corresponding receptors on postsynaptic membranes play an important role in shaping distinct neuronal responses. For example, differences in receptor kinetics can substantially influence the timing of chemical signal transmission. Also, in many cases the co-release of more than one transmitter and/or neuromodulator enables fine-tuning of the postsynaptic potentials. It therefore appears likely that distinct neuronal subtypes also differ in their neurotransmitter profiles at all stages of vestibulo-ocular processing.

In general, excitatory neurotransmission within the VOR is mediated by glutamate and the associated AMPA/kainate and NMDA receptors (see Straka and Dieringer, 2004). A first indication for different functions of these two receptors was given by a study in cats, where AMPA- and NMDA antagonists were systemically applied and VOR responses tested thereafter, suggesting that NMDA receptors predominantly mediate responses to low frequency head motion (0.1 – 1 Hz) whereas higher frequencies (2 – 8 Hz) mainly require excitation through AMPA receptors (Priesol et al., 2000).

Looking at the hair cell – afferent synapse, glutamate is present in (Panzanelli et al., 1994) and released from vestibular hair cells in frogs (Annoni et al., 1984; Zucca et al., 1992), axolotls (Soto and Vega, 1988) and turtles (Cochran and Correia, 1995). In the axolotl, Soto et al. (1994) demonstrated that glycine-modulated NMDA receptors play a major role in the hair cell-afferent transmission of long-lasting stimulation of the vestibular system, whereas non-NMDA receptors are suggested to play a major role in the initial, fast onset of afferent responses. Furthermore, Holstein et al. (2004a,b) showed that a specific subset of toadfish hair cells use GABA in addition to glutamate to shunt afferent responses via $GABA_B$ receptors, thus creating a phase advance of the response. GABA was also immunohistochemically demonstrated in vestibular endorgans of chicken (Usami et al., 1989).

Between vestibular afferents and 2°VNs, glutamatergic transmission again occurs via both AMPA and NMDA receptors. Vestibular afferents can be either purely glutamatergic or co-release glycine, presumably for a modulation of NMDA receptor mediated currents (see Straka et al., 2009). In addition, NMDA receptors are believed to play a major role in the transmission of larger diameter afferent fiber inputs. Furthermore, feed-forward excitatory or inhibitory side-loops via vestibular interneurons shape 2°VN responses to afferent inputs (Fig. 4A). In frogs, feed-forward inhibition can be both GABA- and glycinergic (Biesdorf et al., 2008), supported by immunohistochemical data, showing both GABA- and glycine-positive neurons in the vestibular nuclei (Reichenberger et al., 1997).

Glutamatergic excitatory inputs between 2°VNs and extraocular motoneurons so far have been poorly investigated. Both AMPA (Straka and Dieringer, 1993) as well as NMDA receptors (Durand, 1987; 1991; 1993) have been demonstrated on abducens motoneurons; however, a potentially differential impact of the two on vestibulo-ocular processing remains largely unknown. Inhibitory vestibular inputs onto extraocular motoneurons, such as from the ipsilateral vestibular nuclei onto abducens motoneurons (see above), are believed to be mainly GABAergic in the case of trochlear (IV) and oculomotor (III) motoneurons (Wentzel et al., 1996; Spencer et al., 1989; Spencer and Baker, 1992), and exclusively glycinergic in abducens (VI) motoneurons as shown in cats (Spencer et al., 1989) and frogs (Straka and Dieringer, 1993). However, in addition to glycine, also a sparse GABA labeling was observed within the abducens nucleus (Spencer et al., 1989), and GABAergic terminals (Lahjouji et al., 1995) as well as $GABA_A$ receptors (Lorenzo et al., 2007) were demonstrated on the somata of abducens motoneurons in rats.

III Plasticity

III.1 The VOR is plastic

III.1.a Demands for motor system plasticity

The development and fine-tuning of motor commands underlying the huge variety of different vertebrate motor skills – from "simple" locomotion to highly complex processes such as playing a musical instrument – is mediated by circuitries that display a high degree of neuronal and/or network plasticity throughout life; even though with increasing age, motor learning generally becomes slower (King et al., 2013; VOR plasticity: Gutierrez-Castellanos et al., 2013). As in any other motor system, the output of the vestibulo-ocular reflex is also far from static (see Broussard and Kassardjian, 2004). Since the basic VOR circuitry consists of an open-loop network, feedback about a potentially remaining image slip is required (see Miles and Lisberger, 1981). Only the visual system can provide information about whether head motion-compensating eye movements have appropriate magnitude and timing, and thus shape the sensory-motor transformation whenever necessary (see Boyden et al., 2004). This becomes essential during growth and development of animals – to adapt to changes in size of extraocular muscle fibers or inner ear organs and increased number of neurons or synapses – as well as during aging (see Boyden et al., 2004; Eatock and Songer, 2011). In addition, plasticity mechanisms are – at least in part – capable of restoring VOR functioning after vestibular injuries. For example, unilateral vestibular loss results in numerous processes referred to as "vestibular compensation" that re-balance the asymmetric activity of the ipsi- and contralateral vestibular nuclei (see Dieringer, 1995; Straka et al., 2005; Cullen et al.,

2009; Dutia, 2010). In part, this is mediated by saccadic and/or sensory substitution with neck-proprioceptive or optokinetic inputs, which becomes especially important in the compensation of bilateral vestibular loss, such as after hair-cell damaging pharmacological treatment (e.g. with gentamicin antibiotics) (see Dieringer, 1995; Eatock and Songer, 2011). These inputs, however, are too slow to compensate for deficits during high-frequency head movements (Angelaki et al., 1996; see Eatock and Songer, 2011).

Besides lesion experiments, visuo-vestibular mismatch paradigms are classically used to elicit and investigate the performance of VOR adaptation in the laboratory. Within a stable visual environment, the ideal VOR has a gain of 1.0, meaning that eye movements have the same magnitude as the head motion but in the exactly opposite direction. However, in order to maintain an unblurred visual scene during artificial motion of the visual environment together with the head, an attenuation of the VOR output would be required, ideally down to a gain of zero, such that no eye movements occur during head motion for an unblurred visual scene (lower part of Fig. 5A, from Hirano and Kawaguchi, 2014). On the other hand, motion of the visual environment in the opposite direction of the head requires a facilitation of the VOR gain (upper part of Fig. 5A). Extreme alterations in gain and phase such as complete phase reversal (e.g. Gutierrez-Castellanos et al., 2013) can be achieved during different mismatch paradigms; and even the direction of the VOR can be altered e.g. by concurrent vertical visual and horizontal vestibular stimulation (Harrison et al., 1986; Schultheis and Robinson, 1981; Wei and Angelaki, 2001; Hübner et al., 2014).

III.1.b Mechanisms underlying VOR plasticity

Numerous studies have investigated the mechanisms underlying VOR adaptation, and to date came to the conclusion that multiple sites and mechanisms of plasticity act in concert to mediate VOR motor learning (see Boyden et al., 2004; Kassardjian et al., 2005; Medina, 2011). Generally for motor learning processes – including VOR adaptation – the cerebellum plays a major role (see Broussard and Kassardjian, 2004), however, additional feed-back and feed-forward loops such as via the vestibular efferent system have been argued to assist the flexibility of VOR processing (see Goldberg, 2000; Eatock and Songer, 2011; Chagnaud et al., 2015; Hübner et al., 2015). The plasticity mechanisms considered most relevant shall now be described in more detail.

Plasticity via the cerebellar side loop

Already Marr (1969) and Albus (1971) presented their “theories of the cerebellar cortex” and “cerebellar function”, and introduced the notion that a major part of VOR plasticity occurs

via the cerebellar side-loop (Fig. 5B). Purkinje cells of the vestibulo-cerebellum (cerebellar flocculus) receive vestibular inputs via granule cell parallel fibers from 2°VNs and vestibular afferent fibers, as well as information from the optokinetic system via climbing fibers from the inferior olive (see Boyden et al., 2004). After integration of the two sensory inputs, an inhibitory, GABA-ergic feedback projection to the vestibular nucleus terminates on a subset of 2°VNs – the floccular target neurons – to regulate VOR responses (Babalian and Vidal, 2000; Shin et al., 2012; see Boyden et al., 2004). The Marr-Albus model suggests that

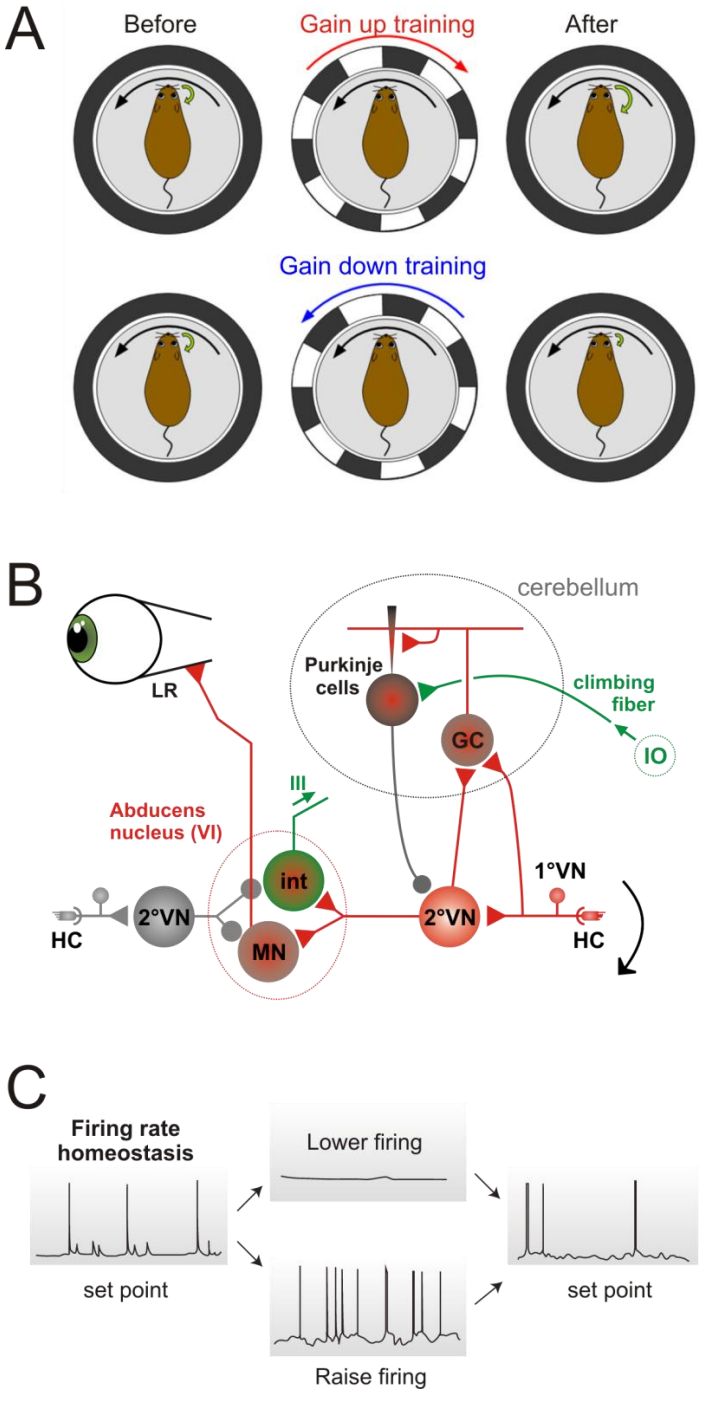

Figure 5: Plasticity of the VOR. ***A,*** Schematics depicting plastic alterations of the VOR gain after visuo-vestibular mismatch training. From Hirano and Kawaguchi, 2014 (no permission required). ***B,*** Schematic showing the horizontal aVOR network including the inhibitory feedback via the cerebellar side loop. ***C,*** Illustration of the homeostatic plasticity of cortical network firing rates in response to lowered or raised overall activity. From Turrigiano, 2012, with permission from Cold Spring Harbor Laboratory Press. 1/2°VN, first/second order vestibular neurons; GC, granule cells; HC, horizontal semicircular canal; int, abducens inter-nuclear neurons; IO, inferior olive LR, lateral rectus; MN, motoneurons

bidirectional VOR plasticity exclusively occurs via long-term strengthening or weakening of the synapse between parallel fibers and Purkinje cells that is guided by the concurrent climbing fiber input whenever abnormal image slip is detected during VOR responses (see Boyden et al., 2004). Evidence for this notion arises from vestibulo-cerebellar lesions and pharmacological blockade of Purkinje cells that cause the adapted VOR gain and phase to immediately return to pre-learning values in goldfish (Michnovicz and Bennett, 1987) and cats (Kassardjian et al., 2005; Broussard et al., 2011). Furthermore, electrical climbing fiber stimulation depresses Purkinje cell responses to parallel fiber inputs in rabbits (Ito et al., 1982) and the Purkinje cell output displays appropriate changes in phase and gain during visuo-vestibular mismatch training to mediate VOR adaptation in primates (Watanabe, 1984; 1985). Despite these findings, an alternative model has been proposed by Miles and Lisberger (1981), suggesting that Purkinje cells do not represent the main site of plasticity but rather send instructive signals for plastic changes to an extra-cerebellar downstream target site, such as the vestibular nucleus (reviewed in Boyden et al., 2004). More recent studies however propose that the two models are not mutually exclusive (see Medina, 2011) and that multiple sites and mechanisms of plasticity act together during motor learning of the VOR (Boyden et al., 2004; Hirata and Highstein, 2001; 2002; Kassardjian et al., 2005; Gao et al., 2012; Clopath et al., 2014). In any case, the presence of an intact cerebellar side loop appears to be the prerequisite for motor learning, since ablation or temporal inactivation of the cerebellum prevents VOR plasticity in goldfish (Michnovicz and Bennett, 1987; Pastor et al., 1994), cats (Schultheis and Robinson, 1981; Luebke and Robinson, 1994; Kassardjian et al., 2005) and primates (Zee et al., 1981; Lisberger et al., 1984; Rambold et al., 2002).

Apart from the integration of visual information, the cerebellar side loop also mediates VOR gain attenuation that occurs during prolonged low-frequency head rotation in the absence of visual feedback (habituation). This phenomenom was demonstrated in goldfish (Dow and Anastasio, 1998; 1999), mice (Gutierrez-Castellanos et al., 2013), monkeys (Jäger and Henn, 1981) and humans (Clément et al., 2008), such as in sailors that can habituate to low-frequency motion on sea with gradually disappearing symptoms of sea-sickness (Schmäl, 2013). Furthermore, it was shown in cats that habituation is a direction-specific rather than global mechanism of the VOR network (Clément et al., 1981).

The cerebellum was also shown to contribute to the integration of active head movements during which compensatory eye movements or postural reflexes might be undesirable (see Cullen and Roy, 2004). Whereas vestibular afferents respond in the same fashion during passive and active head motion, specific subclasses of neurons in the cerebellum and/or vestibular nuclei react differently during both conditions in mice (Medrea and Cullen, 2013) and monkeys (Roy and Cullen, 1998; see Cullen and Roy, 2004; Cullen et al., 2011).

Plasticity at extra-cerebellar sites

Whereas the cerebellum appears to be essential for VOR plasticity during visuo-vestibular mismatch conditions, vestibular compensation following unilateral loss of the labyrinthine endorgans only partially requires cerebellar integrity (see Cullen et al., 2009; Dutia et al., 2010). For example, genetically modified mice with cerebellar deficits show similar time courses of vestibular compensation as the wild-type within the first week after unilateral labyrinthectomy, however long-term restoration is impaired (Beraneck et al., 2008). This suggests that the acute phase of compensation, which levels out the profound asymmetry in resting discharge between the two vestibular nuclei after unilateral ablation of afferent inputs (see Straka et al., 2005), is mediated by modifications within extracerebellar circuits, whereas the cerebellum is required for further improvement of the VOR in the longer term (Beraneck et al., 2008). Extra-cerebellar plasticity mechanisms (see Dutia, 2010) include bilateral changes in intrinsic properties and excitability of 2°VNs (Cameron and Dutia, 1997; Beraneck et al., 2003; 2004), a modified sensitivity to commissural inputs (Farrow and Broussard, 2003; Bergquist et al., 2008; Lim et al., 2010), reorganization of the vestibular pathway connectivity (Goto et al., 2002; Rohregger and Dieringer, 2003), and even neurogenesis in the vestibular nucleui of the ipsilesional side (Tighilet et al., 2007; Dutheil et al., 2009). In addition, vestibular compensation appears to be influenced by neuromodulatory mechanisms such as through steroid hormones or the histaminergic system (see Beraneck and Idoux, 2012), compatible with the finding that the time course of plasticity appears to be influenced by stress, anxiety and arousal (see Dutia, 2010; Beraneck and Idoux, 2012).

III.2 Homeostatic plasticity

Correct functioning of the central nervous system critically depends on the stability of neural networks that is challenged throughout life by imbalances of circuit activity whenever the number or strength of synapses changes during development or learning (see Turrigiano, 2012). “Homeostasis” (“staying the same through change”) not only refers to the maintenance of parameters like body temperature or glucose levels but is also used to describe the plasticity that stabilizes neuronal network activity (see Turrigiano, 2012). To maintain stability around a certain “set point” of activity, neurons must sense any deviation from this point and regulate excitability on a cellular or network level such that the activity returns to the set point (Fig. 5C; see Turrigiano, 2012). This can be achieved by synaptic scaling that for example can alter the expression of NMDA or AMPA receptors on the postsynaptic membrane (Turrigiano et al., 1998; Watt et al., 2000; see Watt and Desai, 2010) or glutamate transporter expression at the presynaptic site (De Gois et al., 2005). Several

molecular mechanisms, usually including calcium concentration-dependent pathways (Ibata et al., 2008; Goold and Nicoll, 2010; see Turrigiano, 2012) underlie synaptic scaling.

Homeostatic plasticity has been demonstrated in various regions of the central and peripheral nervous system. For example, at the neuromuscular junction, the efficiency of motoneuronal inputs adapts according to changes in muscle fiber size during growth, which ensures the appropriate level of depolarization to bring fibers above threshold for an all-or-none contraction (Davis and Goodmann, 1998; Paradis et al., 2001; see Davis and Bezprozvanni, 2001; Turrigiano and Nelson, 2004; Turrigiano, 2012). Homeostatic mechanisms in central neurons however are more complex: Up to thousands of synaptic inputs must be integrated and although short-term fluctuations in activity are essential for information transfer and learning, long-term net changes are undesirable (Turrigiano and Nelson, 2004). Hence, it has been demonstrated that e.g. cortical and hippocampal neurons display a high ability to compensate for long-term deviations from the activity set point (Turrigiano et al., 1998; Burrone et al., 2002; see Turrigiano and Nelson, 2004; Turrigiano, 2012). Furthermore, in the spinal cord, homeostatic plasticity ensures the presence of spontaneous activity required for axonal pathfinding and circuit formation during development (Hanson and Landmesser 2004; Gonzalez-Islas and Wenner 2006). Recently, homeostatic control has also been demonstrated in the brainstem in hypoglossal motoneurons in mice (Tadros et al., 2014). Due to its functional relevance, it appears likely that homeostatic plasticity represents a general strategy present in numerous brain regions (see Watt and Desai, 2010), including the vestibular system (Menzies et al., 2010).

IV Aim of this thesis

Even though the vestibulo-ocular reflex is comprised of only very few processing stages, the understanding of several details of the underlying cellular and network computations is still lacking. Cell-to-cell projection patterns at all stages of the VOR circuitry were extensively studied using anatomical tracing techniques; however, connections across more than one synapse have only started to be investigated with rabies virus tracing in primates (e.g. Ugolini et al., 2006). Parallel, frequency-tuned channels were suggested according to the different cellular subtypes that are present at various stages of VOR processing with similar properties (see Straka et al., 2009) and to date, numerous studies have investigated these subtypes at the level of vestibular hair cells, afferent fibers, 2°VNs and muscle fibers. However, until now few data exist about functionally distinct groups of extraocular motoneurons. A major part of my thesis therefore deals with the classification of abducens motoneurons with respect to their morphology, pharmacology and response profile in the context of a fully functional vestibulo-ocular network in semi-intact larval *Xenopus laevis* preparations.

"Natural" stimulation of the vestibular endorgans using sinusoidal head rotation allowed investigating the potential frequency- and velocity-sensitivities, activation thresholds and phase precisions of individual motor units recorded extracellularly from the abducens nerve. On the other hand, the functional relevance of these individual physiological properties for VOR related eye motion was studied using a computational approach: optimal combinations of motor commands generated by the different motoneuronal subtypes were determined for the simulation of eye movements. Calcium imaging of retrogradely labeled motoneurons with simultaneous abducens nerve recordings revealed a potential link between cell morphology, location and response properties during electrical stimulation of the vestibular endorgans. With respect to pharmacology, the differential roles of AMPA/kainate and NMDA receptors as well as the functionality of GABA- and glycinergic inputs onto abducens motoneurons were extensively studied in this PhD thesis. To date, the two glutamate receptors systems have only been investigated in isolated brains (e.g. Straka et al., 1993; Durand, 1991), lacking the context of an *in vivo*-like activation of the vestibular endorgans. Glycine has been suggested to mediate inhibitory inputs from the ipsilateral vestibular nucleus (Spencer et al., 1989; Straka et al., 1993); however, the role of GABA receptors on abducens motoneurons (Spencer et al., 1989; Lahjouji et al., 1995; Lorenzo et al., 2007) is yet unclear. Selective application of the respective receptor antagonists via focal injection into the abducens nucleus within an otherwise intact VOR circuitry in *Xenopus laevis* helped to resolve these questions and uncover the functional properties underlying this last stage of sensory-motor transformation within the VOR circuitry. In combination, the different aspects of classification of neuronal subtypes achieved during this thesis will potentially be integrated into the so far existing framework of parallel channels in order to further advance the discussion about the theory of VOR processing in frequency-tuned channels.

Another major part of this thesis deals with the plasticity of vestibulo-ocular processing. So far, adaptive mechanisms of the VOR network were mainly studied using visuo-vestibular mismatch paradigms or vestibular lesions (see Boyden et al., 2004; Dutia, 2010). Although several studies have demonstrated habituation effects during prolonged low-frequency vestibular stimulation in the dark (e.g. Jäger and Henn, 1981), thorough analysis of a potential regulation of the VOR gain in the absence of visual inputs is still missing. In larval *Xenopus laevis*, a stimulus amplitude-dependent homeostatic plasticity was observed upon sustained sinusoidal head rotation in the dark, i.e. after dissection of the bilateral optic nerves. Taking advantage of the semi-intact *in vitro* preparation, a potential role of the cerebellar side loop was investigated using lesion experiments. The present findings will contribute to the understanding of the broad spectrum of plastic mechanisms within the VOR circuitry that act in concert for the fine-tuning of the underlying sensory-motor transformations.

Results Part I

Functional organization of vestibulo-ocular responses in abducens motoneurons

Haike Dietrich, Stefan Glasauer and Hans Straka

Final version published in the Journal of Neuroscience on 12.4.2017

Contributions of HD:

- Planning of all experiments
- Performance of all experiments except for the computational modeling
- Analysis of all data except for those of the computational modeling
- Design and assembly of all figures
- Writing and revision of the manuscript

Functional organization of vestibulo-ocular responses in abducens motoneurons

Haike Dietrich[1,2], Stefan Glasauer[3] and Hans Straka[1,*]

[1] Department Biology II, Ludwig-Maximilians-University Munich, Großhaderner Str. 2, 82152 Planegg
[2] Graduate School of Systemic Neurosciences, Ludwig-Maximilians-University Munich, Großhaderner Str. 2, 82152 Planegg
[3] Center for Sensorimotor Research, Ludwig-Maximilians-University, Marchioninistr. 23, 81377 Munich

Abbreviated title: Abducens motoneuronal responses

Abstract: **250** words
Significance statement: **119** words
Introduction: **535** words
Discussion: **1484** words

Number of figures: **8**

Key words: Vestibulo-ocular reflex, semicircular canal, extraocular motoneurons, GABA, glycine, glutamate

Acknowledgments

The authors acknowledge financial support from the German Science Foundation (CRC 870; STR 478/3-1 and GL 342/2-1), the German Federal Ministry of Education and Research under the Grant code 01 EO 0901 and the Munich Center for Neurosciences - Brain and Mind (MCN). The authors are grateful for the help of Tobias Kohl with the spike 2 software scripts for the spike-sorting algorithm and for the help of Alexander Knorr with the eye motion analysis software.

Conflict of interest statement: The authors declare no competing financial interests.

*To whom correspondence should be addressed:

Dr. Hans Straka,

Department Biology II
Ludwig-Maximilians-University Munich
Großhaderner Str. 2
82152 Planegg
Germany
Tel: +49 89 2180 74307

Email: straka@lmu.de

Abstract

Vestibulo-ocular reflexes (VOR) are the dominating contributors to gaze stabilization in all vertebrates. During horizontal head movements, abducens motoneurons form the final element of the reflex arc that integrates visuo-vestibular inputs into temporally precise motor commands for the lateral rectus eye muscle. The large dynamic spectrum from slow, tonic to fast, twitch-like contractions of different extraocular muscle fiber types necessitates an innervation by a similar range of task-specific motoneuronal subgroups. Here, we studied a possible differentiation of abducens motoneurons into subtypes by evaluating their morphology, discharge properties and synaptic pharmacology in semi-intact *in vitro* preparations of larval *Xenopus laevis*. Extracellular nerve recordings during sinusoidal head motion revealed a continuum of resting rates and activation thresholds during vestibular stimulation. Differences in the sensitivity to changing stimulus frequencies and velocities allowed subdividing abducens motoneurons into two subgroups, one encoding the frequency and velocity of head motion (group I), and the other precisely encoding angular velocity independent of stimulus frequency (group II). Computational modeling indicated that group II motoneurons are the major contributor to actual eye movements over the tested stimulus range. The segregation into two functional subgroups coincided with a differential activation of glutamate receptor subtypes, each with relevance for the phase of motion-induced responses. Furthermore, glycine mediated inhibitory inputs during the horizontal VOR while GABA transmitted a tonic non-vestibular inhibition. These findings support the presence of physiologically and pharmacologically distinct functional subgroups of extraocular motoneurons that act in concert to mediate the large dynamic range of extraocular motor commands during gaze-stabilization.

Significance statement

Outward-directed gaze stabilizing eye movements are commanded by abducens motoneurons that combine different sensory inputs including signals from the vestibular system (vestibulo-ocular reflex) about ongoing head movements. Using an amphibian model, this study investigates whether different types of abducens motoneurons exist that become active during different types of eye movements. The outcome of this study demonstrates the presence of specific motoneuronal populations with pharmacological profiles that match their response dynamics. The evolutionary conservation of the vestibulo-ocular circuitry makes it likely that a similar motoneuronal organization is also implemented in other vertebrates. Accordingly, the physiological and pharmacological understanding of specific motoneuronal contributions to eye movements might help designing drug therapies for human eye movement dysfunctions such as abducens nerve palsy.

Introduction

Accurate perception of the visual environment in all vertebrates requires permanently active gaze-stabilization that counteracts retinal image displacements during passive and self-motion. These image-stabilizing eye movements derive from the spatio-temporally precise transformation of visuo-vestibular sensory signals into extraocular motor commands. The large bandwidth of natural motion-related sensory signals likely precludes a signaling pathway composed of dynamically uniform neurons but rather suggests that the underlying sensory-motor transformation occurs in separate, parallel signaling channels with different temporal characteristics (see Straka and Dieringer, 2004; Straka et al., 2009). The necessity of such an organization is particularly obvious for the vestibulo-ocular reflex (VOR) pathway, given the wide dynamic range of this system for motion encoding. While both, vestibular nerve afferents (Jamali et al., 2013; see Goldberg, 2000) and central vestibular neurons (see Straka et al., 2005) subdivide into distinct cellular subtypes, a similarly clear differentiation of extraocular motoneurons into functional phenotypes has so far not

been demonstrated. Except for few studies emphasizing potential differences in motoneuronal response patterns during head motion (Dieringer and Precht, 1986; Evinger and Baker, 1991; Davis-López de Carrizosa et al., 2011), distinct subgroups with respect to intrinsic membrane properties were so far only described for rat oculomotor motoneurons (Nieto-Gonzalez et al., 2007). Nonetheless, vertebrate extraocular motor nuclei appear to form morpho-physiologically heterogeneous populations of neurons with different recruitment thresholds and time constants that match the large behavioral spectrum of eye movements (Sterling, 1977; Delgado-Garcia et al., 1986; Pastor et al., 1991; Pastor and Gonzales-Forero, 2003; Carrascal et al., 2009; Davis-López de Carrizosa et al., 2011).

Heterogeneity is also observed at the extraocular motor periphery where tonic, multiply and twitch-like, singly innervated eye muscle fibers can be distinguished (Büttner-Ennever et al., 2001; Eberhorn et al., 2005, 2006). Assuming different contraction dynamics of the respective fiber types, this structural differentiation is excellently suited to meet the general necessity for eye muscles to cover different motion dynamics such as during saccades, smooth pursuit, gaze holding or slow phase optokinetic responses (Horn and Leigh, 2011). This differential neuromuscular innervation of two separate muscle fiber types suggests a bipartite organization of extraocular motoneurons (Büttner-Ennever et al., 2001; Ugolini et al., 2006). Moreover, to generate dynamically appropriate extraocular motor commands for different eye motion tasks, extraocular motoneurons require functionally adequate synaptic inputs (Dean, 1997). In fact, different types of extraocular motoneurons receive synaptic inputs from spatially segregated ocular motor control regions with complementary functions such as gaze-stabilization or voluntary movement control during saccades or smooth pursuit (Ugolini et al., 2006).

Here, we provide direct evidence that extraocular motoneurons indeed form subgroups that mediate signals with distinct dynamics. During sinusoidal motion stimulation, abducens nerve recordings in semi-intact preparations of *Xenopus laevis* tadpoles revealed two groups of

extraocular motor units that either modulated exclusively with head motion velocity or with both, velocity and frequency components of the head movement. Differential pharmacological blockade of excitatory and inhibitory transmission demonstrated a differential impact of specific neurotransmitter systems and/or receptor subtypes for shaping the motor output of the two motoneuronal subgroups. Computational modeling that linked motor unit discharge with actual eye motion dynamics outlined potential contributions of the different neuronal subtypes to VOR performance. Preliminary data were previously published in abstract form (Dietrich et al., 2014).

Materials and Methods

Animals and experimental preparation

Xenopus laevis tadpoles of either sex (n = 105) at developmental stages 53-54 (Nieuwkoop and Faber, 1994) were obtained from the in house animal breeding facility at the Biocenter-Martinsried (Ludwig-Maximilians-University Munich). Tadpoles were maintained in tanks with non-chlorinated water (17-18°C) at a 12/12 light/dark cycle and were fed daily with *Spirulina* bacteria. Electrophysiological and pharmacological experiments were performed *in vitro* on isolated, semi-intact preparations and comply with the "Principles of animal care", publication No. 86-23, revised 1985 of the National Institute of Health. Permission for these experiments was granted by the respective governmental institution at the Regierung von Oberbayern (55.2-1-54-2532.3-59-12).

For all experiments, tadpoles were anesthetized in 0.05% MS-222 (Pharmaq Ltd. UK) in ice-cold frog Ringer´s solution (75 mM NaCl, 25 mM $NaHCO_3$, 2 mM $CaCl_2$, 2 mM KCl, 0.5 mM $MgCl_2$, and 11 mM glucose, pH 7.4) and decapitated at the level of the upper spinal cord. As previously described (Gensberger et al., 2016), the skin above the brain was removed, the cartilaginous skull opened from dorsal, the forebrain and spinal cord disconnected and both optic nerves transected. The remaining central nervous system and vestibular sensory periphery as well as all afferent connections and extraocular motoneuronal projections were functionally preserved in

this preparation. This allowed a natural activation of the horizontal vestibulo-ocular reflex (VOR) with sinusoidal vertical-axis rotations on a two-axis turntable under controlled *in vitro* conditions (Dietrich and Straka, 2016). Extraocular motor units were recorded from the abducens nerve after isolation of the lateral rectus (LR) nerve branch close to the target muscle. For pharmacological experiments, the trochlear nerve was isolated from the superior oblique (SO) target muscle and used for control recordings. For fluorescent tracer application, nerve branches were similarly prepared and cleaned from surrounding tissue. For all experiments, the preparations were placed in a Sylgard-lined recording chamber that was continuously perfused with oxygenated Ringer´s solution at a constant temperature of 16.8 ± 0.1°C.

Electrophysiology and pharmacology

The recording chamber with the preparation affixed to the Sylgard floor was mounted in the center of the rotation axes of a two-axis computer-controlled motorized turntable (ACT-1002, Acutronic USA Inc., Switzerland) as described earlier (Lambert et al., 2008). Spontaneous and stimulus-evoked spike discharge of the abducens and trochlear nerves were recorded (EXT 10-2F; npi electronics; Tamm, Germany) with individually adjusted glass suction electrodes, digitized at 20 kHz (CED 1401, Cambridge Electronic Design) and stored on computer for offline analysis. Glass microelectrodes for extracellular recordings were produced with a horizontal puller (P-87 Brown/Flaming) and the tips were individually broken to fit the respective nerve diameter. Motion stimuli for natural activation of the horizontal semicircular canals consisted of sinusoidal rotations of the turntable around the vertical axis at frequencies of 0.1 - 1 Hz and peak velocity amplitudes of ± 6°/s - 60°/s for modulating the spike activity of motoneuronal axons in the abducens nerve. Control recordings of the trochlear nerve were performed during horizontal-axis roll motion stimulation at a horizontal position of 45° (for details see Branoner and Straka, 2015; Dietrich and Straka, 2016).

The contribution of different excitatory and inhibitory neurotransmitter systems and receptor subtypes to the transmission of vestibular inputs onto abducens motoneurons was studied using

focal injections of specific antagonists directly into the abducens nucleus through beveled glass microelectrodes. The abducens nucleus was localized using external landmarks such as the entrance of the VIIIth and XIth cranial nerves into the hindbrain and the plainly visible midline along the IVth ventricle. Injection electrodes were inserted into the hindbrain and positioned in the center of the abducens nucleus with a micromanipulator. After pressure injection (0.5 bar; 50 ms) of a volume of 20 - 50 nl containing a particular transmitter receptor antagonist, the electrode was slowly retracted from the brainstem to avoid further leakage. To exclude indirect effects of the injected blockers due to potential spread into the neighboring ipsilateral vestibular nuclei and interference with vestibular signal processing, control recordings of the ipsilateral trochlear nerve were made in parallel to those of the abducens nerve. However, no change in vestibular-evoked trochlear motor activity was encountered after a focal pressure injection of antagonists into the abducens nucleus, indicating that the applied drugs remained strictly confined to the abducens nucleus.

Vestibular-evoked glutamatergic excitation of abducens motoneurons was blocked by focal bolus injections of the α-amino-3-hydroxy-5-methyl-4-isoxazolepropionic acid (AMPA) receptor antagonist 2,3-Dioxo-6-nitro-1,2,3,4-tetrahydrobenzo[*f*]quinoxaline-7-sulfonamide (NBQX disodium salt; 10 µM; Tocris Bioscience, United Kingdom) and by the N-methyl-D-aspartate (NMDA) receptor antagonist D-(-)-2-Amino-5-phosphonopentanoic acid (D-AP5; 500 µM; Tocris Bioscience) into the abducens nucleus. Focal abducens injections of the glycine receptor antagonist strychnine
(10 µM; Tocris Bioscience) and of the $GABA_A$ receptor blocker gabazine (10 µM; Tocris Bioscience) were made to test potential contributions of these inhibitory transmitters to the vestibular-induced modulation of abducens motoneuronal activity. All antagonists were dissolved in frog Ringer´s solution.

Data analysis

Peri-stimulus time histograms (PSTHs) illustrating the average motoneuronal firing patterns over a single cycle of sinusoidal head rotation were obtained from raw data using Spike2 scripts that

allowed analyzing the recorded multi- or single-unit spike discharge (Dietrich and Straka, 2016). For all stimulus parameters (frequencies, amplitudes), average responses were calculated from at least 10 single cycles. The PSTHs were further processed and analyzed statistically using Microcal Origin 6.0G and MathWorks MATLAB® software. PSTHs were normalized and averaged (± SEM; standard error of the mean) for comparison within and between different experiments. The discharge regularity of individual units that were active at rest was quantified using the coefficient of variation 2 (CV2) as described previously (Holt et al., 1996). Spike sorting according to shape and amplitude was performed using Principal Component Analysis included in the Spike2 software.

Anatomy

The location of the principal abducens (VI) nucleus was determined by retrograde labeling of the motoneurons from the LR target muscle in the periphery. The abducens nerve was dissected as for the electrophysiological experiments (see above), placed on a thin piece of parafilm and covered with a small amount of biocytin. After ~10 minutes the preparation was excessively rinsed and kept in freshly oxygenated frog Ringer´s solution overnight at 12°C as described previously (Straka et al., 2001). Subsequently the brain was dissected free and fixed in 4% paraformaldehyde in 0.1 M phosphate buffer, pH 7.4, for 4 hours at 4°C. To visualize the motoneurons, a standard protocol for processing whole-mount preparations with streptavidin-Alexa 488 was applied before mounting the preparation in Vectashield® mounting medium. The hindbrain region containing retrogradely labeled abducens motoneurons was reconstructed from stacks of ~100 - 150 consecutive optical sections after scanning on a Leica SP5-2 confocal microscope at 0.5 - 1 µm z-axis intervals. Z-axis projections and image processing as well as quantification of neuronal numbers and measurement of somal cross-sectional areas were carried out using the Fiji software package (http://fiji.sc/wiki/index.php/Fiji). In order to map the position of retrogradely labeled motoneurons onto the rhombomeric scaffold, preparations were scanned with an illumination wavelength of 633 nm, visualizing the segmental arrangement of midline-crossing axonal pathways (Chagnaud et al., 2015; Hänzi et al., 2015), thereby outlining the rostro-caudal arrangement of the rhombomeres (r).

Eye movement recordings

Eye movements during sinusoidal head rotations were recorded non-invasively from above with a video camera (Grasshopper color, Point Grey Research Inc, Canada) and a zoom objective (Optem Zoom 70XL, Qioptiq Photonics GmbH & Co KG, Germany) with an adequate lens (M25 x 0.75 + 0.25). Eye motion was captured at a frame rate of 50 Hz with the respective software (FlyCap2) and analyzed offline using a custom video-processing algorithm written in Matlab to compute eye position over time (for details see Ramlochansingh et al., 2014). From the raw eye position data, slow drift was removed by high-pass filtering (Gaussian filter, 0.01 Hz). Outliers caused e.g. by resetting fast phases were discarded. The resulting eye position trace was then averaged over all stimulus cycles. The averaged eye position traces over a single cycle were fitted with a sine wave of the same frequency as the stimulus in order to determine gain and phase of the eye movement. The extracted averaged eye position traces were then used for the computational model.

Computational model

The purpose of constructing a model was to evaluate the respective contributions of dynamically different types of abducens motoneurons to tadpole eye movements. To simulate eye movements from measured action potential sequences, the spikes of each neuron, stored as binary values, were first processed by a dual low-pass filter (time constants 20 ms and 40 ms) representing the activation function of the muscle fibers. The resulting muscle activity was then processed with a simplified model of the oculomotor plant (single time constant, 330 ms, measured in *Xenopus* tadpole eye muscles, Schuller and Straka, unpublished results). The activity of contralateral motoneurons was simulated by assuming a discharge with the same spike train as measured in ipsilateral motoneurons, however, phase-shifted by half a cycle such that ipsi- and contralateral neurons act in a push-pull fashion with oppositely oriented directional tuning. To yield an eye movement, weighted signals, generated by both ipsi- and contralateral motoneurons, were summated. The synaptic weights of the motoneurons were determined by a least-squares fit to the

averaged measured eye movement traces using the Matlab function "lsqnonneg", which solves non-negative least-squares constraints problems to account for the fact that synaptic weights at the neuro-muscular junction can only be positive. To avoid a bias towards low-frequency eye movements due to longer cycle durations, traces were resampled to contain 1000 values for one stimulus cycle before fitting. Data for four eye movement frequencies (0.1, 0.2, 0.5 and 1 Hz) of each animal were fitted simultaneously to determine the weights of the best fitting set of neurons for that particular animal. In order to compare between motoneuronal subtypes, the explained variance was calculated for fits of individual subgroups.

Results

Anatomical organization of abducens motoneurons

Application of biocytin to the lateral rectus (LR) branch of the abducens nerve in stage 53-54 *Xenopus* tadpoles retrogradely labeled on average ~40 motoneurons (41.2 ± 6.6, n = 7) within a single hindbrain nucleus (Fig. 1$A_{1\text{-}3}$). The location of the cell bodies close to the midline in rhombomere (r) 5 (Fig. 1A_1 and inset) complies with the known mono-segmental origin of principal abducens motoneurons in other anuran species (Straka et al., 1998, 2006). Axons of all LR innervating abducens motoneurons joined into a ventrally projecting tract, exited the brainstem close to the midline as VIth cranial nerve, coursed rostrally along the pial surface of the brainstem (n.VI in Fig. 1A_2) and left the cranium laterally along with the Vth and VIIth cranial nerves. Somata of these principal abducens motoneurons (Fig. 1A_3) were generally round or oval-shaped with cross-sectional areas that varied considerably within a range of 32 – 204 µm² (n = 275) at the plane of their largest perimeter (Fig. 1$B_{1,2}$). The cell size distribution of motoneurons appeared to form a continuum, however the majority of somata had cross-sectional areas in the range of 50 - 100 µm², even though few very large neurons were regularly encountered (Fig. 1B_1). In order to potentially

distinguish distinct motoneuronal subtypes with respect to cell shape, the circularity of the somata (4π*area/perimeter^2) was determined (Fig. 1B_2). Based on this calculation, most principal abducens motoneurons had round cell bodies (circularity close to 1), however, with a continuous transition towards few motoneurons with oval-shaped somata (Fig. 1B_2). While motoneurons with round somata predominated at midline positions, motoneurons at increasingly more lateral positions within the nucleus tended to be more oval-shaped (Fig. 1C_1). In contrast, no difference in cell shape with respect to the rostro-caudal position was observed (Fig. 1C_2).

Spontaneous and motion-evoked discharge profiles of abducens motoneurons

The discharge patterns of abducens motoneurons at rest and during imposed head motion in semi-intact preparations of *Xenopus* tadpoles were studied by recording the axonal spike activity of the abducens nerve after disconnection from its LR target muscle (Fig. 2$A_{1,2}$,B). In most recordings, the multi-unit discharge of the LR nerve (black trace in Fig. 2C) could be dissociated into the spike activity of individual, single-units by spike shape discrimination (red and blue traces in Fig. 2C) using principal component analysis (Fig. 2D,E; see also Dietrich and Straka, 2016). The functionally preserved inner ear endorgans in these preparations allowed characterizing discharge dynamics of individual abducens motoneurons at rest and during imposed head rotation (Fig. 3$A_{1,2}$). All isolated motor units (n = 46) had a resting activity below ~10 spikes/s (Fig. 3B), including a group of cells (n = 13) with spikes of particularly large amplitude in multi-unit recordings (compare blue and red arrowheads in Fig. 3A_2) that were silent at rest (dark green bar in inset of Fig. 3B) and became discernible only during motion stimulation. At variance with this latter group, spontaneously firing units (n = 33) usually had spikes of smaller amplitude with a highly variable resting firing rate that extended over two decades within this group (~0.1-10 spikes/s; Fig. 3B). The discharge regularity of these neurons covered a correspondingly large range as indicated by the coefficient of variation (CV2; Fig. 3$C_{1,2}$). For motor units with resting rates between 1-10 spikes/s, the average interspike interval (ISI) was linearly correlated with the CV2 (r^2 = 0.345; Fig. 3C_2).

During horizontal sinusoidal rotation, the vast majority of abducens motoneurons became

cyclically active, in phase with the velocity of contraversive head movements (right traces in Fig. 3$A_{1,2}$). In order to facilitate a classification of responses, the discharge rates of different units were normalized, respectively, before population averages were calculated. While the firing rate modulation during sinusoidal motion generally increased in depth with stimulus velocity, the threshold for this modulation varied considerably between different motoneurons (Fig. 3$D_{1,2}$). In fact, motor units that were silent ('s') at rest had relatively high velocity thresholds (33.6 ± 4.2°/s; n = 13; inset in Fig. 3E, Fig. 3D_2), whereas spontaneously active motor units ('sa') exhibited a cyclic discharge modulation (Fig. 3D_1) above a significantly ($p < 0.001$; Mann-Whitney U test) lower peak velocity of the sinusoidal stimulus (3.0 ± 1.03°/s; n = 33; inset in Fig. 3E). Moreover, a more or less continuous range of discharge modulation depths at ±30°/s stimulus peak velocity was observed in different motoneurons that linearly correlated with the rate of the resting discharge of the respective motoneurons (Fig. 3E, r^2 = 0.121), suggesting a continuum of motoneurons with respect to resting rate, discharge regularity and sensitivity to motion stimuli.

Apart from the generally similar VOR response pattern, shared by the majority of motor units, amplitude and phase analyses of sufficiently long periods of response recordings during horizontal sinusoidal head motion (n = 24), allowed a more detailed characterization and classification of abducens motoneuronal response properties. Independent of the distinguishing traits (see below), all tested motoneurons with a spontaneous resting rate (n = 14) exhibited peak firing rates that increased steadily with increasing stimulus magnitude up to ~25 spikes/s and saturated above a peak velocity of ±60°/s at 0.5 Hz (Fig. 3D_1, 4$A_{1,2}$, black and red lines in Fig. 4C_1). The peak response within a given motion cycle was approximately in phase with stimulus velocity, independent of its magnitude (black and red lines in Fig. 4C_3).

While the response profile during increasing peak velocities was essentially indistinguishable among spontaneously active motoneurons, a categorization into two subgroups with respect to the timing of the peak response became obvious when the stimulus frequency was systematically altered while the peak velocity was kept constant at ±30°/s (Fig. 4A,B). Motor units of the first

subgroup (group I; n = 8; Fig. 4A_1) exhibited modulated responses during sinusoidal rotation with a peak firing rate that was maximal at 0.2 Hz and decreased with increasing stimulus frequency (black line in Fig. 4C_2). Importantly, the decrease of the peak response rate in these motor units was accompanied by a large concurrent shift of the timing of the response peak from a phase lead of ~45° at 0.1 Hz to a phase lag of ~40° at 1 Hz (black line in Fig. 4C_4). In contrast, motor units of the second subgroup (group II; n = 6; Fig. 4A_2) exhibited responses that decreased only slightly with increasing stimulus frequency while the phase relation remained constant (red lines in Fig. 4$C_{2,4}$). In summary, the two abducens motoneuronal subgroups appear to be similarly motion-sensitive with respect to head velocity but differ considerably in the amplitude and temporal signature of the responses when stimulus frequencies are altered.

The differentiation into two categories however was not limited to spontaneously active units with low stimulus thresholds but was also encountered in a comparable manner for those neurons that were silent in the absence of motion stimuli (n = 10; Figs. 3A_2,D_2, 4$B_{1,2}$). Common to all of these latter units was the presence of a sharp response peak during contraversive head motion (Fig. 3D_2). Even though the discharge modulation at ±30°/s peak velocity was relatively weak (7.2 ± 1.8 spikes/s), changes in stimulus velocity were precisely encoded once the activation threshold was reached (Fig. 3D_2). Given the absence of a spontaneous resting rate, however, these neurons only encoded the excitatory but not the inhibitory component of the VOR. Similar to the situation in spontaneously active motor units, differences in discharge profiles were mainly observed upon changes in stimulus frequency (Fig. 4$B_{1,2}$,$D_{2,4}$). Here again, the response modulation during sinusoidal head rotation in group I motoneurons (n = 6) changed in amplitude with increasing motion frequency, accompanied by a concurrent shift of the response peak from a phase lead of ~35° at 0.1 Hz to a phase lag of ~38°/s at 1 Hz (Fig. 4B_1, black line in Fig. 4D_4). Silent group II motoneurons (n = 4) exhibited peak responses of similar magnitude and timing, independent of stimulus frequency (black and red lines in Fig. 4B_2) as observed for the corresponding class of spontaneously active motoneurons. However, a modulated spike discharge in the latter neurons

could not be triggered with motion stimuli that had peak velocities less than or equal to ±30°/s (Fig. 4*D*$_1$) or frequencies above 0.2 Hz at ±30°/s (Fig. 4*D*$_2$).

Thus, independent of the presence or extent of spontaneous activity, abducens motoneurons separate into two groups that generate motor commands that are either in phase with the velocity of the sinusoidal motion stimulus or dependent in their response amplitude and timing on stimulus frequency.

Motion-insensitive abducens motoneurons

In addition to the majority of motion-sensitive abducens motor units, a small population of neurons (n = 6) was encountered in different preparations that had no spontaneous spike activity, displayed an occasional burst-like discharge (Fig. 5*A*$_{1,2}$) and in multi-unit recordings exhibited the largest spikes. In contrast to motion-sensitive abducens motoneurons described above, the latter neurons were unresponsive to imposed horizontal rotations but instead often bursted randomly during table motion (Fig. 5*A*$_2$, * in Fig. 5*B*). The absence of any correlation between bursting and rotational stimuli was confirmed by the average activity over a single motion cycle (Fig. 5*A*$_3$). Compatible with the obvious absence of vestibular influence, these motor units continued to fire occasional bursts of spikes (lower trace in Fig. 5*C*) after transection of the contralateral VIIIth nerve, a perturbation that consistently caused complete elimination of the robust cyclic activity of motion-sensitive abducens motor units (compare upper and lower traces in Fig. 5*C*). Even though the activity of these motion-insensitive units is reminiscent of that of accessory abducens motoneurons (Dieringer and Precht, 1986), the distinct isolation of the identified LR nerve branch close to the target muscle in our experiments makes a recording of such motoneurons unlikely. More likely, motion-insensitive units form a particular class of principal abducens motoneurons that are only activated during optokinetically-driven fast resetting eye movements (Schuller et al., 2014) or by locomotor efference copies, known to directly recruit extraocular motoneurons during undulatory swimming in *Xenopus* tadpoles (Lambert et al., 2012).

Vestibular inputs to abducens motoneurons

Bilateral vestibular inputs to vertebrate abducens motoneurons consist of a crossed excitation and an uncrossed inhibition (Precht, 1978). In order to reveal potential differences in the pharmacological profile of the two different groups of abducens motor units, we tested the specific recruitment of transmitter receptor subtypes during motion-driven extraocular motor activity.

Glutamatergic excitatory inputs. The contribution of AMPA and NMDA receptors to motion-induced discharge modulation of abducens motor units was tested by focal pressure injection of specific transmitter blockers (AMPA receptor-blocker: NBQX; NMDA receptor-blocker: D-AP5) into the abducens nucleus, respectively (Fig. 2*B*). Independent of the previously established classification of spontaneously active motor units into group I and II, bolus injections of either D-AP5 (500 µM) or NBQX (10 µM) caused a significant reduction of the spontaneous discharge. The almost instantaneously occurring reduction of the motoneuronal discharge after the injection usually lasted for 10-15 min and was followed by a gradual recovery that reached control values ~45 min after injection of D-AP5, whereas the effect of NBQX was only partially reversible. Both blockers reduced the spontaneous abducens nerve activity (n = 7), however, D-AP5 was significantly more effective than NBQX. While the NMDA blocker decreased the spontaneous discharge rate of single abducens motor units to ~40% (37.2 ± 8.5%) of the control value, NBQX had a significantly smaller effect and reduced the resting rate only to ~75% (75.5 ± 5.8%; p = 0.0156; Wilcoxon signed-rank test) of the control.

During sinusoidal head rotation, the excitatory response component of all recorded single-units in controls (black traces in Fig. 6*A,B*), independent of the presence and extent of spontaneous activity, was consistently reduced following injection of either one of the two glutamate receptor blockers (red and blue traces in Fig. 6*A,B*). However, the relative magnitudes of the unmasked AMPA and NMDA receptor-mediated response components differed between group I and II motoneurons. This differential impact was quantified by comparing the change of the area under the average modulated response curve (integral) over a single cycle before (black trace in Fig. 6*C,D*)

and after injection of the respective drug (red and blue traces in Fig. 6*C,D*). Independent of the presence and/or extent of spontaneous resting activity, D-AP5 reduced the excitatory response component in group I abducens motor units (n = 8) by more than 80%, whereas the NBQX-provoked decrease amounted to only ~50% of the control response (representative examples in Fig. 6$C_{1,2}$). Accordingly, the residual AMPA response component after D-AP5 injection was significantly smaller (18.5 ± 6.6%; p = 0.0078; Wilcoxon signed-rank test) than the NMDA component after NBQX injection (47.2 ± 7.1%; Fig. 6E_1). This suggests that the cyclic discharge modulation of these motoneurons during sinusoidal motion stimulation is predominantly driven by NMDA receptor-mediated excitation, with a smaller contribution of AMPA receptors (Fig. 6E_1). In contrast, in group II motor units (n = 6), NBQX had a larger impact on the excitatory response than D-AP5 and reduced the response by 95%, whereas the NMDA blocker caused a reduction by 85% (Fig. 6$D_{1,2}$). Hence, despite the considerable efficiency of both blockers, the residual NMDA response component after NBQX injection was significantly smaller (4.0 ± 2.2%; p = 0.0313; Wilcoxon signed-rank test) compared to the AMPA component after D-AP5 injection (14.0 ± 3.5%; Fig. 6E_1). In fact, NBQX usually abolished the evoked responses completely in those group II units that were silent at rest (blue trace in Fig. 6D_2), whereas a small response component persisted in spontaneously active group II motor units after injection of the AMPA receptor blocker (blue trace in Fig. 6D_1). These results suggest that excitatory responses during motion stimulation in the two groups of abducens motoneurons are differentially organized with respect to glutamate receptor subtypes. Whereas group II motoneurons are predominantly excited by AMPA receptors, group I motoneurons are mainly activated by an NMDA receptor-mediated component during motion stimulation.

Independent of the relative contributions of AMPA and NMDA receptors to the excitation of group I and II abducens motoneurons, the pharmacological block of the two components also differentially affected the timing of the response peak (Fig. 6$C_{1,2}$,D_1,E_2). Compared to controls (black traces in Fig. 6*C,D*), application of NBQX caused a delay of the response peak with respect

to the sinusoidal stimulus in all tested motor units (blue traces in Fig. 6*C*$_{1,2}$,*D*$_1$). This resulted in a considerable phase lag of the evoked responses by 10-20° and was particularly pronounced in group I motoneurons (blue bars in Fig. 6*E*$_2$). In contrast, application of D-AP5 provoked an opposite shift of the response peak of similar magnitude (red traces in Fig. 6*C*$_{1,2}$,*D*$_{1,2}$, thereby generating a pronounced phase lead of the modulated responses during the block (red bars in Fig. 6*E*$_2$). These reciprocal shifts of the response timing after separate blockade of the two glutamatergic receptor subtypes was independent of stimulus velocity or frequency and suggests that the phase relation of vestibular-driven responses in abducens motoneurons is differentially controlled by AMPA and NMDA receptors.

GABAergic and glycinergic inhibitory inputs. The contribution of uncrossed inhibitory horizontal semicircular canal (HC) inputs to abducens motoneurons was first evaluated by surgical removal of the ipsilateral HC sensory epithelium. This ablation immediately caused a substantial increase in the abducens nerve resting activity from ~40 to ~55 spikes/s (38.9 ± 5.8 to 56.7 ± 4.4 spikes/s; n = 3), compatible with the notion that when the head is stationary, a continuous inhibitory input from the ipsilateral HC balances the tonic excitatory drive from the contralateral side. This augmentation in spontaneous firing rate was accompanied by an increased spike activity of the modulated multiple-unit abducens nerve discharge over the entire head motion cycle (Fig. 7*A*,*B*). The difference to control responses, however, was particularly obvious during rotation towards the ipsilesional side (* in Fig. 7*B*), in agreement with the loss of an uncrossed inhibition in the absence of ipsilateral HC inputs.

In a separate set of experiments, the uncrossed HC-derived inhibition of abducens motoneurons was further characterized by a longitudinal midline section between r1-r8 (Fig. 7*C*; Lambert et al., 2012) that removed crossed excitatory HC inputs as well as a potential amplifying effect of vestibular commissural pathways on vestibulo-ocular signal processing (Malinvaud et al., 2010). The spontaneous discharge of the LR nerve ceased immediately after the surgical invention, however, motoneuronal activity regained a small resting spike activity after 15-30 minutes. The

restored spontaneous firing of abducens motoneurons was cyclically attenuated in a stimulus velocity-dependent manner during sinusoidal rotation in the direction of the ipsilateral HC (Fig. 7*D*, n = 6), thus illustrating the functional impact of the isolated uncrossed vestibular inhibition. A putatively differential contribution of glycine- and $GABA_A$-receptors to the inhibitory component of motion-induced discharge modulation was further evaluated by focal pressure injections of the respective antagonists strychnine and gabazine into the abducens nucleus.

Focal injections of strychnine (10µM) into the abducens nucleus generally resulted in a rather inconsistent, temporarily variable and often fluctuating elevation of the firing rate around which the LR nerve discharge was modulated during motion stimulation. In addition, strychnine often caused extensive and unpredictable bursts and/or repetitive discharge oscillations during motion as reported earlier (Straka and Dieringer, 1993), likely due to an unmasking of excessive excitatory inputs, thus preventing a quantification of the impact of blocked glycinergic transmission. To reduce the overall amount of excitatory drive to abducens motoneurons, in particular from the contralateral vestibular nucleus, and to exclude a potential commissural influence on vestibulo-ocular signal processing, strychnine injections were repeated in preparations with a longitudinal midline transection. As described above, the multi-unit abducens nerve firing rate modulation became strongly reduced compared to control values (blue and black traces, respectively, Fig. 7*E* and inset in Fig. 7*F*), lacking the excitatory component that derives from the contralateral HC. Nonetheless, subsequent focal application of strychnine eliminated the observed residual inhibitory firing rate modulation during the half cycle of ipsiversive rotation (representative example and average PSTH in Fig. 7*E,F*, n = 6), indicating in compliance with previous assumptions (Straka and Dieringer, 1993) that glycine mediates the uncrossed inhibitory component of the horizontal angular VOR.

Focal application of the $GABA_A$-blocker gabazine (10µM) into the abducens nucleus of unimpaired preparations (without longitudinal midline section) considerably increased the spontaneous LR nerve discharge, however without causing oscillatory bursting as observed after strychnine injections. The single- and/or multiple-unit abducens nerve resting rate increased by

~130% (p = 0.0313; Wilcoxon signed-rank test) from 10.6 ± 2.9 spikes/s in controls to 24.6 ± 7.8 spikes/s after gabazine application (n = 6). In addition, the peak firing rate of individual units during sinusoidal motion stimulation at a peak velocity of ±30°/s increased by ~50% (Fig. 7*G,H*). Notably, the absolute gabazine-evoked increases in single-unit peak firing rates were essentially independent of the stimulus peak velocity up to ±30°/s (inset in Fig. 7*H*, n = 7). The relatively smaller increase observed for responses elicited by a higher stimulus peak velocity suggests that peak firing rates reached a maximum, compatible with the assumption that saturation of single-unit response amplitudes occurs at peak velocities of around ±60°/s (see Fig. 4C*1*). Moreover, blocking $GABA_A$ receptors elevated the level around which the discharge was modulated during motion stimulation and thus caused an augmentation of both the excitatory and inhibitory response components. In these experiments, relatively more single-units with no or very low resting rates were recorded (4 out of 7) that only fired spikes during head rotations in the on-direction (Fig. 7*G*). Therefore, an increase in firing rate was mainly observed for the excitatory half-cycle, i.e during contraversive rotation (solid lines in Fig. 7*H*). However, motor units with a spontaneous resting activity (3 out of 7; dotted lines in Fig. 7*H*), displayed a considerable increase in activity over the entire motion cycle, suggesting the presence of a tonic $GABA_A$ receptor mediated inhibition, that, in contrast to glycinergic inputs described above, is independent of modulated ipsilateral vestibular inputs. In summary, this corroborates previous findings (Spencer et al., 1989; Straka and Dieringer, 1993) that indeed glycine and not GABA mediates the transmission of inhibitory VOR inputs onto abducens motoneurons. In addition, a tonic GABAergic input significantly attenuates abducens motoneuronal firing both at rest and during motion-related vestibular activation.

Computational modeling

In order to evaluate the relative contributions of the different subgroups of abducens motoneurons to eye movements, a computational model was constructed and used to simulate eye movements with weighted sums of individual muscle contractions caused by single motor unit activity. As a first step, eye motion during horizontal head rotation (±30°/s peak velocity) was

video-recorded (n = 7; Fig. 8*A*) and averaged over a single motion cycle for different frequencies, respectively (see representative examples in Fig. 8*B*). Evoked eye movements were fitted with a sine wave (blue lines in Fig. 8*B*) that allowed calculating the phase relation of the responses with respect to the stimulus. This analysis revealed that the phase of sinusoidal motion-driven eye movements leads turntable position during low-frequency head rotation (0.1 Hz) and gradually becomes more aligned with the stimulus at higher frequencies (0.5 and 1 Hz; Fig. 8*B*). Thus, eye movements (green lines in Fig. 8*B*) counteracted table motion (gray lines in Fig. 8*B*) in a stimulus frequency-dependent manner, notably however, with concurrently decreasing motion amplitudes (compare 0.5 and 1 Hz in Fig. 8*B*).

The recorded eye motion was simulated using modulated firing patterns of individual abducens motor units during horizontal head rotation. Spike times were extracted from single-unit recordings (left plot in Fig. 8*C*) and fed into a simplified model of the oculomotor plant to generate contraction patterns of individual muscle fibers (middle plot in Fig. 8*C*) and to compute the weighted sum of the latter to optimally simulate each of the recorded eye movements (n = 7). The relative contributions of group I and group II motoneurons to the generation of eye movements were evaluated using simulations of the discharge patterns of different combinations of the two groups (Fig. 8*D*). Across stimulation frequencies, the contribution of group II motoneurons (red lines in Fig. 8*D*) was significantly larger than that of group I motoneurons (blue lines in Fig. 8*D*), however at higher frequencies, group I motoneurons became increasingly more important (compare e.g. 0.1 and 1 Hz in Fig. 8*D*). To quantify the quality of the fit of individual simulations, explained variances were calculated and averaged for all eye movement data for simulations using either all units, units of one of the two subgroups or silent or spontaneously active units individually (Fig. 8*E*). The explained variance was highest using all units for simulation (93.2%). Group II motoneurons contributed more to the average explained variance (81.7%) than group I motoneurons (28.6%). Comparing silent and spontaneously active units revealed that active units contributed more than silent units to the overall fit (active 78.8% *vs.* silent 44.5%). To further quantify the role

of different types of motor units to explain the observed eye movements, the above simulations were repeated using each of these types alone. “Repeated measures analysis of variance” (ANOVA) of logarithmic least-squares error values – to obtain a normal distribution – revealed that depending on the classification scheme (group I - group II, active - silent) each of the different populations are differently well suited to fit the observed eye movements ($F(3,18)=4.38$; $p=0.018$) with the best result for group II units followed by spontaneously active units. The outcome of the simulation suggests that all types of abducens motoneurons contribute to the final VOR output and conjointly create the spatio-temporal precision of counteractive eye movements. However, group II motoneurons appear to play a more dominant role compared to those of the group I subtype while spontaneously active units contribute to eye motion relatively more than motoneurons that are silent at rest, at least during sinusoidal rotations at frequencies between 0.1 and 1 Hz.

Discussion

The principal abducens nucleus in larval *Xenopus* consists of a morphologically heterogeneous population of ~40 motoneurons. Based on differences in discharge profiles during head motion, abducens motoneurons distinguish into two subgroups. Responses of group I motoneurons have a phase relation and peak firing rate that changes systematically with head rotation frequency. In contrast, responses of group II motoneurons are characterized by high phase precision relative to stimulus velocity, independent of the frequency. While AMPA and NMDA receptors contribute differentially to the vestibular-driven excitation of the two neuronal subgroups, a tonic GABAergic and modulated glycinergic vestibular inhibition is present in both populations.

Morphology and function of motoneuronal subtypes in larval Xenopus

The heterogeneity of abducens motoneurons with respect to cell morphology, spontaneous discharge rate, sensitivity and dynamics of vestibular-evoked responses, complies with previous

assumptions that the VOR circuitry is arranged in parallel, frequency-tuned signaling channels, each tuned to a particular range of head motion dynamics (see Straka et al., 2009). First evidence for this was provided by the presence of abducens motor units with markedly different time constants during optokinetic stimulation in adult frogs, suitable for either low-dynamic eye motion and maintenance of excentric eye positions or rapid eye movements, respectively (Dieringer and Precht, 1986). The inverse correlation between motoneuronal cell diameter and input resistance and hence neuronal excitability (see Mendell, 2005), suggests that the large spectrum of somal sizes of abducens motoneurons correlates with motoneuronal task separation during eye movements (Evinger and Baker, 1991). Moreover, the observed morphological differences might directly match the continuum of resting activities as well as the differences in spike amplitude during extracellular multiple-unit recordings (Lambert et al., 2008).

Different morpho-physiological characteristics of abducens motoneurons comply with a task-specific extraocular motor activity (Evinger and Baker, 1991), and a differential origin of presynaptic inputs from distinct eye movement control areas (Ugolini et al., 2006). A dual organization with respect to response dynamics is implemented for vestibular afferents and central neurons in amphibians (Gensberger et al., 2015; Beraneck et al., 2007; Pfanzelt et al., 2008; Rössert et al., 2011) and other vertebrates (see Goldberg, 2000; Straka et al., 2005). If this concept of duality is directly transferable to abducens motoneurons is unclear, however, it is compatible with a categorization for example into silent *vs.* spontaneously active motoneurons. Nevertheless, although a lesser degree of distinction between these units does not conflict with the general concept of duality, it is rather comparable to the large continuum of resting rates and activation thresholds of cat abducens motoneurons (Davis-López de Carrizosa et al., 2011) and might reflect at least partial convergence of dynamically distinct vestibular inputs in single motoneurons. Also the classification of abducens motoneurons into two groups in the current study potentially reflects a functional duality since group I and II motoneurons show responses during head motion that are reminiscent of the two types of vestibular afferents in larval *Xenopus* (Gensberger et al., 2015). This similarity is

584 thus compatible with a VOR organization as frequency-tuned channels from the sensory periphery
585 to the motor plant.

586 Despite the lesser degree of separation of group I and II extraocular motoneurons in
587 *Xenopus*, compared to their tonic and phasic presynaptic vestibular neurons (see Straka et al., 2005),
588 the two motoneuronal subgroups encode different aspects of head movements. While neurons in
589 both subgroups are similarly sensitive to increasing stimulus peak velocities, only responses of
590 group II motoneurons remain in phase with stimulus velocity, largely independent of stimulus
591 frequency. This suggests that these motoneurons selectively and precisely encode the velocity of
592 head motion, its precision being facilitated by the predominance of rapid AMPA receptor-mediated
593 excitatory components (Fig. 6). In contrast, group I motoneurons respond differentially with respect
594 to amplitude and timing to changes in frequency, possibly by integration of the head acceleration
595 component that changes during varying frequencies. Such an integration might be supported by
596 temporally extended responses resulting from NMDA receptor activation (Fig. 6).

597 A likely motoneuronal task-sharing is suggested by data from the modeling approach (Fig.
598 8), since dynamically appropriate compensatory eye movements during head motion require a
599 combined activation of both motoneuronal groups. In general, group II motoneurons appear to be
600 more important for the generation of adequate eye movements (Fig. 8*E*), however predominantly at
601 lower frequencies. In contrast, group I motoneurons contribute weakly at lower stimulus
602 frequencies but become increasingly more important at higher frequencies. In addition, independent
603 of the classification scheme, spontaneously active motoneurons play a predominant role for VOR-
604 related eye movements compared to silent motoneurons. This complies with previous studies
605 suggesting that silent extraocular motoneurons with large spike amplitudes rather trigger high-
606 velocity VOR responses, saccades or eye twitches (Dieringer and Precht, 1986; Büttner-Ennever
607 and Horn, 2002). Furthermore, the extreme ends of the continuum of silent to spontaneously active
608 motoneurons described here comply with a general concept where singly- and multiply-innervated
609 muscle fibers are activated by “twitch-like” (i.e. high-dynamic, silent at rest) and “tonic” (i.e.

spontaneously active, low-dynamic) extraocular motoneurons, respectively (Büttner-Ennever and Horn, 2002; Eberhorn et al., 2006).

Organization of excitatory inputs to abducens motoneurons

Glutamatergic inputs from the contralateral vestibular nucleus form the major excitatory drive for abducens motoneurons that in isolated frog brains was completely abolished by bath-application of the AMPA receptor blocker CNQX (Straka and Dieringer, 1993). In the current study, excitation in all abducens motoneurons is mediated by a mixture of AMPA and NMDA receptors, compatible with the presence of both receptor molecules on their membranes (Durand et al., 1987; Durand, 1991; Keifer and Clark, 2003). The absence of a residual NMDA component after blocking the AMPA component in the previous study (Straka and Dieringer, 1993) is likely due to the lack of background resting activity from the vestibular sensory periphery in isolated frog brains. This notion complies with the spontaneous activity of vestibular afferents in semi-intact tadpole preparations (Gensberger et al., 2015) and the large NMDA sensitivity of abducens motoneuronal resting rates. Moreover, NBQX, used in the current study, is more selective for AMPA receptors than CNQX since the latter also partially blocks NMDA receptor-mediated responses (Birch et al., 1988; Long et al., 1990). Thus, based on the more specific pharmacological intervention in the current study, both glutamate receptor subtypes contribute to the vestibular-driven excitation of abducens motoneurons. Furthermore, the two receptor subtypes independently control the timing of responses during sinusoidal vestibular stimulation, since blockade of AMPA receptors causes a phase lag and NMDA receptor inhibition a phase lead in each abducens motor unit. This differential impact is compatible with the short and long time courses of AMPA and NMDA receptor-activated EPSPs, respectively (see Edmonds et al., 1995) and complies with the different time courses of AMPA receptor-mediated afferent and NMDA receptor-mediated commissural inputs to central vestibular neurons in frog (Dieringer and Precht, 1977; see Straka and Dieringer, 2004). This thus suggests that AMPA receptors mediate the rapid onset of VOR responses, whereas NMDA receptors encode a longer, sustained activity. These findings also

636 comply with a previous pharmacological study (Priesol et al., 2000) demonstrating that AMPA
637 receptor blockade mainly affects the VOR gain during rapid, high frequency head rotation, whereas
638 NMDA receptor blockade predominantly reduces slow and sustained, low frequency VOR
639 responses.

640 *Organization of inhibitory inputs to abducens motoneurons*

641 Inhibitory vestibulo-ocular projections onto horizontal and vertical/oblique extraocular
642 motoneurons exhibit different pharmacological profiles (see Straka and Dieringer, 2004): glycine is
643 the transmitter for the horizontal and GABA for the vertical VOR (Spencer et al., 1989; Straka and
644 Dieringer, 1993). However, rat abducens motoneurons have been shown to possess both glycine and
645 $GABA_A$ receptors, which in slice preparations elicit IPSPs with different time constants,
646 respectively (Lahjouji et al., 1996; Russier et al., 2002, Lorenzo et al., 2007). Compatible with these
647 results, all abducens motoneurons in *Xenopus* tadpoles receive a GABAergic and glycinergic
648 inhibition. The more tonic $GABA_A$ receptor-mediated inhibition, however, is unrelated to sinusoidal
649 rotation, as such of non-vestibular origin and potentially mediated by extrasynaptic $GABA_A$
650 receptors, compatible with a respective location of these receptors in rat abducens motoneurons
651 (Lorenzo et al., 2007). This also complies with the role of $GABA_A$ receptors in regulating neuronal
652 excitability and recruitment threshold of rat oculomotor motoneurons (Torres-Torrelo et al., 2014)
653 and with the robust increase in firing rate following gabazine injections into the abducens nucleus in
654 the current study. The more dendritic location of glycine receptors in rat abducens motoneurons
655 (Lorenzo et al., 2007) is compatible with the rather variable effects of glycinergic inhibition in
656 abducens motoneurons. However, the present experiments with isolated inhibitory vestibular inputs
657 suggest that glycine is nonetheless capable of mediating the inhibitory component of the horizontal
658 angular VOR (Straka and Dieringer, 1993), although it likely predominates in spontaneously active
659 abducens motoneurons similar to the commissural inhibition of tonic but not phasic frog central
660 vestibular neurons (Malinvaud et al., 2010). Single cell intracellular characterization of membrane
661 properties and pharmacological profiles will definitively resolve the functional role and efficiency

of semicircular canal-activated glycinergic inhibition in different types of abducens motoneurons during head rotation.

References

Beraneck M, Pfanzelt S, Vassias I, Rohregger M, Vibert N, Vidal P-P, Moore LE, Straka H (2007) Differential intrinsic response dynamics determine synaptic signal processing in frog vestibular neurons. J Neurosci 27:4283–4296.

Birch PJ, Grossman CJ, Hayes AG (1988) 6,7-Dinitro-quinoxaline-2,3-dion and 6-nitro,7-cyano-quinoxaline-2,3-dion antagonise responses to NMDA in the rat spinal cord via an action at the strychnine-insensitive glycine receptor. Eur J Pharmacol 156:177–180.

Branoner F, Straka H (2015) Semicircular canal-dependent developmental tuning of translational vestibulo-ocular reflexes in Xenopus laevis. Dev Neurobiol 75:1051-1067

Büttner-Ennever JA, Horn AK, Scherberger H, D'Ascanio P (2001) Motoneurons of twitch and nontwitch extraocular muscle fibers in the abducens, trochlear, and oculomotor nuclei of monkeys. J Comp Neurol 438:318–335.

Büttner-Ennever JA, Horn AK (2002) Oculomotor system: a dual innervation of the eye muscles from the abducens, trochlear, and oculomotor nuclei. Mov Disord 17 Suppl 2:S2–S3.

Carrascal L, Nieto-Gonzalez JL, Torres B, Nunez-Abades P (2009) Changes in somatodendritic morphometry of rat oculomotor nucleus motoneurons during postnatal development. J Comp Neurol 514:189–202.

Chagnaud BP, Banchi R, Simmers J, Straka H (2015) Spinal corollary discharge modulates motion sensing during vertebrate locomotion. Nat Commun 6:7982.

685 Davis-López de Carrizosa MA, Morado-Díaz CJ, Miller JM, de la Cruz RR, Pastor AM (2011)
686 Dual encoding of muscle tension and eye position by abducens motoneurons. J Neurosci
687 31:2271–2279.

688 Dean P (1997) Simulated recruitment of medial rectus motoneurons by abducens internuclear
689 neurons: synaptic specificity vs. intrinsic motoneuron properties. J Neurophysiol 78:1531–
690 1549.

691 Delgado-Garcia JM, del Pozo F, Baker R (1986) Behavior of neurons in the abducens nucleus of the
692 alert cat – I. Motoneurons. Neuroscience 17:929–952.

693 Dieringer N, Precht W (1977) Modification of synaptic input following unilateral labyrinthectomy.
694 Nature 269:431–433.

695 Dieringer N, Precht W (1986) Functional organization of eye velocity and eye position signals in
696 abducens motoneurons of the frog. J Comp Physiol A 158:179–194.

697 Dietrich H, Glasauer S, Straka H (2014) Vestibulo-ocular reflexes are mediated by functionally
698 distinct subgroups of extraocular motoneurons. Soc Neurosci Abstr 44:247.07.

699 Dietrich H, Straka H (2016) Prolonged vestibular stimulation induces homeostatic plasticity of the
700 vestibulo-ocular reflex in larval *Xenopus laevis*. Eur J Neurosci 44:1787–1796.

701 Durand J, Engberg I, Tyc-Dumont S (1987) L-glutamate and N-methyl-D-asparatate actions on
702 membrane potential and conductance of cat abducens motoneurones. Neurosci Lett 79:295–
703 300.

704 Durand J (1991) NMDA Actions on Rat Abducens Motoneurons. Eur J Neurosci 3:621–633.

705 Eberhorn AC, Ardeleanu P, Büttner-Ennever JA, Horn AK (2005) Histochemical differences
706 between motoneurons supplying multiply and singly innervated extraocular muscle fibers. J
707 Comp Neurol 491:352–366.

Eberhorn AC, Büttner-Ennever JA, Horn AK (2006) Identification of motoneurons supplying multiply- or singly-innervated extraocular muscle fibers in the rat. Neuroscience 137:891–903.

Edmonds B, Gibb AJ, Colquhoun D (1995) Mechanisms of activation of glutamate receptors and the time course of excitatory synaptic currents. Annu Rev Physiol 57:495–519.

Evinger C, Baker R (1991) Are there subdivisions of extraocular motoneuronal pools that can be controlled separately? In: Motor Control: Concepts and Issues (Humphrey DR, Freund H-J, eds), pp 23–31. John Wiley & Sons, Chichester, UK.

Gensberger KD, Gravot C, Hoffman LF, Paulin M, Straka H (2015) Dynamic diversity of horizontal canal afferent neurons in *Xenopus laevis* tadpoles. Soc Neurosci Abstr 45: 235.07.

Gensberger KD, Kaufmann AK, Dietrich H, Branoner F, Banchi R, Chagnaud BP, Straka H (2016) Galvanic vestibular stimulation: cellular substrates and response patterns of neurons in the vestibulo-ocular network. J Neurosci in press.

Goldberg JM (2000) Afferent diversity and the organization of central vestibular pathways. Exp Brain Res 130:277–297.

Hänzi S, Banchi R, Straka H, Chagnaud BP (2015) Locomotor corollary activation of trigeminal motoneurons: coupling of discrete motor behaviors. J Exp Biol 218:1748–1758.

Holt GR, Softky WR, Koch C, Douglas RJ (1996) Comparison of discharge variability in vitro and in vivo in cat visual cortex neurons. J Neurophysiol 75:1806–1814.

Horn AK, Leigh RJ (2011) The anatomy and physiology of the ocular motor system. Handb Clin Neurol 102:21–69.

Jamali M, Carriot J, Chacron MJ, Cullen KE (2013) Strong correlations between sensitivity and variability give rise to constant discrimination thresholds across the otolith afferent population. J Neurosci 33:11302–11313.

731 Keifer J, Clark TG (2003) Abducens conditioning in in vitro turtle brain stem without cerebellum
732 requires NMDA receptors and involves upregulation of GluR4-containing AMPA receptors.
733 Exp Brain Res 151:405–410.

734 Lahjouji F, Barbe A, Chazal G, Bras H (1996) Evidence for colocalization of GABA and glycine in
735 afferents to retrogradely labelled rat abducens motoneurones. Neurosci Lett 206:161–164.

736 Lambert FM, Beck JC, Baker R, Straka H (2008) Semicircular canal size determines the
737 developmental onset of angular vestibuloocular reflexes in larval *Xenopus*. J Neurosci
738 28:8086–8095.

739 Lambert FM, Combes D, Simmers J, Straka H (2012) Gaze stabilization by efference copy
740 signaling without sensory feedback during vertebrate locomotion. Curr Biol 22:1649–1658.

741 Long SK, Smith DA, Siarey RJ, Evans RH (1990) Effect of 6-cyano-2,3-dihydroxy-7-nitro-
742 quinoxaline (CNQX) on dorsal root-, NMDA-, kainate- and quisqualate-mediated
743 depolarization of rat motoneurones in vitro. Br J Pharmacol 100:850–854.

744 Lorenzo LE, Russier M, Barbe A, Fritschy JM, Bras H (2007) Differential organization of gamma-
745 aminobutyric acid type A and glycine receptors in the somatic and dendritic compartments of
746 rat abducens motoneurons. J Comp Neurol 504:112–126.

747 Malinvaud D, Vassias I, Reichenberger I, Rössert C, Straka H (2010) Functional organization of
748 vestibular commissural connections in frog. J Neurosci 30:3310–3325.

749 Mendell LM (2005) The size principle: a rule describing the recruitment of motoneurons. J
750 Neurophysiol 93:3024–3026.

751 Nieto-Gonzalez JL, Carrascal L, Nunez-Abades P, Torres B (2007) Phasic and tonic firing
752 properties in rat oculomotor nucleus motoneurons, studied in vitro. Eur J Neurosci 25:2682–
753 2696.

754 Nieuwkoop PD, Faber J (1994) Normal Table of *Xenopus* Laevis (Daudin): A Systematical and
755 Chronological Survey of the Development from the Fertilized Egg Till the End of
756 Metamorphosis. Garland Pub.

757 Pastor AM, Torres B, Delgado-Garcia JM, Baker R (1991) Discharge characteristics of medial
758 rectus and abducens motoneurons in the goldfish. J Neurophysiol 66:2125–2140.

759 Pastor AM, Gonzalez-Forero D (2003) Recruitment order of cat abducens motoneurons and
760 internuclear neurons. J Neurophysiol 90:2240–2252.

761 Pfanzelt S, Rössert C, Rohregger M, Glasauer S, Moore LE, Straka H (2008) Differential dynamic
762 processing of afferent signals in frog tonic and phasic second-order vestibular neurons. J
763 Neurosci 28:10349–10362.

764 Precht W (1978) Neuronal operations in the vestibular system. Studies of brain function. Berlin
765 Heidelberg: Springer.

766 Priesol AJ, Jones GE, Tomlinson RD, Broussard DM (2000) Frequency-dependent effects of
767 glutamate antagonists on the vestibulo-ocular reflex of the cat. Brain Res 857:252–264.

768 Ramlochansingh C, Branoner F, Chagnaud BP, Straka H (2014) Efficacy of tricaine
769 methanesulfonate (MS-222) as an anesthetic agent for blocking sensory-motor responses in
770 *Xenopus laevis* tadpoles. PLoS One 9:e101606.

771 Rössert C, Moore LE, Straka H, Glasauer S (2011) Cellular and network contributions to vestibular
772 signal processing: impact of ion conductances, synaptic inhibition, and noise. J Neurosci
773 31:8359–8372.

774 Russier M, Kopysova IL, Ankri N, Ferrand N, Debanne D (2002) GABA and glycine co-release
775 optimizes functional inhibition in rat brainstem motoneurons in vitro. J Physiol 541:123–137.

776 Schuller JM, Knorr AG, Glasauer S, Straka H (2014) Task-specific activation of extraocular
777 motoneurons in *Xenopus laevis*. Soc Neurosci Abstr. 44: 247.06.

778 Spencer RF, Wenthold RJ, Baker R (1989) Evidence for glycine as an inhibitory neurotransmitter of
779 vestibular, reticular, and prepositus hypoglossi neurons that project to the cat abducens
780 nucleus. J Neurosci 9:2718–2736.

781 Sterling P (1977) Anatomy and physiology of goldfish oculomotor system. I. Structure of abducens
782 nucleus. J Neurophysiol 40:557–572.

783 Straka H, Dieringer N (1993) Electrophysiological and pharmacological characterization of
784 vestibular inputs to identified frog abducens motoneurons and internuclear neurons in vitro.
785 Eur J Neurosci 5:251–260.

786 Straka H, Gilland E, Baker R (1998) Rhombomeric organization of brainstem motor neurons in
787 larval frogs. Biol Bull 195:220–222.

788 Straka H, Baker R, Gilland E (2001) Rhombomeric organization of vestibular pathways in larval
789 frogs. J Comp Neurol 437:42–55.

790 Straka H, Dieringer N (2004) Basic organization principles of the VOR: Lessons from frogs. Prog
791 Neurobiol 73:259–309.

792 Straka H, Vibert N, Vidal PP, Moore LE, Dutia MB (2005) Intrinsic membrane properties of
793 vertebrate vestibular neurons: Function, development and plasticity. Prog Neurobiol 76:349–
794 392.

795 Straka H, Baker R, Gilland E (2006) Preservation of segmental hindbrain organization in adult
796 frogs. J Comp Neurol 494:228–245.

797 Straka H, Lambert FM, Pfanzelt S, Beraneck M (2009) Vestibulo-ocular signal transformation in
798 frequency-tuned channels. Ann N Y Acad Sci 1164:37–44.

799 Torres-Torrelo J, Torres B, Carrascal L (2014) Modulation of the input-output function by GABAA
800 receptor-mediated currents in rat oculomotor nucleus motoneurons. J Physiol 592:5047–5064.

Ugolini G, Klam F, Doldan Dans M, Dubayle D, Brandi AM, Büttner-Ennever J, Graf W (2006) Horizontal eye movement networks in primates as revealed by retrograde transneuronal transfer of rabies virus: differences in monosynaptic input to “slow” and “fast” abducens motoneurons. J Comp Neurol 498:762–785.

Figure legends

Figure 1 Anatomical organization of the abducens nucleus in larval *Xenopus laevis*. ***A,*** Confocal reconstruction of a hindbrain whole-mount preparation of a stage 54 tadpole depicting retrogradely labeled abducens motoneurons in rhombomere (r) 5 following uni- (***A*$_{1,3}$**) or bilateral (***A*$_2$**) application of Alexa Fluor 488 dextran to the VIth motor nerve(s) at the level of the lateral rectus muscle; brainstem-crossing fibers, visualized by 633 nm illumination (red staining in ***A*$_1$**), indicate the center of r1-7, respectively; inset in ***A*$_1$** is a higher magnification of the outlined area (VI). ***B,*** Somal size (cross-sectional area, ***B*$_1$**) and circularity (***B*$_2$**) distributions of retrogradely labeled abducens motoneurons (n = 275); Circularity of 1 indicates a round cell body. ***C,*** Dependency of somal circularity on the medio-lateral (***C*$_1$**) and rostro-caudal (***C*$_2$**) motoneuronal position within the abducens nucleus; positions were normalized to the most medial/rostral (0) and most lateral/caudal (1) part of the nucleus, respectively.

Figure 2 Semi-intact *Xenopus* preparations for electrophysiological recordings and pharmacological perturbations of extraocular motor nerve activity. ***A,*** Photomicrographs, depicting in ***A*$_1$** an isolated head of a stage 54 tadpole with intact inner ears, central nervous system and eyes and in ***A*$_2$** the extraocular motor innervation of eye muscles. ***B,*** Schematic of the semi-intact preparation, indicating LR (VI) and SO (IV) nerve recording electrodes and the pipette for pressure injection of drugs into the abducens nucleus; curved double arrows indicate horizontal turntable

rotation. ***C,*** Representative multi-unit abducens nerve discharge (black trace) and the activity of extracted single-units (red and blue traces) based on spike shape analysis. ***D,E,*** Spike templates (s.u. 1 and s.u. 2 in ***D***) of the two single-units isolated in ***C*** and graphical illustration of the principal component analysis (PC1, PC2) used for the spike sorting with respect to spike shape and amplitude (***E***). Dashed gray sine wave in ***C*** indicates head motion stimulus velocity (H_{vel}). Picture in $\boldsymbol{A_2}$ was modified from Lambert et al., 2008.

Figure 3. Discharge properties of silent and spontaneously active abducens motor units. ***A,*** Representative examples of units with moderate ($\boldsymbol{A_1}$) and low (red arrowheads in $\boldsymbol{A_2}$) spontaneous activity and a typical silent unit (blue arrowhead in $\boldsymbol{A_2}$) at rest (left traces in $\boldsymbol{A_{1,2}}$) and during multiple cycles of horizontal sinusoidal head rotation (right traces in $\boldsymbol{A_{1,2}}$). ***B,*** Histogram depicting the distribution of neuronal firing rates at rest; the distribution between 0 and 1 spikes/s (light green bar) is plotted at an extended scale in the inset; the dark green bar indicates units that were silent at rest. ***C,*** Correlation between the mean interspike interval (ISI) and discharge regularity (CV2) in $\boldsymbol{C_1}$ for all spontaneously active units (n = 33) and in $\boldsymbol{C_2}$ for units with a resting discharge between 1 and 10 Hz (gray area in $\boldsymbol{C_1}$; n = 25, linear correlation r^2 = 0.345). Color code in $\boldsymbol{C_2}$: Red, group I units, blue: group II units, black: unspecified units recorded only at a single frequency (0.5 Hz). ***D,*** Average firing rate modulation (±SEM, shaded areas) of a population of spontaneously active (sa; $\boldsymbol{D_1}$) and silent (s; $\boldsymbol{D_2}$) motor units over a single motion cycle at 0.5 Hz and different peak stimulus velocities. ***E,*** Linear correlation between the resting rate and modulation depth of spontaneously active neurons during rotation at 0.5 Hz with a peak velocity of ±30°/s (n = 33, r^2 = 0.121). Inset depicts differences in activation threshold (Act. thr.) between silent (s) and spontaneously active (sa) units. Dashed gray sine waves in ***D*** indicate head motion stimulus velocity (H_{vel}).

Figure 4. Discharge properties of group I and group II abducens motor units. ***A,B,*** Average rotation-evoked firing rate modulation (±SEM, shaded areas) of spontaneously active group I ($\boldsymbol{A_1}$, n

= 8) and group II (***A*****$_2$**, *n* = 6) and silent group I (***B*****$_1$**, *n* = 6) and group II (***B*****$_2$**, *n* = 4) motor units over a single rotation cycle at a stimulus frequency of 0.5 Hz and varying peak velocities (left in ***A*****$_{1,2}$**) and at a stimulus peak velocity of ±30°/s and varying frequencies (right in ***A*****$_{1,2}$**; ***B*****$_{1,2}$**); dashed gray sine waves indicate head motion stimulus velocity (H_{vel}). ***C,D,*** Dependency of the maximal discharge modulation depth (***C*****$_{1,2}$**,***D*****$_{1,2}$**) and phase *re* stimulus velocity (***C*****$_{3,4}$**,***D*****$_{3,4}$**) of rotation-evoked responses (±SEM) on stimulus peak velocity (***C*****$_{1,3}$**,***D*****$_{1,3}$**) and frequency (***C*****$_{2,4}$**,***D*****$_{2,4}$**) in spontaneously active (***C***) and silent (***D***) group I (black) and group II (red) motor units.

Figure 5. Discharge properties of non-VOR abducens motor units. ***A,*** Representative example of a non-VOR unit at rest (***A*****$_1$**) and during sinusoidal head rotation over multiple rotation cycles at 0.5 Hz and ±60°/s peak velocity (***A*****$_2$**) with its average response over a single cycle (***A*****$_3$**). ***B,*** Representative example of a multi-unit abducens nerve discharge during multiple cycles of head rotation at 0.5 Hz and ±30°/s peak velocity. Note that non-VOR units (*) have the highest spike amplitudes. ***C,*** Representative example of a multi-unit abducens nerve discharge during multiple rotation cycles before and after contralateral VIIIth nerve transection. Note that a single non-VOR unit remains active after the lesion (*). Dashed sine waves in ***A*****$_3$** and red and gray sine waves in ***B*** and ***C*** indicate head motion stimulus velocity (H_{vel}). Calibration bar in ***A*****$_1$** applies to ***A*****$_2$**.

Figure 6. Excitatory neurotransmitter profile of group I and group II abducens motor units. ***A,B,*** Representative examples of spontaneously active group I (***A***) and group II (***B***) units before and after focal injection of D-AP5 (red, 500 µM) and NBQX (blue, 10 µM) into the respective abducens nucleus. Single-units (s.u., gray traces) were identified by spike sorting. ***C,D,*** Average normalized firing rate modulation over a single rotation cycle (±SEM, shaded areas) of representative spontaneously active (sa; ***C*****$_1$**,***D*****$_1$**) and silent (s; ***C*****$_2$**,***D*****$_2$**) group I (***C***) and group II (***D***) abducens motor units, at a stimulus frequency of 0.5 Hz and peak velocity of ± 30°/s, before and after D-AP5 (red) and NBQX (blue) injection into the respective abducens nucleus. ***E,*** Bar charts depicting the

879 average (±SEM) residual components of the response integrals (***E₁***) and phase shifts of the response
880 peaks (***E₂***) after NMDA (AP5, red) and AMPA (NBQX, blue) receptor blockade in spontaneously
881 active (sa) and silent (s) group I and group II abducens motoneurons. Dashed gray sine waves in ***A-***
882 ***D*** indicate head motion stimulus velocity (H_{vel}).
883
884 **Figure 7**. Inhibitory neurotransmitter profile of abducens motor units. ***A,B,*** Representative example
885 of a multi-unit abducens nerve discharge over multiple rotation cycles (***A***) and average responses
886 (***B***) over a single cycle (*n* = 3, ±SEM, shaded areas) before (black) and after surgical removal of the
887 ipsilateral horizontal canal cupula (red). ***C,*** Schematic of a semi-intact preparation depicting the
888 recording and stimulation paradigm, ipsilateral neuronal VOR connections and the removal of
889 crossed excitatory vestibular inputs to abducens motoneurons by midline section (dotted line). ***D,***
890 Inhibitory modulation of average multi-unit abducens nerve responses over a single motion cycle (*n*
891 = 6, ±SEM, shaded areas) at 0.5 Hz and different stimulus velocities of head rotation after midline
892 section. ***E,F,*** Representative example (***E***) and average responses (***F***) over a single motion cycle (*n* =
893 6, ±SEM, shaded areas) of the multi-unit abducens nerve discharge before (control, black), after
894 midline section (blue) and subsequent focal strychnine (10 µM) injection into the respective
895 abducens nucleus (red). For comparison, average control responses over a single rotation cycle in
896 the intact preparation are indicated in the inset in ***F***. ***G,H,*** Representative example (***G***) and average
897 responses (***H***) over a single motion cycle (*n* = 7 single-units, ±SEM, shaded areas) of an isolated
898 single-unit before (black) and after focal injection of gabazine (10 µM) into the respective abducens
899 nucleus. Dotted lines in ***H*** represent average responses of spontaneously active units (3 out of 7).
900 The bar chart in the inset in ***H*** shows the average increase in firing rate of all single-units (*n* = 7,
901 ±SEM) at different peak stimulus velocities (at 0.5 Hz). abd, abducens; cup, cupula; VN, vestibular
902 nucleus. Gray (dashed) sine waves in ***A,B,E-H*** indicate head motion stimulus velocity (H_{vel}).
903
904

Figure 8. Computational modeling of eye movements. ***A,*** Schematic depicting video recordings of eye movements in semi-intact *Xenopus* tadpole preparations during horizontal sinusoidal head rotation. ***B,*** Averaged eye positions (green, Eye_{pos}) and corresponding sinusoidal fits (blue, sine fit) over a single cycle of sinusoidal head rotation at three different frequencies (at ±30°/s peak velocity). ***C,*** Schematic view of the model used to evaluate whether observed motoneuron spike patterns sufficiently explain eye movement behavior. Left: spikes recorded from different motoneurons; black: original recordings; red: 180° shifted version to account for the innervation of the contralateral muscle. Middle: time courses of simulated muscle contractions derived from spike trains in the left column. Right: weighted sum (positive weights, wi) of muscle contractions fitted to original VOR eye movement recordings (green trace) in response to head rotation (black dashed trace) and resultant simulations of eye movements (blue trace). ***D,*** Contributions of group I (blue) and group II (red) motor units to the simulation of actual eye movements (green, Eye_{pos}) at 0.1, 0.5 and 1 Hz head rotation. E, Explained variances for eye movement simulations either using all (black) or only group I (blue), group II (red), spontaneously active (sa, gray) or silent (s, gray) abducens motor units. Gray sine waves and dashed black/green vertical lines in ***B*** indicate head motion stimulus position (H_{pos}) and phase relation of the responses, respectively.

Figure 1
Dietrich et al.
Abducens motoneuronal responses

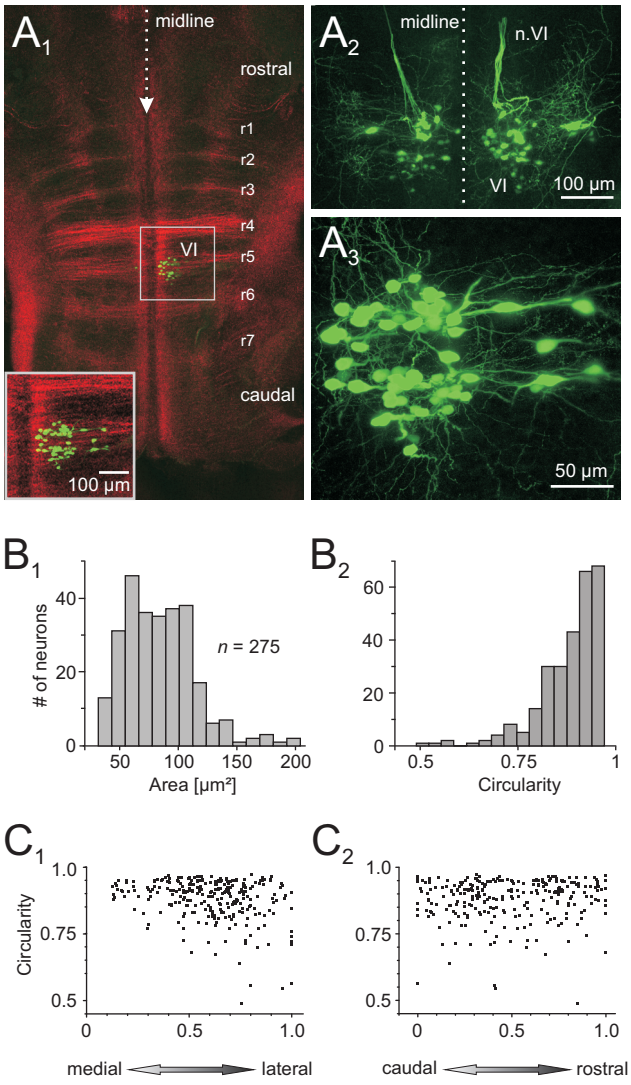

Figure 2
Dietrich et al.
Abducens motoneuronal responses

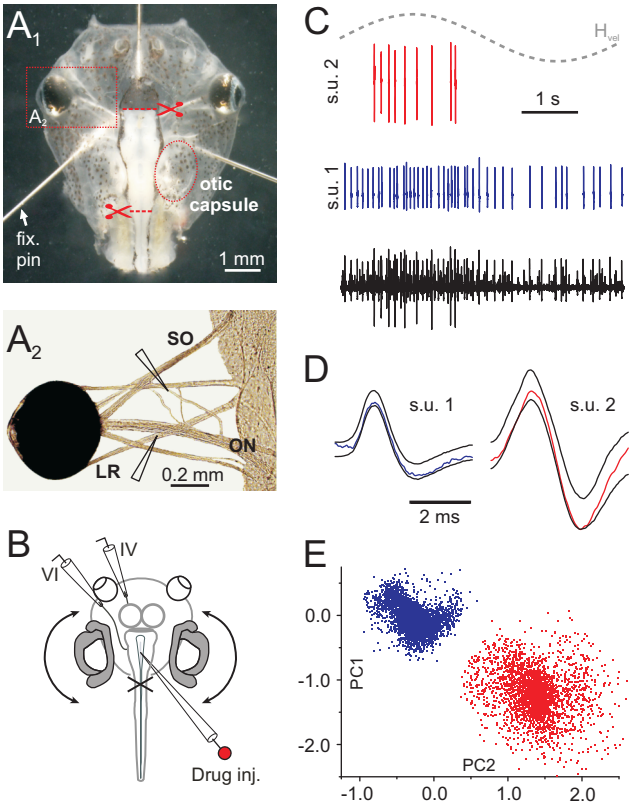

Figure 3
Dietrich et al.
Abducens motoneuronal responses

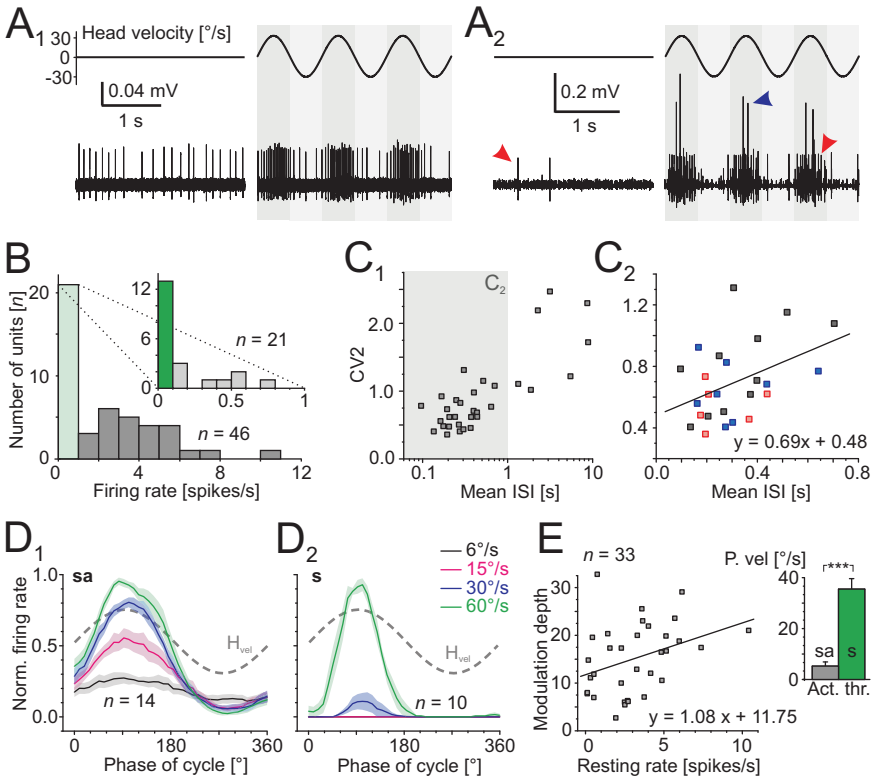

Figure 4
Dietrich et al.
Abducens motoneuronal responses

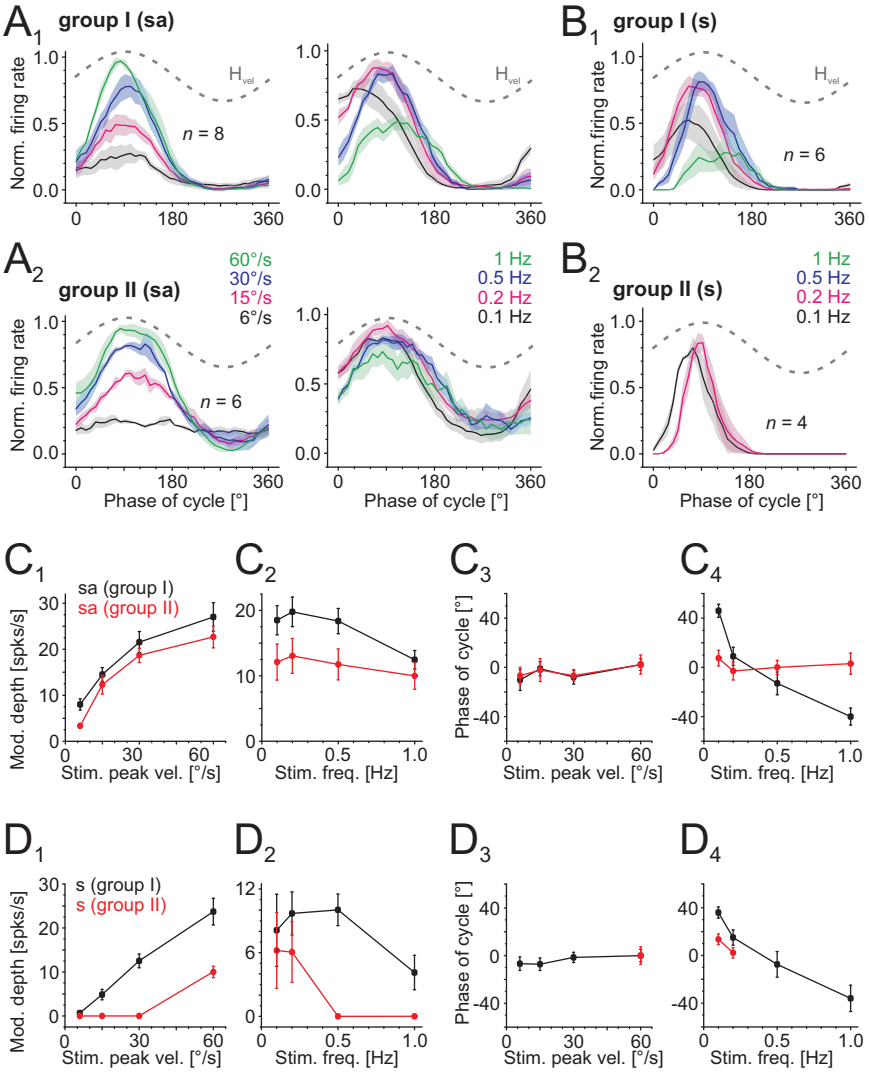

Figure 5
Dietrich et al.
Abducens motoneuronal responses

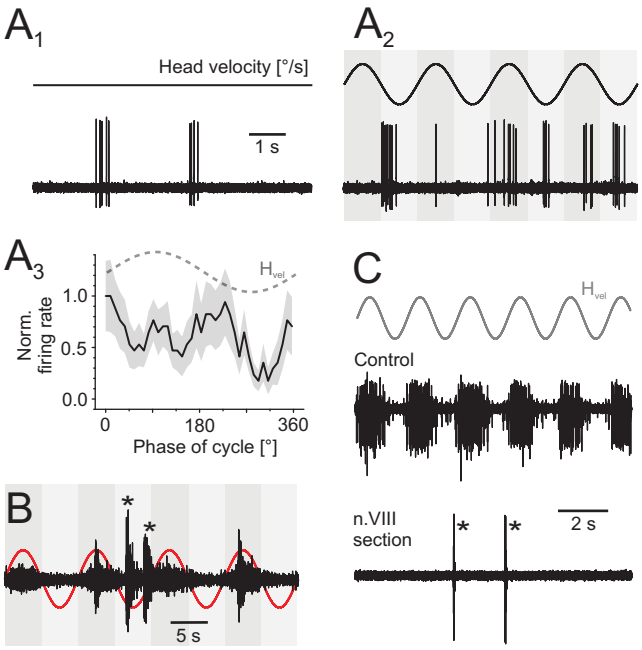

Figure 6
Dietrich et al.
Abducens motoneuronal responses

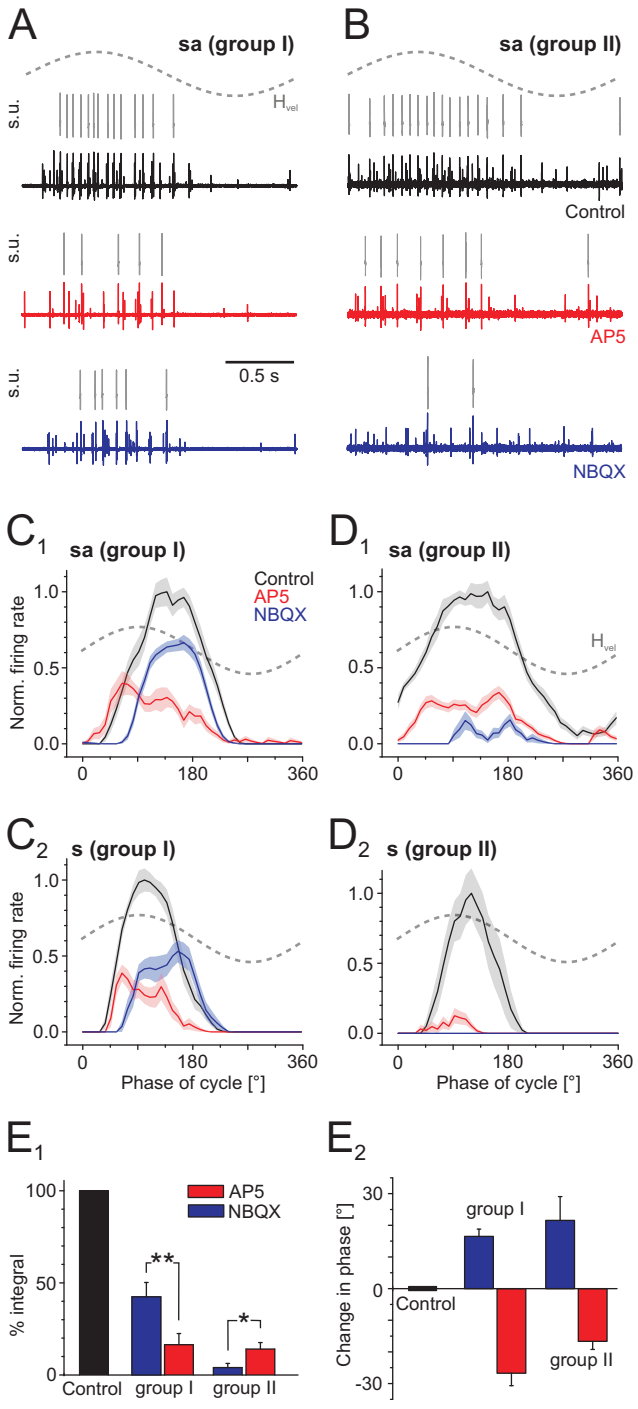

Figure 7
Dietrich et al.
Abducens motoneuronal responses

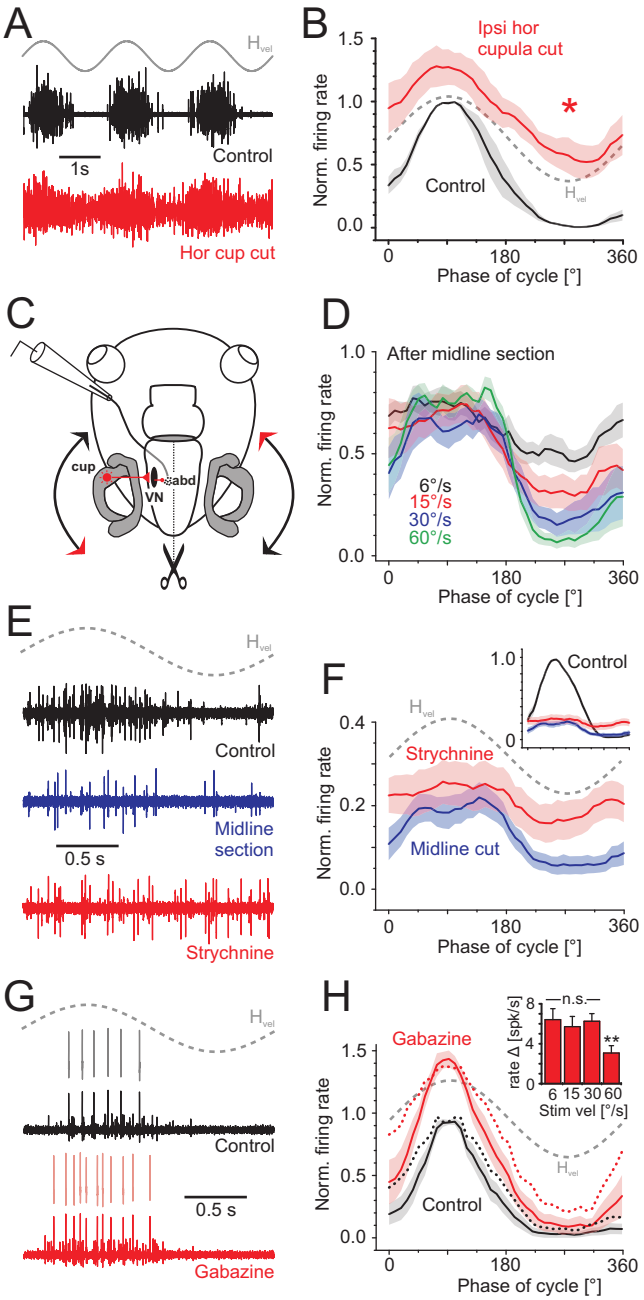

Figure 8
Dietrich et al.
Abducens motoneuronal responses

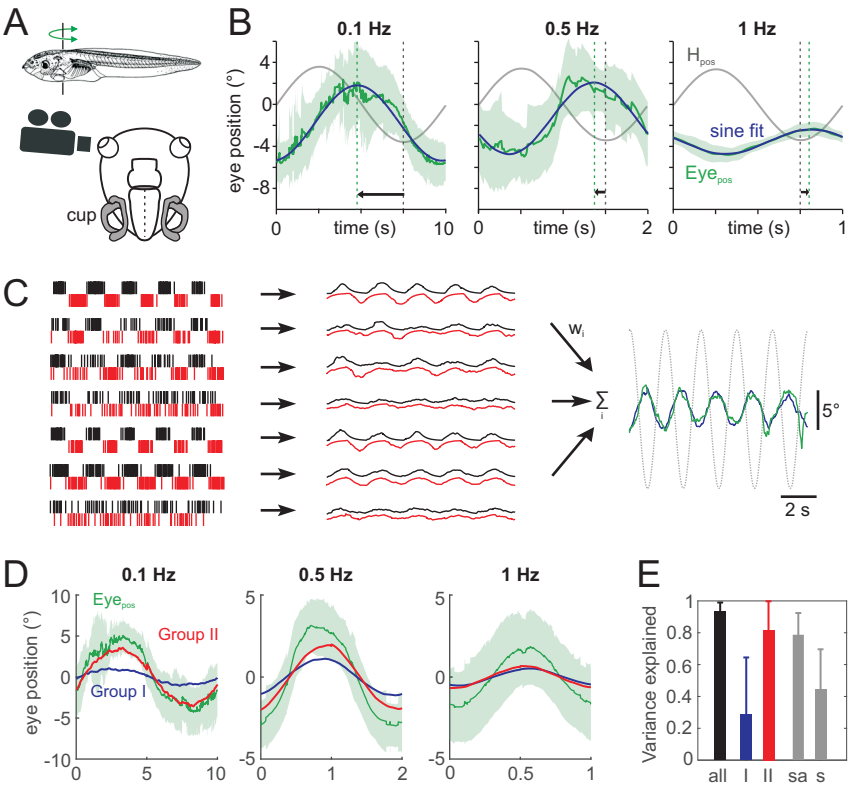

Results Part II

Prolonged vestibular stimulation induces homeostatic plasticity of the vestibulo-ocular reflex in larval *Xenopus laevis*

Haike Dietrich and Hans Straka

European Journal of Neuroscience, 2016

Contributions of HD:

- Planning of all experiments
- Performance of all experiments
- Analysis of all data
- Design and assembly of all figures
- Writing and revision of the manuscript

EJN European Journal of Neuroscience

FENS Federation of European Neuroscience Societies

European Journal of Neuroscience, pp. 1–10, 2016 doi:10.1111/ejn.13269

Prolonged vestibular stimulation induces homeostatic plasticity of the vestibulo-ocular reflex in larval *Xenopus laevis*

Haike Dietrich[1,2] and Hans Straka[1]
[1]Department Biology II, Ludwig-Maximilians-University Munich, Großhaderner Str. 2, Planegg 82152, Germany
[2]Graduate School of Systemic Neurosciences, Ludwig-Maximilians-University Munich, Planegg, Germany

Keywords: adaptation, cerebellum, extraocular motoneurons, semicircular canal

Edited by Ying-Shing Chan
Received 21 January 2016, revised 21 April 2016, accepted 22 April 2016

Abstract

Vestibulo-ocular reflexes (VOR) stabilise retinal images during head/body motion in vertebrates by generating spatio-temporally precise extraocular motor commands for corrective eye movements. While VOR performance is generally robust with a relatively stable gain, cerebellar circuits are capable of adapting the underlying sensory-motor transformation. Here, we studied cerebellum-dependent VOR plasticity by recording head motion-induced lateral rectus and superior oblique extraocular motor discharge in semi-intact preparations of *Xenopus laevis* tadpoles. In the absence of visual feedback, prolonged sinusoidal rotation caused either an increase or decrease of the VOR gain depending on the motion stimulus amplitude. The observed changes in extraocular motor discharge gradually saturated after 20 min of constant rotation and returned to baseline in the absence of motion stimulation. Furthermore, plastic changes in lateral rectus and superior oblique motor commands were plane-specific for horizontal and vertical rotations, respectively, suggesting that alterations are restricted to principal VOR connections. Comparison of multi- and single-unit activity indicated that plasticity occurs in all recorded units of a given extraocular motor nucleus. Ablation of the cerebellum abolished motoneuronal gain changes and prevented the induction of plasticity, thus demonstrating that both acquisition and retention of this type of plasticity require an intact cerebellar circuitry. In conclusion, the plane-specific and stimulus intensity-dependent modification of the VOR gain through the feed-forward cerebellar circuitry represents a homeostatic plasticity that likely maintains an optimal working range for the underlying sensory-motor transformation.

Introduction

Gaze stabilising reflexes are evolutionarily well conserved (Straka *et al.*, 2014), ensure accurate perception of the animals' visual environment during head motion and assist in distinguishing between self- and passive motion (Land, 1999). Vestibulo-ocular reflexes (VOR) play an essential role in image stabilisation due to the rapid transformation of vestibular inputs into extraocular motor commands that elicit counteracting eye movements (Straka & Dieringer, 2004). However, fine-tuning of the spatio-temporal specificity of the three-neuronal VOR pathway necessitates the integration of visual feedback through a cerebellar side loop (Boyden *et al.*, 2004). Furthermore, the cerebellar circuitry implements changes in sensitivity for example during active vs. passive head movements (King, 2013; Brooks *et al.*, 2015), or, on a longer time-scale, during development and ageing (Boyden *et al.*, 2004).

Under experimental conditions, the VOR can be modified by visuo-vestibular mismatch paradigms that induce alterations in eye motion gain and phase depending on the motion direction of the visual world relative to head motion (Boyden *et al.*, 2004). During VOR adaptation, Purkinje cells in the vestibulo-cerebellum receive vestibular inputs via parallel fibres as well as visual motion signals through climbing fibres and provide feedback to the vestibular nucleus about potential mismatch between expected and actual retinal image slip (Boyden *et al.*, 2004). Surgical lesions of the cerebellum impair motor learning in goldfish (Michnovicz & Bennett, 1987), rabbits (Ito *et al.*, 1974), cats (Schultheis & Robinson, 1981) and monkeys (Zee *et al.*, 1981; Lisberger *et al.*, 1984; Rambold *et al.*, 2002) and reversible inactivation of Purkinje cells in cats causes comparable effects (Luebke & Robinson, 1994; Kassardjian *et al.*, 2005). In agreement with the assumption of Marr (1969) and Albus (1971), that neuronal plasticity occurs at the level of Purkinje cells, ablation or glutamatergic blockade of the latter immediately abolishes adapted responses in goldfish (Michnovicz & Bennett, 1987) and cats (Kassardjian *et al.*, 2005; Broussard *et al.*, 2011). However, more recent studies suggest that VOR plasticity occurs both within the vestibulo-cerebellum as well as at multiple extra-cerebellar sites, each with different time courses that contribute

Correspondence: Dr Hans Straka, as above.
E-mail: straka@lmu.de

jointly to VOR motor learning (Hirata & Highstein, 2001; Boyden *et al.*, 2004; Kassardjian *et al.*, 2005; Medina, 2011; Beraneck & Idoux, 2012; Clopath *et al.*, 2014). In addition to adjusting extraocular motor output during visuo-vestibular mismatch, the cerebellum is also involved in habituating VOR performance during prolonged sinusoidal low-frequency rotation in the dark that causes a pronounced depression of extraocular motor responses in goldfish (Dow & Anastasio, 1998, 1999), mice (Gutierrez-Castellanos *et al.*, 2013) and monkeys (Jäger & Henn, 1981). Thus, cerebellum-mediated extraocular motor plasticity occurs under various experimental conditions and presumably acts to adjust VOR performance to specific behavioural requirements.

Here, we tested the possibility to induce VOR plasticity in larval *Xenopus* by prolonged high- or low-magnitude vestibular stimulation in the absence of visual feedback. Using the advantages of semi-intact preparations for recordings and surgical manipulations, plastic changes of the extraocular motor output as well as the role of the cerebellum in modifying VOR performance were investigated.

Materials and methods

Animals and experimental preparation

Xenopus laevis tadpoles ($n = 53$) at developmental stages 53–54 (Nieuwkoop & Faber, 1994) were obtained from the in house animal breeding facility at the Biocenter-Martinsried (Ludwig-Maximilians-University Munich). Tadpoles were maintained in tanks with non-chlorinated water (17 °C) at a 12/12 light/dark cycle. Electrophysiological and pharmacological experiments were performed *in vitro* on isolated, semi-intact preparations and comply with the 'Principles of animal care', publication No. 86-23, revised 1985 of the National Institute of Health. Permission for these experiments was granted by the Regierung von Oberbayern (55.2-1-54-2532.3-59-12).

For all experiments, tadpoles were anaesthetised in 0.05% MS-222 (Pharmaq Ltd., UK), transferred into ice-cold frog Ringer (75 mM NaCl, 25 mM $NaHCO_3$, 2 mM $CaCl_2$, 2 mM KCl, 0.5 mM $MgCl_2$, and 11 mM glucose, pH 7.4) and decapitated at the level of the upper spinal cord. As previously described (Lambert *et al.*, 2012), the skin above the brain was removed, the cartilaginous skull was opened from the top (Fig. 1A), the forebrain was disconnected and both the optic nerves were transected. This procedure preserved the remaining central nervous system and vestibular sensory periphery including afferent connections as well as extraocular motoneuronal projections to the eye muscles, and thus allowed an *in vivo*-like activation of the vestibulo-ocular reflex (VOR) under controlled *in vitro* conditions (Straka & Simmers, 2012; Ramlochansingh *et al.*, 2014). To determine the impact of the cerebellum on the evoked plasticity, a cerebellectomy was performed in 10 preparations. In amphibians such as *Xenopus laevis*, the cerebellum forms a vertically oriented thin sheet at the rostral end of the hindbrain, connected to the latter by the bilateral peduncle (Llinas *et al.*, 1969). The cerebellum was removed by transecting the peduncle on both sides at the base with fine scissors.

Spontaneous and evoked neuronal activity of abducens and trochlear motoneurons was captured as single- or multi-unit recordings from the respective cranial nerve branches that innervate the lateral rectus (LR) and superior oblique (SO) eye muscles (Fig. 1B). Accordingly, LR and SO nerves were detached close to their target muscles and cleaned from surrounding tissue for extracellular nerve recordings with Ringer-filled suction electrodes. For the experiments, preparations were placed in a Sylgard-lined recording chamber that was continuously perfused with oxygenated Ringer solution at a temperature of 16.8 ± 0.2 °C.

Electrophysiology

The recording chamber with the preparation fixed to the Sylgard floor was mounted in the centre of the rotation axes of a two-axis computer-controlled motorised turntable (ACT-1002, Acutronic USA Inc., Switzerland) as described earlier (Lambert *et al.*, 2008). Spike discharge of extraocular motor nerves was recorded extracellularly (EXT 10-2F, npi electronics, Tamm, Germany) with individually adjusted glass suction electrodes, digitised at 20 kHz (CED 1401, Cambridge Electronic Design, UK) and stored on a computer for offline analysis. Glass microelectrodes for extracellular recordings were produced with a horizontal puller (P-87 Brown/Flaming, Sutter Instrument Company, USA) and the tips were individually broken to fit the respective nerve diameter. LR nerve motor units were activated by vertical-axis sinusoidal rotation while SO nerve motor units, which respond optimally to rotations along the plane formed by the ipsilateral posterior (iPC)/contralateral anterior semicircular canals (cAC), were activated by sinusoidal roll-motion in this plane (i.e. 45° relative to the body length axis; Branoner & Straka, 2015). Stimulus frequencies ranged from 0.1 to 1 Hz and peak velocity amplitudes from ±3°/s to ±60°/s.

VOR plasticity paradigm

Plasticity of the horizontal VOR was tested using prolonged vestibular stimulation (up to 30 min) with continuous sinusoidal horizontal head rotations. A 'test stimulus' at 0.5 Hz and a peak velocity of ±30°/s was used to compare LR nerve response modulation before and after prolonged application of a 'conditioning' stimulus that either evoked smaller or larger peak discharges compared to the test response. These conditioning stimuli were applied in random order and were separated by at least 20 min where the preparation remained stationary within the recording chamber. To test the plane specificity of the adaptive plasticity, test responses of the SO nerve (causing upward eye movements) before and after prolonged horizontal rotation served as a control. In addition, in a second set of experiments, VOR plasticity in the vertical plane was tested by recording SO nerve activity during sinusoidal rotation (test stimulus: 0.5 Hz, ±15°/s) along the plane formed by the iPC – cAC, while LR nerve responses served as a control for these experiments. To determine a potential role of the cerebellum in the adaptation of the extraocular motor discharge, prolonged stimulation was applied before and after cerebellectomy.

Data analysis

Peri-stimulus time histograms (PSTHs) of the averaged responses over single motion cycles, illustrating motoneuronal firing rates during sinusoidal head rotations, were obtained from raw data using Spike2 scripts for analysing the recorded multi- or single-unit spike discharge (Lambert *et al.*, 2008). For all stimulus parameters, the average responses were calculated from 10 to 20 successive cycles. PSTHs were further processed and analysed statistically using Microcal Origin 6.0G (OriginLab Corp., USA) and MATLAB® (MathWorks GmbH, USA) software. PSTHs were normalised to individual peak responses where applicable and averaged (±SEM or ±SD) for subsequent statistical comparison of paired parameters (Wilcoxon signed-rank test).

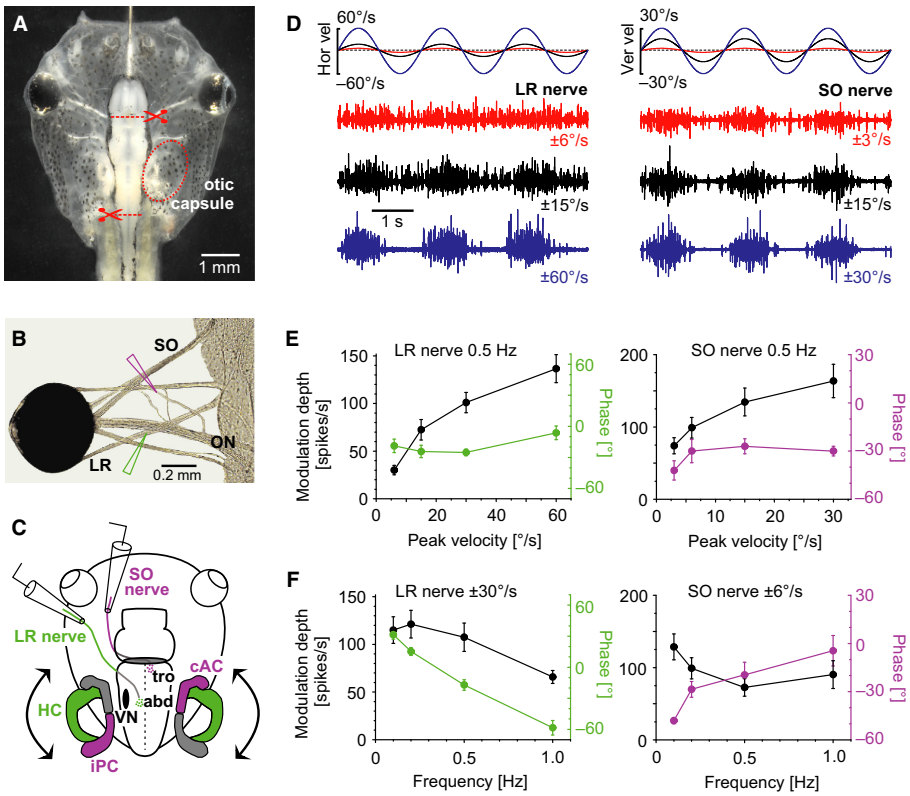

FIG. 1. Extraocular motor discharge during motion stimulation in *Xenopus*. A, Photomicrograph depicting a semi-intact tadpole preparation with functionally intact bilateral otic capsules, central nervous system and eyes. Red dashed lines indicate rostro-caudal positions for forebrain and spinal cord removal. B, Eye muscles and innervating extraocular motor nerve branches, isolated for suction electrode recordings of the lateral rectus (LR) and superior oblique (SO) motor nerves. C, Schematic of the experimental setting depicting the semi-intact preparation as well as the activation of LR (green) and SO (magenta) motor nerves during horizontal and vertical rotational stimulation of the bilateral horizontal (HC, green) or the ipsilateral posterior (iPC, magenta) and contralateral anterior (cAC, magenta) semicircular canals respectively. D, Representative example of multi-unit LR (left) and SO (right) nerve spike discharge over three cycles of horizontal and vertical head rotation (0.5 Hz) at three different stimulus peak velocities. E,F, Dependency of peak amplitude (black curves) and phase (green and magenta curves respectively) of rotation-evoked cyclic multi-unit LR (left) and SO (right) motor nerve responses (±SEM; n = 10) on stimulus peak velocity (E) and frequency (F). abd, abducens nucleus; hor/ver vel, horizontal/vertical head velocity; ON, optic nerve; tro, trochlear nucleus; VN, vestibular nucleus. Image in B was modified from Lambert *et al.* (2008).

Results

Motion-induced responses of lateral rectus and superior oblique motor nerves

VOR-related neuronal activity in abducens and trochlear motoneurons during sinusoidal head rotation was recorded as single- or multi-unit discharge from isolated LR (abducens) and SO (trochlear) nerves in semi-intact preparations of *Xenopus* tadpoles (Fig. 1C). The multi-unit spike discharge characteristics of the two extraocular motor nerves were determined at rest and during sinusoidal head motion (n = 10 for LR, n = 6 for SO nerve recordings). Based on the spatially specific semicircular canal – extraocular motor connectivity of the angular VOR in vertebrates (Straka & Dieringer, 2004), LR and SO nerve discharges modulated maximally during turntable rotation in the horizontal semicircular canal plane (green HC in Fig. 1C) and in a plane formed by the ipsilateral PC/contralateral AC (magenta iPC, cAC in Fig. 1C) respectively. In the absence of motion stimulation, the average multi-unit resting rate of 33.8 ± 7.4 spikes/s (n = 10) in the LR nerve was lower than the average rate of 52.0 ± 12.9 spikes/s (n = 6) in the SO nerve, possibly because the latter allowed a longer part of the nerve trajectory to be isolated and accessed by the suction electrode and thus more motor units to be recorded. During passive sinusoidal head rotation, both LR and SO nerve discharges were cyclically modulated (Fig. 1D). The peak discharge of modulated LR nerve responses coincided with contraversive horizontal turntable motion that maximally activated the contralateral horizontal canal, while the SO nerve peak discharge was aligned with motion in the direction of activation of the ipsilateral PC (Fig. 1D). At a given stimulus frequency (0.5 Hz in the first set of experiments), the peak firing rate increased asymptotically with increasing stimulus peak velocity in both the LR and SO nerves and reached 136.5 ± 14.7 and 163.5 ± 23.1 spikes/s, respectively, at maximal stimulus peak velocity (Fig. 1E). In addition, the timing (phase) of the peak response remained relatively constant over the range of employed stimulus velocities (green and magenta curves in Fig. 1E).

In contrast to the increase with stimulus velocity, the peak discharge of LR and SO nerve responses decreased with increasing stimulus frequencies between 0.1 and 1 Hz, although differently for the two extraocular motor nerves (compare black curves in left and right plots of Fig. 1F). For LR nerve responses, this decrease in peak amplitude was accompanied by a concurrent shift of the peak response from a phase lead of 31.5 ± 4.3° with respect to stimulus velocity at a frequency of 0.1 Hz to a phase lag of 58.5 ± 7.0° with respect to the stimulus at 1 Hz (at a peak velocity of ±30°/s; left plot of Fig. 1F). In contrast, the considerable phase lag of the SO nerve peak discharge of 48.0 ± 1.9° with respect to the stimulus at

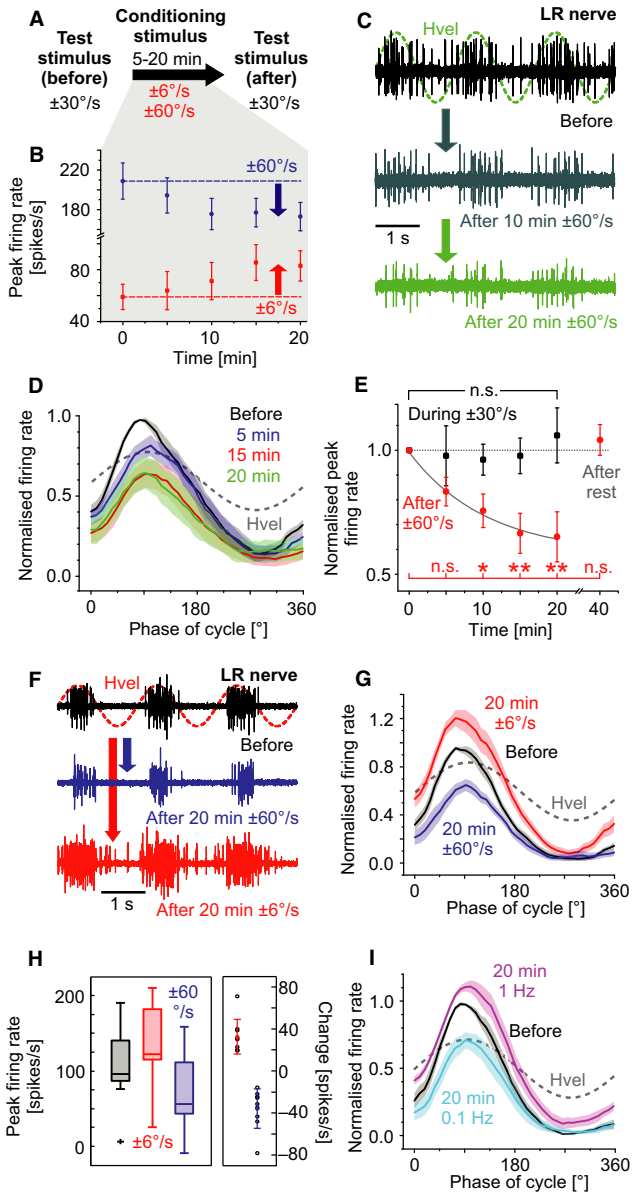

FIG. 2. Alterations of LR nerve discharge magnitudes following prolonged horizontal head rotation. A, Schematic depicting the experimental paradigm used for the induction of bidirectional plastic changes of the extraocular motor output. B, Time-dependent alterations of LR nerve peak firing rates (±SEM; $n = 9$) during prolonged sinusoidal rotation at 0.5 Hz with either high (±60°/s, blue) or low (±6°/s, red) stimulus peak velocities (conditioning stimulus amplitudes). C, Representative example of a multi-unit LR nerve discharge over three cycles of horizontal head rotation (Hvel, dashed green line) at the test stimulus intensity (0.5 Hz, ±30°/s peak velocity) before and after 10 and 20 min (colour-coded traces) of high-amplitude conditioning stimulation. D, Normalised LR nerve firing rate modulation (±SEM, shaded areas) at the test stimulus intensity averaged over a single cycle ($n = 9$) before and after different durations of prolonged high-amplitude conditioning stimulation (colour-coded curves). E, Dependency of the normalised peak firing rate of LR nerve test responses on the duration of high-amplitude conditioning stimulation (red symbols and line of exponential decay fit with a time constant of $\tau = 10.4$ s) and after keeping the preparation stationary for 20 min. Black symbols depict unaltered peak firing rates during prolonged stimulation at the test stimulus (±SEM; $n = 6$). F,G, Representative example of a multi-unit LR nerve discharge over three cycles of horizontal head rotation (Hvel, dashed red line) at the test stimulus intensity (F) and respective normalised LR nerve test responses averaged over a single cycle (±SEM, shaded areas; $n = 9$) (G) before (black) and after 20 min of high (blue) and low (red) amplitude conditioning stimulation respectively. H, Box plots depicting peak firing rates of test responses (left) and individual differences in peak firing rates (right) before (black) and after 20 min of prolonged low (red) and high (blue) amplitude conditioning stimulation ($n = 9$). Boxes indicate median and lower and upper quartiles; bars represent minimum and maximum values and crosses outliers (left). Individual differences are plotted as open black circles; mean ± SD in red and blue respectively (right). I, LR test responses (0.5 Hz, ±30°/s) averaged over a single motion cycle (±SEM, shaded areas; $n = 6$) before (black) and after 20 min conditioning stimulation at a constant peak velocity but lower (0.1 Hz; light blue) or higher (1 Hz; magenta) stimulus frequency. Dashed lines in D,G,I indicate head motion stimulus velocity (Hvel). *, $P < 0.05$; ** $P < 0.01$.

a frequency of 0.1 Hz decreased such that it was almost in phase (lag of 4.5 ± 9.5°) with the stimulus at 1 Hz (at a peak velocity of ±6°/s; right plot in Fig. 1F). The general phase lag of SO nerve responses over the entire range of stimulus frequencies, in contrast to LR nerve responses, is likely due to a co-activation of semicircular canal and utricular pathways during roll motion, with the influence of the gravity-sensitive otolith organ being largest at maximal turntable excursion (position). Thus, the combined contribution of semicircular canal and otolith signals to the extraocular motor output, each with different dynamics, causes an overall larger phase lag of motion-driven responses in the SO compared to the LR nerve. In addition, the modulation of SO nerve responses (Fig. 1D,E) usually required smaller stimulus intensities, again likely due to the additional contribution of otolith signals during roll motion. This difference in sensitivity prompted us to use different magnitudes for the test stimuli for LR (0.5 Hz; ±30°/s) and SO nerve responses (0.5 Hz; ±15°/s), respectively, when evaluating in the subsequent experiments whether extraocular motor responses were altered by prolonged stimulation.

Time-dependent homeostatic plasticity of the VOR

Potential homeostatic plasticity of vestibulo-ocular responses was explored by studying the consequences of prolonged motion stimulation. Control responses of the LR nerve to the 'test stimulus' were obtained before and immediately after continuous sinusoidal rotation of the preparation in the horizontal plane for 5–20 min with a stimulus amplitude or frequency that evoked extraocular motor responses with either larger or smaller peak discharge amplitudes ('conditioning stimulus'; Fig. 2A). During the period over which a high-magnitude conditioning stimulus (±60°/s, 0.5 Hz) was continuously applied, the discharge rate of the LR peak response (208.8 ± 18.3 spikes/s) decreased gradually by ~20% and saturated at a lower level (173.0 ± 14.4 spikes/s) after ~10 min of continuous sinusoidal rotation ($n = 9$, blue symbols in Fig. 2B). This attenuation of the peak firing rate also extended onto responses that were elicited by a stimulus with a lower magnitude such as the test stimulus (±30°/s, 0.5 Hz). In fact, the peak discharge of the LR nerve test response was also reduced to an extent that depended on the duration of the applied conditioning stimulus (Fig. 2C–E). A significant attenuation was observed after 10 min of rotation at the higher intensity conditioning stimulus (dark green trace in Fig. 2C). This reduction became even more pronounced after 15 and 20 min of continuous rotation (green trace in Fig. 2C, pooled data in Fig. 2D,E, $n = 6$) and followed a first-order exponential decay time course (grey line in Fig. 2E, $r^2 = 0.99$, $\tau = 10.4$ s). As stimulation times of >20 min did not cause further attenuation ($n = 3$, data not shown), test responses were compared before and after applying the conditioning stimulus for 20 min during all subsequent experiments. Quantification of the LR nerve test response attenuation following continuous

sinusoidal rotation at ±60°/s (blue trace in Fig. 2F) revealed a decrease of the peak firing rate from ~130 spikes/s to ~95 spikes/s (box plot in Fig. 2H) as indicated by the normalised averaged response over a single motion cycle (Fig. 2G, blue curve). The average difference of 36.0 ± 6.3 spikes/s corresponds to a decrease of 27% (n = 9, P = 0.0039, right plot in Fig. 2H). In contrast to this attenuation observed after prolonged high-intensity stimulation, continuous rotation for 20 min at the test stimulus intensity had no effect on the peak discharge of LR nerve responses (black symbols in Fig. 2E, n = 6).

In a second set of experiments, we tested whether prolonged stimulation with a low-magnitude conditioning stimulus (±6°/s, 0.5 Hz) provoked corresponding changes in the amplitude of LR nerve peak responses (Fig. 2A). During the period over which the low-magnitude conditioning stimulus was applied, the peak discharge of LR nerve responses (59.0 ± 9.8 spikes/s) increased gradually by ~50% and saturated at a peak firing rate of 82.9 ± 11.6 spikes/s after 15–20 min (n = 9, red symbols in Fig. 2B). Moreover, 20 min of sinusoidal rotation at the lower peak velocity of the conditioning stimulus (red trace/curve in Fig. 2F/G) also caused a facilitation of the LR nerve test response. Quantification of this effect revealed an increase of the peak discharge of the test responses from ~130 spikes/s to ~160 spikes/s (box plot in Fig. 2H) corresponding to an increase of 32.5 ± 5.5 spikes/s (25%, n = 9, P = 0.0039, right plot in Fig. 2H).

We further tested whether extraocular motor plasticity could also be induced by prolonged stimulation with different rotation frequencies that either evoked larger (0.1 Hz) or smaller extraocular motor discharge gains (1 Hz; Fig. 1F) compared to test responses of the LR nerve, evoked at 0.5 Hz (Fig. 2I). Indeed, prolonged conditioning stimulation for 20 min at 0.1 Hz resulted in an attenuation of the test responses from ~130 to ~95 spikes/s (difference: 35.5 ± 7.4 spikes/s; n = 6; P = 0.0313), corresponding to a decrease of 27%. In a complimentary fashion, continuous rotation of the preparation for 20 min with a conditioning stimulus at 1 Hz provoked a facilitation of the test response of 15% from ~130 to ~150 spikes/s (19.0 ± 4.9 spikes/s; n = 6; P = 0.0313).

LR nerve responses consistently returned to baseline values when keeping the semi-intact preparations stationary for 20 min after adaptation had occurred (data point at 40 min in Fig. 2E, n = 6). Thus, homeostatic plasticity of the VOR described here was not permanently consolidated as long-term changes of the motor output, but response magnitudes returned to initial values when the respective vestibular stimulation ceased for at least 20 min. Furthermore, control experiments where semi-intact preparations remained stationary in the recording chamber for up to 4 h (i.e. in the absence of a conditioning stimulus) revealed that the test response magnitude of the LR discharge remained unaltered, thus excluding unspecific effects related to extended periods of experimentation on *in vitro* preparations.

In seven experiments, one or more single units could be isolated from multi-unit LR nerve recordings (n = 11 units; see representative example of two single units in Fig. 3A,B). This allowed investigating plastic changes in individual motoneurons, in particular to address the question of whether the observed plasticity was due to alterations in the entire population of LR motoneurons or limited to some motor units while the discharge of others remained unaffected. To confirm that the same units were recorded during prolonged experimentation times, overlays of the spikes were made before and after 20 min of low- or high-magnitude stimulation (Fig. 3B, representative example of the same two units shown in Fig. 3A). Most isolated single units (8 out of 11 units) displayed a change in peak firing rate in both directions after application of the two different conditioning stimuli, similar to those observed in multi-unit recordings (e.g. unit 1 in Fig. 3A,C). However, in some cases, single units showed plastic changes only in one direction, as illustrated for the LR nerve single unit 2 in Fig. 3A,D. The peak discharge of this motor unit became facilitated after application of a weak conditioning stimulus, but did not express an attenuation of the test response after prolonged sinusoidal rotation at ±60°/s peak velocity (Fig. 3A, D). A possible explanation might derive from the response dynamics of this LR nerve motor unit during increasing stimulus intensities that revealed a saturation of the peak discharge above a stimulus velocity of ±30°/s (black and blue lines in Fig. 3E). Accordingly, application of the stronger conditioning stimulus (±60°/s) evoked

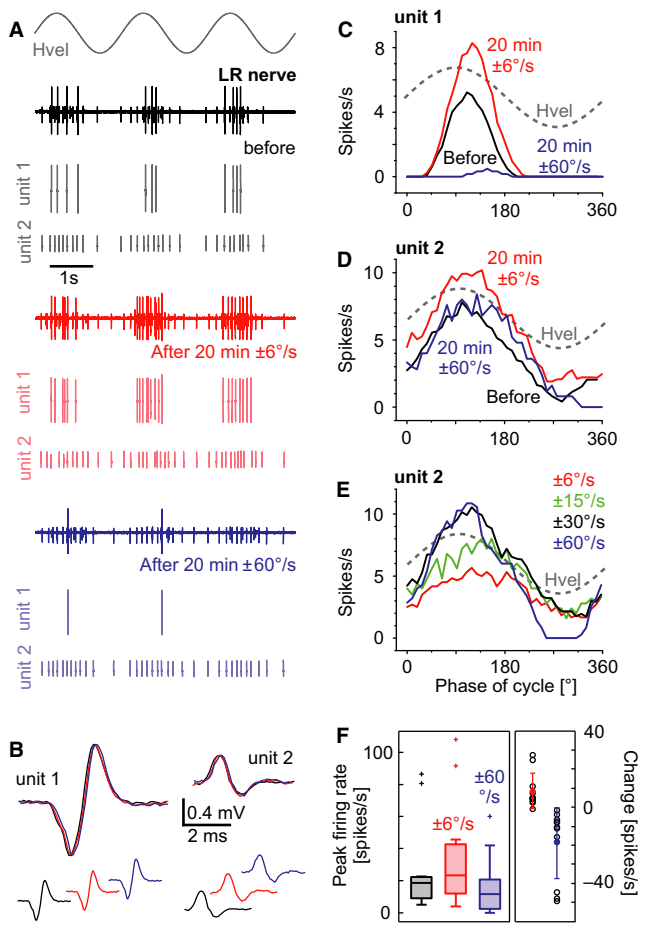

FIG. 3. Alterations in discharge magnitudes of single LR motor units following prolonged horizontal head rotation. A–D, Representative examples of two isolated LR motor units (unit 1 and 2) during three cycles (0.5 Hz) of horizontal head rotation (Hvel; A) and overlays of the corresponding spike shapes before (black) and after 20 min of low- (red) and high-amplitude (blue) conditioning stimulation respectively (B). Firing rate modulation of unit 1 (C) and unit 2 (D) averaged over a single cycle at the test stimulus intensity (±30°/s peak velocity) before (black) and after 20 min of low (red) and high (blue) amplitude conditioning stimulation respectively. E, Averaged firing rate modulation of unit 2 over a single cycle at the same stimulus frequency (0.5 Hz), but different peak velocities (colour-coded). F, Box plots depicting peak firing rates of single unit test responses (left) and individual differences in peak firing rates (right) before (black) and after 20 min of prolonged low- (red) and high-amplitude (blue) conditioning stimulation (n = 11). Boxes indicate median and lower and upper quartiles; bars represent minimum and maximum values and crosses outliers. Individual differences are plotted as open black circles; mean ± SD in red and blue respectively (right). Dashed lines in C–E indicate head motion stimulus velocity (Hvel).

responses with similar peak firing rates as the test stimulus (±30°/s). This potentially prevented a recalibration that in most other motor units was induced by prolonged stimulation with stronger stimuli. Quantification of the changes for all single units indicated an overall facilitation of the peak discharge of the test responses from ~25 spikes/s to ~35 spikes/s after prolonged rotation at ±6°/s peak velocity (red box plot in Fig. 3F) corresponding to an increase of 8.5 ± 2.8 spikes/s (31%, $n = 11$, $P = 0.002$, right plot in Fig. 3F). Prolonged stimulation at ±60°/s caused an attenuation of the response from ~25 spikes/s to ~ 15 spikes/s (blue box plot in Fig. 3F), corresponding to an overall decrease of 10.4 ± 4.0 spikes/s (46%, $n = 11$, $P = 0.0029$, right plot in Fig. 3F).

Plane specificity of VOR adaptation

To test whether the observed attenuation and facilitation of LR nerve responses following prolonged horizontal rotation also extends onto the oblique/vertical VOR output such as SO motoneurons in the trochlear nerve, the discharge of both LR and SO nerves was recorded simultaneously. While the SO nerve discharge remained largely insensitive to horizontal rotation at 0.5 Hz and ±30°/s (representative example in Fig. 4A, $n = 20$), rotation in the iPC/cAC plane at 0.5 Hz and ±15°/s evoked cyclically modulated responses (Figs 1, 4B). These roll motion-evoked responses (before; black trace in Fig. 4B) remained unaltered following prolonged horizontal rotation at either high (blue trace in Fig. 4B) or low stimulus intensities (red trace in Fig. 4B). Calculation of the average SO nerve discharge over a single roll-motion cycle (Fig. 4D, $n = 6$) confirmed this insensitivity to prolonged horizontal stimulation, presumably due to the lack of sufficiently modulated activity during rotation in this plane.

However, prolonged application of conditioning rotational stimuli in the plane of the iPC/cAC caused plasticity of the SO nerve discharge in the same fashion as observed in the LR nerve during horizontal rotation. An attenuation of the test responses (0.5 Hz, ±15°/s) was observed after 20 min of continuous roll-motion with a high-magnitude conditioning stimulus (±30°/s, 0.5 Hz). The mean SO nerve peak firing rate decreased by 23.7 ± 6.1 spikes/s ($n = 6$, $P = 0.0313$), corresponding to a reduction of 12% from ~200 spikes/s to ~175 spikes/s as illustrated by the representative example in Fig. 4C (pooled data in Fig. 4E,F). Similarly, an average increase of the test response from ~200 to ~215 spikes/s (15.8 ± 3.8 spikes/s ($n = 6$, $P = 0.0313$), corresponding to a facilitation of 8% was observed after prolonged low-magnitude roll-motion conditioning stimulation (±3°/s, 0.5 Hz; Fig. 4C,E,F). Hence, the observed plasticity of vestibulo-ocular responses, as indicated by LR and SO nerve recordings, is spatially specific and in both extraocular nerves related to a stronger or weaker discharge modulation during conditioning stimuli relative to the test stimulus.

Cerebellar role in homeostatic VOR plasticity

A cerebellar contribution to VOR plasticity through inhibitory Purkinje cells that project to cerebellar target neurons in the vestibular nucleus (Fig. 5A; Babalian & Vidal, 2000) has been demonstrated using visuo-vestibular mismatch paradigms (e.g. Gittis & du Lac, 2006). In order to reveal a potential contribution of the cerebellar circuitry to plane-specific homeostatic plasticity in *Xenopus* tadpoles, we tested whether a bilateral cerebellectomy (Fig. 5B) had an effect on the facilitation or attenuation of the LR nerve discharge observed after prolonged motion stimulation.

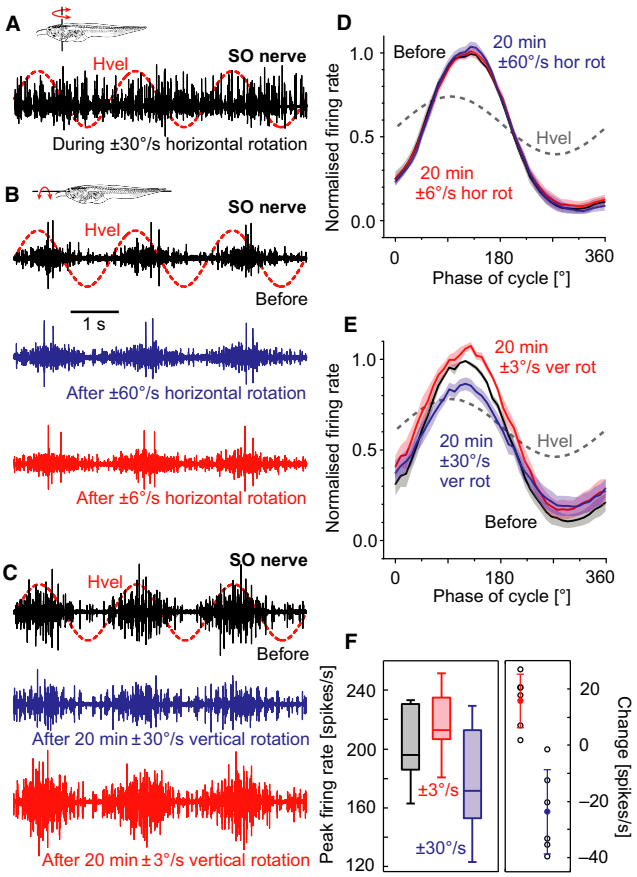

FIG. 4. Plane-specific alterations of the SO nerve discharge following prolonged horizontal head rotation. A, Representative example of a multi-unit SO nerve discharge over three cycles of horizontal head rotation (Hvel, dashed red line; pictogram) at the test stimulus intensity (0.5 Hz, ±30°/s peak velocity). B–E, Representative examples of a multi-unit SO nerve discharge over three cycles of vertical head rotation along the iPC-cAC plane (dashed red lines; pictogram) at the test stimulus intensity for vertical rotation (0.5 Hz, ±15°/s peak velocity; B,C) and firing rate modulation averaged over a single cycle (D,E; $n = 6$, respectively; ±SEM, shaded areas); recordings were obtained before (black) and after 20 min of conditioning stimulation at high (blue) and low (red) amplitude horizontal (B,D) and vertical (C,E) sinusoidal head rotation respectively; note alterations of SO nerve responses following vertical but not horizontal conditioning stimulation. F, Box plots depicting peak firing rates of SO nerve test responses (left) and individual differences in peak firing rates (right) before (black) and after 20 min of prolonged low (red) and high (blue) amplitude conditioning stimulation in the iPC-cAC plane (vertical rotation; $n = 6$). Boxes indicate median and lower and upper quartiles; bars represent minimum and maximum values. Individual differences are plotted as open black circles; mean ± SD in red and blue respectively (right). Dashed lines in D,E indicate head motion stimulus velocity (Hvel). hor/ver rot, horizontal/vertical head rotation.

After establishing homeostatic plasticity in a given semi-intact preparation, the cerebellum was surgically removed following attenuation of the LR test responses ($n = 6$) by prolonged high-magnitude conditioning stimulation (±60°/s, 0.5 Hz). Immediately after the cerebellum had been disconnected by bilateral transection of the peduncle (see Methods), the attenuated LR nerve test response (Fig. 5C, blue line in Fig. 5D) reversed approximately to baseline level prior to the prolonged stimulation (compare green and black lines in Fig. 5D; $n = 6$). A similar cerebellar lesion-induced reversal of homeostatic plasticity was observed after facilitation of LR nerve responses and also for SO nerve responses that were subjected to prolonged stimulation in the iPC/cAC plane ($n = 2$ in both cases,

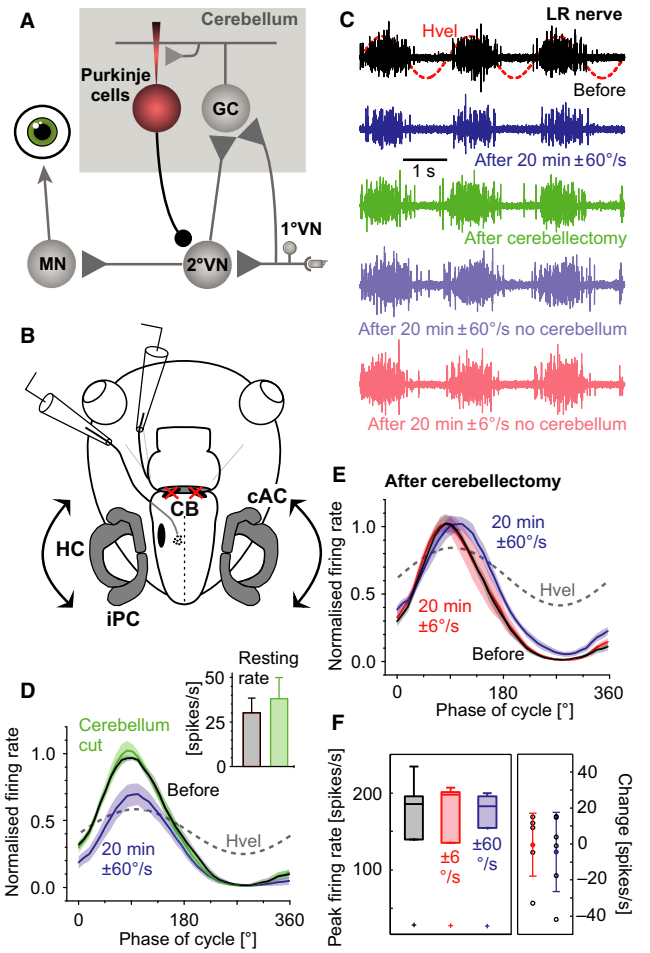

FIG. 5. Cerebellar role in extraocular motor plasticity. A,B, Schematics depicting the three-neuronal vestibulo-ocular pathway and the cerebellar side loop, controlling the VOR output (A) and the site of surgical removal of the cerebellum in the semi-intact *Xenopus* preparation (B). C, Representative example of a multi-unit LR nerve discharge over three cycles of horizontal head rotation (Hvel, dashed red line) at the test stimulus intensity (0.5 Hz, ±30°/s peak velocity); recordings were obtained in the same preparation before (black), after 20 min of high-amplitude conditioning stimulation (blue), immediately after cerebellectomy (green), after 20 min of low-amplitude conditioning stimulation (light red) and 20 min after high-amplitude conditioning stimulation (light blue), both of the latter in the absence of the cerebellum. D,E, LR firing rate modulation averaged over a single cycle at the test stimulus intensity (n = 6; ±SEM, shaded areas) before (black) and after 20 min of high-amplitude conditioning stimulation immediately before (blue) and after cerebellectomy (green) (D) as well as after 20 min of low- (red) and high-amplitude (blue) conditioning stimulation in the absence of the cerebellum (E). Inset in D shows LR nerve resting rates before (black) and after (green) cerebellectomy (±SEM; n = 7). ***F,*** Box plots depicting peak firing rates of LR nerve test responses (n = 6) in the absence of the cerebellum before (black) and after 20 min of prolonged low (red) and high (blue) amplitude stimulation (left) and individual differences in peak firing rates before and after prolonged stimulation (right). Boxes indicate median and lower and upper quartiles; bars represent minimum and maximum values and crosses outliers. Individual differences are plotted as open black circles; mean ± SD in red and blue respectively (right). Dashed lines in D,E indicate head motion stimulus velocity (Hvel). 1°VN, 2°VN, first- and second-order vestibular neurons; CB, cerebellum; cAC, contralateral anterior canal; GC, granule cells; HC, horizontal canal; iPC, ipsilateral posterior canal; MN, extraocular motoneurons.

data not shown). This indicates that an intact cerebellar circuitry is required for the maintenance of induced homeostatic plasticity. An increase in the LR nerve resting discharge after cerebellectomy was observed in five out of seven cases (inset in Fig. 5D) and complies with the removed tonic inhibitory influence on vestibulo-ocular signal processing (see Straka & Dieringer, 2004).

To test whether the cerebellum is also involved in the acquisition of homeostatic VOR plasticity, prolonged horizontal rotation at either low or high magnitudes was applied after cerebellectomy. In contrast to the reliable attenuation and facilitation of extraocular motor responses observed in preparations with an intact cerebellum, prolonged vestibular stimulation consistently failed to induce significant changes of the LR nerve test response after cerebellectomy (Fig. 5C,E). Neither 20 min stimulation with ±6°/s nor prolonged head rotation at ±60°/s caused significant changes of the peak firing rate of 161.6 ± 29.5 spikes/s (n = 6; Fig. 5F), indicating that the cerebellum is required for both inducing as well as maintaining homeostatic plasticity.

Discussion

Angular and translational vestibulo-ocular reflexes (VOR) contribute to retinal image stabilisation during head/body motion by generating extraocular motor commands for counteractive eye movements. Here, we show that prolonged sinusoidal rotation causes plasticity of the extraocular motor output in *Xenopus* tadpoles. The observed bidirectional changes in rotational VOR gain depend on the amplitude and duration of the prolonged stimulus and are plane-specific for horizontal and vertical rotations respectively. Ablation of the cerebellum abolishes changes in extraocular motor gain and prevents further induction of homeostatic plasticity.

Vestibulo-ocular reflex plasticity

Numerous studies employing various modes of experimental perturbations have demonstrated a remarkable plasticity of vestibulo-ocular reflexes (reviewed in e.g. Miles & Lisberger, 1981; Raymond & Lisberger, 2000; Gittis & du Lac, 2006). In addition to gain changes, also response timing and even the direction of compensatory eye movements can be altered under experimental conditions that create a sensory conflict where visual feedback no longer matches the concurrent vestibular input (reviewed in e.g. Boyden *et al.*, 2004). Such visuo-vestibular mismatch training causes an adaptation of extraocular motor commands by changing the underlying sensory-motor transformation that accounts for the retinal image slip in the experimentally perturbed sensory environment. In general, VOR plasticity is necessary to adjust the extraocular motor output to changes in sensory and/or motor system functionality that naturally occur during development and ageing (Boyden *et al.*, 2004) or after uni- or bilateral vestibular impairments (e.g. Angelaki *et al.*, 1996; reviewed in Dieringer, 1995; Cullen *et al.*, 2009; Dutia, 2010). Furthermore, an attenuation of the VOR gain was demonstrated during prolonged low-frequency vestibular stimulation in darkness in goldfish (Dow & Anastasio, 1998), mice (Gutierrez-Castellanos *et al.*, 2013) and monkeys (Jäger & Henn, 1981), which was interpreted as habituation.

While VOR plasticity is usually induced by visuo-vestibular mismatch conditions, the changes in VOR efficacy in this study occur in the absence of conflicting visuo-vestibular signals, since visual inputs were eliminated by bilateral optic nerve transection prior to the experiments. Moreover, the bidirectionality of the observed plasticity also excludes classical habituation as the only explanation. We rather suggest that the VOR attenuation and facilitation described here represents a homeostatic plasticity that is well-suited to level out prolonged elevated or diminished cellular/network activity and

to maintain stability of the neuronal encoding as previously described in other brain areas (Turrigiano, 2012). Evidence for this assumption derives from the fact that the observed attenuation or facilitation of extraocular motor commands persists when the amplitude or frequency of stimulation is changed (compare the concurrent decrease and increase of conditioning and test stimulus responses). In addition, plastic gain changes are completely abolished after a comparable period without motion stimulation, indicating that the resting activity in the vestibulo-ocular circuitry is sufficient to reset VOR performance to the pre-conditioning level. Together with the observed bidirectional gain changes under our experimental conditions, this suggests that the pre-conditioning baseline activity corresponds to the amount of spontaneous vestibular discharge and/or to VOR activity during head motion typically experienced by the intact animal. Independent of whether the VOR gain is increased or decreased, the relatively short time period (<20 min) in which plasticity occurs complies with the fastest adaptation times reported in e.g. cats, where vestibular adaptation is most prominent within the first 30 min of visuo-vestibular mismatch training (Luebke & Robinson, 1994; Broussard *et al.*, 2011) or in monkeys, where gain changes during passive rotation appear already after 15 min of stimulation (Broussard & Kassardjian, 2004). Furthermore, this study together with previous findings in monkeys (Miles & Eighmy, 1980) and goldfish (Michnovicz & Bennett, 1987), suggest that VOR adaptation generally follows an exponential time course.

Evaluation of the responses of single extraocular motor units (Fig. 3) revealed that most neurons express bidirectional changes. However, some units display adaptive plasticity only in one direction, e.g. facilitation but not attenuation. This could be explained by the lack of sufficient sensitivity of these neurons to input changes over the range of applied test- and/or conditioning stimulus magnitudes. Sensitivity as a functional prerequisite for adaptive plasticity is plausible also with respect to the observed plane specificity. In general, a particular set of extraocular motoneurons predominantly receives coplanar semicircular canal-related inputs via principal VOR connections. These inputs are supplemented by less efficient signals from auxiliary pathways that compensate for some of the spatial misalignments between semicircular canals and sets of extraocular muscles (Straka & Dieringer, 2004). Accordingly, extraocular motoneurons being especially sensitive to changes in stimuli activating principal vestibulo-ocular pathways, display homeostatic plasticity in this particular plane of activation. In contrast, weaker auxiliary connections, such as between horizontal canals and SO motoneurons, that cause only a minor modulation of the extraocular motor discharge, are insufficient to induce an adaptation.

Homeostatic plasticity is cerebellum-dependent

Surgical removal of the cerebellum prevents both the acquisition as well as the maintenance of homeostatic changes in motion-induced extraocular motor activity. This not only confirms that the cerebellum is required for the induction of motor adaptation by modifying the efficacy of sensory-motor transformations underlying the VOR but also indicates that it is the principal site for retaining modified responses, in agreement with the mechanistic explanation for classical short-term VOR learning (Boyden *et al.*, 2004). First evidence for a continuous online control of vestibulo-ocular network activity derives from the observed elevation of the resting discharge of LR motoneurons (Fig. 5D inset) after cerebellectomy. This is likely caused by the removal of tonic inhibitory Purkinje cell inputs onto second-order vestibular neurons, reported for e.g. ranid frogs (Straka & Dieringer, 2004) and goldfish (Michnovicz & Bennett, 1987). The observed retention of plasticity within the cerebellum also complies with previous reports in goldfish (Michnovicz & Bennett, 1987) and cats (Robinson, 1976; Kassardjian *et al.*, 2005) where adapted VOR gains are fully reversed to baseline levels after cerebellectomy. Moreover, recordings from Purkinje cells responsible for horizontal eye movements in monkeys revealed that their output correlates with an up- or down-regulation of the VOR gain (Watanabe, 1985). Also, VOR adaptation is prevented by electrical deactivation of Purkinje cells in cats (Luebke & Robinson, 1994) or by cerebellectomy in rabbits (Ito *et al.*, 1974), goldfish (Michnovicz & Bennett, 1987) and monkeys (Lisberger *et al.*, 1984) compatible with the present finding that the cerebellum is required for inducing VOR plasticity in *Xenopus* tadpoles.

Importantly, classical VOR learning appears to consolidate after longer training periods by a process during which the site of plasticity transfers from Purkinje cells to downstream target neurons, such as the deep cerebellar nuclei or central vestibular neurons (Kassardjian *et al.*, 2005; Titley *et al.*, 2007). In contrast, the return of VOR gains to baseline levels after cerebellectomy in this study excludes consolidation of plastic changes at an extra-cerebellar site, at least under our experimental conditions. Even though it is possible that 20 min of stimulation are insufficient for a permanent retention, it appears more plausible that the observed homeostatic plasticity represents a rapid, continuous online adjustment of the VOR network activity when visual feedback is missing. We thus conclude that, in the absence of motion-related retinal image slip signals, prolonged application of strong or weak vestibular stimuli suffices to regulate VOR gain via modifications of the cerebellar Purkinje cell output. Furthermore, these findings suggest that attenuation or facilitation of vestibulo-ocular responses is introduced at the level of cerebellar target neurons in the vestibular nuclei, even though, additional adaptive processes of motoneuronal activity itself cannot be excluded at present.

Functional implications – flexible adjustment of gain control

VOR adaptation in this study differs from classical VOR motor learning, such as visuo-vestibular mismatch training or habituation, and rather matches the description of postsynaptic homeostatic plasticity initially observed in cortical circuits (see Turrigiano & Nelson, 2004). Assuming that VOR neurons and circuits also have an optimal encoding range with a set point that is intrinsically predetermined, the plasticity observed in this study can be interpreted as an attempt of VOR neuronal elements to maintain an optimal working range for sensory-motor transformations. The indifference level at which no homeostatic change in the extraocular motor discharge to prolonged stimulation was encountered (i.e. the employed test stimulus) represents an intensity that causes responses with amplitudes approximately halfway between activation threshold and saturation. This corresponds to a stimulus where extraocular motoneurons in *Xenopus* tadpoles respond more or less linearly to changes in head velocity for both rotational directions (see Fig. 1). Thus, it appears very plausible that during prolonged head rotation at weak stimuli close to threshold or strong stimuli close to saturation levels of the VOR output, the system recalibrates vestibulo-ocular signal processing with the help of the cerebellar side loop to generate extraocular motor commands that remain within the linear input–output range and display maximal sensitivity. However, critical to this explanation is the fact that experiments in this study were performed in the absence of visual inputs, which would serve in the intact animal as sensory feedback of the intended VOR gaze stabilisation. In that case, one might

speculate that during prolonged vestibular stimulation in light, the extraocular motor output would remain unchanged, since visual feedback allows fine-tuning of the respective extraocular motor commands. In this study, however, the observed homeostatic plasticity represents a specific cerebellum-dependent mechanism that shows the capacity to adapt and thus optimise the encoding of motion signals within the VOR pathway in isolation (absence of visual feedback signals).

Conflict of interest statement

The authors declare no competing interests.

Acknowledgments

The authors thank Dr. Francisco Branoner, Dr. Boris Chagnaud and Sara Hänzi for critical reading of the manuscript. The authors acknowledge financial support from the German Science Foundation (CRC 870, TP B12; STR 478/3-1; GRK 1373), the German Federal Ministry of Education and Research under the Grant code 01 EO 0901, the Bernstein Center for Computational Neuroscience Munich (B-T1) and the Munich Center for Neurosciences – Brain and Mind (MCN).

Abbreviations

cAC, contralateral anterior canal; HC, horizontal canal; iPC, ipsilateral posterior canal; LR, lateral rectus; SO, superior oblique; VOR, vestibulo-ocular reflex.

References

Albus, J.S. (1971) A theory of cerebellar function. *Math. Biosci.*, **10**, 25–61.

Angelaki, D.E., Hess, B.J.M., Arai, Y. & Suzuki, J. (1996) Adaptation of primate vestibuloocular reflex to altered peripheral vestibular inputs. I. Frequency-specific recovery of horizontal VOR after inactivation of the lateral semicircular canals. *J. Neurophysiol.*, **76**, 2941–2953.

Babalian, A.L. & Vidal, P.-P. (2000) Floccular modulation of vestibuloocular pathways and cerebellum-related plasticity: An in vitro whole brain study. *J. Neurophysiol.*, **84**, 2514–2528.

Beraneck, M. & Idoux, E. (2012) Reconsidering the role of neuronal intrinsic properties and neuromodulation in vestibular homeostasis. *Front. Neurol.*, **3**, 25.

Boyden, E.S., Katoh, A. & Raymond, J.L. (2004) Cerebellum-dependent learning: the role of multiple plasticity mechanisms. *Annu. Rev. Neurosci.*, **27**, 581–609.

Branoner, F. & Straka, H. (2015) Semicircular canal-dependent developmental tuning of translational vestibulo-ocular reflexes in *Xenopus laevis*. *Dev. Neurobiol.*, **75**, 1051–1067.

Brooks, J.X., Carriot, J. & Cullen, K.E. (2015) Learning to expect the unexpected: rapid updating in primate cerebellum during voluntary self-motion. *Nat. Neurosci.*, **18**, 1310–1317.

Broussard, D.M. & Kassardjian, C.D. (2004) Learning in a simple motor system. *Learn. Memory*, **11**, 127–136.

Broussard, D.M., Titley, H.K., Antflick, J. & Hampson, D.R. (2011) Motor learning in the VOR: the cerebellar component. *Exp. Brain Res.*, **210**, 451–463.

Clopath, C., Badura, A., De Zeeuw, C.I. & Brunel, N. (2014) A cerebellar learning model of vestibulo-ocular reflex adaptation in wild-type and mutant mice. *J. Neurosci.*, **34**, 7203–7215.

Cullen, K.E., Minor, L.B., Beraneck, M. & Sadeghi, S.G. (2009) Neural substrates underlying vestibular compensation: contribution of peripheral versus central processing. *J. Vestibul. Res.*, **19**, 171–182.

Dieringer, N. (1995) "Vestibular compensation": neural plasticity and its relations to functional recovery after labyrinthine lesions in frogs and other vertebrates. *Prog. Neurobiol.*, **46**, 97–129.

Dow, E.R. & Anastasio, T.J. (1998) Analysis and neural network modeling of the nonlinear correlates of habituation in the vestibulo-ocular reflex. *J. Comput. Neurosci.*, **5**, 171–190.

Dow, E.R. & Anastasio, T.J. (1999) Dual-frequency habituation and dishabituation of the goldfish vestibulo-ocular reflex. *NeuroReport*, **10**, 1729–1734.

Dutia, M.B. (2010) Mechanisms of vestibular compensation: recent advances. *Curr. Opin. Otolaryngo. Head Neck Surg.*, **18**, 420–424.

Gittis, A.H. & du Lac, S. (2006) Intrinsic and synaptic plasticity in the vestibular system. *Curr. Opin. Neurobiol.*, **16**, 385–390.

Gutierrez-Castellanos, N., Winkelman, B.H.J., Tolosa-Rodriguez, L., De Gruijl, J.R. & De Zeeuw, C.I. (2013) Impact of aging on long-term ocular reflex adaptation. *Neurobiol. Aging*, **34**, 2784–2792.

Hirata, Y. & Highstein, S.M. (2001) Acute adaptation of the vestibuloocular reflex: signal processing by floccular and ventral parafloccular Purkinje cells. *J. Neurophysiol.*, **85**, 2267–2288.

Ito, M., Shiida, T., Yagi, N. & Yamamoto, M. (1974) Visual influence on rabbit horizontal vestibulo-ocular reflex presumably effected via the cerebellar flocculus. *Brain Res.*, **65**, 170–174.

Jäger, J. & Henn, V. (1981) Habituation of the vestibulo-ocular reflex (VOR) in the monkey during sinusoidal rotation in the dark. *Exp. Brain Res.*, **41**, 108–114.

Kassardjian, C.D., Tan, Y.-F., Chung, J.-Y.J., Heskin, R., Peterson, M.J. & Broussard, D.M. (2005) The site of a motor memory shifts with consolidation. *J. Neurosci.*, **25**, 7979–7985.

King, W.M. (2013) Getting ahead of oneself: anticipation and the vestibulo-ocular reflex. *Neuroscience*, **236**, 210–219.

Lambert, F.M., Beck, J.C., Baker, R. & Straka, H. (2008) Semicircular canal size determines the developmental onset of angular vestibuloocular reflexes in larval *Xenopus*. *J. Neurosci.*, **28**, 8086–8095.

Lambert, F.M., Combes, D., Simmers, J. & Straka, H. (2012) Gaze stabilization by efference copy signaling without sensory feedback during vertebrate locomotion. *Curr. Biol.*, **22**, 1649–1658.

Land, M.F. (1999) Motion and vision: why animals move their eyes. *J. Comp. Physiol. - A Sensory, Neural. Behav. Physiol.*, **185**, 341–352.

Lisberger, S.G., Miles, F.A. & Zee, D.S. (1984) Signals used to compute errors in monkey vestibuloocular reflex: possible role of flocculus. *J. Neurophysiol.*, **52**, 1140–1153.

Llinas, R., Bloedel, J.R. & Hillman, D.E. (1969) Functional characterization of neuronal circuitry of frog cerebellar cortex. *J Neurophysiol.*, **32**, 847–870.

Luebke, A.E. & Robinson, D.A. (1994) Gain changes of the cat's vestibulo-ocular reflex after flocculus deactivation. *Exp. Brain Res.*, **98**, 379–390.

Marr, D. (1969) A theory of cerebellar cortex. *J. Physiol.*, **202**, 437–470.

Medina, J.F. (2011) The multiple roles of Purkinje cells in sensori-motor calibration: to predict, teach and command. *Curr. Opin. Neurobiol.*, **21**, 616–622.

Michnovicz, J.J. & Bennett, M.V. (1987) Effects of rapid cerebellectomy on adaptive gain control of the vestibulo-ocular reflex in alert goldfish. *Exp. Brain Res.*, **66**, 287–294.

Miles, F.A. & Eighmy, B.B. (1980) Long-term adaptive changes in primate vestibuloocular reflex. I. Behavioral observations. *J. Neurophysiol.*, **43**, 1406–1425.

Miles, F.A. & Lisberger, S.G. (1981) Plasticity in the vestibulo-ocular reflex: a new hypothesis. *Annu. Rev. Neurosci.*, **4**, 273–299.

Nieuwkoop, P.D. & Faber, J. (1994) *Normal Table of Xenopus Laevis (Daudin): A Systematical and Chronological Survey of the Development from the Fertilized Egg Till the End of Metamorphosis, Daudin?*: A Systematical and Chronological Survey of the Development from the Fertilized Egg Till the End of Metamorp. Garland Pub, New York.

Rambold, H., Churchland, A., Selig, Y., Jasmin, L. & Lisberger, S.G. (2002) Partial ablations of the flocculus and ventral paraflocculus in monkeys cause linked deficits in smooth pursuit eye movements and adaptive modification of the VOR. *J. Neurophysiol.*, **87**, 912–924.

Ramlochansingh, C., Branoner, F., Chagnaud, B.P. & Straka, H. (2014) Efficacy of tricaine methanesulfonate (MS-222) as an anesthetic agent for blocking sensory-motor responses in *Xenopus laevis* tadpoles. *PLoS One*, **9**, e101606.

Raymond, J.L. & Lisberger, S.G. (2000) Hypotheses about the neural trigger for plasticity in the circuit for the vestibulo-ocular reflex. *Prog. Brain Res.*, **124**, 235–246.

Robinson, D.A. (1976) Adaptive gain control of vestibuloocular reflex by the cerebellum. *J. Neurophysiol.*, **39**, 954–969.

Schultheis, L.W. & Robinson, D.A. (1981) Directional plasticity of the vestibuloocular reflex in the cat. *Ann. N. Y. Acad. Sci.*, **374**, 504–512.

Straka, H. & Dieringer, N. (2004) Basic organization principles of the VOR: lessons from frogs. *Prog. Neurobiol.*, **73**, 259–309.

Straka, H. & Simmers, J. (2012) *Xenopus laevis*: an ideal experimental model for studying the developmental dynamics of neural network assembly and sensory-motor computations. *Dev. Neurobiol.*, **72**, 649–663.

Straka, H., Fritzsch, B. & Glover, J.C. (2014) Connecting ears to eye muscles: evolution of a "simple" reflex arc. *Brain Behav. Evol.*, **83**, 162–175.

Titley, H.K., Heskin-Sweezie, R., Chung, J.-Y.J., Kassardjian, C.D., Razik, F. & Broussard, D.M. (2007) Rapid consolidation of motor memory in the vestibuloocular reflex. *J. Neurophysiol.*, **98**, 3809–3812.

Turrigiano, G.G. (2012) Homeostatic synaptic plasticity: local and global mechanisms for stabilizing neuronal function. *Cold Spring Harb. Perspect. Biol.*, **4**, a005736.

Turrigiano, G.G. & Nelson, S.B. (2004) Homeostatic plasticity in the developing nervous system. *Nat. Rev. Neurosci.*, **5**, 97–107.

Watanabe, E. (1985) Role of the primate flocculus in adaptation of the vestibulo-ocular reflex. *Neurosci. Res.*, **3**, 20–38.

Zee, D.S., Yamazaki, A., Butler, P.H. & Gücer, G. (1981) Effects of ablation of flocculus and paraflocculus of eye movements in primate. *J. Neurophysiol.*, **46**, 878–899.

Results Part III

Galvanic Vestibular Stimulation: Cellular Substrates and Response Patterns of Neurons in the Vestibulo-Ocular Network

Kathrin D. Gensberger*, Anna-Kristin Kaufmann*, **Haike Dietrich**, Francisco Branoner, Roberto Banchi, Boris P. Chagnaud and Hans Straka

*KD and AK contributed equally to this work

Journal of Neuroscience, 2016

Contributions of HD:

- Planning of experiments
- Recording and analysis of motion-induced extraocular motor activity (Figure 3)
- Recording and analysis of extraocular motor activity during in phase- *vs* out of phase-galvanic vestibular stimulation (Figure 5*M*,*N*)
- Recording and analysis of LR *vs* SO nerve activity during galvanic stimulation of the bilateral horizontal canals (Figure 5*L*)
- Design of figures containing contributed data together with HS
- Writing and revision of the manuscript

Systems/Circuits

Galvanic Vestibular Stimulation: Cellular Substrates and Response Patterns of Neurons in the Vestibulo-Ocular Network

Kathrin D. Gensberger,[1*] Anna-Kristin Kaufmann,[1*] Haike Dietrich,[1,2,3] Francisco Branoner,[1] Roberto Banchi,[1,2,3] Boris P. Chagnaud,[1] and Hans Straka[1,3]

[1]Department Biology II, [2]Graduate School of Systemic Neurosciences, and [3]German Center for Vertigo and Balance Disorders, Ludwig-Maximilians-University Munich, 82152 Planegg, Germany

Galvanic vestibular stimulation (GVS) uses modulated currents to evoke neuronal activity in vestibular endorgans in the absence of head motion. GVS is typically used for a characterization of vestibular pathologies; for studies on the vestibular influence of gaze, posture, and locomotion; and for deciphering the sensory–motor transformation underlying these behaviors. At variance with the widespread use of this method, basic aspects such as the activated cellular substrate at the sensory periphery or the comparability to motion-induced neuronal activity patterns are still disputed. Using semi-intact preparations of *Xenopus laevis* tadpoles, we determined the cellular substrate and the spatiotemporal specificity of GVS-evoked responses and compared sinusoidal GVS-induced activity patterns with motion-induced responses in all neuronal elements along the vestibulo-ocular pathway. As main result, we found that, despite the pharmacological block of glutamatergic hair cell transmission by combined bath-application of NMDA (7-chloro-kynurenic acid) and AMPA (CNQX) receptor blockers, GVS-induced afferent spike activity persisted. However, the amplitude modulation was reduced by ~30%, suggesting that both hair cells and vestibular afferent fibers are normally recruited by GVS. Systematic alterations of electrode placement with respect to bilateral semicircular canal pairs or alterations of the bipolar stimulus phase timing yielded unique activity patterns in extraocular motor nerves, compatible with a spatially and temporally specific activation of vestibulo-ocular reflexes in distinct planes. Despite the different GVS electrode placement in semi-intact *X. laevis* preparations and humans and the more global activation of vestibular endorgans by the latter approach, this method is suitable to imitate head/body motion in both circumstances.

Key words: extraocular motor; galvanic stimulation; hair cells; inner ear; vestibular; *Xenopus laevis*

Significance Statement

Galvanic vestibular stimulation is used frequently in clinical practice to test the functionality of the sense of balance. The outcome of the test that relies on the activation of eye movements by electrical stimulation of vestibular organs in the inner ear helps to dissociate vestibular impairments that cause vertigo and imbalance in patients. This study uses an amphibian model to investigate at the cellular level the underlying mechanism on which this method depends. The outcome of this translational research unequivocally revealed the cellular substrate at the vestibular sensory periphery that is activated by electrical currents, as well as the spatiotemporal specificity of the evoked eye movements, thus facilitating the interpretation of clinical test results.

Introduction

Ever since LeRoy (1755) produced visual sensations by passing current through the eye and Galvani (1791) used current to evoke contractions of frog muscles, electrical stimulation has been used in neuroscientific research to activate excitable cellular elements (Thompson et al., 2014). After the descriptions of balance problems and equilibrium disturbances when passing current through the human head (Purkinje, 1820) or applying currents to both

Received Nov. 25, 2015; revised July 12, 2016; accepted July 14, 2016.

Author contributions: H.S. designed research; K.D.G., A.-K.K., H.D., F.B., R.B., B.P.C., and H.S. performed research; K.D.G., A.-K.K., H.D., F.B., R.B., B.P.C., and H.S. analyzed data; K.D.G., A.-K.K., H.D., F.B., R.B., B.P.C., and H.S. wrote the paper.

The authors acknowledge the assistance of Alexander Knorr with the eye motion analysis.

This work was supported by the Collaborative Research Center 870 (CRC 870) and the Graduate Program (GRK 1373) of the German Science Foundation, the German Federal Ministry of Education and Research (Grants 01 EO 0901 and 01 GQ 1407), and the Graduate School of Systemic Neurosciences at Ludwig-Maximilians-University Munich.

The authors declare no competing financial interests.

*K.D.G. and A.K.K. contributed equally to this work.

Correspondence should be addressed to Hans Straka, Department Biology II, Ludwig-Maximilians-Universität Munich, Grosshaderner Str. 2, 82152 Planegg, Germany. E-mail: straka@lmu.de.

DOI:10.1523/JNEUROSCI.4239-15.2016

 0270-6474/16/360001-14$15.00/0

ears (Hitzig, 1871), galvanic vestibular stimulation (GVS) became routine to stimulate vestibular sense organs (Bos and Jongkees, 1963; Curthoys, 2010). So far, GVS has been used to investigate the role of vestibular signals in gaze, posture, and locomotor control, as well as motion and spatial perception in human subjects under pathophysiological conditions and in clinical practice (Fitzpatrick and Day, 2004; Curthoys, 2010; St George and Fitzpatrick, 2011; Hsu et al., 2012; Ferrè et al., 2013; Grasso et al., 2013; Fitzpatrick and Watson, 2015). In addition, GVS has assisted in deciphering cellular aspects of vestibular signal processing in various animal models (Goldberg, 2000).

Galvanic currents influence the discharge of otolith and semicircular canal nerve afferents (Goldberg et al., 1984; Schneider et al., 2002; Fitzpatrick and Day, 2004; Kim and Curthoys, 2004; Curthoys and Macdougall, 2012); however, different approaches are used to achieve this goal. Stimulus electrodes in different vertebrate species were either inserted unilaterally or bilaterally into the perilymphatic space of the semicircular canals (Ezure et al., 1983; Goldberg et al., 1984; Angelaki and Perachio, 1993), placed in the middle ear cavity (Kim and Curthoys, 2004; Shanidze et al., 2012; Kim, 2013a, 2013b), or noninvasively attached to the neck for transmastoidal stimulation in human subjects (Fitzpatrick and Day, 2004). The latter two methods preserve inner ear function and thus permit experimental perturbations of motion-induced responses (Shanidze et al., 2012). Independent of the stimulus method, GVS at low intensity activates irregular vestibular afferents, whereas higher stimulus intensities also recruit regular afferents (Goldberg et al., 1984; Kim and Curthoys, 2004; Kim et al., 2011). This stimulus-amplitude-dependent activation allows determining various details of vestibular signal processing, such as fiber-specific origins of monosynaptic and disynaptic inputs to central vestibular neurons (Highstein et al., 1987; Minor and Goldberg, 1991; Angelaki and Perachio, 1993; Straka and Dieringer, 2000) or the organization of vestibulo-motor and vestibulo-autonomous reflexes (Courjon et al., 1987; Cohen et al., 2011; Shanidze et al., 2012; Kim, 2013a).

However, despite an apparent consensus regarding induction and specificity of GVS-induced responses (Wardman and Fitzpatrick, 2002), no definitive experimental proof for the cellular substrate that is activated by GVS is yet available. Although some experimental studies assume a direct activation of vestibular afferents by GVS (Goldberg et al., 1984), recent clinical evidence indicates that GVS might also activate hair cells (Aw et al., 2013). Unequivocal knowledge about the activated structure, however, is necessary to differentiate between human patients suffering from Ménière's disease (Aw et al., 2013) or vestibular migraine (Clarke, 2010; Curthoys, 2010). To resolve basic functional principles of GVS, including activated substrates, studies on tractable animal models are required that allow stimulation of individual endorgans within intact inner ears, recordings from individual vestibulo-ocular reflex (VOR) neuronal elements, as well as pharmacological manipulations. Given the well described vestibulo-ocular signal processing in amphibians (Straka and Dieringer, 2004) and the highly conserved morpho–physiological organization of the VOR circuitry in vertebrates, including vestibular nerve afferent and extraocular motor activity patterns (Straka et al., 2014), *Xenopus laevis* tadpoles are an ideal model system with which to decipher basic aspects of GVS.

Here, we used semi-intact tadpole preparations to compare the induction and modulation of the activity in vestibular nerve afferents, central vestibular neurons, and extraocular motoneurons, as well as eye movements during head rotation and GVS. Systematic manipulations of stimulus electrode position, stimulus parameters, and pharmacological block of the glutamatergic transmission were used to determine the spatiotemporal specificity and morphological substrate of GVS-evoked responses. Preliminary data were published in abstract form previously (Kaufmann et al., 2013).

Materials and Methods

Animals. X. laevis tadpoles of either sex were obtained from the in-house animal breeding facility at the Biocenter–Martinsried of the Ludwig-Maximilians-University Munich. Tadpoles were kept in tanks filled with 17–18°C nonchlorinated water at a 12/12 light/dark cycle and were fed daily with *Spirulina* bacteria. A total of 88 animals at developmental stages 53–55 (Nieuwkoop and Faber, 1994) were used for this study. Experiments were performed *in vitro* on isolated, semi-intact preparations and comply with the National Institutes of Health publication entitled *Principles of Animal Care No. 86-23* (revised 1985). Permission for these experiments was granted by the governmental institution at the Regierung von Oberbayern/Government of Upper Bavaria (55.2–1-54–2532.3–59-12).

Isolated semi-intact in vitro *preparations.* For all experiments, tadpoles were anesthetized in 0.05% 3-aminobenzoic acid ethyl ester (MS-222; Pharmaq) in frog Ringer's solution containing the following (in mM): 75 NaCl, 25 $NaHCO_3$, 2 $CaCl_2$, 2 KCl, 0.5 $MgCl_2$, and 11 glucose, pH 7.4, and decapitated at the level of spinal segments 5–10. The skin covering the top of the head was removed, the soft skull tissue and rostral vertebrae opened, and the forebrain disconnected. This surgical procedure anatomically preserved all vestibular endorgans within the otic capsule on both sides (Fig. 1*A*,*B*), the CNS, the extraocular motor innervation, and eye muscles and allowed prolonged *in vitro* experimentation (Ramlochansingh et al., 2014), including an *in vivo*-like activation of the VOR during motion or electrical stimulation (Straka and Simmers, 2012).

Vestibular and extraocular motor nerve recordings. For recordings of vestibular afferent activity, the VIIIth nerve was transected at the entrance into the brainstem, leaving the peripheral portion along with the ganglion of Scarpa and the sensory innervation of all vestibular endorgans in the otic capsule intact. The brain was removed to facilitate the visibility and access to the cut surface of the peripheral portion of the VIIIth nerve for electrophysiological recordings. For recordings of extraocular motor nerve activity, the skin surrounding the eye was removed and the nerve branches innervating the lateral rectus (LR) or the superior oblique (SO) eye muscles were disconnected from their target muscles. Thereafter, preparations were rinsed in freshly oxygenated Ringer's solution (95% O_2, 5% CO_2; Carbogen) and mechanically secured to the Sylgard-lined floor of the recording chamber (volume, 5 ml). During the experiments, preparations were continuously superfused with oxygenated Ringer's solution at a rate of ~2 ml/min. The temperature of the bath solution was maintained at 17.0 ± 0.2°C.

Extracellular multiunit spike discharge from the isolated extraocular motor nerves (LR, SO; $n = 44$) or multiunit ($n = 8$) and single-unit activity of vestibular nerve afferent fibers ($n = 39$) was recorded by targeting glass suction electrodes with a micromanipulator to the cut end of the extraocular motor nerves or the fasciculated cut end of the VIIIth nerve. Glass microelectrodes were made with a horizontal puller (P-87; Sutter Instruments) and were individually adjusted at the tip to fit the diameter of the respective target nerves. Vestibular and extraocular motor nerve activity was recorded (EXT 10–2F; npi electronic), digitized at 10–20 kHz (CED 1401, Cambridge Electronic Design) and stored on a computer for offline analysis. For the analysis, responses obtained during 8–60 repetitions of sinusoidal turntable oscillations or sinusoidally modulated current stimuli were averaged to obtain the mean response over a single cycle. Data from particular sets of experiments were averaged and presented as mean ± SEM or SD.

Eye motion recordings. After isolation, preparations were mechanically secured to the Sylgard floor of the recording chamber. Because of the maintained neuronal innervation of the extraocular muscles, this semi-intact preparation allowed the activation of eye movements by vestibular stimulation (Straka and Simmers, 2012). As described previously (Ram-

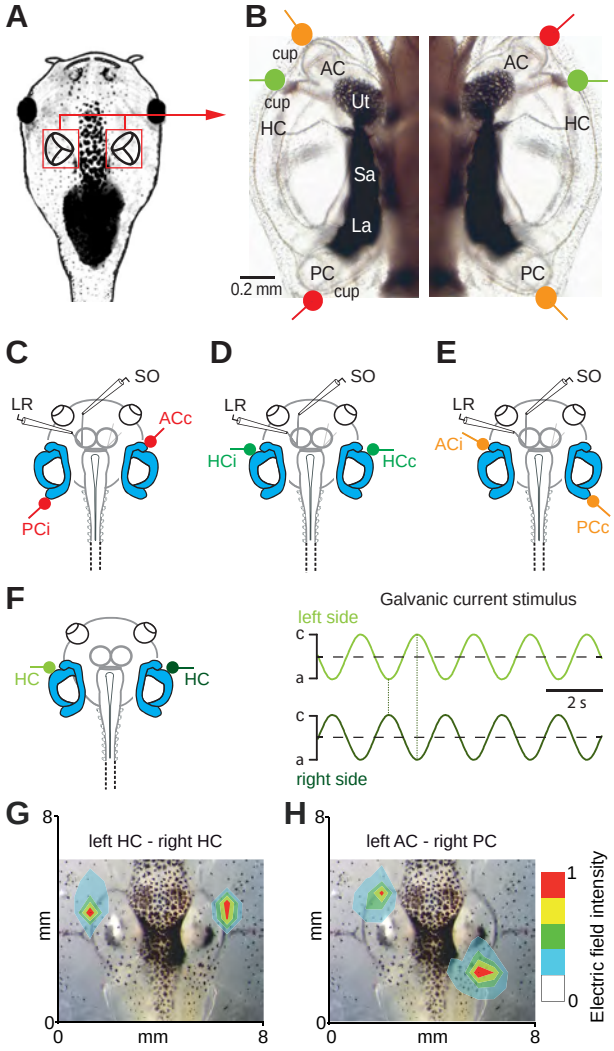

Figure 1. Anatomical substrate, electrode positions for extraocular motor nerve recordings, and application of galvanic vestibular current stimuli. ***A***, ***B***, Schematic of a semi-intact *X. laevis* preparation highlighting the location of the otic capsules (***A***) and photomicrograph depicting the arrangement of bilateral vestibular endorgans and the location of the semicircular canal epithelia as marker for positioning the electrodes on the outer surface of the otic capsules for bipolar electrical stimulation of the three (red, green, orange) coplanar semicircular canal pairs, exemplarily shown in a stage 50 larva (***B***). ***C–E***, Schematics illustrating the location of the electrodes for LR and SO motor nerve recordings, along with the three basic positions of the stimulus electrodes for activating plane-specific bilateral semicircular canal pairs. ***F–H***, Sinusoidally modulated currents with alternating phase relation of the anodal/cathodal (a,c) GVS currents (±100 μA) were applied through bilateral stimulus electrodes (***F***); amplitude distribution plot of the generated electric field evoked by GVS of the bilateral HCs (***G***) and the left AC–right PC (***H***) superimposed on bright-field images of the respective head region; relative amplitude magnitudes are indicated by color code. Cup, Semicircular canal cupula; i,c, ipsilateral, contralateral with respect to the recorded extraocular motor nerve; La, lagena; Sa, saccule; Ut, utricle.

lochansingh et al., 2014), eye movements were recorded noninvasively with a video camera (Grasshopper color, Point Gray Research) and a zoom objective (Optem Zoom 70XL; Qioptiq Photonics) with an adequate lens (M25 × 0.75 + 0.25). This system was mounted on top of the experimental setup to visualize the motion of one eye from above during natural or galvanic vestibular stimulation at a video capture frame rate of 30 Hz with the FlyCap2 software (version 2.3.2.14). Eye motion profiles and parameters were extracted from the captured video sequences using a custom video-processing algorithm written in Matlab (for details, see Ramlochansingh et al., 2014). To calculate the motion of the eye, an ellipse was drawn around the eyeball and the angle between the minor axis of the ellipse and the longitudinal axis of the head was calculated in each frame of a given video sequence (Beck et al., 2004). Based on the frame rate (30 Hz), the change in eye position over time was computed. The generation of peristimulus time histograms for a single cycle, obtained from 8–60 sinusoidal stimulus oscillations was used to calculate the eye motion gain (ratio eye/table motion).

Natural and galvanic vestibular stimulation. The recording chamber with the semi-intact *X. laevis* preparations was mounted on a computer-controlled, motorized two-axis turntable with the preparation centered in the horizontal and vertical rotation axes to provide optimal activation of semicircular canal organs (Lambert et al., 2008, 2013). Motion stimuli consisted of sinusoidal rotations across frequencies that ranged from 0.1 to 5.0 Hz (peak velocities: ±6–60°/s) in either the vertical (yaw) or horizontal (roll) axis to stimulate the bilateral horizontal or the ipsilateral posterior–contralateral anterior vertical semicircular canal pair preferentially as major modulatory vestibular inputs to LR and SO motoneurons, respectively. The limitation of motion stimulus frequencies to 5 Hz maximally is mainly due to the relatively soft cartilage of the *X. laevis* skull that prevents a firm fixation of the preparation to the recording chamber as tightly as in mammalian species, in which the bony skull is usually secured with a head holder to a stereotactic frame. In addition, the absence of considerable tissue above the neural targets, as well as the fluid pressure on the electrode shank, induced by inertia-related liquid motion at the Ringer's surface, impaired in particular stable recordings of single vestibular afferent fibers at higher rotation frequencies.

Sinusoidally modulated galvanic currents were applied by stimulus electrodes that consisted of two Teflon-coated silver wires (diameter: 0.76 mm; AG 25-T; Science Products) placed on the outer surface of the otic capsule (Fig. 1*A*,*B*). The two stimulus electrodes were cut at the tip, chlorinated to minimize polarization, and separately attached to a micromanipulator to enable precise positioning under visual guidance. The placement of the electrodes for GVS of a particular semicircular canal was facilitated by the clear visibility of all labyrinthine endorgans and sensory structures inside the transparent cartilaginous otic capsule of the semi-intact larval *X. laevis* preparation (Fig. 1*A*,*B*). For most experiments, electrodes were placed bilaterally in close proximity of the visible cupulae of a specific coplanar semicircular canal pair (Fig. 1*B–E*). For the recording of vestibular nerve afferents, electrodes were placed unilaterally with one electrode close to either the horizontal or the anterior vertical semicircular canal cupula and the second electrode at a distance of ~15 mm from the first in the Ringer's solution of the recording chamber. For most of the experiments, sine waves for GVS were produced with a linear stimulus isolator (WPI A395; World Precision Instruments), triggered by the analog output from a waveform function generator (Digital VCG Model 113; Wavetek) or by the analog output from an analog/digital converter (CED 1401). For Ca^{2+}-imaging experiments, GVS sine waves were produced by a stimulus generator with an integrated isolation unit (STG 4004; Multichannel Systems). In most experiments, the galvanic currents were applied to the two electrodes in phase opposition and consisted of sinusoidally modulated currents at frequencies of 0.05-10 Hz and amplitudes of ±10–350 μA. The applied sinusoidal current generated an alteration of the cathode and anode between the two electrodes, respectively (Fig. 1*F*), and a local electric field that decreased in magnitude with the distance from the electrode (Fig. 1*G*,*H*). In some experiments, the sinusoidally modulated currents, applied to a bilateral semicircular canal pair, were in phase. In this case, the current was applied through two independently controlled sets of stimulus electrodes, each with one electrode close to the semicircular canal cupula and the second one at a distance of ~15 mm from the first in the Ringer's solution of the recording chamber.

Imaging of Ca^{2+} transients in central vestibular neurons. Ca^{2+} transients were recorded in identified vestibulo-ocular neurons, retrogradely labeled from the midbrain oculomotor nucleus with a calcium sensor (Calcium Green-1 dextran, 3000 MW; Thermo Fisher Scientific). For this purpose, tadpoles were anesthetized in 0.05% MS-222, transferred into oxygenated, ice-cold Ringer's solution, and decapitated. After opening the skull on the ventral side and disconnecting the forebrain, the Ringer's solution was temporarily removed and crystals of Calcium Green-1 dextran, melted to an injection needle, were inserted unilaterally

into the oculomotor nucleus, identified by the exit of the III rd cranial nerve as described previously (Straka et al., 2001). Thereafter, surplus tracer was removed with excess Ringer's solution and preparations were incubated for 24–48 h at 14°C in oxygenated Ringer's solution. Imaging of Ca^{2+} transients in these vestibulo-ocular neurons during GVS of specific bilateral semicircular canal pairs was performed by using a fixed-stage microscope (Axio Examiner Z1; Carl Zeiss) equipped with a 40× (1.0) water-immersion objective and connected to a CCD camera (Axiocam HSM; Carl Zeiss). The microscope and camera were driven by a control unit and a signal distribution box (Examiner Control and SVB1; Carl Zeiss). Timing of GVS-induced image acquisition at a rate of 10–20 frames/s and data storage of the latter were controlled with the Axiovision software SE64 (Carl Zeiss). Fluorescence signal acquisition started 2–3 s before the onset of the first GVS sine wave to determine the background fluorescence level (F_0). Images were analyzed offline using the "intensity versus time" algorithm in the MBF-ImageJ Java software package (http://rsb.info.nih.gov/ij/). The background fluorescence was subtracted and bleaching effects were corrected using a linear regression algorithm written in IgorPro (Wavemetrics). All data are presented as relative changes in fluorescence (dF/F).

Pharmacology. Motion- or GVS-induced responses were completely blocked by bath application of a mixture of 15 μM CNQX (Tocris Bioscience) and 50 μM 7-chloro-kynurenic acid (7-Cl-KYNA; Tocris Bioscience). The two substances block AMPA- and NMDA-receptor-mediated components of glutamatergic transmission, respectively. A drug-related reduction of the responses in these isolated preparations usually occurred after 3–5 min and reached steady state after 15 min (Biesdorf et al., 2008). The reversible block of AMPA- and NMDA-receptor-mediated components by combined application of CNQX and 7-Cl-KYNA allowed evaluation of the neural substrate of galvanic stimulation as well as the specificity of the stimulated structures.

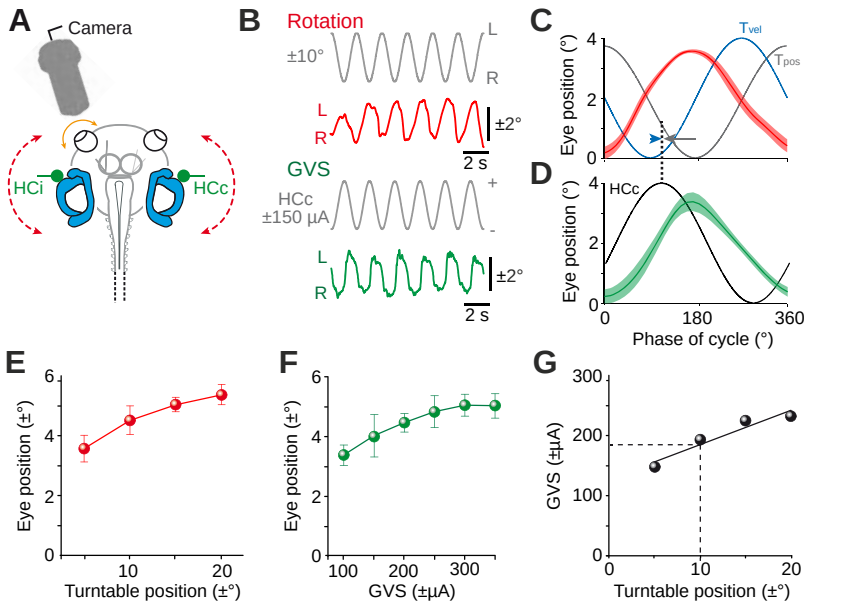

Figure 2. Motion- and GVS-induced eye movements. ***A***, Experimental setting for video recordings of eye movements (orange arrow) during horizontal turntable rotation (red dashed arrows) and GVS of the bilateral HC cupulae (green HCc and HCi electrodes). ***B***, Representative example of horizontal positional oscillations of the left eye during head rotation (±10°; red trace) and GVS (±150 μA; green trace) at 0.5 Hz, extracted from video sequences; stimulus waveforms indicate left–right positional oscillations (top gray trace) and current oscillations of the HCc (bottom gray trace). ***C***, ***D***, Averaged responses (±SEM, shaded areas) over a single cycle (from 20 cycles, respectively; $n = 9$) during horizontal rotation (***C***) and GVS (***D***) of the bilateral HCs; stimulus in ***C*** is plotted both as position (T_{pos}; gray trace) and velocity (T_{vel}; blue trace) of the table motion and in ***D*** as current waveform of the HCc electrode; note that responses in ***C*** and ***D*** were aligned to their respective peak, illustrating that the galvanic stimulus is more closely aligned (dotted line) with T_{vel} (blue arrowhead) than T_{pos} (gray arrow). ***E***, ***F***, Dependency of eye position (mean ± SD) on maximal turntable excursion (***E***) and galvanic current intensity (***F***). ***G***, Calibration of GVS with respect to turntable positional oscillations based on eye movement magnitudes; imitation of a rotation amplitude of ±10° (at 0.5 Hz) requires a GVS current of ±180 μA (dashed lines).

Results

Experimental setting for galvanic vestibular stimulation

Oppositely oriented sinusoidally modulated currents were applied to two stimulus electrodes, placed at the outer surface of the transparent otic capsule close to the cupulae of a bilateral coplanar semicircular canal pair, respectively (color-coded electrodes in Fig. 1*C–E*). These sinusoidal currents caused reciprocal oscillations of the anodal and cathodal current peaks at the electrode tips close to the semicircular canal sensory epithelia (Fig. 1*F*). To estimate the spatial extent of current spread during GVS, voltage amplitudes evoked by GVS of ±100 μA were systematically recorded with a glass microelectrode (tip diameter: ~10 μm; resistance: ~1 $\mu\Omega$) that was filled with 2 M sodium chloride. Recordings were made along a grid of 8 × 6 mm (1 mm spacing) that covered the spatial dimensions of the preparation ($n = 5$) between the two stimulus electrodes (Fig. 1*G*,*H*). For evaluating the spatial extent of voltage magnitude distributions, two electrodes were placed close to the cupulae of either the bilateral horizontal semicircular canals (HC, Fig. 1*G*) or the anterior (AC) on the left and the posterior semicircular canal (PC) on the right side (Fig. 1*H*). As indicated by the color-coded 2D voltage distribution plot, the peak amplitude at the site of the stimulus electrode dropped to ~20% at a distance of ~1 mm. Therefore, this stimulation method causes only minimal current spread to susceptible structures other than the two targeted semicircular canal cupulae. In particular, the relatively distant location of the utricle (~1.5 mm), saccule (~2 mm), and lagena (~2 mm) with respect to the closest semicircular canal stimulus electrode (Fig. 1*B*) minimizes an undesired electrical activation of otolith organs, suggesting that evoked responses are largely semicircular canal specific.

Motion- and GVS-induced eye movements

Horizontal sinusoidal rotation at a stimulus frequency of 0.5 Hz (red dashed line in Fig. 2*A*) provoked oscillatory movements of both eyes in isolated semi-intact *in vitro* preparations of *X. laevis* tadpoles ($n = 9$). Video recordings revealed the timing and amplitude of the evoked eye movements (red trace in Fig. 2*B*) that were oppositely oriented with respect to the rotation direction (Fig. 2*C*). Responses were approximately in phase with table position (T_{pos}; gray trace in Fig. 2*C*) and thus phase-lagged with respect to table velocity (T_{vel}; blue trace in Fig. 2*C*). Rotation-evoked eye movements increased in amplitude with increasing stimulus magnitudes (Fig. 2*E*) with a gain (ratio eye/table motion) of 0.28 ± 0.02 at ±30°/s peak velocity (0.5 Hz, ±10° left–right table excursion; $n = 9$). These responses were thus very similar, both in gain and phase, to the VOR observed under *in vivo* conditions for larval *X. laevis* at the same developmental stage (Lambert et al., 2008; Straka and Simmers, 2012).

In the same preparations that had been subjected to rotational stimulation ($n = 9$), eye movements were also elicited by sinu-

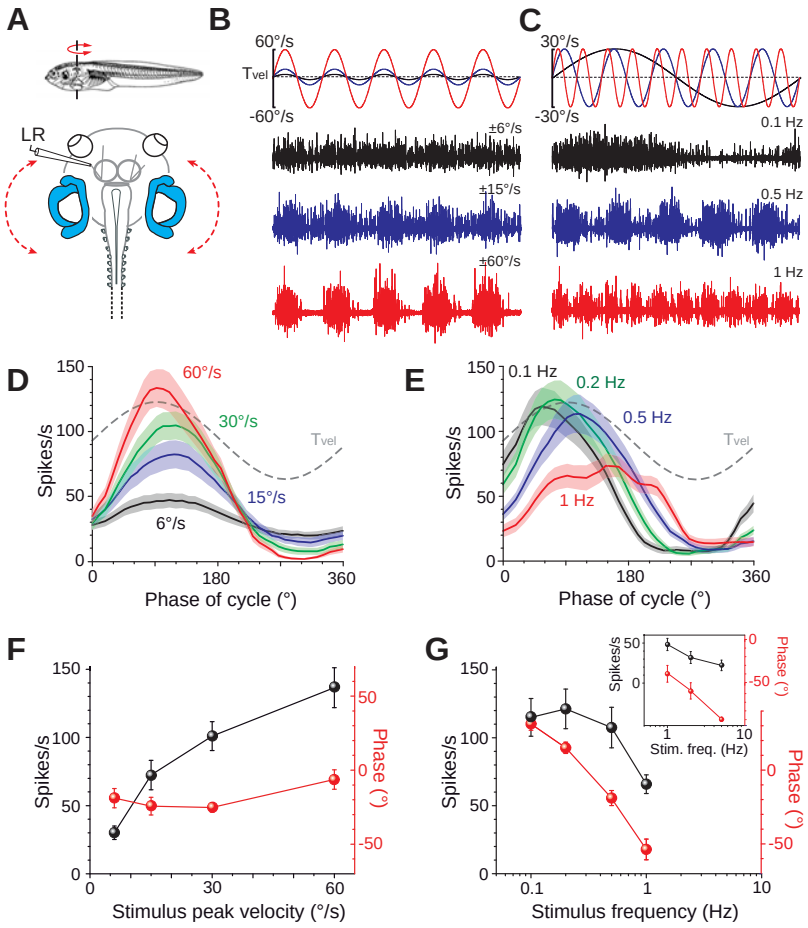

Figure 3. Response parameters of motion-induced extraocular motor activity. ***A***, Multiunit recordings of the LR nerve during horizontal turntable rotation (red dashed arrow). ***B***, ***C***, LR nerve discharge during turntable rotation at a frequency of 0.5 Hz (***B***, top traces) and three peak velocities (black, blue, red trace); and a peak velocity of ±30°/s (***C***, top traces) and three stimulus frequencies (black, blue, red trace). ***D***, ***E***, Averaged firing rate modulation (±SEM, shaded areas) over a single cycle (from 10 to 50 cycles, respectively; $n = 10$) at 0.5 Hz and different peak velocities (color-coded traces in ***D***) and at ±30°/s and different stimulus frequencies (color-coded traces in ***E***); dashed lines in ***D*** and ***E*** indicate stimulus velocity. ***F***, ***G***, Dependency of response peak amplitude (black symbols in ***F***, ***G***) and phase (red symbols in ***F***, ***G***) of rotation-evoked cyclic LR nerve responses (±SEM; $n = 10$) with respect to stimulus peak velocity (***F***) and frequency (***G***). Inset in ***G*** shows data obtained in a separate set of experiments ($n = 7$) in which the response dynamics at stimulus frequencies between 1 and 5 Hz were explored. Scale bar in ***C*** also applies to ***B***.

soidal GVS of the bilateral HC cupulae at a stimulus frequency of 0.5 Hz [contralateral HC (HCc)/ipsilateral HC (HCi) in Fig. 2*A*)]. GVS triggered horizontal oscillatory movements of both eyes with dynamic characteristics comparable to those observed during head rotation (cf. green and red traces in Fig. 2*B*). More specific, leftward movements of both eyes were generated during depolarization of the right HC (HCc; bottom gray trace in Fig. 2*B*) and concurrent hyperpolarization of the left HC (stimulus not plotted) and vice versa. This pattern complies with a reciprocal cathodal excitation and anodal inhibition of the two sensory epithelia, respectively, thus imitating rightward–leftward head oscillations. Temporal alignment of GVS-induced eye movements (green trace in Fig. 2*D*) and rotation-induced responses (red trace in Fig. 2*C*) indicated that the electrical stimulus reflected the velocity much more closely (blue arrowhead in Fig. 2*C*) than the position component of the turntable motion (gray arrow in Fig. 2*C*). Therefore, with respect to evoked responses, GVS essentially imitates the velocity component of a head rotation.

With increasing head motion magnitude (Fig. 2*E*) as well as current intensity (Fig. 2*F*), the amplitude of the evoked eye movements increased steadily until eventually saturation occurred at higher amplitudes. Direct comparison of current- and motion-evoked eye movements allowed calibrating GVS-induced eye movements with respect to eye motion, thus offering the possibility to use sinusoidal GVS to mimic a dynamically defined angular VOR behavior in the absence of effective motion. According to this calibration, imitation of a cyclic turntable rotation of, for example, ±10° left–right position excursion at 0.5 Hz (peak velocity: ±30°/s), required a GVS amplitude of approximately ±180 μA (black dashed lines in Fig. 2*G*).

Motion-induced extraocular motor discharge

To evaluate the general conditions for inducing eye movements with sinusoidal GVS, we first tested the impact of systematically altered motion stimulus parameters on the spatiotemporal specificity of extraocular motor activity. This evaluation was facilitated by the greater sensitivity to changes in stimulus conditions of extraocular motor spike discharge compared with effective eye motion. Therefore, the multiunit spike activity of disconnected and isolated extraocular motor nerves was recorded in semi-intact *in vitro* preparations (Straka and Simmers, 2012) during imposed head rotation that activated particular semicircular canal pairs (horizontal canals in Fig. 3*A*). Accordingly, during horizontal sinusoidal turntable rotation, the spontaneous multiunit discharge (33.8 ± 7.4 spikes/s; $n = 10$) of the LR nerve was cyclically modulated (Fig. 3*B*,*C*).

With increasing peak velocities from ±6°/s to ±60°/s at a stimulus frequency of 0.5 Hz (Fig. 3*B*), the LR nerve peak discharge became larger, as indicated by the averaged responses over a single motion cycle, respectively, and reached up to ~140 spikes/s (141.1 ± 16.1 spikes/s; $n = 10$) at a peak velocity of ±60°/s (Fig. 3*D*,*F*). Whereas the spike rate increased steadily with peak velocity (black symbols in Fig. 3*F*), the corresponding phase lag of the responses of ~10–20° relative to stimulus velocity was largely independent of stimulus magnitude (red symbols in Fig. 3*F*). The overall change in LR nerve response amplitude and phase relation with increasing stimulus amplitude (Fig. 3*F*) is qualitatively very similar to that of rotation-induced eye movements (Fig. 2*E*). However, a direct translation of the presynaptic extraocular motor discharge into effective eye movements suffers from several unknown parameters, such as the dynamics at the neuromuscular junction and the required buildup and relaxation of muscle strength.

With increasing stimulus frequencies from 0.1 to 1 Hz at a peak velocity of ±30°/s (Fig. 3*C*), the peak firing rate of the modulated responses decreased after reaching a maximum at 0.2 Hz (Fig. 3*E*,*G*). This decline (black symbols in Fig. 3*G*) was accompanied by a considerable change in the timing of the response

peak over the range of applied stimuli (red symbols in Fig. 3*G*). In fact, responses evoked at a stimulus frequency of 0.1 Hz were phase advanced by ~30° (31.5° ± 4.3°; $n = 10$), whereas those evoked at 1 Hz were phase lagged by ~50° (−49.8° ± 6.6°; $n = 17$). In several preparations ($n = 7$), successful LR nerve recordings were made during horizontal rotations at frequencies from 1 to 5 Hz (inset in Fig. 3*G*). With increasing stimulus frequencies >1 Hz, the modulated peak firing rate decreased further to a peak firing rate of ~20 spikes/s at 5 Hz (22.1 ± 6.5 spikes/s; $n = 7$), whereas the corresponding phase lagged stimulus velocity by ~90° (−92.6° ± 2.6°; $n = 7$; inset in Fig. 3*G*). These motion-induced extraocular motor responses and their respective dynamic characteristics were used in the following for a comparison with GVS-induced responses.

GVS-induced extraocular motor discharge: response dynamics

As a next step in evaluating the efficacy of GVS, we determined the correlation between extraocular motor discharge and stimulus current amplitude. Sinusoidal GVS of the bilateral HCs (Fig. 4*A*, top traces in *B*) caused a cyclic modulation of the multiunit LR nerve discharge ($n = 8$) that depended on the intensity of the applied current stimulus (color coded traces in Fig. 4*B*). The spontaneous LR nerve discharge of ~35 spikes/s was already noticeably modulated at a minimal current of ±10 μA, as indicated by the averaged responses over a single cycle (black curve in Fig. 4*E*). With larger current amplitudes, the peak firing rate of the modulated multiunit spike activity gradually increased and reached ~200 spikes/s at an intensity of ±100 μA (Fig. 4*E*). Even larger current amplitudes of up to ±300 μA, however, failed to further increase the peak firing rate, causing instead a saturation of the maximal discharge rate (green symbols in Fig. 4*G*) that was accompanied by a gradually increasing phase lead of the peak response (Fig. 4*E*). Comparable to the temporal characteristics of motion-velocity-induced responses of LR motoneurons (Fig. 3), the peak firing rate of the modulated LR nerve response approximately coincided with the peak of the GVS half cycle that simultaneously depolarized the HCc and hyperpolarized the HCi (Fig. 4*E*).

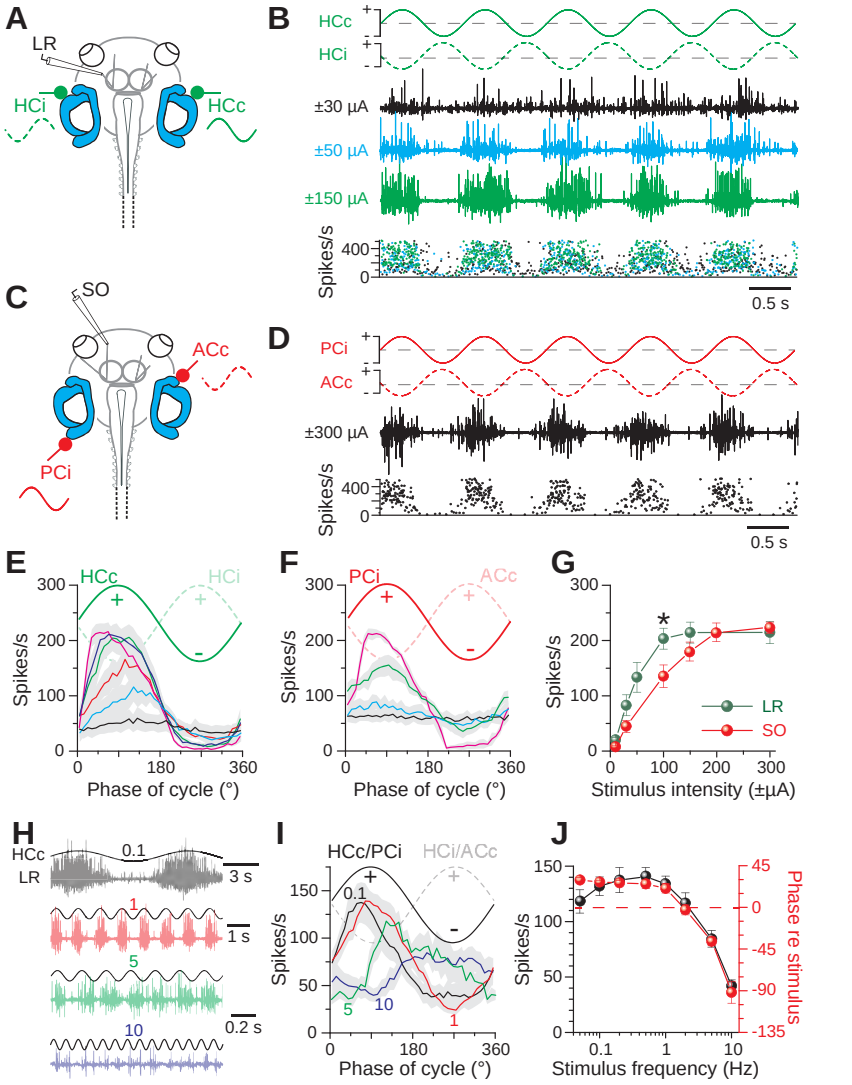

Figure 4. Frequency and intensity dependence of GVS-induced multiple-unit discharge modulation in extraocular motor nerves. ***A***, ***C***, Extracellular recordings of the left LR (***A***) and SO (***C***) nerves during GVS of the bilateral HC cupulae (green HCc and HCi) and the left PC (PCi) and right AC (ACc) cupulae, respectively. ***B***, Left LR nerve discharge during 1 Hz sinusoidal GVS of the bilateral HC cupulae (traces in top row) at three current intensities (black, blue, green traces) with peak firing rates (instantaneous rate, bottom plot) that increased with GVS amplitude. ***D***, Left SO nerve discharge (black trace) and instantaneous firing rate (bottom plot) during sinusoidal GVS of the left PC and right AC cupulae (traces in top row). ***E***, ***F***, Averaged LR (***E***, $n = 8$) and SO nerve responses (***F***, $n = 8$) over a single GVS cycle at 1 Hz (from 16 cycles, ±SEM, gray shaded areas) increased with stimulus amplitude (color-coded responses were evoked by increasing currents: ±10, ±30, ±50, ±100, ±150, ±300 μA in ***E***; ±10, ±30, ±100, ±200 μA in ***F***). ***G***, Dependency of averaged LR and SO nerve peak firing rates on GVS intensity; significance of difference between responses of the two nerves is indicated. *$p < 0.05$ (Mann–Whitney *U* test). ***H–J***, LR nerve discharge during sinusoidal GVS (±100 μA) of the bilateral HCs at four different stimulus frequencies (color-coded traces; ***H***); averaged LR/SO nerve responses (from 16 cycles, ±SEM, gray shaded areas) over a single GVS cycle at 0.1, 1, 5, and 10 Hz (color-coded curves) and a stimulus intensity of ±100 μA ($n = 8$; ***I***) reveal amplitude (black symbols) and phase dependency (red symbols) of the responses on stimulus frequency (***J***). The stimulus in ***H*** indicates polarization of the HCc; numbers in ***H*** and ***I*** indicate frequency in Hz.

To generalize the findings obtained for the horizontal angular VOR, the evaluation of GVS-induced extraocular motor discharge modulation was extended onto other combinations of semicircular canals and extraocular motor nerves. Therefore, we recorded multiunit spike activity of the SO motor nerve during sinusoidal GVS of the ipsilateral posterior (PCi) and contralateral anterior vertical semicircular canals (ACc; Fig. 4*C*). This latter bilateral semicircular canal pair is spatially coaligned with the pulling direction of the SO muscle and thus forms the major modulatory drive for the respective extraocular motoneurons (Branoner and Straka, 2015). Sinusoidally alternating GVS of the PCi and ACc (red traces in Fig. 4*D*) provoked a cyclic modulation (black trace in Fig. 4*D*) of the spontaneous multiunit SO nerve activity (62.5 ± 7.2 spikes/s; $n = 8$). The peak discharge of the modulated responses coincided with the GVS half cycle, during which the PCi was depolarized and the ACc was simultaneously

hyperpolarized (Fig. 4*F*). A first modulation of the SO nerve discharge usually occurred at a current of ±30 μA, as indicated by the averaged responses over a single cycle (blue curve in Fig. 4*F*). With larger current amplitudes, the average peak firing rate of the modulated multiunit spike activity increased and saturated at ~220 spikes/s at current amplitudes above ±200 μA (red symbols in Fig. 4*G*). Although the overall dependency of GVS-induced responses on current intensity was similar for the LR and SO nerves, the modulation threshold and saturation of the peak firing rates required larger currents for SO compared with LR nerve responses (cf. green and red symbols in Fig. 4*G*). This difference is likely due to the topographic relation between electrode tip and sensory epithelium that allows a closer placement of the stimulus electrode to the HC than the PC or AC sensory epithelia.

The dynamics of GVS-induced extraocular motor responses was characterized by modulating the LR and SO nerve activity with sinusoidal currents over a frequency range of 0.05–10 Hz ($n = 12$; Fig. 4*H*). At GVS frequencies up to ~1 Hz, the peak discharge of the modulated LR nerve responses remained relatively synchronized (black and red traces in Fig. 4*H*) and coincided with the GVS half cycle that depolarized the HCc (Fig. 4*I*). Averaging both LR and SO nerve responses over a single cycle, respectively, revealed that, at stimulus frequencies >1 Hz, the modulated discharge became more and more asynchronous, resulting in a decrease of the peak firing rate of the modulated extraocular motor discharge (green and blue traces/curves in Fig. 4*H*,*I*; black symbols in Fig. 4*J*). This decrease in peak firing rate with increasing GVS frequency was accompanied by a concurrent shift in the timing of the response peak (red symbols in Fig. 4*J*). At stimulus frequencies up to 1 Hz, responses were phase advanced by 15–30°, whereas, at stimulus frequencies of >1 Hz, LR and SO response peaks became more and more phase lagged, reaching −90° at a stimulus frequency of 10 Hz (Fig. 4*I*, red symbols in *J*).

GVS-induced extraocular motor discharge

Independent control of bilateral push–pull inputs

The synaptic connectivity underlying the angular VOR includes for each set of extraocular motoneurons a reciprocal crossed excitatory and uncrossed inhibitory input from bilateral semicircular canal pairs coaligned with the pulling direction of the respective eye muscles (Graf and Simpson, 1981). Accordingly, the extraocular motor response modulation during sinusoidal head rotation consists of an alternating increase and decrease of the spontaneous motoneuronal discharge (Straka and Dieringer, 2004). Therefore, we next attempted to influence the two components of GVS-induced extraocular motor responses separately. This was achieved by independently altering the position of the two GVS electrodes ($n = 6$) that provoked the semicircular canal-related excitatory and inhibitory responses, respectively (Fig. 5*A*). Maximal modulation of SO nerve responses evoked at a stimulus intensity of ±100 μA was obtained when the two GVS electrodes were placed in close proximity (0 mm in Fig. 5*A*) to the epithelia of the PCi and ACc, respectively (gray trace in Fig. 5*B*). Retraction of the ACc electrode to a distance of 2 mm from the epithelium while maintaining the second electrode close to the PCi epithelium (Fig. 5*A*) caused a visible reduction of the inhibitory component (blue trace in Fig. 5*B*). In contrast, retraction of the PCi electrode to a distance of 2 mm from the epithelium while maintaining the second electrode close to the ACc epithelium (Fig. 5*A*) caused an obvious decrease of the peak discharge that reflects the excitatory VOR component (red trace in Fig. 5*B*). The independent reciprocal diminishment of the two components (red and blue asterisks in Fig. 5*C*) became particularly evident when averaging the modulated responses over a single cycle (Fig. 5*C*). This independent reduction of excitatory and inhibitory components, respectively, was gradual and correlated in magnitude with the distance between stimulus electrode and epithelium (red and blue asterisks in Fig. 5*D*). At the most distant position of the stimulus electrodes from the epithelium (2 mm), the amplitudes of the two components, respectively, reached the level of the spontaneous resting rate (gray bar in Fig. 5*E*). Therefore, the systematic manipulation of the positions of the two GVS electrodes allowed an independent control of excitatory and inhibitory extraocular motor responses from particular bilateral semicircular canal pairs.

Spatial specificity of stimulation sites

As another primary purpose of the comparison between motion- and GVS-evoked responses, we evaluated whether GVS through carefully placed electrodes on bilateral coplanar semicircular pairs evokes vestibulo-ocular responses with the same spatial specificity as during a rotation along the same canal plane. Accordingly, stimulus electrodes were repositioned systematically relative to the semicircular canal epithelia along the lateral aspect of the otic capsule ($n = 10$; Fig. 5*F*,*H*). Placement of the two GVS electrodes in close proximity of the bilateral HC (position 1 in Fig. 5*F*; stimulus intensity: ±50 μA) or PCi/ACc epithelia (position 1 in Fig. 5*H*; stimulus intensity: ±100 μA) provoked a maximal extraocular motor discharge modulation in the LR (trace 1 in Fig. 5*G*) and SO nerves, respectively, by the applied sinusoidal current (red and green curves in Fig. 5*I*). Simultaneous symmetric repositioning of the two HC electrodes caudally toward the PC epithelia (bilateral positions 2 and 3 in Fig. 5*F*) caused a gradual reduction of the LR nerve discharge modulation (traces 2 and 3 in Fig. 5*G*; green curves in Fig. 5*J*,*K*). A similar repositioning of the bilateral PCi/ACc stimulation electrodes to the reciprocal stimulus sites [i.e., ipsilateral AC (ACi)/PCc; bilateral positions 2 and 3 in Fig. 5*H*] caused a correspondingly diminished discharge modulation of the SO nerve activity (red curves in Fig. 5*J*,*K*). This stimulus-site-specific alteration of the discharge modulation of the LR and SO nerves was further confirmed by simultaneous recordings of the two nerves during GVS (0.5 Hz; ±50 μA) of the bilateral HC cupulae ($n = 4$; Fig. 5*L*). At variance with the clear discharge modulation of the LR nerve (top trace in Fig. 5*L*), the SO nerve discharge did not display any modulation (bottom trace in Fig. 5*L*) up to a stimulus intensity of about ±150 μA, corroborating a semicircular canal-specific activation of extraocular motor nerves at low to moderate stimulus intensities.

Central to the GVS-induced cyclic modulation of extraocular motor discharge and the imitation of a sinusoidal head rotation is the application of sine wave currents with oppositely oriented polarities of the bilaterally positioned electrodes. This arrangement causes activation on one side and disfacilitation of peripheral neuronal elements on the other side of, for example, the bilateral HC that was comparable to the situation during horizontal head rotations. This assumption was further tested by comparing LR nerve responses that were evoked by GVS of the bilateral HC (Fig. 5*M*,*N*) with either opposite phase (out of phase; top trace in Fig. 5*M*) or with phase alignment (in phase; bottom trace in Fig. 5*M*) of the sinusoidal current applied to the two stimulus electrodes. At variance with the clear discharge modulation during out-of-phase stimulation (black curve in Fig. 5*N*; $n = 7$), GVS with an in-phase relation of the cyclic currents (cf. green stimulus traces in top and bottom plots of Fig. 5*M*) did not provoke a modulation of the LR nerve activity (red curve in

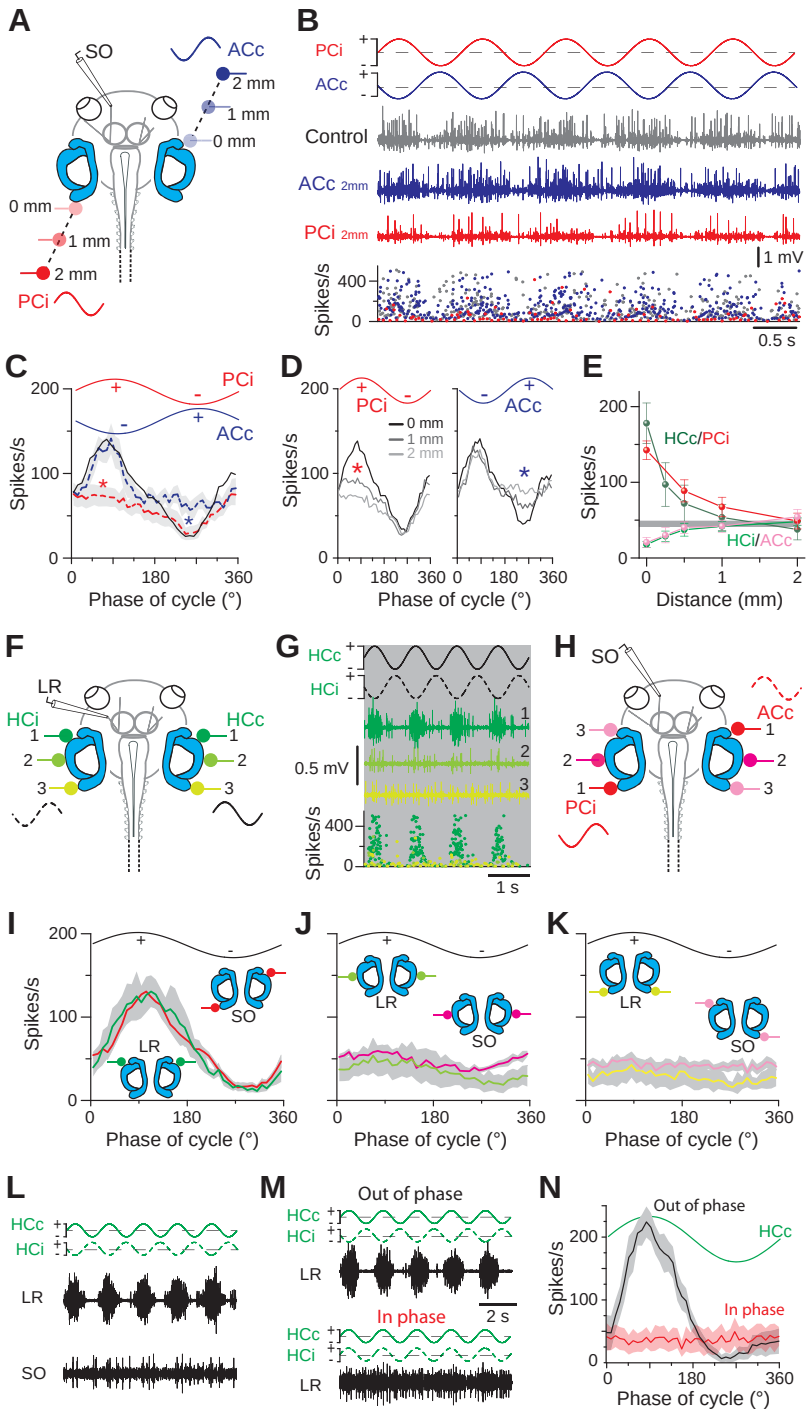

Figure 5. Stimulus site dependency of GVS-induced multi unit discharge modulation in extraocular motor nerves. ***A***, Extracellular recordings of the SO nerve during GVS of the left PC (PCi) and right AC (ACc) cupulae at different distances from the sensory epithelia (color-coded stimulus electrodes). ***B***, Left SO nerve discharge (middle traces) and instantaneous firing rate (bottom plot) during sinusoidal GVS of the left PC and right AC cupulae (traces in top row), with both electrodes close to the respective cupula (gray trace) and after independent repositioning of the ACc (blue trace) or PCi electrode (red trace) to a distance of 2 mm from the respective cupulae. ***C***, Averaged responses over a single GVS cycle (from 16 cycles; ±SEM, gray shaded areas; $n = 6$) with both stimulus electrodes close to the cupulae (black trace) and with the ACc (blue dashed trace) or PCi electrode (red dashed trace) at a distance of 2 mm from the cupula; Note the absence of either the inhibitory (blue asterisk) or the excitatory component (red asterisk) under the latter two stimulus conditions. ***D***, Averaged responses over a single GVS cycle (from 16 cycles in $n = 6$ preparations) with the PCi or ACc electrode at increasing distances from the epithelium; note the gradual reduction of excitatory (red asterisk) and inhibitory components (blue asterisk), respectively. ***E***, Dependency of HCc/PCi-evoked excitatory and HCi/ACc-evoked inhibitory response components in the LR and SO nerves on electrode position; the horizontal gray bar indicates the mean ± SEM of the LR/SO resting rates. ***F***, ***H***, Recordings of the LR (***F***) and SO nerve (***H***) during GVS of the HCc/HCi and the PCi/ACc cupulae and after bilateral electrode repositioning ($n = 10$; color-coded electrodes 1–3 in ***F***, ***H***). ***G***, Left LR nerve discharge (color-coded traces) and instantaneous rate (bottom plot) during sinusoidal GVS of the HCc/HCi cupulae (traces in top row) at three stimulus electrode positions (1–3, defined in ***F***). ***I–K***, Averaged responses of the LR and SO nerves over a single GVS cycle (from 16 cycles, ±SEM, gray shaded areas; $n = 10$) evoked with both electrodes close to the cupulae (HCc/HCi, PCi/ACc in ***I***) and after bilateral repositioning of the electrodes (***J***, ***K***; color-coded electrodes also in ***F***, ***H***). ***L***, Simultaneous recordings of the left LR (top trace) and SO (bottom trace) nerve during 0.5 Hz sinusoidal GVS (±50 μA) of the bilateral HC cupulae. ***M***, ***N***, LR nerve discharge during sinusoidal GVS (0.5 Hz; ±100 μA) of the bilateral HC cupulae with sinusoids that polarized the two stimulus electrodes either in phase opposition (out of phase; top traces in ***M***) or in phase alignment (in phase; bottom traces in ***M***); averaged extraocular motor responses (***N***, $n = 7$) over a single GVS cycle at 0.5 Hz (from 16 cycles, ±SEM, gray and light red shaded areas) with out-of-phase (black curve) or in-phase (red curve) polarization. Scale bar in ***M*** applies also to ***L***.

Fig. 5*N*; $n = 7$). This lack of modulation is compatible with a concurrent activation of excitatory and inhibitory vestibulo-ocular connections when the semicircular canal sensory peripheries on both sides are simultaneously activated/disfacilitated.

The systematic reduction of cyclic LR and SO nerve activity by altering the distances of the stimulus electrodes from the respective sensory epithelia in a stepwise manner indicates that the optimal semicircular canal position has a high specificity for the electrical activation of the three-neuronal VOR with respect to a particular spatial plane. Although the stimulus-site-specific alterations are consistent with the spatially limited extension of the electric field for GVS (Fig. 1*G*,*H*), this specificity also complies with the conserved main VOR connections between particular semicircular canals and sets of extraocular motoneurons (Precht, 1978; Straka and Dieringer, 2004).

GVS-induced modulation of Ca^{2+} transients in central vestibular neurons

The pattern of GVS-induced neuronal activity was studied by Ca^{2+} imaging of identified vestibulo-ocular projection neurons (green fibers and cell bodies in Fig. 6*A*) labeled retrogradely with a Ca^{2+} sensor (Calcium Green-1 dextran) from the oculomotor nucleus. With respect to the injection site, clusters of oculomotor-nucleus-projecting VOR neurons were consistently labeled ipsilateral in rhombomeres (r) 2–3 and contralateral in r5-6 (white outlined areas in Fig. 6*A*), compatible with earlier studies (Straka et al., 2001, 2002a). The two populations coincide with the known segmental positions of VOR neurons that receive excitatory vestibular afferent inputs from an ipsilateral vertical semicircular canal (Straka et

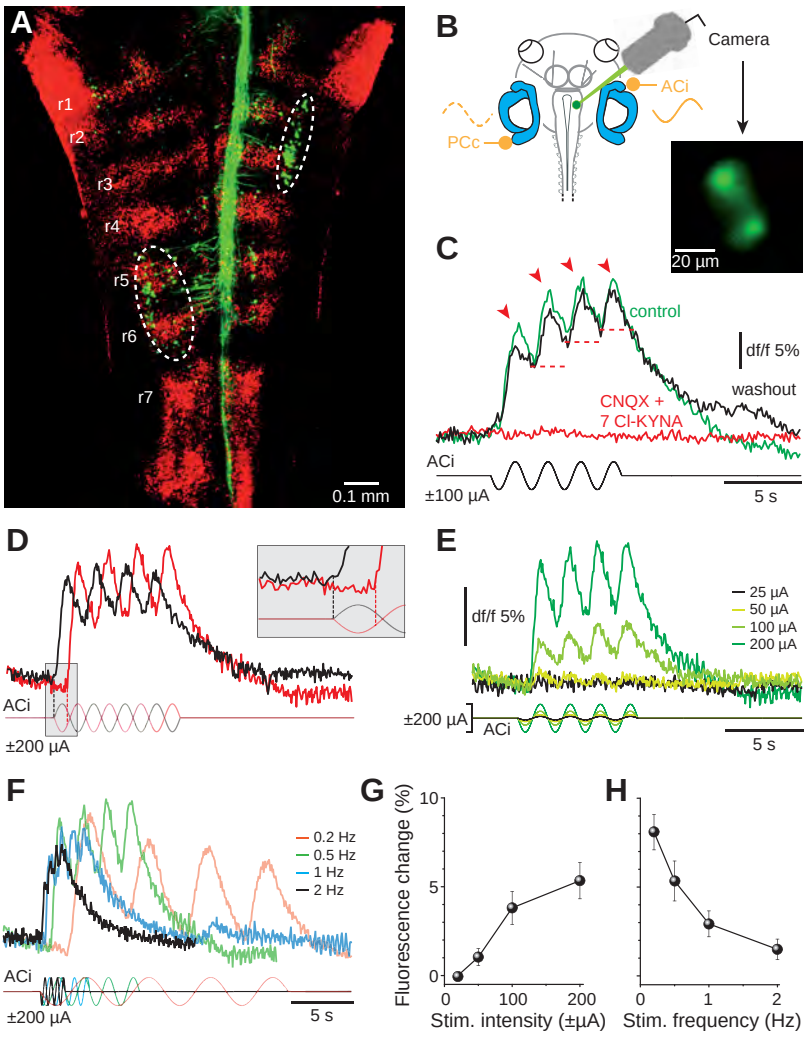

Figure 6. GVS-induced calcium dynamics in vestibulo-ocular neurons. ***A***, Confocal reconstruction of hindbrain whole mounts after application of Alexa Fluor 488 dextran to the right oculomotor nucleus depicting retrogradely labeled vestibulo-ocular projection neurons (green) in ipsilateral r2-3 and contralateral r5-6 (white encircled areas); rhombomeres (red) were visualized with 633 nm illumination. ***B***, Recording of Ca^{2+} transients in r2-3 vestibulo-ocular neurons (green neurons in inset) during GVS of the ACi and PCc; neurons were retrogradely labeled with the Ca^{2+}-sensor (Calcium Green-1 dextran) from the ipsilateral oculomotor nucleus. ***C***, GVS-induced Ca^{2+} transients before (green trace, control), during (red trace), and after 30 min of wash-out (black trace) of CNQX (15 μM) and 7-Cl-KYNA (50 μM); arrowheads indicate cyclic phase-timed fluorescence peaks; red dashed lines indicate successively elevated Ca^{2+} levels. ***D–F***, Ca^{2+} transients induced by GVS with opposite stimulus polarities (red and black stimulus traces, ***D***), increasing current stimulus amplitudes (color-coded traces, ***E***) and increasing stimulus frequency (color-coded traces, ***F***). Inset in ***D*** illustrates a half-cycle shift in response onset with inversion of the stimulus polarity. ***G***, ***H***, Dependency of fluorescence peak amplitude (***G***) and cyclic fluorescence oscillations (***H***) on stimulus intensity and frequency, respectively. Fluorescence calibration (d*F*/*F*) in ***E*** also applies to ***D*** and ***F***.

al., 2002b) and commissural inhibitory inputs from the corresponding contralateral coplanar semicircular canal (Holler and Straka, 2001). Accordingly, we simultaneously stimulated the ipsilateral AC and contralateral PC with sinusoidal GVS (Fig. 6*B*) and recorded Ca^{2+} transients of identified VOR neurons in r2-3 that were backfilled with the Ca^{2+} sensor (green neurons in Fig. 6*B*). The majority of these neurons (12 of 16 neurons in five preparations) exhibited fluorescence changes during GVS (Fig. 6*C*). At a stimulus frequency of 0.5 Hz, these Ca^{2+} responses consisted of cyclic fluorescence oscillations (red arrowheads in Fig. 6*C*), with the peaks being phase timed to the depolarization of the ipsilateral AC. During the alternating hyperpolarization, the fluorescence failed to reach the initial baseline, likely due to the low dynamics of the Ca^{2+} sensor, thus causing each subsequent transient to start from a successively higher Ca^{2+} level (red dashed lines in Fig. 6*C*).

To demonstrate that the observed GVS-induced Ca^{2+}-responses were mediated synaptically, rather than by direct electrical activation of central vestibular neurons, we pharmacologically blocked the glutamatergic transmission between vestibular nerve afferents and second-order vestibular neurons (Fig. 6*C*). Combined bath application of the AMPA receptor blocker CNQX (15 μM) and NMDA blocker 7-Cl-KYNA (50 μM) reversibly abolished the stimulus-evoked fluorescence modulation (red trace in Fig. 6*C*), thus excluding a direct activation of central vestibular neurons by GVS. Accordingly, Ca^{2+} transients in VOR neurons were provoked by vestibular nerve afferent discharge after activation of cellular elements in the semicircular canal epithelium. However, this activation exhibited a distinct specificity with respect to the polarity of the galvanic stimulus. In fact, Ca^{2+} transients of imaged VOR neurons were only activated by cathodal currents at the electrode close to the ipsilateral AC cupula (Fig. 6*D*). Accordingly, after inversion of the stimulus polarity, the response onset was shifted by a half cycle, coinciding again with a depolarization of the ACi epithelium (compare red and black traces in inset of Fig. 6*D*).

The activation of VOR neurons through bilateral GVS of the ACi/PCc was further evaluated by systematically altering stimulus amplitude and frequency (Fig. 6*E*,*F*). With increasing GVS magnitude (±25–200 μA), the amplitude of the fluorescence peaks (Fig. 6*E*,*G*), as well as the fluorescence level from which the Ca^{2+} transients started during each successive depolarizing half cycle, increased gradually (see also red dashed lines in Fig. 6*C*). A similar augmentation of the fluorescence level over the stimulus period was observed with increasing frequencies (0.2–2 Hz), whereas, at the same time, the cyclic-phase-timed fluorescence peaks became gradually smaller and less discernible (Fig. 6*F*,*H*). This latter decline is again likely due to the slow decay time constant of the evoked Ca^{2+}-responses that restricts a dissociation of individual peaks with increasing GVS frequencies. Nonetheless, individual Ca^{2+} oscillations were still distinguishable up to a stimulus frequency of 2 Hz (Fig. 6*H*).

GVS-induced modulation of vestibular nerve afferent discharge

GVS-induced extraocular motor activity or discharge of VOR neurons depends on the activation of excitable cells in the vestibular sensory epithelium. Because the membrane potential of both hair cells and afferent fibers is sensitive to electrical currents, GVS could either trigger action potentials in vestibular afferents di-

rectly or indirectly through hair cell depolarization and increased transmitter release or recruit both cellular substrates. To differentiate between these possibilities, we recorded multiunit spike discharge from the anterior branch of the VIIIth nerve and the spike activity of single afferent nerve fibers during sinusoidal rotation and GVS of the HC or AC sensory epithelium (Fig. 7*A*). During sinusoidal turntable rotation, the multiunit discharge (dark red trace in Fig. 7*B*) and the spike activity of individual afferents (HC afferent fiber; light red trace in Fig. 7*B*) became cyclically modulated with an increase of the discharge during ipsiversive motion. However, independent of the number of recorded units, the peak firing rate of the multiunit recording ($n = 8$) increased gradually with peak velocity over the used stimulus range (red shaded area in Fig. 7*D*). This discharge profile was confirmed by single-unit HC ($n = 34$) and AC ($n = 5$) nerve afferent recordings; however, as expected, single units had peak firing rates that were lower than those of the multiunit recordings [cf. multiunit (M) and single-unit (S) recordings in left plot of Fig. 7*C*]. Nonetheless, the increase in maximal firing rate with peak stimulus velocity was very similar between single-unit and multiunit recordings (cf. red symbols with red shaded area in Fig. 7*D*) and not significantly different from each other (Mann–Whitney *U* test). The relatively wide range of resting rates between 0.1 and 14.1 spikes/s (mean rate ± SD: 5.10 ± 4.95 spikes/s; $n = 39$) and discharge regularity between 0.30 and 1.46 (mean CV± SD: 0.83 ± 0.32; $n = 39$) of the recorded single units suggest that a relatively broad population of dynamically different vestibular nerve afferent fibers has been included in the analysis (Honrubia et al., 1989).

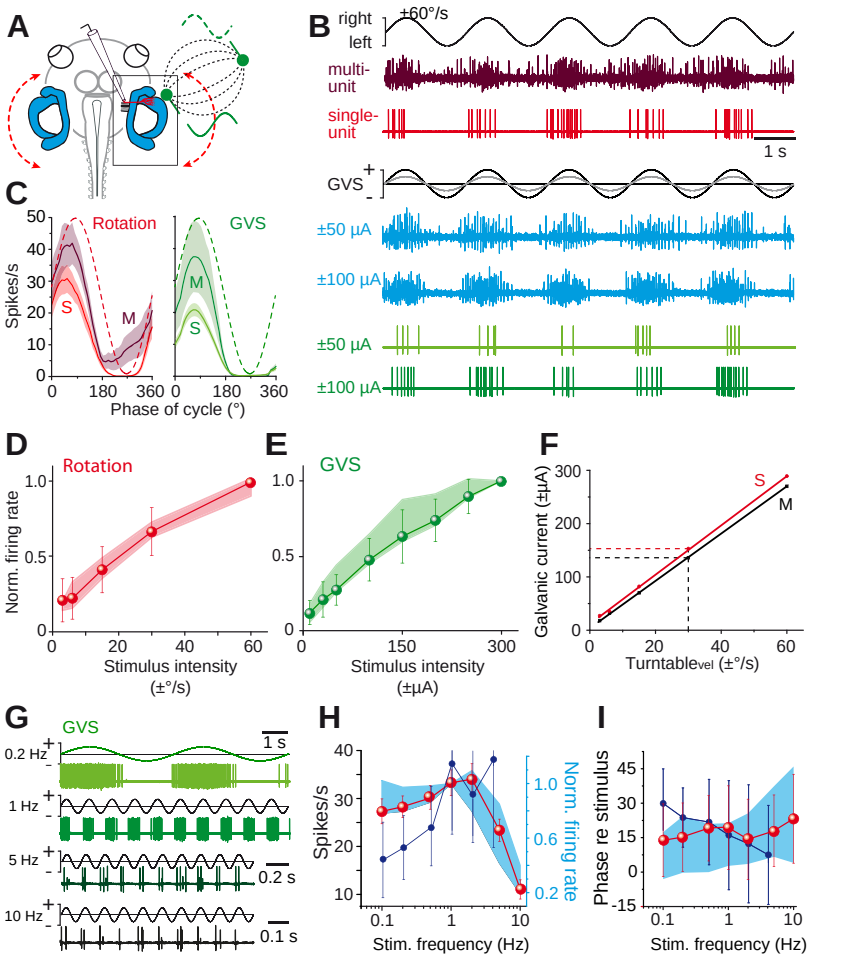

Figure 7. Dynamics of rotation- and GVS-evoked HC afferent neuronal discharge. ***A***, Extracellular recordings of afferent fibers in the anterior branch of the right VIIIth nerve during horizontal rotation (red dashed curve) and GVS of the right HC cupula (green electrode); note the electric field (black dashed field lines) between the HC and a second electrode in the bath solution (green electrode). ***B***, Multiunit discharge (dark red trace; blue traces) and HC single-unit discharge (light red trace; green traces) during horizontal sinusoidal turntable rotation (0.5 Hz; top traces) and GVS of the HC at two current intensities (bottom traces). ***C***, Averaged multiunit (M; $n = 8$) and single-unit (S; $n = 39$) responses over a single rotation and GVS cycle, respectively (from 16 cycles, ±SEM, shaded areas); red and green dashed sinusoids indicate the current stimulus. ***D***, ***E***, Dependency of the normalized multiunit (colored areas, ±SD in ***D***, ***E***; $n = 8$) and HC/AC single-unit (colored symbols in ***D***, ***E***; $n = 34$ HC, $n = 5$ AC afferent fibers) firing rates on rotation (***D***) and GVS stimulus intensities (***E***). ***F***, Calibration of the GVS with respect to turntable peak velocity based on corresponding multiunit (M, black line) and single-unit (S, red line) firing rates; imitation of 30°/s turntable peak velocity (at 0.5 Hz) requires GVS currents of ±140 µA and ±155 µA, respectively (dashed lines). ***G***, HC single-unit discharge during sinusoidal GVS (±100 µA) of the HC at 4 stimulus frequencies ($n = 5$). ***H***, ***I***, Average amplitude (***H***) and phase (***I***) of multiunit responses during sinusoidal GVS (blue areas, ±SD in ***H***, ***I***; $n = 8$) and of HC single-unit responses during sinusoidal GVS (red symbols in ***H***, ***I***; $n = 20$) and sinusoidal rotation (dark blue symbols in ***H***, ***I***; $n = 26$) at different stimulus frequencies; note that multiunit firing rates were normalized in ***H***. Scale bar in ***B*** applies to all traces; calibration bar in ***G*** for 0.2 Hz applies also to 1 Hz.

During GVS of the HC or AC cupula, the afferent spike discharge (HC single-unit: green traces; multiunit: blue traces in Fig. 7*B*) was sinusoidally modulated with a similar difference in peak firing rates between multiunit and single-unit recordings (cf. M and S in right plot of Fig. 7*C*) as seen for the corresponding responses during rotational stimuli (left plot of Fig. 7*C*). With increasing GVS currents, the peak firing rate increased for both multiunit recordings (blue traces in Fig. 7*B*) and single-unit recordings (green traces in Fig. 7*B*). In fact, the maximal firing rate augmented similarly with current intensity in both cases (cf. green symbols with green shaded area in Fig. 7*E*) and was not significantly different from each other (Mann–Whitney *U* test). The relatively linear correlation between vestibular afferent peak firing rate and stimulus intensity over a wide range during rotation and GVS, respectively (Fig. 7*D*,*E*), allowed calibrating the GVS current with respect to the motion stimulus amplitude (red and black line in Fig. 7*F*). Using the peak discharge of vestibular nerve afferents obtained from single-unit (S, red line) and multiunit (M, black line) recordings during rotation and GVS as common parameter, this comparison allowed translating peak head velocity into GVS current amplitude and vice versa. Given the matching dependency of single-unit and multiunit discharge on stimulus intensities, respectively (Fig. 7*D*,*E*), the calibration yielded similar results in both cases (red and black lines in Fig. 7*F*). Accordingly, imitation of the discharge during a sinusoidal rotation with a peak velocity of 30°/s requires a GVS current of approximately ±150 µA.

Whereas multiunit and single-unit recordings revealed similar afferent response dynamics, the multiunit recording from the anterior branch of the VIIIth nerve captured the activity of a rather heterogeneous group of fibers that very likely also included

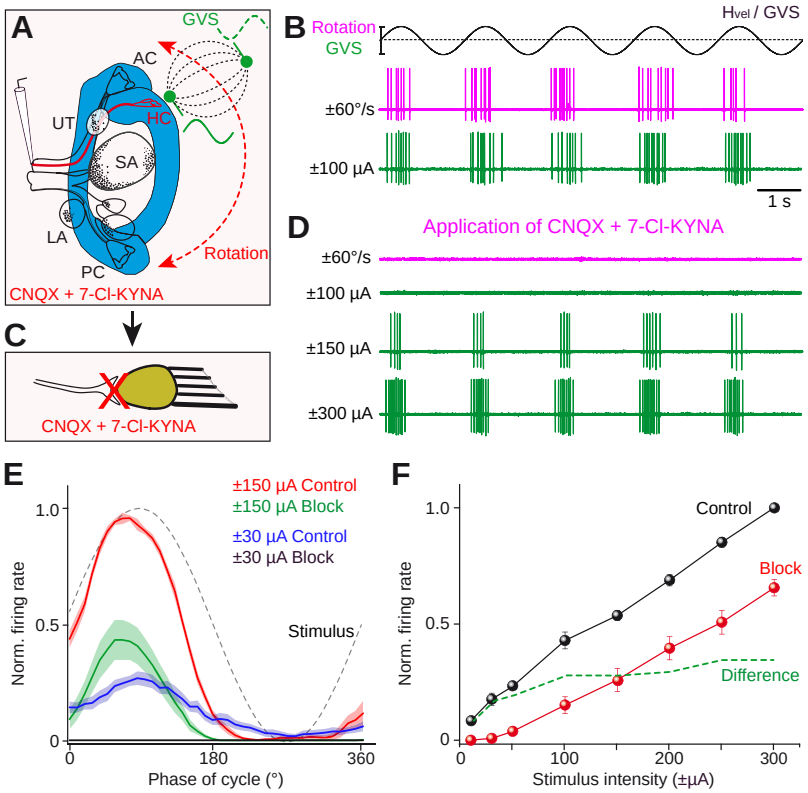

Figure 8. Determination of the cellular substrate underlying GVS-induced spike discharge in vestibular nerve afferents. ***A***, Single-unit recordings of HC afferents during horizontal turntable rotation (red dashed arrow) and GVS of the HC cupula (green stimulus electrode); note that the GVS electric field (dashed field lines) expands between the HC electrode and a distant one in the Ringer's solution. ***B–D***, Single HC afferent fiber discharge during horizontal rotation (magenta traces in ***B***, ***D***) and GVS of the HC cupula (green traces in ***B***, ***D***) before (***B***) and during (***D***) bath application of CNQX (15 μM) and 7-Cl-KYNA (50 μM) that blocked the synaptic transmission between hair cells and vestibular afferent fibers pharmacologically (***C***). ***E***, ***F***, Averaged single-unit afferent discharge over one cycle of GVS (from 16 cycles, ±SEM, shaded areas; $n = 13$) at two stimulus intensities (±30 μA, ±150 μA; ***E***) and dependency of GVS-induced peak afferent firing rate on stimulus intensity (***F***) before (control, black symbols) and during pharmacological block of the glutamatergic hair cell–afferent synapse (red symbols); green dashed line in ***F*** depicts the arithmetic difference between the two conditions, indicating the magnitude of hair cell contribution to the GVS-induced afferent discharge. Scale bar in ***B*** applies to all traces in ***B*** and ***D***.

utricular afferents along with HC and AC afferents. To obtain a more homogeneous population of afferent fibers for further analysis, we restricted our sampling to identified HC and AC single units ($n = 26$). GVS of the HC or AC at different stimulus frequencies (0.1–10 Hz) caused an afferent discharge modulation (Fig. 7*G*) with a maximal peak discharge at a stimulus frequency of ~1–2 Hz (red symbols in Fig. 7*H*), which was similar to that of multiunit recordings (blue area in Fig. 7*H*). This pattern is similar to that of motion-induced responses in the same afferent population with the exception of a further increase in sensitivity above a motion frequency of 1 Hz (dark blue symbols in Fig. 7*H*) and generally complies with the dynamics of mammalian afferent fibers despite their separation into different subtypes (Kim et al., 2011). The concurrent phase lead of GVS-induced responses with respect to stimulus velocity in the range of 10–20° at 0.1 Hz was relatively constant over the tested range of stimulus frequencies for both single-unit responses (red symbols in Fig. 7*I*) and multiunit responses (blue area in Fig. 7*I*). This phase independence was similar to the phase relation of the responses during sinusoidal head motion (dark blue symbols in Fig. 7*I*), which, however, in the current study could only be evaluated up to a stimulus frequency of 4 Hz due to the impaired stability of the afferent recordings at even higher stimulus frequencies. Unfortunately, this prevented a direct comparison of phase values of GVS- and motion-induced responses at higher frequencies as in mammals (Kim et al., 2011). In the current study, the broad distribution of amplitude modulation and phase values over the range of used frequencies is likely related to the relatively broad spectrum of recorded single units, as indicated by the range of resting rates and CVs (see above).

Cellular substrate for galvanic stimulation of semicircular canals

To resolve the question of which cellular substrate(s), hair cells and/or vestibular nerve afferents are activated by GVS, we recorded the galvanically induced discharge modulation of HC and AC afferent fibers ($n = 13$) during pharmacological blockade of the synaptic transmission between hair cells and vestibular afferent fibers (Fig. 8*A*,*C*). All recorded afferent fibers were robustly modulated during either horizontal rotation (HC afferents) or rotation in the direction of the ipsilateral AC (AC afferents), as well as during GVS before drug application (magenta and green traces in Fig. 8*B*). Combined bath application of AMPA receptor (CNQX: 15 μM) and NMDA receptor (7-Cl-KYNA: 50 μM) antagonists completely blocked the motion-induced discharge modulation (magenta trace in Fig. 8*D*), confirming the suppression of the glutamatergic transmission between hair cells and vestibular nerve afferents (Fig. 8*C*). Similarly, the discharge modulation induced by low GVS intensities was blocked under this condition (cf. green traces at a GVS of ±100 μA in Fig. 8*B*,*D*). However, the discharge modulation evoked by higher GVS currents persisted (green traces at a GVS of ±150 and 300 μA in Fig. 8*D*), even though peak firing rates were markedly reduced (Fig. 8*E*,*F*). The failure to induce a discharge modulation by GVS at stimulus intensities <50 μA (Fig. 8*F*) in the presence of glutamatergic antagonists suggests a preferential recruitment of hair cells at low stimulus intensities, with only limited increase at higher currents (dashed line in Fig. 8*F*). Therefore, the partial reduction of GVS-induced vestibular afferent discharge modulation, when the hair cell–afferent synaptic transmission was blocked (Fig. 8*E*,*F*), indicates that, under control conditions, both hair cells and afferent fibers are recruited by galvanic vestibular stimulation even though a direct activation of vestibular afferents predominated at higher stimulus intensities.

Discussion

Sinusoidal galvanic stimulation of semicircular canals provokes a modulation of neuronal activity in all VOR elements. The GVS site dependency of response magnitudes and matching spatio-temporal profiles during GVS and rotation demonstrate that applied currents activate canal-specific circuits and imitate natural head movements over a broad range of frequencies and amplitudes. The partially reduced GVS-evoked vestibular afferent dis-

charge following a block of the glutamatergic transmission indicates that galvanic currents recruit both hair cells and vestibular nerve afferent fibers.

Cellular substrate of GVS-evoked responses

Clinical interpretation of galvanically evoked responses in patients with inner ear pathologies depends on the knowledge of the cellular substrate that is activated by GVS. Ever since the study by Goldberg et al. (1984), the relatively unchallenged notion was that GVS activates vestibular nerve afferents directly at the action potential trigger site, bypassing hair cell synapses (see Fitzpatrick and Day, 2004). Based on axon diameters, cathodal and anodal galvanic currents predominantly recruit and silence irregular afferent fibers, respectively, with a limited influence on regularly firing afferents at higher stimulus intensities (Ezure et al., 1983; Goldberg et al., 1984; Kim and Curthoys, 2004; Kim et al., 2011; Shanidze et al., 2012). However, until now, no direct experimental demonstration was available showing that GVS-evoked responses in vestibulo-motor circuitries are activated without hair cell contribution. Nonetheless, the view that vestibular afferents are the exclusive origin of GVS-induced vestibular responses still prevails. Recently, however, electrical induction of VORs in gentamicin-treated human patients has challenged this assumption (Aw et al., 2008). The impairment of evoked eye movements in the latter study was interpreted as evidence that GVS-induced responses depend, at least in part, on the electrical recruitment of hair cells (Aw et al., 2008).

A significant hair cell contribution to GVS-induced afferent discharge was in fact confirmed in the present study (Fig. 8). After complete pharmacological blockade of the glutamatergic transmission between hair cells and afferent fibers, GVS-induced responses persisted, although at reduced magnitudes (Fig. 8*F*). The loss of part of the GVS-induced afferent activity suggests that a direct activation of hair cells normally contributes to the discharge modulation, a result that complies with the findings in patients with gentamicin-induced vestibular deficits (Aw et al., 2008). Whereas our approach benefited from spatially specific locations of stimulation electrodes and preservation of intact inner ears, an activation of both peripheral excitable elements in other species or with other electrode placements is likely and might finally reconcile previously opposing views on the cellular substrate of GVS. This general extension of our finding is also supported by very similar species-independent dynamics of GVS-induced vestibular afferent responses (Ezure et al., 1983; Kim et al., 2011) and by the overall evolutionary conservation of the vertebrate inner ear (Goldberg, 2000; Fritzsch and Straka, 2014).

Spatial specificity of vestibular end-organ activation by GVS

Placement of GVS electrodes outside the intact otic capsule in close proximity to the semicircular canal cupulae in the present study was facilitated by the plain visibility of the inner ear in *X. laevis* tadpoles (Straka and Simmers, 2012). This experimental condition has the advantage of leaving endolymph motion-driven cupula displacements unaffected. The locally restricted electric field (Fig. 1*G*) and the stimulus site dependency of responses (Fig. 5*C*,*D*,*I–K*) indicate that single or pairs of bilateral coplanar semicircular canals, and thus plane-specific vestibulo-motor pathways, can be activated separately, compatible with the effects of a multichannel vestibular prosthesis in monkeys (Dai et al., 2013). This spatiotemporal specificity of GVS-evoked extraocular motor responses was validated by our experiments indicating that careful placement of the electrodes evokes responses with the same spatial specificity as during a rotation along the same canal plane. This also largely excludes concurrent electrical activation of other semicircular canals or the more distant otolith organs. Accordingly, stimulus electrode placement on a specific semicircular canal in *X. laevis* is more precise compared with most studies on mammalian species/humans in which electrodes were inserted into the perilymphatic space of the inner ear (Ezure et al., 1983; Kim et al., 2011; Shanidze et al., 2012), the middle ear cavity (Kim and Curthoys, 2004; Kim, 2013a, 2013b), or onto the skin (Fitzpatrick and Day, 2004) and activated all vestibular end organs, as evidenced by, for example, current-evoked eye (Schneider et al., 2002) or head (Kim, 2013a) movements.

Despite the different positions of the internally placed stimulus electrodes, relatively similar current intensities ($\pm$100 μA) were required to evoke responses in vestibular afferents (Kim and Curthoys, 2004; Kim et al., 2011; this study) and central vestibular pathways or to effectively trigger VOR behavior (Shanidze et al., 2012). Minor variations are likely related to size/resistance of the stimulus electrodes and/or leak currents. These values, however, differ by ~10-fold from those required for transmastoidal stimulation in human subjects (Fitzpatrick and Day, 2004). Although absolute values depend largely on the experimental approach, a comparison of motion- and GVS-induced responses allowed calibrating the current stimulus (Fitzpatrick and Day, 2004). With regard to eye movements (Fig. 2) and vestibular afferent discharge (Fig. 7) in *X. laevis* tadpoles, the respective general patterns and dynamics of current- and motion-induced responses match very well (Figs. 2*G*, 7*F*). Moreover, the corresponding calibration of GVS-induced afferent discharge and eye movements indicates that a representative sample of neurons was recorded at each synaptic level of the VOR. Moreover, the similarity of responses in this study compared with other studies (Ezure et al., 1983) suggests that the interpretation of our results can be extended onto other GVS models.

Dynamic properties of GVS-evoked responses

Most previous studies used current pulses to study GVS-induced neuronal responses and vestibulo-motor behaviors or to perturb activity patterns during motion stimulation (Shanidze et al., 2012; Kim, 2013a, 2013b). In addition, current- and motion-evoked responses were generally compared at one level of the VOR circuitry (Kim and Curthoys, 2004; Kim et al., 2011). In contrast, our approach, which probed each synaptic stage of the VOR, allowed estimating the dynamic similarity of motion and GVS-induced responses at multiple levels. This attempt revealed that sinusoidal GVS corresponds more closely to the velocity than the position component of head movements (Fig. 2*C*,*D*), with similar phase relations between GVS- and motion-evoked responses in VOR neuronal elements over most of the tested frequency range (~0.2-1 Hz). The tendency of more phase-advanced GVS-compared with motion-induced responses >1 Hz in our study is likely due to a direct activation of vestibular afferents, which bypasses canal fluid dynamics, cilial bundle deflection, and synaptic transmission between hair cells and afferent fibers, a finding that is even more pronounced in the cat (Ezure et al., 1983) and chinchilla (Kim et al., 2011), in which higher stimulus frequencies were used. The further increasing sensitivity of afferents for motion-evoked responses >2 Hz at variance with GVS-induced afferent discharge (Fig. 7*H*) is compatible with data from the chinchilla (Kim et al., 2011) and might be related to an altered efficacy of GVS at higher frequencies. Moreover, specific differences between GVS- and rotation-evoked response dynamics in mammals and amphibians might

be related to afferent fiber types, stimulus frequencies used, and/or electrode placement. Because recruitment order and activation threshold of hair cells and afferent fibers differ between electrical and motion stimulation, any comparison between GVS- and motion-induced responses requires careful interpretation (Kim and Curthoys, 2004; Kim et al., 2011).

In contrast, differences in timing between GVS-induced extraocular motor discharge and eye movements are similar to those of respective motion-induced responses and are likely related to the additional synapse between motoneurons and muscle fibers and the buildup of muscle strength. The available response dynamics of various VOR neuronal elements in the same animal model allows determining transfer functions that might be also relevant for other species. Although GVS pulses are convenient to determine response onsets (Goldberg et al., 1984), sinusoidally oscillating stimuli appear to be more suitable for activating irregular vestibular afferents given their particularly fast response dynamics (Goldberg, 2000), which in part are due to voltage-dependent K^+-channels (Eatock and Songer, 2011).

The possibility of using GVS to imitate body motion will facilitate the conduction of fluorescence imaging experiments in central nervous circuits that render natural vestibular stimulation challenging. The possibility of differentiating GVS-induced responses temporally during Ca^{2+} imaging up to 2 Hz (Fig. 6) will facilitate studies that aim at understanding the organization of frequency-tuned vestibular pathways for sensory–motor transformation (Straka et al., 2005). Moreover, knowledge of the activated cellular substrates allows a more faithful categorization of vestibular disorders (Curthoys, 2010) or further improvement of vestibular prostheses (Fridman and Della Santina, 2013). In animals (Gong and Merfeld, 2000; Dai et al., 2011; Mitchell et al., 2013) and human patients (Phillips et al., 2015), vestibular prostheses provide controlled inputs that trigger vestibular reflexes (Dai et al., 2013; Lewis, 2015). Whereas prosthetic rate stimulation activates ampullary nerve fibers directly, modulated DC currents might also recruit hair cells, if intact. However, more insight into the mechanistic basis of GVS is required to understand the differential activation of excitable elements within the vestibular epithelia. Once this is resolved, GVS will considerably facilitate the diagnosis and treatment of vestibular deficits and the understanding of basic aspects of sensory–motor transformations.

References

Angelaki DE, Perachio AA (1993) Contribution of irregular semicircular canal afferents to the horizontal vestibuloocular response during constant velocity rotation. J Neurophysiol 69:996–999. Medline

Aw ST, Todd MJ, Aw GE, Weber KP, Halmagyi GM (2008) Gentamicin vestibulotoxicity impairs human electrically evoked vestibulo-ocular reflex. Neurology 71:1776–1782. CrossRef Medline

Aw ST, Aw GE, Todd MJ, Halmagyi GM (2013) Enhanced vestibulo-ocular reflex to electrical vestibular stimulation in Meniere's disease. J Assoc Res Otolaryngol 14:49–59. CrossRef Medline

Beck JC, Gilland E, Baker R, Tank DW (2004) Instrumentation for measuring oculomotor performance and plasticity in larval organisms. Methods Cell Biol 76:385–413. CrossRef Medline

Biesdorf S, Malinvaud D, Reichenberger I, Pfanzelt S, Straka H (2008) Differential inhibitory control of semicircular canal nerve afferent-evoked inputs in second-order vestibular neurons by glycinergic and GABAergic circuits. J Neurophysiol 99:1758–1769. CrossRef Medline

Bos JH, Jongkees LB (1963) On galvanic stimulation of the labyrinth. Pract Otorhinolaryngol (Basel) 25:345–348. Medline

Branoner F, Straka H (2015) Semicircular canal-dependent developmental tuning of translational vestibulo-ocular reflexes in *Xenopus laevis.* Dev Neurobiol 75:1051–1067. CrossRef Medline

Clarke AH (2010) Laboratory testing of the vestibular system. Curr Opin Otolaryngol Head Neck Surg 18:425–430. CrossRef Medline

Cohen B, Martinelli GP, Ogorodnikov D, Xiang Y, Raphan T, Holstein GR, Yakushin SB (2011) Sinusoidal galvanic vestibular stimulation (sGVS) induces a vasovagal response in the rat. Exp Brain Res 210:45–55. CrossRef Medline

Courjon JH, Precht W, Sirkin DW (1987) Vestibular nerve and nuclei unit responses and eye movement responses to repetitive galvanic stimulation of the labyrinth in the rat. Exp Brain Res 66:41–48. Medline

Curthoys IS (2010) A critical review of the neurophysiological evidence underlying clinical vestibular testing using sound, vibration and galvanic stimuli. Clin Neurophysiol 121:132–144. CrossRef Medline

Curthoys IS, Macdougall HG (2012) What galvanic vestibular stimulation actually activates. Front Neurol 3:117. CrossRef Medline

Dai C, Fridman GY, Davidovics NS, Chiang B, Ahn JH, Della Santina CC (2011) Restoration of 3D vestibular sensation in rhesus monkeys using a multichannel vestibular prosthesis. Hear Res 281:74–83. CrossRef Medline

Dai C, Fridman GY, Chiang B, Rahman MA, Ahn JH, Davidovics NS, Della Santina CC (2013) Directional plasticity rapidly improves 3D vestibulo-ocular reflex alignment in monkeys using a multichannel vestibular prosthesis. J Assoc Res Otolaryngol 14:863–877. CrossRef Medline

Eatock RA, Songer JE (2011) Vestibular hair cells and afferents: two channels for head motion signals. Annu Rev Neurosci 34:501–534. CrossRef Medline

Ezure K, Cohen MS, Wilson VJ (1983) Response of cat semicircular canal afferents to sinusoidal polarizing currents: implications for input-output properties of second-order neurons. J Neurophysiol 49:639–648. Medline

Ferrè ER, Longo MR, Fiori F, Haggard P (2013) Vestibular modulation of spatial perception. Front Hum Neurosci 7:660. CrossRef Medline

Fitzpatrick RC, Day BL (2004) Probing the vestibular system with galvanic stimulation. J Appl Physiol 96:2301–2316. Medline

Fitzpatrick RC, Watson SR (2015) Passive motion reduces vestibular balance and perceptual responses. J Physiol 593:2389–2398. CrossRef Medline

Fridman GY, Della Santina CC (2013) Safe direct current stimulation to expand capabilities of neural prostheses. IEEE Trans Neural Syst Rehabil Eng 21:319–328. CrossRef Medline

Fritzsch B, Straka H (2014) Evolution of mechanosensory hair cells and inner ears: identifying stimuli to select altered molecular development toward new morphologies. J Comp Physiol A Neuroethol Sens Neural Behav Physiol 200:5–18. CrossRef Medline

Galvani L (1791) *De viribus electicitatis in motu musculari commentarius.* Translated by Foley, M.G. as *Luigi Galvani: Commentary of the Effects of Electricity on Muscular Motion.* 1953, Burndy Library: Norwalk.

Goldberg JM (2000) Afferent diversity and the organization of central vestibular pathways. Exp Brain Res 130:277–297. CrossRef Medline

Goldberg JM, Smith CE, Fernández C (1984) Relation between discharge regularity and responses to externally applied galvanic currents in vestibular nerve afferents of the squirrel monkey. J Neurophysiol 51:1236–1256. Medline

Gong W, Merfeld DM (2000) Prototype neural semicircular canal prosthesis using patterned electrical stimulation. Ann Biomed Eng 28:572–581. CrossRef Medline

Graf W, Simpson JI (1981) The relations between the semicircular canals, the optic axis, and the extraocular muscles in lateral-eyed and frontal-eyed animals. In: Progress in oculomotor research, developments in neuroscience, Vol 12 (Fuchs A, Becker W, eds), pp 411–420. Elsevier: New York.

Grasso C, Orsini P, Bruschini L, Manzoni D, Barresi M (2013) A new technique to investigate vestibulo-spinal reflexes. Arch Ital Biol 151:54–66. CrossRef Medline

Highstein SM, Goldberg JM, Moschovakis AK, Fernández C (1987) Inputs from regularly and irregularly discharging vestibular nerve afferents to secondary neurons in the vestibular nuclei of the squirrel monkey. II. Correlation with output pathways of secondary neurons. J Neurophysiol 58:719–738. Medline

Hitzig E (1871) Über galvanischen Schwindel. Arch Ohren-, Nasen- Kehlkopfheilk 5/6:34–37.

Holler S, Straka H (2001) Plane-specific brainstem commissural inhibition in frog second order semicircular canal neurons. Exp Brain Res 137:190–196. CrossRef Medline

Honrubia V, Hoffman LF, Sitko S, Schwartz IR (1989) Anatomic and physiological correlates in bullfrog vestibular nerve. J Neurophysiol 61:688–701. Medline

Hsu LJ, Zelenin PV, Orlovsky GN, Deliagina TG (2012) Effects of galvanic vestibular stimulation on postural limb reflexes and neurons of spinal postural network. J Neurophysiol 108:300–313. CrossRef Medline

Kaufmann AK, Gensberger K, Dietrich H, Branoner F, Banchi R, Chagnaud

BP, Straka H (2013) Mechanistic basis and spatiotemporal specificity of galvanic vestibular stimulation in *Xenopus laevis*. Soc Neurosci Abstr 39:164.04.

Kim J (2013a) Head movements suggest canal and otolith projections are activated during galvanic vestibular stimulation. Neuroscience 253: 416–425. CrossRef Medline

Kim J (2013b) Tonic eye movements induced by bilateral and unilateral galvanic vestibular stimulation (GVS) in guinea pigs. Brain Res Bull 90: 72–78. CrossRef Medline

Kim J, Curthoys IS (2004) Responses of primary vestibular neurons to galvanic vestibular stimulation (GVS) in the anaesthetised guinea pig. Brain Res Bull 64:265–271. CrossRef Medline

Kim KS, Minor LB, Della Santina CC, Lasker DM (2011) Variation in response dynamics of regular and irregular vestibular-nerve afferents during sinusoidal head rotations and currents in the chinchilla. Exp Brain Res 210:643–649. CrossRef Medline

Lambert FM, Beck JC, Baker R, Straka H (2008) Semicircular canal size determines the developmental onset of angular vestibuloocular reflexes in larval *Xenopus*. J Neurosci 28:8086–8095. CrossRef Medline

Lambert FM, Malinvaud D, Gratacap M, Straka H, Vidal PP (2013) Restricted neural plasticity in vestibulospinal pathways after unilateral labyrinthectomy as the origin for scoliotic deformations. J Neurosci 33: 6845–6856. CrossRef Medline

LeRoy C (1755) Où l'on rend compte de quelques tentatives que l'on a faites pour guérir plusieurs maladies par l'électricité. Hist Acad Roy Sciences (Paris), Mémoire Math Phys 60:87–95.

Lewis RF (2015) Advances in the diagnosis and treatment of vestibular disorders: psychophysics and prosthetics. J Neurosci 35:5089–5096. CrossRef Medline

Minor LB, Goldberg JM (1991) Vestibular nerve inputs to the vestibulo-ocular reflex: A functional ablation study in the squirrel monkey. J Neurosci 11:1636–1648. Medline

Mitchell DE, Dai C, Rahman MA, Ahn JH, Della Santina CC, Cullen KE (2013) Head movements evoked in alert rhesus monkey by vestibular prosthesis stimulation: implications for postural and gaze stabilization. PLoS One 8:e78767. CrossRef Medline

Nieuwkoop PD, Faber J (1994) Normal table of *Xenopus laevis* (Daudin): a systematical and chronological survey of the development from the fertilized egg till the end of metamorphosis. New York: Garland.

Phillips JO, Ling L, Nie K, Jameyson E, Phillips CM, Nowack AL, Golub JS, Rubinstein JT (2015) Vestibular implantation and longitudinal electrical stimulation of the semicircular canal afferents in human subjects. J Neurophysiol 113:3866–3892. CrossRef Medline

Precht W (1978) Neuronal operations in the vestibular system: studies of brain function. Berlin Heidelberg: Springer.

Purkinje J (1820) Beiträge zur näheren Kenntnis des Schwindels. Med Jahrb k u k Staates (Wien) 6:23–35.

Ramlochansingh C, Branoner F, Chagnaud BP, Straka H (2014) Tricaine methanesulfonate (MS-222) as an effective anesthetic agent for blocking sensory-motor responses in *Xenopus laevis* tadpoles. PLoS ONE 9:e101606. CrossRef Medline

Schneider E, Glasauer S, Dieterich M (2002) Comparison of human ocular torsion patterns during natural and galvanic vestibular stimulation. J Neurophysiol 87:2064–2073. Medline

Shanidze N, Lim K, Dye J, King WM (2012) Galvanic stimulation of the vestibular periphery in guinea pigs during passive whole body rotation and self-generated head movement. J Neurophysiol 107:2260–2270. CrossRef Medline

St George RJ, Fitzpatrick RC (2011) The sense of self-motion, orientation and balance explored by vestibular stimulation. J Physiol 589:807–813. CrossRef Medline

Straka H, Dieringer N (2000) Convergence pattern of uncrossed excitatory and inhibitory semicircular canal-specific inputs onto second-order vestibular neurons of frogs. Exp Brain Res 135:462–473. CrossRef Medline

Straka H, Dieringer N (2004) Basic organization principles of the VOR: lessons from frogs. Prog Neurobiol 73:259–309. CrossRef Medline

Straka H, Simmers J (2012) *Xenopus laevis*: an ideal experimental model for studying the developmental dynamics of neural network assembly and sensory-motor computations. Dev Neurobiol 72:649–663. CrossRef Medline

Straka H, Baker R, Gilland E (2001) Rhombomeric organization of vestibular pathways in larval frogs. J Comp Neurol 437:42–55. CrossRef Medline

Straka H, Baker R, Gilland E (2002a) The frog as a unique vertebrate model for studying the rhombomeric organization of functionally identified hindbrain neurons. Brain Res Bull 57:301–305. CrossRef Medline

Straka H, Holler S, Goto F (2002b) Patterns of canal and otolith afferent input convergence in frog second-order vestibular neurons. J Neurophysiol 88:2287–2301. CrossRef Medline

Straka H, Vibert N, Vidal PP, Moore LE, Dutia MB (2005) Intrinsic membrane properties of vertebrate vestibular neurons: Function, development and plasticity. Prog Neurobiol 76:349–392. CrossRef Medline

Straka H, Fritzsch B, Glover JC (2014) Connecting ears to eye muscles: evolution of a 'simple' reflex arc. Brain Behav Evol 83:162–175. CrossRef Medline

Thompson DM, Koppes AN, Hardy JG, Schmidt CE (2014) Electrical stimuli in the central nervous system microenvironment. Annu Rev Biomed Eng 16:397–430. CrossRef Medline

Wardman DL, Fitzpatrick RC (2002) What does galvanic vestibular stimulation stimulate? Adv Exp Med Biol 508:119–128. CrossRef Medline

Discussion

I The developing *Xenopus laevis*: an ideal model organism for studying the VOR

Due to its indispensable role for gaze stabilization, the vestibulo-ocular reflex represents one of the evolutionarily most conserved networks of the central nervous system and can therefore be studied in a variety of different species from fish to mammals (Straka, 2010). Amphibians, as almost all other vertebrates, have three semicircular canals for detecting angular acceleration, two otolith organs for horizontal and vertical linear motion detection respectively, and a cerebellar side loop for plastic modifications of the VOR (see Straka and Dieringer, 2004). Besides the numerous methodological advantages of using semi-intact *Xenopus laevis* preparations for studying the basic concepts of VOR processing (see Introduction), this model organism also allows the investigation of developmental aspects and plasticity underlying vestibulo-ocular processing. During metamorphosis, *Xenopus* change their locomotor strategy from tadpole undulatory swimming to adult propulsive limb kicks (Combes et al., 2004), although as frogs they are rather inactive predators (Avila and Frye, 1978). Presumably, these behavioral changes are directly linked to the concurrent changes in VOR performance. During free swimming, larval semicircular canals experience head movements with angular peak velocities of up to 2500°/s (Hänzi et al., 2015). Although spinal efference copies appear to play a major role for gaze stabilization during rhythmic locomotion in *Xenopus* tadpoles (Combes et al., 2008; Lambert et al., 2012), also a robust angular VOR response occurs during passive rotation of the head (for review, see Straka and Dieringer, 2004). Notably, this aVOR is "lost" during metamorphosis and around developmental stage 60, a huge reduction in VOR performance can be observed (see Fig. 1), in accordance with the decline in ocular motility described previously in *Xenopus* (Horn et al., 1986; see Straka and Dieringer, 2004; Schuller et al., 2011) and bullfrogs (Stehouwer, 1988). Due to the appearance of a neck, adult frogs rather use compensatory head instead of eye movements (Dieringer and Precht, 1982; see Straka and Dieringer, 2004) to stabilize gaze. On the other hand, tadpoles at younger developmental stages have semicircular canals that are too small for the detection of angular accelerations, delaying the onset of angular VOR responses to stage 49, even though the vestibulo-ocular circuitry is already established and the otolith-driven linear VOR is already functional at earlier stages (Lambert et al., 2008). At stage 49, VOR gains are yet small (0.17) and improve slightly up to stage 52 (0.26) (Lambert et al., 2008). These findings suggest that tadpoles somewhere between stages 52 and 60 display largest VOR responses, hence during my thesis, mostly animals of stage 54 were used for experimentation. This stage also appeared optimal for recordings of the

abducens motor output, since at earlier stages (e.g. 52), spontaneous bursting activity was more frequently observed (arrows in Fig. 1), compromising the analysis of VOR performance especially at lower frequencies of head motion. Furthermore, morphological investigation of *Xenopus* abducens motoneurons during development suggests that the general patterns of dendritic arborization and somal shape resemble those of adult frogs after stage 54 (Matesz, 1990). In rats, changes in complexity of the dendritic tree of oculomotor motoneurons occur in steps, one of which is correlated with the establishment of the vestibular circuitry (Carrascal et al., 2009). If similar mechanisms are assumed in the *Xenopus*, fully developed dendrites at stage 54 comply with the notion that the developmental fine-tuning of the vestibulo-ocular network is completed by then, making it ideally suitable for studying the mechanisms underlying the VOR.

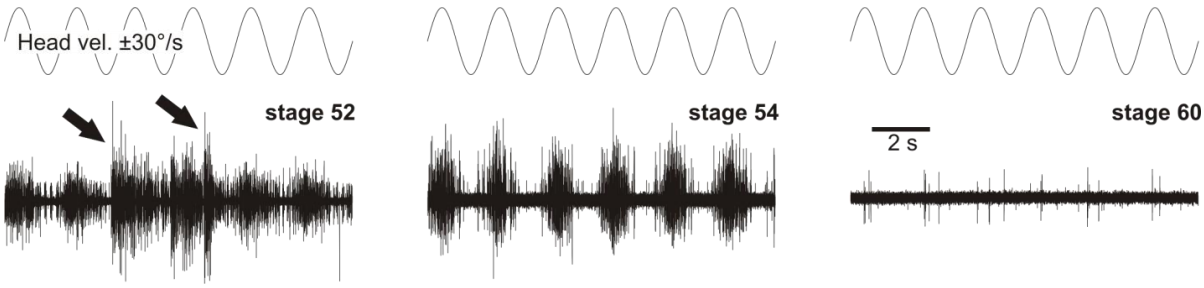

Figure 1: Modulated abducens nerve discharge during sinusoidal head rotation in the horizontal plane at 0.5 Hz in *Xenopus* tadpole preparations of three different stages. Note the decline in extraocular motor activity at stage 60 (right) and the occurrence of spontaneous discharge bursts at stage 52 (left).

II Electrophysiological properties of abducens motoneurons

A major part of this thesis concerns the classification of abducens motoneurons with respect to their response characteristics during vestibulo-ocular processing. Resting discharge and regularity as well as the modulated activity during sinusoidal stimulation in the horizontal plane were studied in single units isolated from extracellular abducens nerve recordings in semi-intact *Xenopus laevis* preparations. Several subtypes of abducens motoneurons have been demonstrated with this approach, some with characteristics reminiscent of the phasic and tonic properties described for vestibular afferent fibers and second order vestibular neurons (2°VNs) as well as of the fast (twitch) and slow (tonic) fiber responses of the extraocular musculature. A major question concerns how the present findings can be integrated into the theory of parallel, frequency-tuned VOR channels. This together with the origin and functional relevance of the different subtypes for VOR-related eye motion shall now be discussed in detail.

II.1 Abducens motoneurons: both continuum and distinct groups

In general, two major neuronal subtypes with respect to their dynamic properties appear to be responsible for vestibular information processing – irregular and phasic, and regular and tonic (see Straka and Dieringer, 2004; Straka et al., 2005; Straka et al., 2009) – although clear segregation between the two subgroups is not possible with respect to all distinguishing traits. For example, the resting discharge of vestibular afferents displays a continuum of different regularities, measured as the coefficient of variation (CV) (Boyle and Highstein, 1990; Honrubia et al., 1989; Kim et al., 2011). Notably, in the present study, such a continuum is also observed for spontaneously active abducens motoneurons. In fact, the vestibular afferent CV ranges from 0.12 to 2.5 (regular to irregular) in bullfrogs (Honrubia et al., 1989) and 0.30 to 1.46 in *Xenopus* (see Results III) very closely resemble the range of CVs observed in spontaneously active abducens motoneurons in the *Xenopus* (see Results I, Fig. 3C).

Furthermore, it was shown here that the motoneuronal CV is inversely related to the resting rate of the cell (see Results I, Fig. 3C) and modulation depth during vestibular stimulation (see Results I, Fig. 3E). Irregularly firing motoneurons (high CV) display a more transient, "phasic-tonic" response to sinusoidal stimuli, and higher thresholds of activation during motion stimuli. In fact, most transient, "phasic" responses and the highest activation thresholds of abducens motoneurons are observed in units that are entirely silent at rest (see Results I, Fig. 3D,E). On the other hand, "tonic" motoneurons with the highest spontaneous discharge rates and low CVs represent the other end of a continuum of tonic to phasic discharge characteristics (see Results I, Fig. $3A_1$). The same correlation between CV and response during activation has also previously been demonstrated for vertebrate vestibular afferent fibers, where irregular fibers have more phasic responses than regular afferents firing rather tonically upon stimulation (Goldberg, 2000; Eatock and Songer, 2011). Hence, a similar continuum of neuronal subtypes both with respect to discharge regularity and responses to vestibular activation can be observed in extraocular motoneurons and vestibular afferent fibers, indicative of similar organizational principles and an information transfer in parallel, separate channels from the vestibular periphery to the extraocular motor plant. This is further supported by the presence of tonic and phasic second order vestibular neurons (2°VNs, see Straka et al., 2005) that, according to the notion of parallel processing, might relay information from tonic vestibular afferents to tonic motoneurons and from phasic afferents to phasic motoneurons, via the corresponding types of 2°VNs (see Straka et al., 2009).

II.1.a The origin of two different subgroups

In addition to the observed continuum of abducens motoneurons from "tonic" and spontaneously active to "phasic" and silent at rest, two distinct subgroups were observed with respect to their sensitivity to different frequencies of sinusoidal head rotation in larval *Xenopus* (Results I, Fig. 4). The modulation depth and timing (phase) of the peak response of group I motoneurons is altered during changes in stimulus frequency while keeping the peak head velocity constant. At low frequency head rotation (0.1 Hz), a large phase lead of the response can be observed that gradually decreases and eventually turns into a phase lag at higher frequencies (1 Hz), together with a decline in the modulation depth. On the other hand, group II motoneurons display similar modulation depths upon changes in frequency with response peaks that are always aligned with the velocity peak of the head motion. Notably, both spontaneously active as well as silent cells can be of either group I or II; however, silent neurons with rather transient responses are more frequently of the second subtype.

The fact that similar response types were also observed in vestibular afferent fibers of *Xenopus* tadpoles, although with generally larger phase leads (Gensberger et al., 2013), again suggests that afferent responses are transmitted via 2°VNs to extraocular motoneurons in parallel channels to preserve the temporal properties throughout the entire VOR network. The small lag of motoneuronal firing compared to afferent responses is compatible with synaptic delays introduced by the intermediate processing steps at the level of 2°VNs.

Interpretation of the origin and functional relevance of the two subgroups with respect to vestibulo-ocular processing is challenging since to date only few studies have approached this issue at all. First of all, it is important to consider which parameter of head motion most likely correlates with hair cell responses. Highstein et al. (2005) have claimed that the fluid displacement within semicircular canals is proportional to angular accelerations in the low frequency range. However, with increasing frequencies, fluid motion in the slender lumen of the canal creates viscous forces that lead to a real-time integration of the fluid displacement such that it aligns with the motion velocity of the head rather than acceleration (Highstein et al., 2005). According to this finding, the present results can be interpreted in two ways. One possibility is that the change in timing of group I afferent and motoneuronal responses with increasing frequencies directly reflects the change from acceleration to velocity-dependent endolymph motion, since at lower frequencies (0.1 Hz) the response peak is shifted towards the acceleration peak, whereas at higher frequencies it becomes more and more aligned with the velocity peak (Results I, Fig. 4). As a consequence, some integration would be required to generate responses of neurons of the group II subtype. Alternatively, the frequencies applied in the present study are already in the range where fluid motion inside the semicircular canals aligns with the velocity of head motion. In this case, group II afferents or motoneurons would

reflect the "default" situation and responses of group I afferents/motoneurons would require some form of differentiation to shift the peak towards acceleration. However, investigation of semicircular canal diameters and actual endolymph motion in *Xenopus* tadpoles would be required to resolve this question.

Similar responses as in *Xenopus* group I motoneurons were observed in vestibular afferents of the bullfrog that were almost in phase with acceleration at low frequencies (0.0125 Hz) and shifted towards the velocity component of head motion at higher frequencies (0.4 Hz) (Honrubia et al., 1989). This might indicate that indeed responses of group I motoneurons are the "default state" that can be predicted by physical properties of the semicircular canals in amphibians. On the other hand, a scenario with two distinct groups of vestibular afferents has been observed in toadfish (see Highstein et al., 2005). The first subtype encodes angular acceleration and velocity for lower and higher frequencies respectively, again reminiscent of group I motoneuronal responses in the *Xenopus*. The other subtype of toadfish vestibular afferents encodes angular acceleration – even at frequencies where the endolymph displacement is known to follow head velocity – due to an integration mediated by the co-release of GABA and glutamate from vestibular hair cells (see introduction, Holstein et al., 2004a,b). Whether or not a corresponding group of vestibular afferents exists and exhibits similar forms of computation as observed in group II motoneurons in the *Xenopus* remains to be determined, for example by focal injections of $GABA_B$ receptor antagonists into the semicircular canal cupulae. However, since group II responses observed in this study are aligned with head velocity rather than acceleration, which would correlate with a delay rather than advance of the response peak at low stimulus frequencies, other or additional mechanisms of neuronal integration appear more likely.

II.1.b Functional relevance of the two different subgroups for VOR eye motion

In order to investigate the functional relevance of silent *vs* spontaneously active as well as of group I *vs* group II abducens motoneurons, a computational approach was applied. Using a standard model of the extraocular motor plant, video-recorded eye movements of semi-intact *Xenopu*s tadpole preparations were simulated with muscle twitches following spike times of different combinations of motoneuronal subtypes (Results I, Methods; Fig. 8). This revealed that eye movements indeed are best fitted when all recorded types of motoneurons are used for the simulation (Results I, Fig. 8E). Simulations also suggested that motoneurons of group II are generally more relevant for VOR associated eye motion than those of the group I subtype, especially at lower frequencies. This finding is not surprising considering the temporal precision of group II motoneuronal responses that are always aligned with the velocity component of the head motion. Group I motoneurons in turn might be required to

supplement eye muscle innervation or simply reflect an undifferentiated, possibly immature type of response that follows semicircular canal fluid motion without further integration. Furthermore, motoneurons that are silent at rest play a minor role for vestibulo-ocular processing as compared to spontaneously active neurons (Results I, Fig. 8E). Considering that these neurons require higher head velocities for activation and display larger spike amplitudes during multiple-unit recordings than spontaneously active neurons (Results I, Fig. 3; Dieringer and Precht, 1986), it appears likely that they represent the population of abducens motoneurons innervating fast-twitch eye muscle fibers with fast axon conduction velocities (see below; e.g. Ugolini et al., 2006), mainly responsible for rapid, high velocity VOR responses, fast phases during resetting eye movements or during other behaviors such as escape.

In general, it was observed that eye movements are approximately aligned with head position rather than head velocity, at least during rotations at 0.5 and 1 Hz (Results I, Fig. 8B), which is what would be expected from "ideal" gaze stabilizing reflexes. Since motoneuronal responses are approximately aligned with head velocity, the delay introduced at the neuromuscular junction as well as the dynamics of muscle fiber contractions must mediate the integration of velocity-related motor commands to position-related eye movements. Mechanistically it appears obvious that, as long as a constant delay of muscular responses is assumed, motoneuronal discharge peaks that are aligned with the velocity of head motion will only result in position-aligned eye movement peaks at a stimulus frequency where a shift in 90° (i.e. from velocity to position) is equivalent to the muscular delay in the time domain. A time constant of 330 ms was measured for the extraocular motor plant in *Xenopus* tadpoles (Knorr et al., 2012; see Results I, methods section). A shift from velocity to position (90°) would correspond to a time delay of 250 ms at 1 Hz and 500 ms at 0.5 Hz sinusoidal head rotation. In fact, at these two frequencies, eye motion is approximately aligned with head position (Results I, Fig. 8B), compatible with the measured time constant of 330 ms. At 0.1 Hz however, a large phase lead with respect to head position can be observed (Results I, Fig. 8B). This is compatible with the assumption that a combination of group I and II motor commands, both with phase advances with respect to stimulus velocity (Results I, Fig. $4C_4$), is unable to induce a delay of >90°, i.e. >2.5 s at the level of extraocular muscle fibers as would be required to align eye movements with head position at this stimulation frequency.

Such "imperfect" VOR responses in the *Xenopus*, especially at low frequencies, can be explained by the notion that the perfect alignment of eye movements with head position (i.e. a gain of 1.0) is not necessary in these animals, compatible with previously reported VOR gains of ~0.25 in *Xenopus* tadpoles of stage 52 (Lambert et al., 2008) and the fact that frogs have no foveated vision. Therefore, gaze stabilization mediated by the observed counteractive eye movements might be sufficiently precise for *Xenopus* behavior. However, it should be

noted that the present findings are based on experiments during which the vestibulo-ocular reflex was isolated from other sensory inputs that usually act in concert for optimal gaze stabilization. For example, since both optic nerves were transected, optokinetic inputs were fully abolished that under normal circumstances mediate a substantial portion of counteractive eye movements considering that *Xenopus* tadpoles display optokinetic gains of up to 0.5 (Lambert et al., 2008). Hence, it appears likely that head motion counteracting eye movements, both with respect to gain and timing, are more precise in animals with intact optokinetic reflexes.

II.2 Different subgroups of abducens motoneurons: evidence for parallel channels?

In the present study, abducens motoneurons were shown to display "tonic" and "phasic" properties similar to those observed "upstream" in 2°VNs and vestibular afferent fibers and "downstream" in extraocular muscle fibers. This serves as a first indication that dynamic cellular properties are conserved throughout the entire pathway of VOR processing and that each subtype relays certain temporal aspects of head motion in separate, "frequency-tuned" channels (see Straka et al., 2009). Furthermore, in *Xenopus*, vestibular afferents reminiscent of the two subtypes of abducens motoneurons with respect to stimulus frequency-sensitivity have been described (Gensberger et al., 2013), suggesting that these response properties are also conserved throughout the VOR pathway. Hence, the present findings support the notion of parallel VOR processing that so far has been suggested on the basis of numerous anatomical and physiological studies (see Introduction). For example, separate sets of extraocular motoneurons with at least partially distinct presynaptic input areas can be distinguished in monkeys from retrograde rabies virus labeling of "slow" and "fast" muscle fibers respectively (Ugolini et al., 2006). Electrophysiological evidence for parallel processing within two dynamic systems has been obtained from studies in frogs: some abducens motoneurons display synaptic responses that arise exclusively from phasic 2°VNs, indicating that at least phasic responses are individually processed at this level without additional convergence of tonically active neurons (see Straka et al., 2009). Furthermore, adaptive changes in VOR gain driven by visuo-vestibular mismatch conditions were shown to be specific for the frequency of head motion applied during the training, suggesting that also plastic processes are mediated by frequency-tuned, separate channels rather than by global mechanisms (Lisberger et al., 1983).

Despite these findings, several studies have reported or at least suggested a substantial amount of convergence between hair cells and afferent fibers (Fernández et al., 1988), afferent fibers and 2°VNs (Straka and Dieringer, 2000; Goldberg, 2000; Dickman and Angelaki, 2002; Straka et al., 2002) as well as 2°VNs and extraocular motoneurons (Graf et

al., 1993). Nevertheless, this does not necessarily conflict with the parallel-channel theory. Firstly, it is possible that in addition to purely "tonic, regular" and "phasic, irregular" pathways, intermediate responses, such as "phasic-tonic" extraocular motoneurons in the present study, require combined inputs from the two extreme ends of the dynamic spectrum (Fig. 2). Secondly, convergence does not exclude "frequency-tuned" channels since it is nonetheless possible that the properties of the majority of inputs correlate with the dynamics of the output. However, in general, it allows neurons to combine and integrate information from multiple presynaptic cells, and hence minimize uncertainty as suggested by Bayesian models (e.g. Vilares and Kording, 2011). This principle also underlies the advantages of convergence between or within sensory systems, such as the integration of semicircular canal- and spatially related otolith organs (Dickman and Angelaki, 2002; Straka et al., 2002). Thirdly, natural head movements usually consist of a variety of different dynamic components (Carriot et al., 2014) and in order to generate appropriate task-specific gaze stabilizing responses, it appears likely that at least some neurons and/or pathways within the VOR network are "tuned" to such combined dynamics.

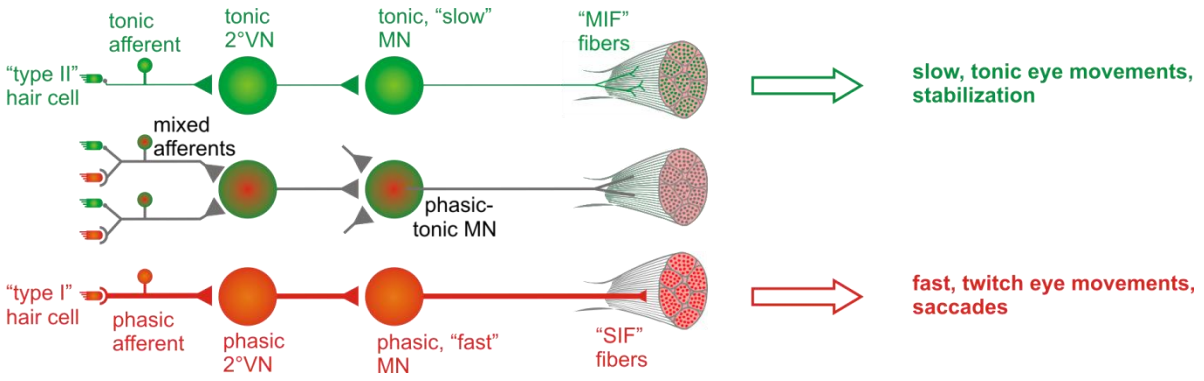

Figure 2: Schematic displaying a suggested model of parallel VOR processing channels. On the extreme ends, information from "type II"-like hair cells is separately processed in a pathway of "tonic" afferents, 2°VNs and motoneurons (MN) that project to multiply-innervated muscle fibers (MIF), whereas the "type I" hair cell output is processed by the "phasic" pathway that terminates on singly-innervated muscle fibers (SIF). In between the two extreme ends, convergence occurs at multiple stages of the VOR circuitry.

III Calcium imaging and morphological correlates to physiology

During the present thesis, morphological properties of abducens neurons were investigated in addition to their electrophysiological and pharmacological profiles by means of retrograde tracing as well as calcium imaging techniques.

The abducens nucleus of *Xenopus* consists of ~40 motoneurons that display a continuum of cell sizes with cross-sectional areas ranging from approximately 30 to 200 µm² (Results I, Fig. 1). In general, it has long been accepted that different motoneuronal sizes inversely correlate with the input resistance and hence excitability of the cell (Mendell, 2005; Henneman et al., 1965a,b); larger neurons for example have a lower input resistance and excitability. Following this notion of a "size principle" it is possible that the continuum of cell sizes in the abducens nucleus correlates with the observed continuum of excitability from spontaneously active to silent abducens motoneurons, such that cells that are silent at rest and require stronger inputs for activation have the largest somata. Furthermore, a relation between the size of a motoneuron and its axonal diameter/conduction speed has long been postulated by Ramón and Cajal (1909), suggesting that large cells also have thicker axons, again compatible with the continuum of axonal diameters described previously in frogs (Dieringer and Precht, 1986). In addition, larger axons are known to give rise to larger relative spike amplitudes in multiple-unit extracellular recordings (Dieringer and Precht, 1986). Indeed, "silent" units with high thresholds of activation have larger spikes and thus presumably axons with a larger diameter than spontaneously active units (Results I, Fig. 3). If axonal and somal sizes correlate, it appears likely that spontaneously active motor units with small relative spike amplitudes represent the smallest cells with smallest axonal diameters, and thus higher input resistance and increased excitability. In contrast, larger cells/axons appear to make up the population of abducens motoneurons that is less active or even silent at rest. This is compatible with findings in abducens (Grantyn and Grantyn, 1978) and oculomotor (Grantyn et al., 1977) motoneurons in cats where a clear correlation between somal size and excitability was demonstrated. In addition to VOR-driven motoneurons, some even larger units were identified in the present study in *Xenopus* that are independent of VOR inputs (Results I, Fig. 5) and it is likely that these are responsible for rapid, fast-phase eye movements that require the fastest axonal transduction speed and fire "spontaneously", e.g. upon touch of the skin or acoustic stimulation, as suggested previously (Dieringer and Precht, 1986).

Within the VOR circuitry, correlations between the size and physiological properties of neurons have also been demonstrated for vestibular afferent fibers in a variety of species (Goldberg and Fernández, 1977; Honrubia et al., 1989; see also Goldberg, 2000; Eatock and Songer, 2011). Furthermore, a continuum of somal diameters was observed in 2°VNs in mice (Sekirnjak and du Lac, 2006), compatible with the often suggested continuum of response characteristics (du Lac and Lisberger, 1995). Hence, an interaction between morphology and physiology appears to be a general principle for VOR processing.

In order to investigate the activity of abducens motoneurons beyond extracellular nerve recordings, calcium imaging experiments were performed during the course of this thesis.

The somata of these neurons were retrogradely labeled from the abducens nerve at its neuromuscular junction with a calcium sensitive dye (Calcium Green^{TM} –1 dextran) and imaged subsequently during galvanic vestibular stimulation (GVS) of the contralateral horizontal canal cupula. With the latter stimulation method it was possible to imitate different velocities of natural head rotation by altering the applied current amplitude (see Results III). This, together with the employment of various stimulation frequencies, allowed recruiting several subtypes of abducens motoneurons differentially, according to their individual thresholds of activation. Unfortunately, the slow time constant of the calcium signal (Grewe et al., 2010) did not allow discriminating between spontaneously active or silent cells at rest with the applied methods of analysis, indicating that the changes in intracellular calcium concentration during resting discharge are not sufficient to elicit a change in calcium related fluorescence intensity. Similarly, during vestibular activation, the time constant of calcium signals did not reveal obvious differences between "tonic" and "phasic" motoneuronal activity, preventing the direct classification of motoneuronal subtypes from their calcium signal alone. However, more detailed analysis of the recorded calcium signals with suitable fitting and modeling techniques might allow gaining further insight into different activity patterns of the respective cell types.

Nevertheless, in the present study, calcium signals were correlated with motoneuronal activity by recording the multiple-unit motor output of the abducens nerve along with imaging of cell somata of the respective nucleus (n = 3; representative example in Fig. 3). During weak, low frequency galvanic vestibular stimulation, usually only spontaneously active motor units with small spike amplitudes were activated (Fig. $3A_1$), whereas stronger galvanic stimuli additionally recruited larger amplitude units that were silent at rest (Fig. $3B_1$). Simultaneous calcium imaging of several cells within the abducens nucleus revealed that during the activation of small units, calcium signals are only observed in neurons close to the midline (cells #1, 5, 6 in Fig. $3A_2$). On the other hand, larger unit activity appears to exclusively correlate with calcium responses of motoneurons that are located more lateral within the nucleus (cells #2, 3, 4 in Fig. $3B_2$).

These findings suggest that different types of abducens motoneurons are spatially segregated within the nucleus such that spontaneously active cells are located close to the midline; whereas neurons that are silent at rest and display more transient activity are found at more lateral positions. This complies with data from monkeys where slow, "tonic" motoneurons are located at the medial periphery of the abducens nucleus and fast, "twitch" motoneurons further lateral (Ugolini et al., 2006). However, in the case of *Xenopus*, such spatial segregation would also indicate that somal sizes play a minor role for distinguishing between "tonic" and "phasic" cell types: calcium dye-filled neurons close to the midline were generally not smaller than more lateral cells, and also retrograde tracing studies demonstrated

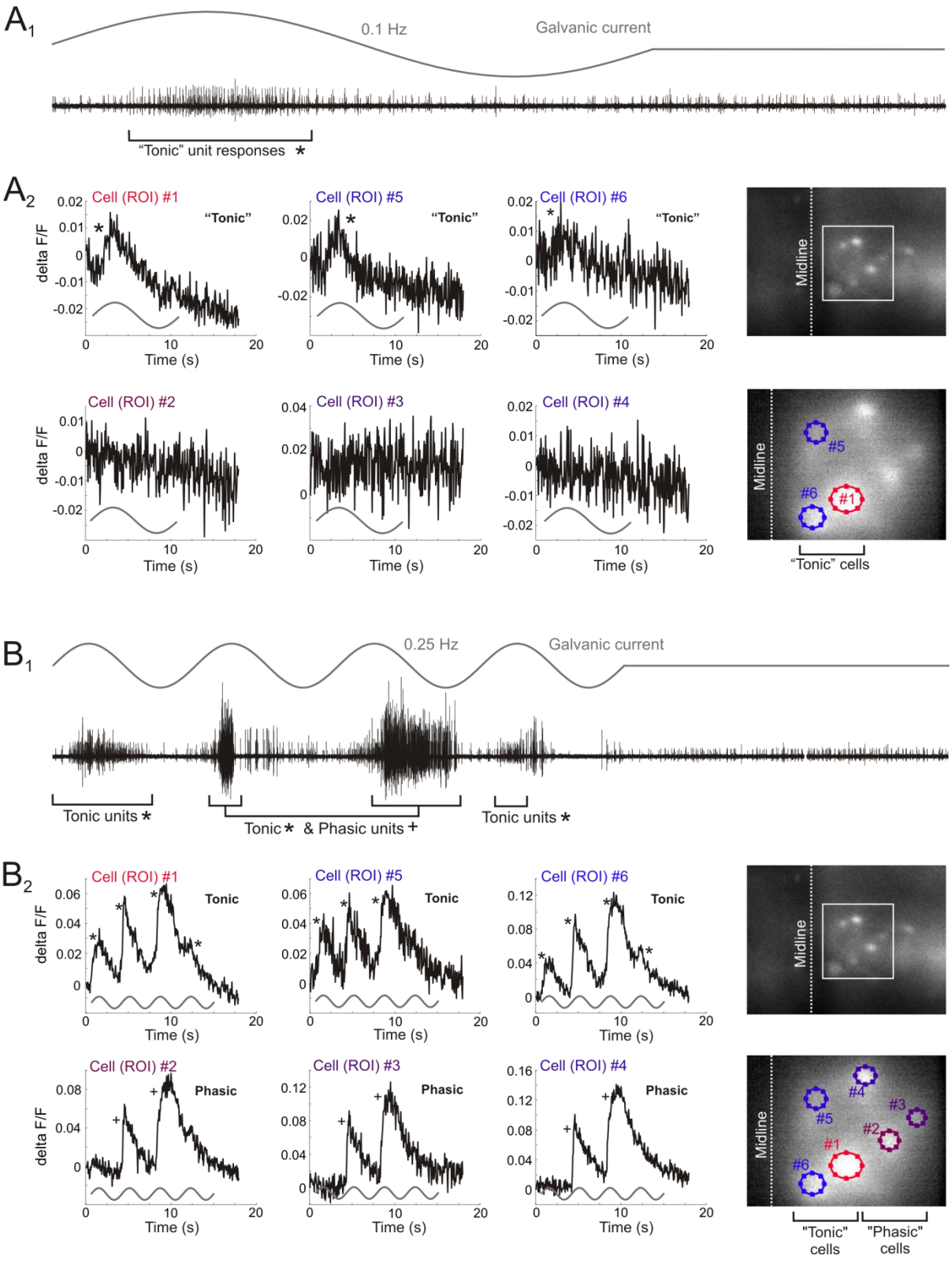

Figure 3: Extracellular nerve recordings (A_1 and B_1) and simultaneous calcium responses (A_2 and B_2) of several retrogradely labeled abducens motoneurons during galvanic vestibular stimulation at 0.1 Hz (A) and 0.25 Hz (B). Note that cells #1,5,6 close to the midline are active during "tonic" motoneuronal repsonses whereas more lateral cells #2,3,4 are only activated during more transient, "phasic" responses. * and + indicate "tonic" and "phasic" responses respectively.

no relation between the medio-lateral position of the cell body and cross-sectional area (Results I, Fig. 1). On the other hand, a trend was observed that more lateral neurons are more oval in shape (Results I, Fig. 1), suggesting that "phasic" motoneurons with more transient responses have more oval-shaped somata, potentially due to a wider axon hillock corresponding to a larger axon. This notion appears plausible considering that also motoneurons of the accessory abducens nucleus, which exclusively display "burst"-like activity are also more oval-shaped (Matesz, 1990).

In conclusion, the present findings suggest that spontaneously active, "tonic" abducens motoneurons have small axons independent of somal size and are present close to the midline, where cell bodies are round. In turn, silent, "phasic" abducens motoneurons have larger axons and are located at more lateral positions within the nucleus with more oval-shaped cell bodies (presumably due to the larger axon and axon hillock). Generally, it can be assumed that axonal rather than somal sizes are the crucial parameter for distinguishing different types of extraocular motoneurons. However, the combination of calcium imaging and extracellular nerve recordings can only serve as a preliminary study; a clear correlation of the two activity patterns on a single cell level would require other techniques such as path-clamp and/or imaging with voltage sensitive dyes.

IV Pharmacology of the VOR

A major aspect of this thesis concerns the excitatory and inhibitory neurotransmission at the 2°VN-abducens motoneuronal synapse, investigated via focal injection of specific receptor antagonists into the respective abducens nucleus (see Results I). Previous studies have reported that glutamate mediates excitatory vestibular inputs to extraocular motoneurons (Straka and Dieringer, 1993); however, a putative differential role of AMPA/kainate and NMDA receptors for VOR processing has remained largely unknown. Moreover, the function of glycine and GABA in mediating inhibitory inputs to abducens motoneurons was investigated here, assuming that the receptors of both transmitters are present on the membrane of abducens motoneurons (Spencer et al., 1989; Lorenzo et al., 2007), although inhibitory vestibular inputs from ipsilateral 2°VNs were suggested to be purely glycinergic (Straka and Dieringer, 1993). During this study, the yet open questions concerning excitatory and inhibitory neurotransmitter systems on abducens motoneurons were thoroughly addressed. Functional implications of these findings with respect to VOR processing shall now be discussed in more detail.

IV.1 Excitatory neurotransmitter systems

Both the resting rate and modulated discharge of single abducens units during vestibular stimulation were investigated before and after injection of selective antagonists of either AMPA or NMDA receptors. In all units, neuronal firing rates were strongly decreased or even fully abolished after AMPA or NMDA blockade, indicating that excitatory transmission always occurs via both glutamate receptor subtypes. However, more detailed investigation of the degree of firing rate reduction revealed significant differences between AMPA and NMDA receptor blockade with respect to several aspects.

The resting rate of individual spontaneously active abducens motor units, irrespective of whether they belong to the group I or II subtype, was more strongly decreased after NMDA than AMPA blockade (Results I). This suggests that continuous, "tonic" inputs from spontaneously active 2°VN and thus indirectly from vestibular afferents (see Goldberg, 2000; Eatock and Songer, 2011) mainly excite abducens motoneurons through a higher proportion of NMDA receptors. It is also important to note that after transsection of the hindbrain midline and thus a complete elimination of contralateral excitatory vestibular inputs, spontaneous abducens activity ceases entirely for around 30 minutes. This indicates that under normal circumstances, abducens motoneurons are not intrinsically active but obtain their spontaneous discharge from continuous presynaptic vestibular activity. On the other hand, the fact that some units regain a resting rate after around half an hour suggests the presence of plasticity mechanisms – possibly homeostatic – that compensate for the loss of excitatory inputs in order to restore the tonic extraocular muscle innervation required to stabilize the eye at rest (Büttner-Ennever and Horn, 2002a).

With respect to the modulated abducens motoneuronal activity during sinusoidal head rotation, it was originally assumed that the application of an AMPA receptor antagonist alone was sufficient to entirely block excitatory vestibular inputs in frogs (Straka and Dieringer, 1993). In fact, the present study confirmed a significant reduction of the motoneuronal output in all recorded units after focal injection of a selective AMPA receptor blocker. However, the dominant expression of NMDA receptors on abducens motoneurons (Durand, 1987; 1991; 1993) as well as the dual role of AMPA and NMDA receptors for high- and low frequency VOR processing respectively (Priesol et al., 2002), as shown in other species, encouraged a re-investigation of the function of the two glutamate receptors in larval frogs on a single-unit level.

Firstly, the observed shifts in response peak after injection of the respective antagonists (Results I, Fig. 6) suggest that AMPA and NMDA receptors are responsible for different phases of the modulated response: AMPA receptors mediate the initial onset whereas NMDA receptors are critical for the later, sustained phase of the response, in compliance with the fast

and slower, delayed response dynamics of the two channels respectively (see Edmonds et al., 1995 for review). Secondly, investigating the magnitude of the decrease revealed no stimulus frequency-specific differential effects of AMPA and NMDA receptor blockade within individual abducens motoneurons (unpublished observations). However, the degree of activity reduction varied significantly between group I and group II abducens motor units, irrespective of whether they were spontaneously active or silent at rest. Group I motoneurons displayed a higher NMDA than AMPA sensitivity whereas cells of the second subtype showed the opposite dependency (Results I, Fig. 6). Task-sharing of the two glutamate receptors with respect to dynamic cellular properties was also assumed "upstream" in the VOR circuitry in frogs, where vestibular neurons receiving input from thick afferent fibers presumably have a higher relative NMDA receptor content than those contacted by thin fibers (Straka et al., 1996). Whether the observed differences in glutamate receptor expression on the level of abducens motoneurons are necessary for transmitting specific dynamics of presynaptic activity, or whether they even play a part in shaping the different response profiles of the two subtypes remains unknown. For example, it could be argued that in group II motoneurons, the higher AMPA receptor concentration causes the observed frequency-independent phase precision due to their fast, time-precise channel opening dynamics. On the other hand, an alternative explanation for the varying AMPA and NMDA receptor distribution arises from a developmental approach. For example, in rats it was demonstrated that the different subunits of the two receptors are differentially expressed during postnatal development in 2°VNs (Sans et al., 2000). Furthermore, NMDA receptors are transiently expressed in spinal motoneurons during early postnatal development in rats (Kalb et al., 1992; Hori and Kanda, 1996), where they presumably play a role in the formation of the dendritic arbor (Kalb, 1994). Assuming similar mechanisms for abducens motoneurons, it is possible that the differences in NMDA *vs* AMPA receptor content are related to the fact that the present study was conducted in developing (stage 54) larval *Xenopus*. More precisely, group I motoneurons that display a higher NMDA receptor contribution might represent a population of not yet fully mature cells, compatible with results from a computational approach (Results I, Fig. 8) suggesting that group II motoneurons are more important for VOR processing than those of the first subtype. This notion is further supported by the fact that in even younger animals (e.g. stage 50) almost exclusively group I motor units were recorded (unpublished observations).

IV.2 Inhibitory neurotransmitter systems

As part of the push-pull organization of the VOR, not only excitatory but also inhibitory vestibular projections terminate on extraocular motoneurons (see Introduction). In the case of

abducens motoneurons, previous studies have reported that inhibitory vestibular inputs from ipsilateral 2°VNs are exclusively glycinergic in nature (Spencer et al., 1989; Straka and Dieringer, 1993). In the present study, this was confirmed in *Xenopus* by focal injections of the glycine antagonist strychnine into the abducens nucleus after isolating the inhibitory pathway from all excitatory inputs and commissural pathways by complete dissection of the hindbrain midline: the initial stimulus velocity-dependent inhibitory modulation during ipsiversive head motion was abolished entirely after glycine receptor blockade (Results I, Fig. 7). In some cases, a small remaining modulation of abducens nerve activity could be observed during sinusoidal rotation, presumably due to additional, auxiliary connections from the ipsilateral vertical semicircular canals (Straka et al., 2002) that are co-activated by fluid motion during horizontal rotation (Ifediba et al., 2007). In addition, mono- or disynaptic utricular inputs onto abducens motoneurons might contribute to the response (Uchino et al., 1994), although activation of otolith organs by linear acceleration is supposed to be minimal by placing the preparation in the center of the turntable rotation axis.

Importantly, the absolute change (increase) in firing rate of abducens motoneurons after blocking glycinergic inputs from ipsilateral 2°VNs in midline-sectioned preparations is substantially smaller than the increase in motoneuronal output observed after surgical removal of the ipsilateral horizontal canal cupula (Results I, Fig. 7). This suggests that the removal of ipsilateral vestibular inputs not only affects direct inhibitory connections to abducens motoneurons but also strongly influences overall VOR activity including the contralateral excitatory drive via commissural pathways between the two vestibular nuclei (Malinvaud et al., 2010).

Several anatomical studies have additionally reported both GABAergic terminals as well as corresponding $GABA_A$ receptors on abducens motoneurons (Spencer et al., 1989; Lahjouji et al., 1995; Russier et al., 2002; Lorenzo et al., 2007). In addition to glycine, I thus tested the influence of $GABA_A$ receptor blockade on the output of multiple and individual abducens motor units by focal gabazine injections. These experiments demonstrated that in all motoneurons, independent of the degree of spontaneous activity and response characteristics during vestibular stimulation, neuronal firing rates were increased after gabazine application both at rest as well as during the entire cycle of sinusoidal head rotation (Results I, Fig. 7). This suggests that abducens motoneurons are tonically inhibited by GABAergic inputs that are independent of vestibular activation, compatible with the fact that GABAergic terminals are mostly present on the cell somata rather than the dendritic tree (Lorenzo et al., 2007). Whether this tonic inhibition is achieved via extrasynaptic GABA receptors (Lorenzo et al., 2007), local inhibitory interneurons, or a combination of the two, remains unknown. After dissection of the hindbrain midline, gabazine injection into the abducens nucleus still caused

an increase in activity without influencing the extent of modulation (unpublished data), which excludes a contralateral origin of the GABAergic inputs. Furthermore, the unaltered inhibitory modulation after $GABA_A$ receptor blockade suggests that indeed ipsilateral vestibular inputs are exclusively glycinergic.

In view of the present findings it thus appears plausible that in the case of abducens motoneurons, glycine and GABA "share tasks" for transmitting ipsilateral vestibular and extra-VOR inputs respectively. Functionally, the GABAergic inhibition might serve to regulate the general neuronal excitability and recruitment threshold, as described previously for rat oculomotor motoneurons (Torres-Torrelo et al., 2014), although inhibitory vestibular inputs to the oculomotor nucleus are also known to be GABAergic, impeding a clear separation of VOR- and non-VOR related pathways.

V Plasticity of the VOR

Plastic modifications of the vestibulo-ocular reflex with respect to both gain and phase of the response have been studied extensively in a variety of different animal models and human subjects (see Broussard and Kassardjian, 2005). The fact that the VOR gain can be reduced to almost zero on one hand and doubled on the other (e.g. Michnovicz and Bennett, 1987) as well as the possibility to induce up to a complete phase reversal of the VOR (e.g. Gutierrez-Castellanos et al., 2013) demonstrate the enormous adaptability of this reflex to changes in the visual environment relative to vestibular signals. This is in contrast to the hard-wired nature of most other short reflexes, such as the patellar reflex ("knee-jerk"; see Purves et al., 2011) and probably related to the fact that gaze stabilization plays such a crucial role for an animal's survival that it must be maintained during natural changes in both the visual and vestibular systems during growth and aging and should be restored as optimally as possible after lesions, such as uni- or bilateral vestibular damage (see Boyden et al., 2004; Dutia, 2010; Eatock and Songer, 2011).

In the present study, a different form of plasticity of the VOR was investigated that is independent of visuo-vestibular interactions and critically depends on the integrity of the cerebellar feed-back circuitry (Results II). In the dark (i.e. after dissection of both optic nerves), the gain of the VOR can be altered by prolonged high- or low-magnitude stimulation in a manner that resembles homeostatic plasticity (see e.g. Turrigiano, 2012): Prolonged "strong" vestibular stimulation close to saturation induces an attenuation of the single- and multiple-unit VOR gain such that the continuous high activity is reduced to more intermediate levels, whereas prolonged "weak" stimulation close to detection thresholds results in a facilitation of the gain, again to more intermediate levels (Results II). This

suggests that in the absence of visual feedback, the performance of the VOR is adjusted to a certain set point between threshold and saturation, hence in the linear range of the stimulus-response curve; presumably to maximize sensitivity to vestibular stimulation under non-physiological "vestibular-only" conditions (see also Results II, discussion). Whether or not these homeostatic mechanisms play a role in fine-tuning gaze-stabilizing reflexes in the intact animal however remains to be determined. In general, it should be noted that changes in VOR performance during prolonged stimulation would be highly undesirable in the intact animal, where optimal gaze stabilization requires a gain of exactly 1.0 (see Straka and Dieringer, 2004). Nevertheless, in several species it was demonstrated that prolonged vestibular stimulation in the dark can result in habituation (i.e. attenuation) of the VOR gain (Dow and Anastasio, 1998; Gutierrez-Castellanos et al., 2013; Jäger and Henn, 1981; Clément et al., 2008). It appears plausible that this is governed by a mechanism similar to the homeostatic plasticity described in the present study during high-magnitude stimulation considering that in both cases, the VOR gain is down-regulated upon prolonged vestibular-only stimulation and that both mechanisms are cerebellum-dependent (Results II; Dow and Anastasio, 1998). On the other hand, facilitation of the VOR gain upon prolonged low-magnitude stimulation in the dark is a novel finding.

Homeostatic plasticity of the VOR was shown to be independent of and persist across different frequencies and velocities of head motion (Results II) indicating that stimulus "strength" indeed is the only critical parameter for inducing homeostatic changes. This differs from "classical" visuo-vestibular adaptation that was shown to be frequency- (Lisberger et al., 1983) and/or velocity-specific (Hübner et al., 2014). Nevertheless, homeostatic plasticity was found to be plane-specific, suggesting that not only the primary VOR network but also the cerebellar side loop, mediating plastic changes, comprises head motion direction specific, parallel processing pathways, reminiscent of "principal VOR connections" (see Straka and Dieringer, 2004).

Importantly, it was demonstrated in the present study that homeostatic plasticity of the VOR – in contrast to adaptation after visuo-vestibular mismatch training (Titley et al., 2007, Anzai et al., 2010; see Broussard et al., 2011) – does not consolidate (Results II), at least with the stimulation times applied (>20 – max. 40 minutes). Notably, homeostatic changes were immediately abolished after surgical ablation of cerebellar purkinje cells (Results II); hence the site of plasticity was restricted to the level of the vestibulocerebellum, compatible with the absence of memory consolidation that in other studies was suggested to occur at downstream synaptic sites such as the deep cerebellar nuclei and/or cerebellar target neurons in the vestibular nuclei (Kassardjian et al., 2005). In the case of the homeostatic plasticity observed in *Xenopus* tadpoles, either the time of prolonged stimulation was too short for

consolidation to occur or this type of plasticity does not consolidate in general. In cats, consolidation appears after around 60 minutes after gain-up or gain-down visuo-vestibular mismatch training (Titley et al., 2007), and although 40 minutes of stimulation fall into a similar time frame, it is possible that an additional hour might lead to consolidation of the gain change in *Xenopus*. However, it appears likely that this is not the case considering that homeostatic plasticity generally represents an "on-line", activity dependent mechanism (see Turrigiano, 2012). Furthermore, without visual feedback, the brain is unable to assess whether VOR performance is optimal and should be stored permanently or not.

VI Summary and Outlook

VI.1 Classification of abducens motoneurons

During a major part of this thesis, substantial knowledge about the morphological, electrophysiological and pharmacological properties of abducens motoneurons could be gained. In addition, using semi-intact preparations of larval *Xenopus* allowed investigating the functions of distinct properties for VOR processing. For example, retrograde labeling of abducens nuclei and calcium imaging experiments suggested that axon diameter rather than soma size correlates with the phasic-tonic characteristics of extraocular motoneurons and that tonically active neurons are more round than those recruited only during stimulation (Discussion, Fig. 3). Specific pharmacological blockade of neurotransmitter receptors during vestibular stimulation revealed a "task-sharing" for early and late phases of the VOR response of AMPA- and NMDA receptors respectively, and a likely correlation between the ratio of the two glutamate receptors and neuronal subtype (Results I, Fig. 6). Furthermore, the previously suggested (e.g. Straka and Dieringer, 1993) role of glycine for ipsilateral inhibitory vestibular inputs could be confirmed and a tonic GABAergic inhibition on abducens motoneurons was revealed (Results I, Fig. 7). With respect to individual response profiles of different abducens units, a continuum of activation thresholds – hence "tonic" to "phasic" properties – during vestibular stimulation was suggested, reminiscent of the often described continuum of vestibular afferents (e.g. Boyle and Highstein, 1990) and 2°VNs (e.g. du Lac and Lisberger, 1995). Further, particular units that are completely independent of VOR inputs were identified (Results I, Fig. 5). In addition, a novel classification of two groups of VOR-responsive abducens motoneurons was attempted according to the differences in response amplitude and timing during changing head motion frequencies (Results I, Fig. 4).

For consistency, only *Xenopus* tadpoles around developmental stage 54 were used for this study. An interesting and so far neglected aspect would be to investigate possible changes in

motoneuronal properties during the development of these animals from the onset of the horizontal aVOR around stage 49 (Lambert et al., 2008) to metamorphosis. During my thesis, occasionally also single units were recorded in younger animals around stages 50 – 52 (unpublished data) and it appeared as if units of the group I subtype are more prevalent in these younger larvae than group II motoneurons. Considering that group II motoneurons generally appear to be more important for VOR-related eye movements (Results I, Fig. 8), this raises the question whether group I motoneurons actually represent a more immature subtype and whether these cells eventually turn into group II motoneurons with increasing age. Further support for this idea might be given by the larger relative NMDA component in group I motoneurons, in agreement with findings in spinal neurons of neonatal rats where considerably larger NMDA currents were observed in younger animals (Hori and Kanda, 1996). However, it also remains to be determined whether changes in canal size during development play a role in determining group I/II motoneurons.

A drawback of the present study is the limited range of stimulation frequencies and velocities applied. Obtaining responses of individual abducens units for a larger range of velocities and/or head motion frequencies, such as beyond 1 Hz and below 0.1 Hz, would allow a more detailed investigation of the threshold and saturation levels of individual units both with respect to the velocity and frequency of stimulation. In addition, it would be interesting to investigate whether responses of group II motoneurons remain in phase with the stimulus also at frequencies beyond 1 Hz, since multiple-unit recordings revealed substantial phase lags of up to ~90° at 5 Hz head rotations (Results III, Fig. 3). Due to limitations of the two-axis turntable setup and problems with the stability of single-unit extracellular recordings at higher velocities and frequencies, such extended analyses are impossible at present and will probably require further equipment and/or experimental techniques.

Another interesting extension to the present study would be to apply constant velocity step stimuli in addition to sinusoidal head rotation to distinguish between individual motor units, since current steps were also used to distinguish between phasic and tonic 2°VNs during intracellular recordings in frogs (Beraneck et al., 2007). In fact, most ideally, intracellular recordings using patch-clamp techniques during electrical vestibular stimulation should be performed to identify the passive and active membrane properties of abducens motoneurons and compare them to those already described for 2°VNs. This would also reveal whether extraocular motoneurons themselves are tonic/phasic, or if they simply “transfer” the output of 2°VNs to the eye muscles. Intracellular recordings would also allow a detailed analysis of neurotransmitter systems and ion channels, such as low-voltage activated K^+ channels, as observed for mammalian vestibular afferent fibers (Kalluri et al., 2010) and frog 2°VNs (Beraneck et al., 2007). Although stable intracellular recordings would not allow for a

"natural" vestibular stimulation, galvanic vestibular stimulation would serve as a reasonable imitation of motion stimuli (Results III), as already applied during calcium imaging experiments in the present study.

Calcium imaging of a population of retrogradely labeled abducens motoneurons with simultaneous extracellular abducens nerve recordings on the same side gave a first indication that the location of individual motoneurons correlates with their response properties (Discussion Fig. 3). However, in the future, these experiments could be substantially improved by using voltage-sensitive dyes to directly monitor individual action potentials of the cells with a high camera frame rate. Calcium signals are too slow to resolve the tonic firing of spontaneously active cells, hence upon activation calcium responses appear equal in somata of "phasic" and "tonic" neurons. In addition, simultaneous application of voltage-sensitive dyes to several VOR-related brain regions might allow recording the activity of the entire network from afferent fibers to extraocular motoneurons.

Simultaneous recordings on various levels of the VOR – either with voltage-sensitive dyes or double-recordings using patch electrodes – would also help to reveal whether signal processing occurs exclusively in parallel channels or, if not, how much convergence occurs on each level. This yet open question could also be answered using rabies virus labeling techniques in a mammalian model organism. In a previous study in primates (Ugolini et al., 2006), this labeling was limited to two synaptic stages, i.e. from extraocular muscles to motoneurons and their respective presynaptic areas; however, a third synapse would already allow staining the entire VOR pathway from afferent fibers via 2°VNs and extraocular motoneurons. Alternatively, in the *Xenopus*, intracellular labeling with patch-clamp electrodes would enable tract-tracing the pathway of individual neurons, e.g. distinct types of motoneurons and their termination sites on possibly distinct types of muscle fibers.

VI.2 Homeostatic plasticity of the VOR

The second major project of my PhD concerned plastic alterations of the VOR under open-loop conditions (i.e. in the absence of visual inputs) that displayed the typical attributes of homeostatic plasticity (Results II, Fig. 2; Turrigiano, 2012). The observed alterations in VOR gain were found to be plane-specific (Results II, Fig. 4) and cerebellum-dependent (Results II, Fig. 5). Plastic changes in gain were reset to baseline values after keeping the preparation at rest for 20 minutes (Results II, Fig. 2), hence, no memory consolidation was observed. In addition, bilateral cerebellectomy directly after plasticity had been established also caused an immediate return of the gain to baseline values (Results II, Fig. 5), suggesting that the memory was not consolidated at extra-cerebellar sites such as the vestibular nuclei. However,

the time of prolonged stimulation never exceeded ~40 minutes in the present study and thus, further experiments should be performed to reveal if consolidation occurs with even longer stimulus durations.

In the present study, homeostatic plasticity was only described for the horizontal and vertical angular VOR. However, since this type of plasticity represents a rather global strategy to maintain stable networks in the brain (Turrigiano, 2012), the question arises if similar phenomena exist also for the linear VOR. Making use of a linear accelerator, this could be tested in future studies in *Xenopus* to complement the present findings.

Another important aspect would be testing whether homeostatic plasticity following prolonged vestibular stimulation also occurs in light, i.e. with both optic nerves intact and an appropriate visual environment such as a striped drum. The hypothesis would be that with visual feedback, gain alterations should not occur due to the online feedback of a correctly functioning VOR that must not be altered. The hypothesis is that homeostatic plasticity represents a compensatory mechanism for maintaining an optimal VOR working range only when the brain is “blind” without visual inputs and unable to assess the appropriateness of the respective gain. Future studies in the same *Xenopus* preparation will help to solve this question.

References/Bibliography

Albus JS (1971) A theory of cerebellar function. Math Biosci 10:25–61.

Angelaki DE, Hess BJM, Arai Y, Suzuki J (1996) Adaptation of primate vestibuloocular reflex to altered peripheral vestibular inputs. I. Frequency-specific recovery of horizontal VOR after inactivation of the lateral semicircular canals. J Neurophysiol 76:2941–2953.

Annoni JM, Cochran SL, Precht W (1984) Pharmacology of the vestibular hair cell-afferent fiber synapse in the frog. J Neurosci 4:2106–2116.

Anzai M, Kitazawa H, Nagao S (2010) Effects of reversible pharmacological shutdown of cerebellar flocculus on the memory of long-term horizontal vestibulo-ocular reflex adaptation in monkeys. Neurosci Res 68:191–198.

Avila VL, Frye PG (1978) Feeding Behavior of the African Clawed Frog (*Xenopus laevis* Daudin): (Amphibia, Anura, Pipidae): Effect of Prey Type. J Herpetol 12:391-396.

Babalian AL, Vidal P-P (2000) Floccular modulation of vestibuloocular pathways and cerebellum-related plasticity: An in vitro whole brain study. J Neurophysiol 84:2514–2528.

Baird RA, Lewis ER (1986) Correspondences between afferent innervation patterns and response dynamics in the bullfrog utricle and lagena. Brain Res 369:48–64.

Baird RA (1992) Morphological and electrophysiological properties of hair cells in the bullfrog utriculus. Ann N Y Acad Sci 656:12–26.

Baker RG, Mano N, Shimazu H (1969) Postsynaptic potentials in abducens motoneurons induced by vestibular stimulation. Brain Res 15:577–580.

Baker R, Highstein SM (1975) Physiological identification of interneurons and motoneurons in the abducens nucleus. Brain Res 91:292–298.

Barnes GR (1993) Visual-vestibular interaction in the control of head and eye movement: the role of visual feedback and predictive mechanisms. Prog Neurobiol 41:435–472.

Batini C, Ito M, Kado RT, Jastreboff PJ, Miyashita Y (1979) Interaction between the horizontal vestibulo-ocular reflex and optokinetic response in rabbits. Exp Brain Res 37:1–15.

Beraneck M, Hachemaoui M, Idoux E, Ris L, Uno A, Godaux E, Vidal P-P, Moore LE, Vibert N (2003) Long-term plasticity of ipsilesional medial vestibular nucleus neurons after unilateral labyrinthectomy. J Neurophysiol 90:184–203.

Beraneck M, Idoux E, Uno A, Vidal P-P, Moore LE, Vibert N (2004) Unilateral labyrinthectomy modifies the membrane properties of contralesional vestibular neurons. J Neurophysiol 92:1668–1684.

Beraneck M, Pfanzelt S, Vassias I, Rohregger M, Vibert N, Vidal P-P, Moore LE, Straka H (2007) Differential intrinsic response dynamics determine synaptic signal processing in frog vestibular neurons. J Neurosci 27:4283–4296.

Beraneck M, McKee JL, Aleisa M, Cullen KE (2008) Asymmetric recovery in cerebellar-deficient mice following unilateral labyrinthectomy. J Neurophysiol 100:945–958.

Beraneck M, Idoux E (2012) Reconsidering the role of neuronal intrinsic properties and neuromodulation in vestibular homeostasis. Front Neurol 3:1–13.

Bergquist F, Ludwig M, Dutia MB (2008) Role of the commissural inhibitory system in vestibular compensation in the rat. J Physiol 586:4441–4452.

Biesdorf S, Malinvaud D, Reichenberger I, Pfanzelt S, Straka H (2008) Differential inhibitory control of semicircular canal nerve afferent-evoked inputs in second-order vestibular neurons by glycinergic and GABAergic circuits. J Neurophysiol 99:1758–1769.

Blackiston DJ, Levin M (2013) Ectopic eyes outside the head in *Xenopus* tadpoles provide sensory data for light-mediated learning. J Exp Biol 216:1031–1040.

Blanks RHI, Precht W (1976) Functional characterization of primary vestibular afferents in the frog. Exp Brain Res 25:369–390.

Boyden ES, Katoh A, Raymond JL (2004) Cerebellum-dependent learning: the role of multiple plasticity mechanisms. Annu Rev Neurosci 27:581–609.

Boyle R, Highstein SM (1990) Resting discharge and response dynamics of horizontal semicircular canal afferents of the toadfish, *Opsanus tau*. J Neurosci 10:1557–1569.

Boyle R, Carey JP, Highstein SM (1991) Morphological correlates of response dynamics and efferent stimulation in horizontal semicircular canal afferents of the toadfish, *Opsanus tau*. J Neurophysiol 66:1504–1521.

Branoner F, Straka H (2015) Semicircular canal-dependent developmental tuning of translational vestibulo-ocular reflexes in *Xenopus laevis*. Dev Neurobiol 75:1051–1067.

Bronstein AM, Hood JD (1986) The cervico-ocular reflex in normal subjects and patients with absent vestibular function. Brain Res 373:399–408.

Broussard DM, Kassardjian CD (2004) Learning in a simple motor system. Learn Mem 11:127–136.

Broussard DM, Titley HK, Antflick J, Hampson DR (2011) Motor learning in the VOR: The cerebellar component. Exp Brain Res 210:451–463.

Büttner-Ennever JA, Horn AKE, Scherberger H, D'ascanio P (2001) Motoneurons of twitch and nontwitch extraocular muscle fibers in the abducens, trochlear, and oculomotor nuclei of monkeys. J Comp Neurol 438:318–335.

Büttner-Ennever JA, Horn AKE (2002a) The neuroanatomical basis of oculomotor disorders: the dual motor control of extraocular muscles and its possible role in proprioception. Curr Opin Neurol 15:35–43.

Büttner-Ennever JA, Horn AKE (2002b) Oculomotor system: a dual innervation of the eye muscles from the abducens, trochlear, and oculomotor nuclei. Mov Disord 17 Suppl 2:S2–S3.

Büttner-Ennever JA (2007) Anatomy of the oculomotor system. Dev Ophthalmol 40:1–14.

Burrone J, O'Byrne M, Murthy VN (2002) Multiple forms of synaptic plasticity triggered by selective suppression of activity in individual neurons. Nature 420:414–418.

Cameron SA, Dutia MB (1997) Cellular basis of vestibular compensation: changes in intrinsic excitability of MVN neurones. Neuroreport 8:2595–2599.

Carrascal L, Nieto-Gonzalez JL, Torres B, Nunez-Abades P (2009) Changes in somatodendritic morphometry of rat oculomotor nucleus motoneurons during postnatal development. J Comp Neurol 514:189–202.

Carriot J, Jamali M, Chacron MJ, Cullen KE (2014) Statistics of the vestibular input experienced during natural self-motion: implications for neural processing. J Neurosci 34:8347–8357.

Caston J, Precht W, Blanks RHI (1977) Response characteristics of frog's lagena afferents to natural stimulation. J Comp Physiol A 118:273–289.

Chagnaud BP, Simmers J, Straka H (2012) Predictability of visual perturbation during locomotion: implications for corrective efference copy signaling. Biol Cybern 106:669–679.

Chagnaud BP, Banchi R, Simmers J, Straka H (2015) Spinal corollary discharge modulates motion sensing during vertebrate locomotion. Nat Commun 6:7982.

Chen JW, Eatock RA (2000) Major potassium conductance in type I hair cells from rat semicircular canals: characterization and modulation by nitric oxide. J Neurophysiol 84:139–151.

Clément G, Courjon JH, Jeannerod M, Schmid R (1981) Unidirectional habituation of vestibulo-ocular responses by repeated rotational or optokinetic stimulations in the cat. Exp Brain Res 42:34–42.

Clément G, Tilikete C, Courjon J-H (2008) Retention of habituation of vestibulo-ocular reflex and sensation of rotation in humans. Exp Brain Res 190:307–315.

Clopath C, Badura A, De Zeeuw CI, Brunel N (2014) A cerebellar learning model of vestibulo-ocular reflex adaptation in wild-type and mutant mice. J Neurosci 34:7203–7215.

Cochran SL, Dieringer N, Precht W (1984) Basic optokinetic-ocular reflex pathways in the frog. J Neurosci 4:43–57.

Cochran SL, Kasik P, Precht W (1987) Pharmacological aspects of excitatory synaptic transmission to second-order vestibular neurons in the frog. Synapse 1:102–123.

Cochran SL, Correia MJ (1995) Functional support of glutamate as a vestibular hair cell transmitter in an amniote. Brain Res 670:321–325.

Combes D, Merrywest SD, Simmers J, Sillar KT (2004) Developmental segregation of spinal networks driving axial- and hindlimb-based locomotion in metamorphosing *Xenopus laevis*. J Physiol 559:17–24.

Combes D, Le Ray D, Lambert FM, Simmers J, Straka H (2008) An intrinsic feed-forward mechanism for vertebrate gaze stabilization. Curr Biol 18:R241–R243.

Cox PG, Jeffery N (2008) Geometry of the semicircular canals and extraocular muscles in rodents, lagomorphs, felids and modern humans. J Anat 213:583–596.

Cullen KE, Roy JE (2004) Signal Processing in the Vestibular System During Active Versus Passive Head Movements. J Neurophysiol 91:1919–1933.

Cullen KE, Minor LB, Beraneck M, Sadeghi SG (2009) Neural substrates underlying vestibular compensation: contribution of peripheral versus central processing. J Vestib Res 19:171–182.

Cullen KE, Brooks JX, Jamali M, Carriot J, Massot C (2011) Internal models of self-motion: Computations that suppress vestibular reafference in early vestibular processing. Exp Brain Res 210:377–388.

Davis GW, Bezprozvanny I (2001) Maintaining the stability of neural function: a homeostatic hypothesis. Annu Rev Physiol 63:847–869.

Davis GW, Goodman CS (1998) Synapse-specific control of synaptic efficacy at the terminals of a single neuron. Nature 392:82–86.

De Gois S, Schäfer MK-H, Defamie N, Chen C, Ricci A, Weihe E, Varoqui H, Erickson JD (2005) Homeostatic scaling of vesicular glutamate and GABA transporter expression in rat neocortical circuits. J Neurosci 25:7121–7133.

Dickman JD, Angelaki DE (2002) Vestibular convergence patterns in vestibular nuclei neurons of alert primates. J Neurophysiol 88:3518–3533.

Dieringer N, Precht W (1982) Compensatory head and eye movements in the frog and their contribution to stabilization of gaze. Exp Brain Res 47:394–406.

Dieringer N, Precht W (1986) Functional organization of eye velocity and eye position signals in abducens motoneurons of the frog. J Comp Physiol A 158:179–194.

Dieringer N (1995) "Vestibular compensation": Neural plasticity and its relations to functional recovery after labyrinthine lesions in frogs and other vertebrates. Prog Neurobiol 46:97–129.

Dietrich H, Straka H (2016) Prolonged vestibular stimulation induces homeostatic plasticity of the vestibulo-ocular reflex in larval *Xenopus laevis*. Eur J Neurosci 44:1787–1796.

Dow ER, Anastasio TJ (1998) Analysis and neural network modeling of the nonlinear correlates of habituation in the vestibulo-ocular reflex. J Comput Neurosci 5:171–190.

Dow ER, Anastasio TJ (1999) Dual-frequency habituation and dishabituation of the goldfish vestibulo-ocular reflex. Neuroreport 10:1729–1734.

du Lac S, Lisberger SG (1995) Membrane and firing properties of avian medial vestibular nucleus neurons *in vitro*. J Comp Physiol A 176:641–651.

Durand J (1989) Electrophysiological and morphological properties of rat abducens motoneurones. Exp Brain Res 76:141–152.

Durand J (1991) NMDA Actions on Rat Abducens Motoneurons. Eur J Neurosci 3:621–633.

Durand J (1993) Synaptic excitation triggers oscillations during NMDA receptor activation in rat abducens motoneurons. Eur J Neurosci 5:1389–1397.

Dutheil S, Brezun JM, Leonard J, Lacour M, Tighilet B (2009) Neurogenesis and astrogenesis contribution to recovery of vestibular functions in the adult cat following unilateral vestibular neurectomy: cellular and behavioral evidence. Neuroscience 164:1444–1456.

Dutia MB (2010) Mechanisms of vestibular compensation: recent advances. Curr Opin Otolaryngol Head Neck Surg 18:420–424.

Eatock RA, Songer JE (2011) Vestibular hair cells and afferents: two channels for head motion signals. Annu Rev Neurosci 34:501–534.

Eberhorn AC, Ardeleanu P, Büttner-Ennever JA, Horn AKE (2005) Histochemical differences between motoneurons supplying multiply and singly innervated extraocular muscle fibers. J Comp Neurol 491:352–366.

Edmonds B, Gibb AJ, Colquhoun D (1995) Mechanisms of activation of glutamate receptors and the time course of excitatory synaptic currents. Annu Rev Physiol 57:495–519.

Elliott KL, Fritzsch B (2010) Transplantation of *Xenopus laevis* ears reveals the ability to form afferent and efferent connections with the spinal cord. Int J Dev Biol 54:1443–1451.

Elliott KL, Houston DW, Decook R, Fritzsch B (2015a) Ear manipulations reveal a critical period for survival and dendritic development at the single-cell level in Mauthner neurons. Dev Neurobiol:1339–1351.

Elliott KL, Houston DW, Fritzsch B (2015b) Sensory afferent segregation in three-eared frogs resemble the dominance columns observed in three-eyed frogs. Sci Rep 5:8338.

Farrow K, Broussard DM (2003) Commissural inputs to secondary vestibular neurons in alert cats after canal plugs. J Neurophysiol 89:3351–3353.

Fernández C, Baird RA, Goldberg JM (1988) The Vestibular Nerve of the Chinchilla. I. Peripheral Innervation Patterns in the Horizontal and Superior Semicircular Canals. J Neurophysiol 60:182–203.

Gao Z, van Beugen BJ, De Zeeuw CI (2012) Distributed synergistic plasticity and cerebellar learning. Nat Rev Neurosci 13:619–635.

Gensberger KD, Dietrich H and Straka H (2013) Parallel signaling pathways as principle for vestibulo-ocular reflexes in *Xenopus laevis*. 106th Annual Meeting of the German Zoological Society, Munich, PP-NB-24.

Gensberger KD, Gravot C, Hoffman LF, Paulin M, Straka H (2015) Dynamic diversity of horizontal canal afferent neurons in *Xenopus laevis* tadpoles. Soc Neurosci Abstr 235:07.

Gestrin P, Sterling P (1977) Anatomy and physiology of goldfish oculomotor system. II. Firing patterns of neurons in abducens nucleus and surrounding medulla and their relation to eye movements. J Neurophysiol 40:573–588.

Goldberg JM, Fernández C (1977) Conduction times and background discharge of vestibular afferents. Brain Res 122:545–550.

Goldberg JM, Brichta AM (1998) Evolutionary trends in the organization of the vertebrate crista ampullaris. Otolaryngol Head Neck Surg 119:165–171.

Goldberg JM (2000) Afferent diversity and the organization of central vestibular pathways. Exp Brain Res 130:277–297.

Gonzalez-Islas C, Wenner P (2006) Spontaneous network activity in the embryonic spinal cord regulates AMPAergic and GABAergic synaptic strength. Neuron 49:563–575.

Goold CP, Nicoll RA (2010) Single-cell optogenetic excitation drives homeostatic synaptic depression. Neuron 68:512–528.

Goto F, Straka H, Dieringer N (2002) Gradual and reversible central vestibular reorganization in frog after selective labyrinthine nerve branch lesions. Exp Brain Res 147:374–386.

Graf W, Baker J, Peterson BW (1993) Sensorimotor transformation in the cat's vestibuloocular reflex system. I. Neuronal signals coding spatial coordination of compensatory eye movements. J Neurophysiol 70:2425–2441.

Graf W, Spencer R, Baker H, Baker R (1997) Excitatory and inhibitory vestibular pathways to the extraocular motor nuclei in goldfish. J Neurophysiol 77:2765–2779.

Grantyn R, Grantyn A, Schaaf P (1977) Conduction velocity, input resistance and size of cat ocular motoneurons stained with Procion yellow. Brain Res 135:167–173.

Grantyn R, Grantyn A (1978) Morphological and electrophysiological properties of cat abducens motoneurons. Exp Brain Res 31:249–274.

Grewe BF, Langer D, Kasper H, Kampa BM, Helmchen F (2010) High-speed *in vivo* calcium imaging reveals neuronal network activity with near-millisecond precision. Nat Methods 7:479–479.

Guth PS, Perin P, Norris CH, Valli P (1998) The vestibular hair cells: post-transductional signal processing. Prog Neurobiol 54:193–247.

Guth PS, Fermin CD, Pantoja M, Edwards R, Norris CH (1994) Hair cells of different shapes and their placement along the frog crista ampullaris. Hear Res 73:109–115.

Gutierrez-Castellanos N, Winkelman BHJ, Tolosa-Rodriguez L, De Gruijl JR, De Zeeuw CI (2013) Impact of aging on long-term ocular reflex adaptation. Neurobiol Aging 34:2784–2792.

Hackett JT (1972) Electrophysiological properties of neuronal circuits in the frog cerebellum *in vitro*. Brain Res 48:385–389.

Hanson MG, Landmesser LT (2004) Normal patterns of spontaneous activity are required for correct motor axon guidance and the expression of specific guidance molecules. Neuron 43:687–701.

Hänzi S, Hoffman L, Paulin M, Straka H (2015) Changes in swimming parameters during the development of *Xenopus* tadpoles. Soc Neurosci Abstr 753.13.

Harrison REW, Baker JF, Naokiisu, Wickland CR, Peterson BW (1986) Dynamics of adaptive change in vestibulo-ocular reflex direction. I. Rotations in the horizontal plane. Brain Res 371:162–165.

Hellsten U et al. (2010) The genome of the Western clawed frog *Xenopus tropicalis*. Science 328:633–636.

Henneman E, Somjen G, Carpenter DO (1965a) Functional Significance of Cell Size in Spinal Motoneurons. J Neurophysiol 28:560–580.

Henneman E, Somjen G, Carpenter DO (1965b) Excitability and inhibitability of motoneurons of different sizes. J Neurophysiol 28:599–620.

Hess BJ, Precht W (1984) Identification of vestibular sense organs responsible for maculo-ocular reflexes in the frog. Exp Brain Res 55:570–573.

Highstein SM, Baker R (1978) Excitatory termination of abducens internuclear neurons on medial rectus motoneurons: relationship to syndrome of internuclear ophthalmoplegia. J Neurophysiol 41:1647–1661.

Highstein SM, Rabbitt RD, Boyle R (1996) Determinants of semicircular canal afferent response dynamics in the toadfish, *Opsanus tau*. J Neurophysiol 75:575–596.

Highstein SM, Rabbitt RD, Holstein GR, Boyle RD (2005) Determinants of spatial and temporal coding by semicircular canal afferents. J Neurophysiol 93:2359–2370.

Hirano T, Kawaguchi S (2014) Regulation and functional roles of rebound potentiation at cerebellar stellate cell-Purkinje cell synapses. Front Cell Neurosci 8:42.

Hirata Y, Highstein SM (2001) Acute adaptation of the vestibuloocular reflex: signal processing by floccular and ventral parafloccular Purkinje cells. J Neurophysiol 85:2267–2288.

Hirata Y, Highstein SM (2002) Plasticity of the vertical VOR: a system identification approach to localizing the adaptive sites. Ann N Y Acad Sci 978:480–495.

Holstein GR, Martinelli GP, Henderson SC, Friedrich VL, Rabbitt RD, Highstein SM (2004a) Gamma-aminobutyric acid is present in a spatially discrete subpopulation of hair cells in the crista ampullaris of the toadfish *Opsanus tau*. J Comp Neurol 471:1–10.

Holstein GR, Rabbitt RD, Martinelli GP, Friedrich VL, Boyle RD, Highstein SM (2004b) Convergence of excitatory and inhibitory hair cell transmitters shapes vestibular afferent responses. Proc Natl Acad Sci USA 101:15766–15771.

Honrubia V, Hoffman LF, Sitko S, Schwartz IR (1989) Anatomic and physiological correlates in bullfrog vestibular nerve. J Neurophysiol 61:688–701.

Hori Y, Kanda K (1996) Developmental alterations in NMDA receptor-mediated currents in neonatal rat spinal motoneurons. Neurosci Lett 205:99–102.

Horn E, Mack R, Lang HG (1986) The development of the static vestibulo-ocular reflex in the southern clawed toad, *Xenopus laevis*. II. Animals with acute vestibular lesions. J Comp Physiol A 159:879–885.

Hübner PP, Khan SI, Migliaccio AA (2014) Velocity-selective adaptation of the horizontal and cross-axis vestibulo-ocular reflex in the mouse. Exp Brain Res 232:3035–3046.

Hübner PP, Khan SI, Migliaccio AA (2015) The mammalian efferent vestibular system plays a crucial role in the high-frequency response and short-term adaptation of the vestibuloocular reflex. J Neurophysiol 114:3154–3165.

Hultborn H, Nielsen JB (2007) Spinal control of locomotion – From cat to man. Acta Physiol 189:111–121.

Huterer M, Cullen KE (2002) Vestibuloocular reflex dynamics during high-frequency and high-acceleration rotations of the head on body in rhesus monkey. J Neurophysiol 88:13–28.

Ibata K, Sun Q, Turrigiano GG (2008) Rapid synaptic scaling induced by changes in postsynaptic firing. Neuron 57:819–826.

Ifediba MA, Rajguru SM, Hullar TE, Rabbitt RD (2007) The role of 3-canal biomechanics in angular motion transduction by the human vestibular labyrinth. Ann Biomed Eng 35:1247–1263.

Ito M (1982) Cerebellar control of the vestibulo-ocular reflex – around the flocculus hypothesis. Annu Rev Neurosci 5:275–296.

Ito M, Sakurai M, Tongroach P (1982) Climbing fibre induced depression of both mossy fibre responsiveness and glutamate sensitivity of cerebellar Purkinje cells. J Physiol 324:113–134.

Iwasaki S, Chihara Y, Komuta Y, Ito K, Sahara Y (2008) Low-voltage-activated potassium channels underlie the regulation of intrinsic firing properties of rat vestibular ganglion cells. J Neurophysiol 100:2192–2204.

Jäger J, Henn V (1981) Habituation of the vestibulo-ocular reflex (VOR) in the monkey during sinusoidal rotation in the dark. Exp Brain Res 41:108–114.

Johnston AR, MacLeod NK, Dutia MB (1994) Ionic conductances contributing to spike repolarization and after-potentials in rat medial vestibular nucleus neurones. J Physiol 481:61–77.

Jones MS, Ariel M (2008) Morphology, intrinsic membrane properties, and rotation-evoked responses of trochlear motoneurons in the turtle. J Neurophysiol 99:1187–1200.

Kalb RG, Lidow MS, Halsted MJ, Hockfield S (1992) N-methyl-D-aspartate receptors are transiently expressed in the developing spinal cord ventral horn. Proc Natl Acad Sci USA 89:8502–8506.

Kalb RG (1994) Regulation of motor neuron dendrite growth by NMDA receptor activation. Development 120:3063–3071.

Kalluri R, Xue J, Eatock RA (2010) Ion channels set spike timing regularity of mammalian vestibular afferent neurons. J Neurophysiol 104:2034–2051.

Kassardjian CD, Tan Y-F, Chung J-YJ, Heskin R, Peterson MJ, Broussard DM (2005) The site of a motor memory shifts with consolidation. J Neurosci 25:7979–7985.

Kelders WPA, Kleinrensink GJ, van der Geest JN, Feenstra L, De Zeeuw CI, Frens MA (2003) Compensatory increase of the cervico-ocular reflex with age in healthy humans. J Physiol 553:311–317.

Khorevin VI (2008) The lagena (the third otolith endorgan in vertebrates). Neurophysiology 40:142–159.

Kim KS, Minor LB, Della Santina CC, Lasker DM (2011) Variation in response dynamics of regular and irregular vestibular-nerve afferents during sinusoidal head rotations and currents in the chinchilla. Exp Brain Res 210:643–649.

King BR, Fogel SM, Albouy G, Doyon J (2013) Neural correlates of the age-related changes in motor sequence learning and motor adaptation in older adults. Front Hum Neurosci 7:142.

Knorr AG, Schuller JM, Straka H and Glasauer S (2012) A model of the optokinetic reflex system in larval *Xenopus*. Front Comput Neurosci Conference Abstract: Bernstein Conference 2012.

Lahjouji F, Bras H, Barbe A, Chazal G (1995) GABAergic innervation of rat abducens motoneurons retrogradely labelled with HRP: quantitative ultrastuctural analysis of cell bodies and proximal dendrites. J Neurocytol 24:29–44.

Lambert FM, Beck JC, Baker R, Straka H (2008) Semicircular canal size determines the developmental onset of angular vestibuloocular reflexes in larval *Xenopus*. J Neurosci 28:8086–8095.

Lambert FM, Combes D, Simmers J, Straka H (2012) Gaze stabilization by efference copy signaling without sensory feedback during vertebrate locomotion. Curr Biol 22:1649–1658.

Land MF (1973) Head Movement of Flies during Visually Guided Flight. Nature 243:299–300.

Land MF (1999) Motion and vision: why animals move their eyes. J Comp Physiol A 185:341–352.

Lewis ER, Li CW (1975) Hair cell types and distributions in the otolithic and auditory organs on the bullfrog. Brain Res 83:35–50.

Lewis ER, Baird RA, Leverenz EL, Koyama H (1982) Inner ear: dye injection reveals peripheral origins of specific sensitivities. Science 215:1641–1643.

Lim R, Callister RJ, Brichta AM (2010) An increase in glycinergic quantal amplitude and frequency during early vestibular compensation in mouse. J Neurophysiol 103:16–24.

Lisberger SG, Miles FA, Optican LM (1983) Frequency-selective adaptation: evidence for channels in the vestibulo-ocular reflex? J Neurosci 3:1234–1244.

Lisberger SG, Miles FA, Zee DS (1984) Signals used to compute errors in monkey vestibuloocular reflex: possible role of flocculus. J Neurophysiol 52:1140–1153.

Lorente de Nó R (1933) Anatomy of the eighth nerve. The central projection of the nerve endings of the internal ear. Laryngoscope 43:1–38.

Lorenzo L-E, Russier M, Barbe A, Fritschy J-M, Bras H (2007) Differential organization of gamma-aminobutyric acid type A and glycine receptors in the somatic and dendritic compartments of rat abducens motoneurons. J Comp Neurol 504:112–126.

Luebke AE, Robinson DA (1994) Gain changes of the cat's vestibulo-ocular reflex after flocculus deactivation. Exp Brain Res 98:379–390.

Luksch H, Walkowiak W, Muñoz A, Ten Donkelaar HJ (1996) The use of in vitro preparations of the isolated amphibian central nervous system in neuroanatomy and electrophysiology. J Neurosci Methods 70:91–102.

Magherini PC, Giretti ML, Precht W (1975) Cerebellar control of vestibular neurons of the frog. Pflügers Arch Eur J Physiol 356:99–109.

Malinvaud D, Vassias I, Reichenberger I, Rössert C, Straka H (2010) Functional organization of vestibular commissural connections in frog. J Neurosci 30:3310–3325.

Marder E, Bucher D (2001) Central pattern generators and the control of rhythmic movements. Curr Biol 11:986–996.

Marr D (1969) A theory of cerebellar cortex. J Physiol 202:437–470.

Matesz C (1990) Development of the abducens nuclei in the *Xenopus laevis*. Dev Brain Res 51:179–184.

McArthur KL, Zakir M, Haque A, Dickman JD (2011) Spatial and temporal characteristics of vestibular convergence. Neuroscience 192:361–371.

Medina JF (2011) The multiple roles of Purkinje cells in sensori-motor calibration: to predict, teach and command. Curr Opin Neurobiol 21:616–622.

Medrea I, Cullen KE (2013) Multisensory integration in early vestibular processing in mice: The encoding of passive versus active motion. J Neurophysiol 110:2704–2717.

Mendell LM (2005) The size principle: a rule describing the recruitment of motoneurons. J Neurophysiol 93:3024–3026.

Menzies JRW, Porrill J, Dutia M, Dean P (2010) Synaptic plasticity in medial vestibular nucleus neurons: comparison with computational requirements of VOR adaptation. PLoS One 5 10.1371/journal.pone.0013182

Michnovicz JJ, Bennett M V (1987) Effects of rapid cerebellectomy on adaptive gain control of the vestibulo-ocular reflex in alert goldfish. Exp Brain Res 66:287–294.

Miles FA, Lisberger SG (1981) Plasticity in the vestibulo-ocular reflex: a new hypothesis. Annu Rev Neurosci 4:273–299.

Nieto-Gonzalez JL, Carrascal L, Nunez-Abades P, Torres B (2007) Phasic and tonic firing properties in rat oculomotor nucleus motoneurons, studied *in vitro*. Eur J Neurosci 25:2682–2696.

Nieuwkoop PD, Faber J (1994) Normal Table of *Xenopus Laevis* (Daudin): A Systematical and Chronological Survey of the Development from the Fertilized Egg Till the End of Metamorphosis. Garland Pub.

Pantle C, Dieringer N (1998) Spatial transformation of semicircular canal signals into abducens motor signals. A comparison between grass frogs and water frogs. J Comp Physiol A 182:475–487.

Panzanelli P, Valli P, Cantino D, Fasolo A (1994) Glutamate and carnosine in the vestibular system of the frog. Brain Res 662:293–296.

Paradis S, Sweeney ST, Davis GW (2001) Homeostatic control of presynaptic release is triggered by postsynaptic membrane depolarization. Neuron 30:737–749.

Pastor AM, de la Cruz RR, Baker R (1994) Cerebellar role in adaptation of the goldfish vestibuloocular reflex. J Neurophysiol 72:1383–1394.

Paul BYH, Nalbacht H, Varju D (1990) Eye Movements in the Rock Crab *Pachygrapsus Marmoratus* Walking Along Straight and Curved Paths. J Exp Biol 154:81–97.

Peterson EH, Cotton JR, Grant JW (1996) Structural variation in ciliary bundles of the posterior semicircular canal. Quantitative anatomy and computational analysis. Ann N Y Acad Sci 781:85–102.

Pratt DW (1982) Saccadic eye movements are coordinated with head movements in walking chickens. J Exp Biol 97:217–223.

Priesol AJ, Jones GE, Tomlinson RD, Broussard DM (2000) Frequency-dependent effects of glutamate antagonists on the vestibulo-ocular reflex of the cat. Brain Res 857:252–264.

Purves D, Augustine GJ, Fitzpatrick D, Hall WC, LaMantia A-S, White LE (2011) Neuroscience 5th edition. Sinauer Associates.

Rambold H, Churchland A, Selig Y, Jasmin L, Lisberger SG (2002) Partial ablations of the flocculus and ventral paraflocculus in monkeys cause linked deficits in smooth pursuit eye movements and adaptive modification of the VOR. J Neurophysiol 87:912–924.

Ramón y Cajal S (1909) Histologie du système nerveux de l'homme & des vertébrés. Paris: Maloine.

Reichenberger I, Dieringer N (1994) Size-related colocalization of glycine and glutamate immunoreactivity in frog and rat vestibular afferents. J Comp Neurol 349:603–614.

Reichenberger I, Straka H, Ottersen OP, Streit P, Gerrits NM, Dieringer N (1997) Distribution of GABA, Glycine, and Glutamate Immunoreactivities in the Vestibular Nuclear Complex of the Frog. J Comp Neurol 377:149–164.

Rohregger M, Dieringer N (2002) Principles of linear and angular vestibuloocular reflex organization in the frog. J Neurophysiol 87:385–398.

Rohregger M, Dieringer N (2003) Postlesional vestibular reorganization improves the gain but impairs the spatial tuning of the maculo-ocular reflex in frogs. J Neurophysiol 90:3736–3749.

Roy JE, Cullen KE (1998) A neural correlate for vestibulo-ocular reflex suppression during voluntary eye-head gaze shifts. Nat Neurosci 1:404–410.

Russier M, Kopysova IL, Ankri N, Ferrand N, Debanne D (2002) GABA and glycine co-release optimizes functional inhibition in rat brainstem motoneurons in vitro. J Physiol 541:123–137.

Russier M, Carlier E, Ankri N, Fronzaroli L, Debanne D (2003) A-, T-, and H-type currents shape intrinsic firing of developing rat abducens motoneurons. J Physiol 549:21–36.

Sadeghi SG, Chacron MJ, Taylor MC, Cullen KE (2007) Neural variability, detection thresholds, and information transmission in the vestibular system. J Neurosci 27:771–781.

Sadeghi SG, Minor LB, Cullen KE (2011) Multimodal integration after unilateral labyrinthine lesion: single vestibular nuclei neuron responses and implications for postural compensation. J Neurophysiol 105:661–673.

Sans NA, Montcouquiol ME, Raymond J (2000) Postnatal developmental changes in AMPA and NMDA receptors in the rat vestibular nuclei. Dev Brain Res 123:41–52.

Sato F, Sasaki H (1993) Morphological correlations between spontaneously discharging primary vestibular afferents and vestibular nucleus neurons in the cat. J Comp Neurol 333:554–566.

Schmäl F (2013) Neuronal mechanisms and the treatment of motion sickness. Pharmacology 91:229–241.

Schuller JM, Chagnaud BP, Straka H (2011) Interaction of visual and spinal central pattern generator-derived signals during locomotor activity in larval *Xenopus*. Soc Neurosci Abstr 699.08.

Schultheis LW, Robinson DA (1981) Directional plasticity of the vestibuloocular reflex in the cat. Ann N Y Acad Sci 374:504–512.

Sekirnjak C, du Lac S (2006) Physiological and anatomical properties of mouse medial vestibular nucleus neurons projecting to the oculomotor nucleus. J Neurophysiol 95:3012–3023.

Serafin M, de Waele C, Khateb A, Vidal P-P, Mühlethaler M (1991) Medial vestibular nucleus in the guinea-pig. I. Intrinsic membrane properties in brainstem slices. Exp Brain Res 84:417–425.

Shao M, Popratiloff A, Hirsch JC, Peusner KD (2009) Presynaptic and postsynaptic ion channel expression in vestibular nuclei neurons after unilateral vestibular deafferentation. J Vestib Res 19:191–200.

Shin M, Moghadam SH, Sekirnjak C, Bagnall MW, Kolkman KE, Jacobs R, Faulstich M, du Lac S (2011) Multiple types of cerebellar target neurons and their circuitry in the vestibulo-ocular reflex. J Neurosci 31:10776–10786.

Shu D-G, Luo H-L, Conway Morris S, Zhang X-L, Hu S-X, Chen L-Z, Han J, Zhu M, Li Y, Chen L-Z (1999) Lower Cambrian vertebrates from south China. Nature 402:42–46.

Simpson JI, Graf W (1981) Eye-muscle geometry and compensatory eye movements in lateral-eyed and frontal-eyed animals. Ann N Y Acad Sci 374:20–30.

Soto E, Vega R (1988) Actions of excitatory amino acid acid agonists and antagonists on the primary afferents of the vestibular system of the axolotl (*Ambystoma mexicanum*). Brain Res 462:104–111.

Soto E, Flores A, Vega R (1994) NMDA-mediated potentiation of the afferent synapse in the inner ear. Neuroreport 5:1963–1965.

Spencer RF, Wenthold RJ, Baker R (1989) Evidence for glycine as an inhibitory neurotransmitter of vestibular, reticular, and prepositus hypoglossi neurons that project to the cat abducens nucleus. J Neurosci 9:2718–2736.

Spencer RF, Baker R (1992) GABA and glycine as inhibitory neurotransmitters in the vestibuloocular reflex. Ann N Y Acad Sci 656:602–611.

Stehouwer DJ (1988) Metamorphosis of behavior in the bullfrog (*Rana catesbeiana*). Dev Psychobiol 21:383–395.

Sterling P (1977) Anatomy and physiology of goldfish oculomotor system. I. Structure of abducens nucleus. J Neurophysiol 40:557–572.

Stirn Kranjc B, Smerdu V, Erzen I (2009) Histochemical and immunohistochemical profile of human and rat ocular medial rectus muscles. Graefes Arch Clin Exp Ophthalmol 247:1505–1515.

Straka H, Dieringer N (1993) Electrophysiological and pharmacological characterization of vestibular inputs to identified frog abducens motoneurons and internuclear neurons *in vitro*. Eur J Neurosci 5:251–260.

Straka H, Dieringer N (1996) Uncrossed disynaptic inhibition of second-order vestibular neurons and its interaction with monosynaptic excitation from vestibular nerve afferent fibers in the frog. J Neurophysiol 76:3087–3101.

Straka H, Reichenberger I, Dieringer N (1996a) Size-related properties of vestibular afferent fibers in the frog: uptake of and immunoreactivity for glycine and aspartate/glutamate. Neuroscience 70:685–696.

Straka H, Debler K, Dieringer N (1996b) Size-related properties of vestibular afferent fibers in the frog: differential synaptic activation of N-methyl-D-aspartate and non-N-methyl-D-aspartate receptors. Neuroscience 70:697–707.

Straka H, Dieringer N (2000) Convergence pattern of uncrossed excitatory and inhibitory semicircular canal-specific inputs onto second-order vestibular neurons of frogs. Organization of vestibular side loops. Exp Brain Res 135:462–473.

Straka H, Holler S, Goto F (2002) Patterns of canal and otolith afferent input convergence in frog second-order vestibular neurons. J Neurophysiol 88:2287–2301.

Straka H, Dieringer N (2004) Basic organization principles of the VOR: Lessons from frogs. Prog Neurobiol 73:259–309.

Straka H, Beraneck M, Rohregger M, Moore LE, Vidal P-P, Vibert N (2004) Second-order vestibular neurons form separate populations with different membrane and discharge properties. J Neurophysiol 92:845–861.

Straka H, Vibert N, Vidal P-P, Moore LE, Dutia MB (2005) Intrinsic membrane properties of vertebrate vestibular neurons: Function, development and plasticity. Prog Neurobiol 76:349–392.

Straka H, Lambert FM, Pfanzelt S, Beraneck M (2009) Vestibulo-ocular signal transformation in frequency-tuned channels. Ann N Y Acad Sci 1164:37–44.

Straka H (2010) Ontogenetic rules and constraints of vestibulo-ocular reflex development. Curr Opin Neurobiol 20:689–695.

Straka H, Simmers J (2012) *Xenopus laevis*: an ideal experimental model for studying the developmental dynamics of neural network assembly and sensory-motor computations. Dev Neurobiol 72:649–663.

Straka H, Fritzsch B, Glover JC (2014) Connecting ears to eye muscles: evolution of a “simple” reflex arc. Brain Behav Evol 83:162–175.

Straka H, Zwergal A, Cullen KE (2016) Vestibular animal models: contributions to understanding physiology and disease. J Neurol 263 Suppl 1:S10–23.

Tadros MA, Farrell KE, Schofield PR, Brichta AM, Graham BA, Fuglevand AJ, Callister RJ (2014) Intrinsic and synaptic homeostatic plasticity in motoneurons from mice with glycine receptor mutations. J Neurophysiol 111:1487–1498.

Takazawa T, Saito Y, Tsuzuki K, Ozawa S (2004) Membrane and firing properties of glutamatergic and GABAergic neurons in the rat medial vestibular nucleus. J Neurophysiol 92:3106–3120.

Tighilet B, Brezun JM, Sylvie GDD, Gaubert C, Lacour M (2007) New neurons in the vestibular nuclei complex after unilateral vestibular neurectomy in the adult cat. Eur J Neurosci 25:47–58.

Titley HK, Heskin-Sweezie R, Chung J-YJ, Kassardjian CD, Razik F, Broussard DM (2007) Rapid consolidation of motor memory in the vestibuloocular reflex. J Neurophysiol 98:3809–3812.

Torres-Torrelo J, Torres B, Carrascal L (2014) Modulation of the input-output function by $GABA_A$ receptor-mediated currents in rat oculomotor nucleus motoneurons. J Physiol 592:5047–5064.

Turrigiano GG, Leslie KR, Desai NS, Rutherford LC, Nelson SB (1998) Activity-dependent scaling of quantal amplitude in neocortical neurons. Nature 391:892–896.

Turrigiano G (2012) Homeostatic synaptic plasticity: local and global mechanisms for stabilizing neuronal function. Cold Spring Harb Perspect Biol 4:a005736.

Turrigiano GG, Nelson SB (2004) Homeostatic plasticity in the developing nervous system. Nat Rev Neurosci 5:97–107.

Uchino Y, Ikegami H, Sasaki M, Endo K, Imagawa M, Isu N (1994) Monosynaptic and disynaptic connections in the utriculo-ocular reflex arc of the cat. J Neurophysiol 71:950–958.

Udin SB (2007) The instructive role of binocular vision in the *Xenopus* tectum. Biol Cybern 97:493–503.

Ugolini G (2010) Advances in viral transneuronal tracing. J Neurosci Methods 194:2–20.

Ugolini G, Klam F, Doldan Dans M, Dubayle D, Brandi A-M, Büttner-Ennever J, Graf W (2006) Horizontal eye movement networks in primates as revealed by retrograde transneuronal transfer of rabies virus: differences in monosynaptic input to “slow” and “fast” abducens motoneurons. J Comp Neurol 498:762–785.

Usami S, Hozawa J, Tazawa M, Igarashi M, Thompson GC, Wu JY, Wenthold RJ (1989) Immunocytochemical study of the GABA system in chicken vestibular endorgans and the vestibular ganglion. Brain Res 503:214–218.

Vilares I, Kording K (2011) Bayesian models: the structure of the world, uncertainty, behavior, and the brain. Ann N Y Acad Sci 1224:22–39.

von Uckermann G, Le Ray D, Combes D, Straka H, Simmers J (2013) Spinal efference copy signaling and gaze stabilization during locomotion in juvenile *Xenopus* frogs. J Neurosci 33:4253–4264.

Walls GL (1962) The evolutionary history of eye movements. Vision Res 2:69–80.

Watanabe E (1984) Neuronal events correlated with long-term adaptation of the horizontal vestibulo-ocular reflex in the primate flocculus. Brain Res 297:169–174.

Watanabe E (1985) Role of the primate flocculus in adaptation of the vestibulo-ocular reflex. Neurosci Res 3:20–38.

Watt AJ, Desai NS (2010) Homeostatic Plasticity and STDP: Keeping a Neuron’s Cool in a Fluctuating World. Front Synaptic Neurosci 2:5.

Watt AJ, van Rossum MC, MacLeod KM, Nelson SB, Turrigiano GG (2000) Activity coregulates quantal AMPA and NMDA currents at neocortical synapses. Neuron 26:659–670.

Wei M, Angelaki DE (2001) Cross-axis adaptation of the translational vestibulo-ocular reflex. Exp Brain Res 138:304–312.

Wentzel PR, Gerrits NM, De Zeeuw CI (1996) GABAergic and glycinergic inputs to the rabbit oculomotor nucleus with special emphasis on the medial rectus subdivision. Brain Res 707:314–319.

Yakushin SB, Kolesnikova OV, Cohen B, Ogorodnikov DA, Suzuki J-I, Della Santina CC, Minor LB, Raphan T (2011) Complementary gain modifications of the cervico-ocular (COR) and angular vestibulo-ocular (aVOR) reflexes after canal plugging. Exp Brain Res 210:549–560.

Zakir M, Kushiro K, Ogawa Y, Sato H, Uchino Y (2000) Convergence patterns of the posterior semicircular canal and utricular inputs in single vestibular neurons in cats. Exp Brain Res 132:139–148.

Zee DS, Yamazaki A, Butler PH, Gücer G (1981) Effects of ablation of flocculus and paraflocculus of eye movements in primate. J Neurophysiol 46:878–899.

Zucca G, Botta L, Milesi V, Dagani F, Valli P (1992) Evidence for L-glutamate release in frog vestibular organs. Hear Res 63:52–56.

Appendix

I Abbreviations

2°VN second-order vestibular neuron

4-AP 4-Aminopyridine

aVOR angular vestibulo-ocular reflex

AC anterior semicircular canal

CPG central pattern generator

CV coefficient of variation

GVS galvanic vestibular stimulation

HC horizontal semicircular canal

K_{LV} low-voltage activated K^+

lVOR linear vestibulo-ocular reflex

MIF multiply-innervated muscle fiber

OKR optokinetic reflex

PC posterior semicircular canal

SIF singly-innervated muscle fiber

VOR vestibulo-ocular reflex

II List of publications

I. **Dietrich H.**, Glasauer S. and Straka H. (2017) Functional organization of vestibulo-ocular responses in abducens motoneurons. J Neuroscience 37:4032-4045.

II. **Dietrich H.** and Straka H. (2016) Prolonged vestibular stimulation induces homeostatic plasticity of the vestibulo-ocular reflex in larval *Xenopus laevis*. Eur J Neuroscience 44:1787–1796.

III. Gensberger K.D., Kaufmann A.K., **Dietrich H.**, Branoner F., Banchi, R., Chagnaud B. and Straka H. (2016) Galvanic Vestibular Stimulation: Cellular Substrates and Response Patterns of Neurons in the Vestibulo-Ocular Network. J Neuroscience 36:9097-9110.

III Declaration of author contributions

I. Functional organization of vestibulo-ocular responses in abducens motoneurons

Haike Dietrich, Stefan Glasauer and Hans Straka

Journal of Neuroscience, 2017

Contributions of HD:

- Planning of all experiments
- Performance of all experiments except for the computational modeling
- Analysis of all data except for those of the computational modeling
- Design and assembly of all figures
- Writing and revision of the manuscript

Contributions of SG:

- Planning of the computational modeling
- Performance and analysis of the computational modeling (Fig. 8)
- Writing and revision of the manuscript

Contributions of HS:

- Planning of all experiments
- Writing and revision of the manuscript

II. Prolonged vestibular stimulation induces homeostatic plasticity of the vestibulo-ocular reflex in larval *Xenopus laevis*

Haike Dietrich and Hans Straka

European Journal of Neuroscience, 2016

Contributions of HD:

- Planning of all experiments
- Performance of all experiments
- Analysis of all data
- Design and assembly of all figures
- Writing and revision of the manuscript

Contributions of HS:

- Planning of all experiments
- Writing and revision of the manuscript

III. Galvanic Vestibular Stimulation: Cellular Substrates and Response Patterns of Neurons in the Vestibulo-Ocular Network

Kathrin D. Gensberger*, Anna-Kristin Kaufmann*, **Haike Dietrich**, Francisco Branoner, Roberto Banchi, Boris P. Chagnaud and Hans Straka

*KD and AK contributed equally to this work

Journal of Neuroscience, 2016

Contributions of HD:

- Planning of experiments
- Recording and analysis of motion-induced extraocular motor activity (Figure 3)
- Recording and analysis of extraocular motor activity during in phase- *vs* out of phase-galvanic vestibular stimulation (Figure 5*M*,*N*)
- Recording and analysis of LR *vs* SO nerve activity during galvanic stimulation of the bilateral horizontal canals (Figure 5*L*)
- Design of figures containing contributed data together with HS
- Writing and revision of the manuscript

Contributions of KG:

- Planning of experiments
- Recording and analysis of motion- and GVS-induced vestibular afferent activity (Figure 7)
- Recording and analysis of pharmacological experiments to determine the cellular substrate underlying GVS-induced vestibular afferent activity (Figure 8)
- Design of figures containing contributed data together with HS
- Writing and revision of the manuscript

Contributions of AK:

- Planning of experiments
- Recording and analysis of GVS-induced extraocular motor activity (Figures 4, 5*A*-*K*)
- Revision of the manuscript

Contributions of FB:

- Planning of experiments
- Recording and analysis of the electric field generated by GVS electrodes (Figure 1*G*,*H*)

- Recording and analysis of motion- and GVS-induced eye movements (Figure 2)
- Design of figures containing contributed data together with HS
- Writing and revision of the manuscript

Contributions of RB:

- Recording and analysis of GVS-induced Ca^{2+} signals in central vestibular neurons (Figure 6)
- Design of figure containing contributed data together with HS

Contributions of BC:

- Planning of experiments
- Recording and analysis of GVS-induced Ca^{2+} signals in central vestibular neurons (Figure 6)
- Design of figure containing contributed data together with HS
- Writing and revision of the manuscript

Contributions of HS:

- Planning of experiments
- Design and assembly of all figures
- Writing and revision of the manuscript

IV Copyrights

Introduction Figure 1

A: Copyright © 1994 from "Normal Table of *Xenopus Laevis* (Daudin): A Systematical & Chronological Survey of the Development from the Fertilized Egg till the End of Metamorphosis" by P.D. Nieuwkoop and J. Faber. Reproduced by permission of Taylor and Francis Group, LLC, a division of Informa plc.

Introduction Figure 3

C: Reprinted from Hearing Research, Vol. 73; Authors: P.S. Guth, C.D. Fermin, M. Pantoja, R. Edwards, C. Norris; Title: "Hair cells of different shapes and their placement along the frog crista ampullaris"; Pages 109 - 115, Copyright © 1994, with permission from Elsevier.

D: Reprinted from Brain Research, Vol. 83; Authors: E.R. Lewis, C.W. Li; Title: "Hair cell types and distributions in the otolithic and auditory organs of the bullfrog"; Pages 35 – 50, Copyright © 1975, with permission from Elsevier.

E: Reprinted from PNAS, Vol. 101; Authors G.R. Holstein, R.D. Rabbitt, G.P. Martinelli, V.L. Friedrich, Jr., R.D. Boyle, S.M. Highstein; Title: "Convergence of excitatory and inhibitory hair cell transmitters shapes vestibular afferent responses"; Pages 15766 – 15771, Copyright © 2004, with permission from National Academy of Sciences, U.S.A.

Introduction Figure 4

C: Reprinted from Progress in Neurobiology, Vol. 76; Authors: H. Straka, N. Vibert, P.P. Vidal, L.E. Moore, M.B. Dutia; Title: "Intrinsic membrane properties of vertebrate vestibular neurons: Function, development and plasticity"; Pages 349 - 392, Copyright © 2005, with permission from Elsevier.

E: Reprinted from Journal of Vestibular Research, Vol. 19; Authors: M. Shao, A. Popratiloff, J.C. Hirsch, K.D. Peusner; Title: "Presynaptic and postsynaptic ion channel expression in vestibular nuclei neurons after unilateral vestibular deafferentation"; Pages 191 - 200, Copyright © 2009, with permission from IOS press.

Introduction Figure 5

C: Reprinted from Cold Spring Harbor Perspectives in Biology, Vol. 4:a005736; Author: G. Turrigiano; Title: "Homeostatic Synaptic Plasticity: Local and Global Mechanisms for Stabilizing Neuronal Function"; Copyright © 2012, with permission from Cold Spring Harbor Laboratory Press.

V Affidavit (Eidesstattliche Erklärung)

Hiermit versichere ich an Eides statt, dass ich die vorliegende Dissertation „**Functional characterization and plasticity of extraocular motor responses in *Xenopus laevis***“ selbstständig angefertigt habe, mich außer der angegebenen keiner weiteren Hilfsmittel bedient und alle Erkenntnisse, die aus dem Schrifttum ganz oder annähernd übernommen sind, als solche kenntlich gemacht und nach ihrer Herkunft unter Bezeichnung der Fundstelle einzeln nachgewiesen habe.

I hereby confirm that the dissertation “**Functional characterization and plasticity of extraocular motor responses in *Xenopus laevis***” is the result of my own work and that I have only used sources or materials listed and specified in the dissertation.